SiPM characterization for nEXO

PRESENTED BY TIZIANO BUZZIGOLI

Wright Laboratory Yale

Double-beta decay

Yale

Double-beta decay

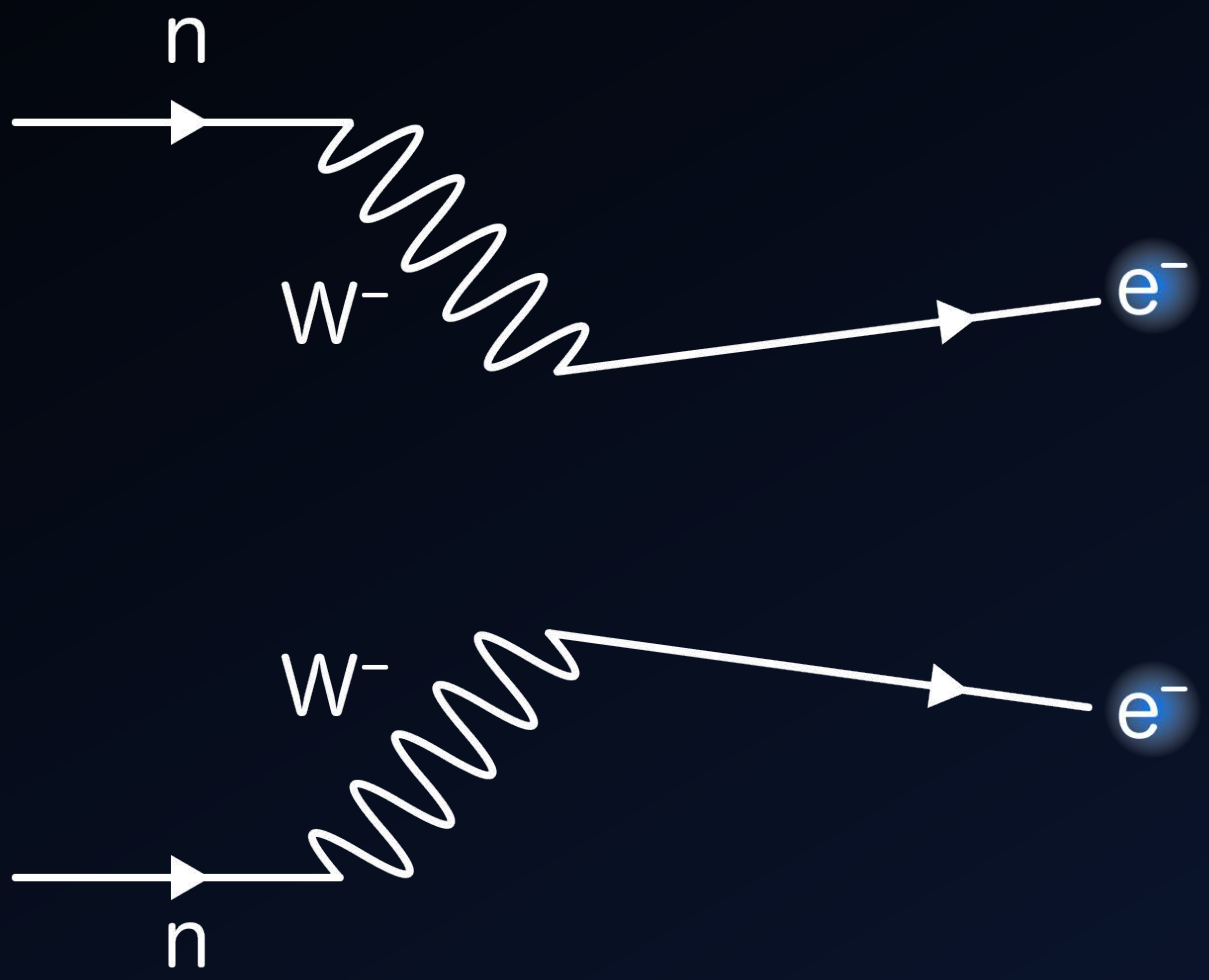

Yale

Double-beta decay

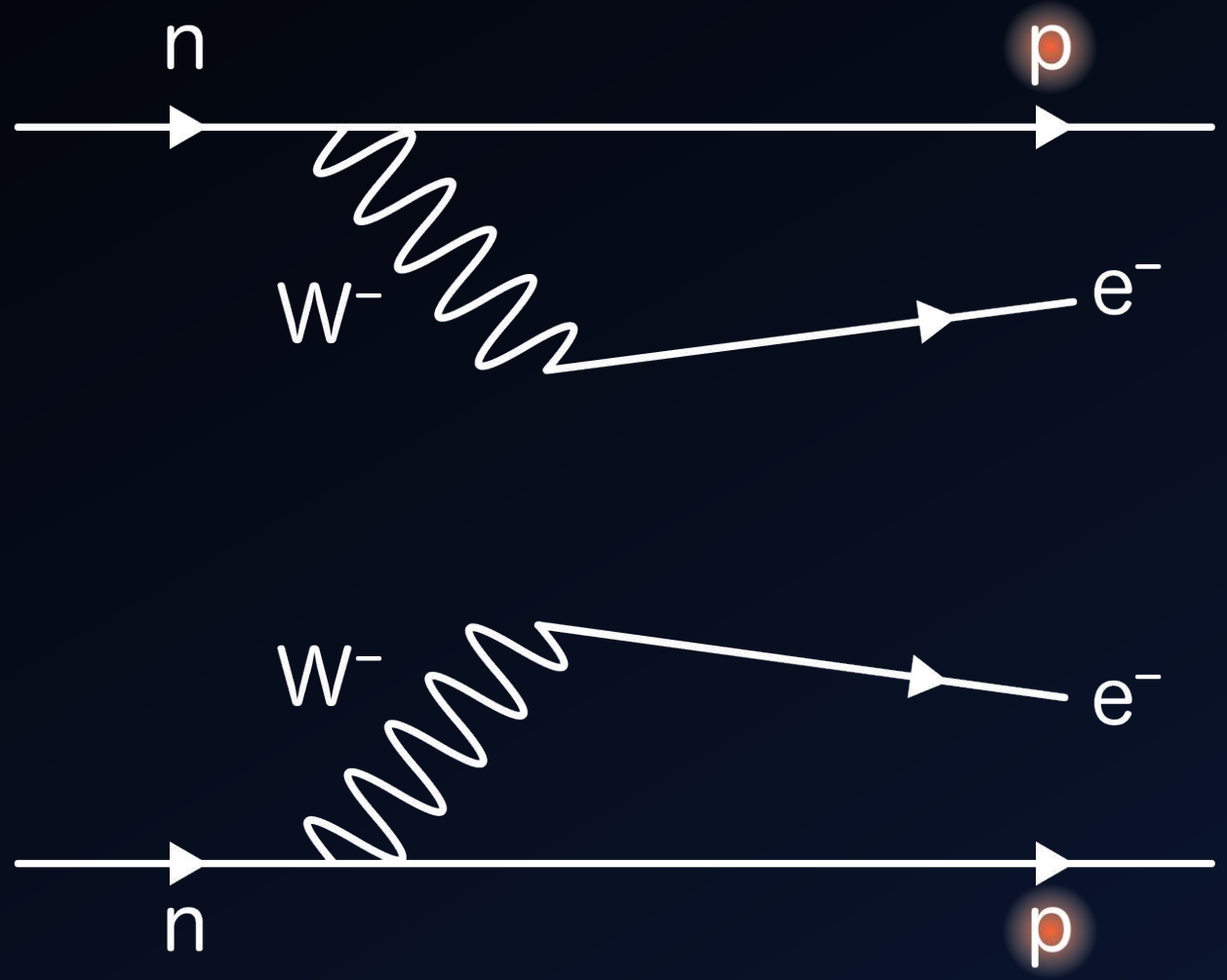

Yale

Double-beta decay

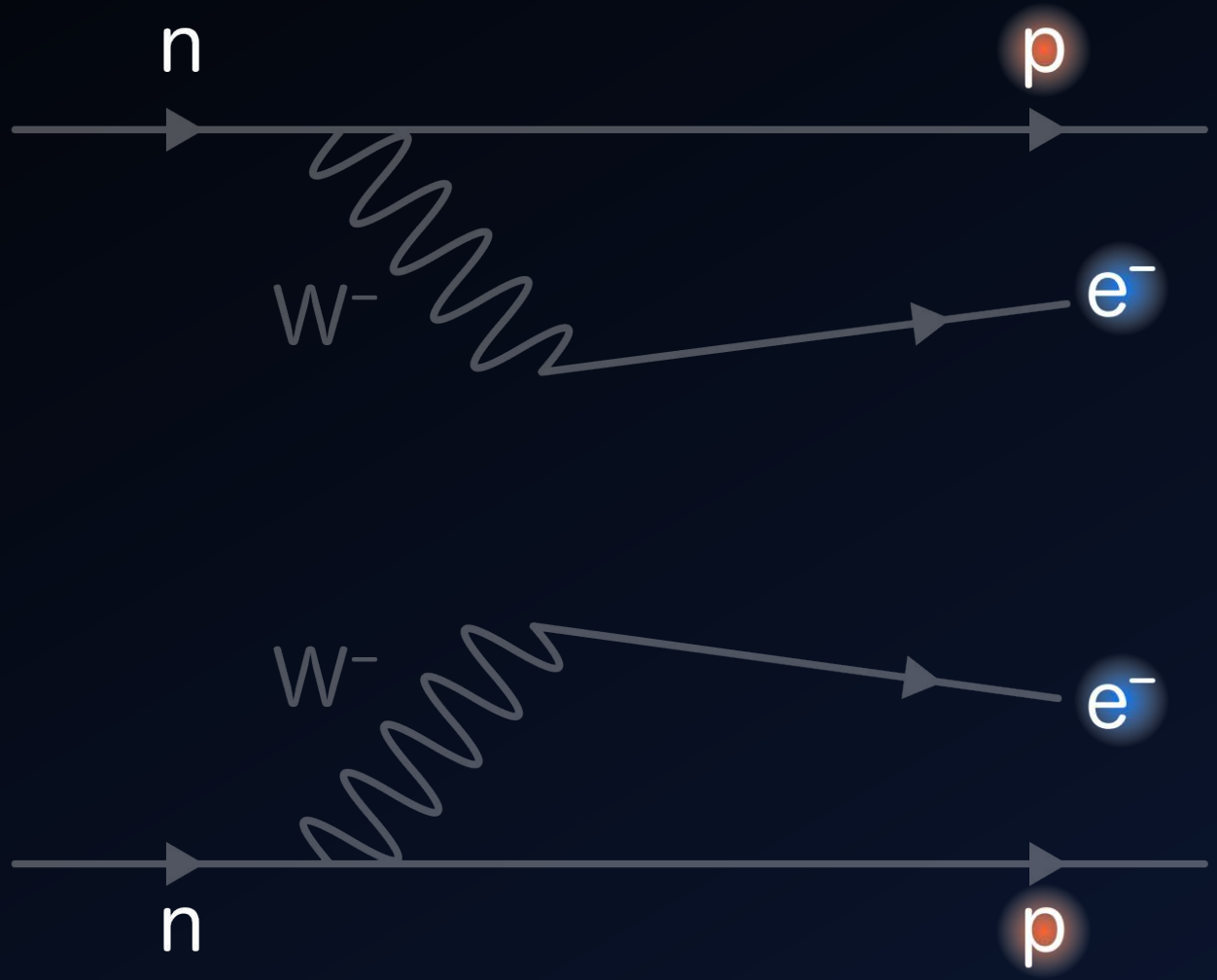

Yale

Double-beta decay

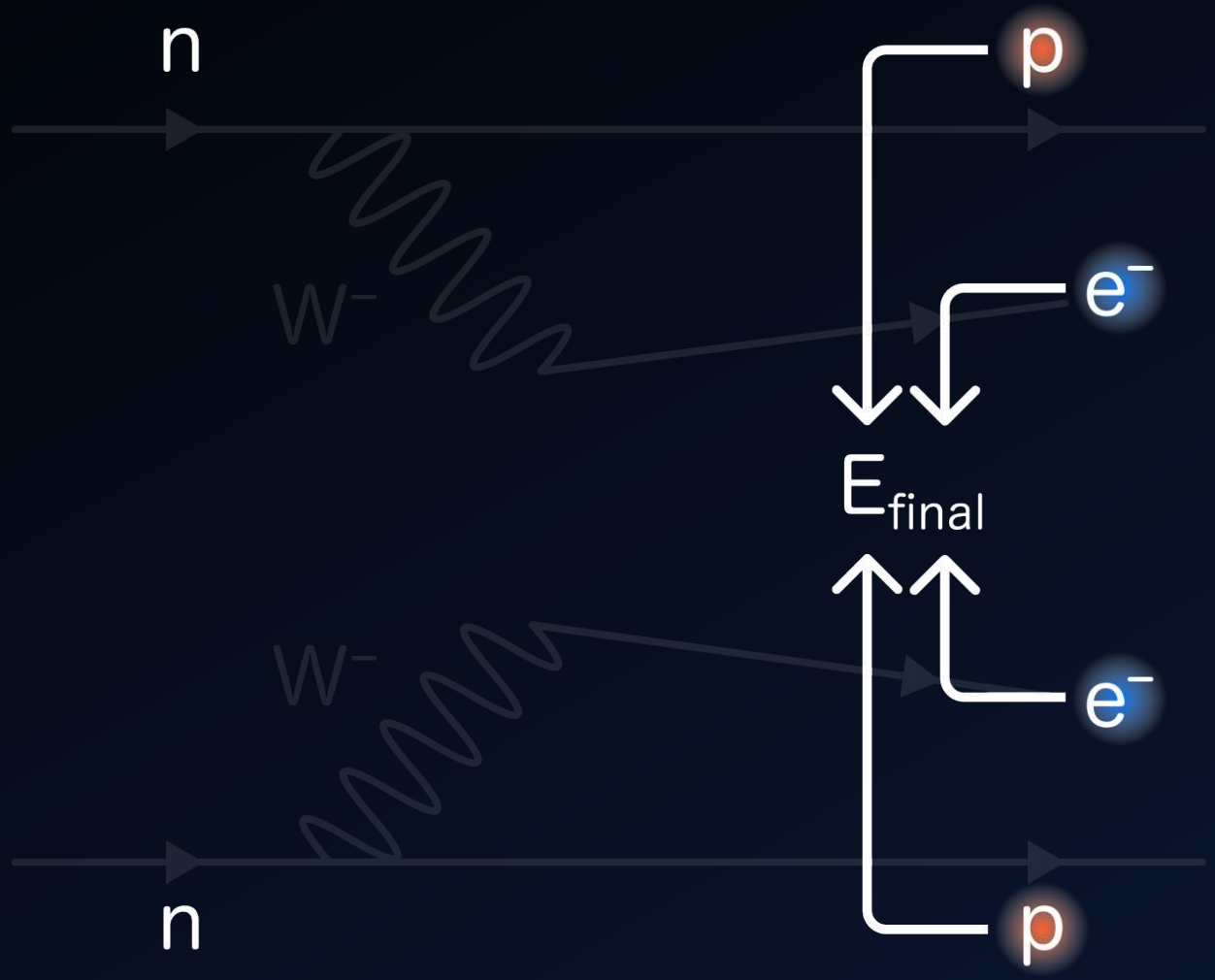

Yale

Double-beta decay

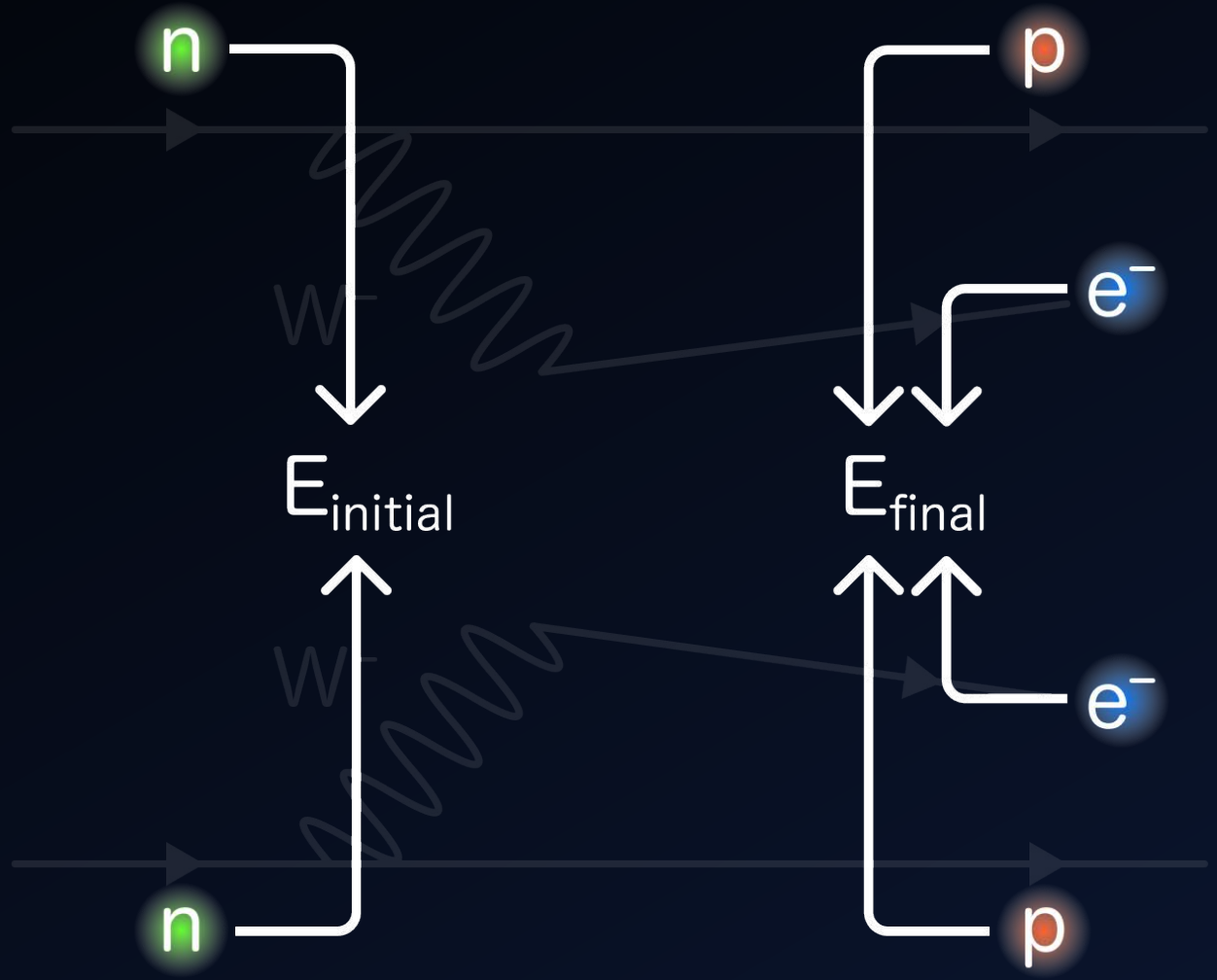

Yale

Double-beta decay

$E_{initial}$ E_{final}

Yale

Double-beta decay

$$E_{initial} > E_{final}$$

Yale

Double-beta decay

$$E_{initial} = E_{final} + \text{Q-value}$$

Yale

Double-beta decay

Yale

Double-beta decay

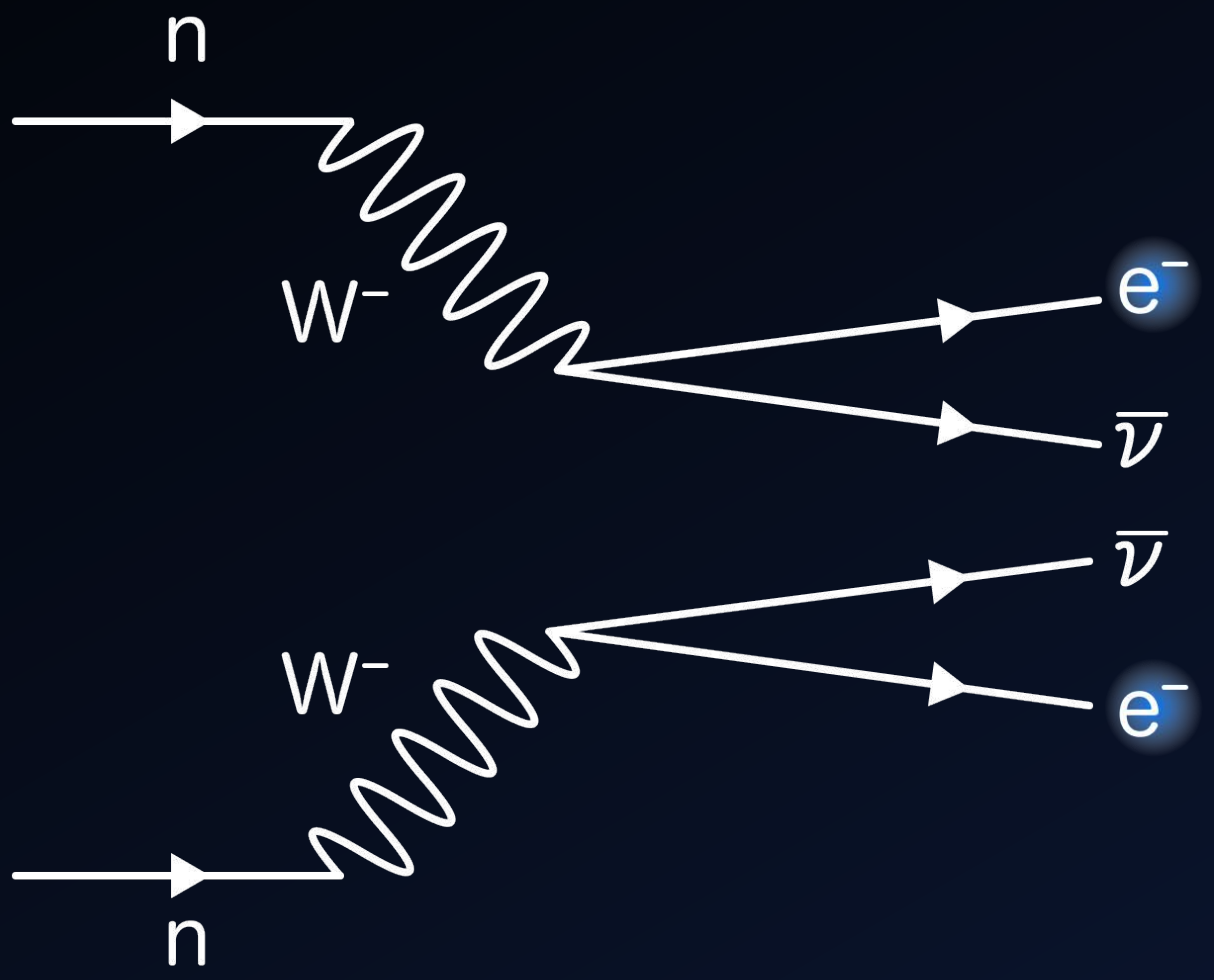

Yale

Double-beta decay

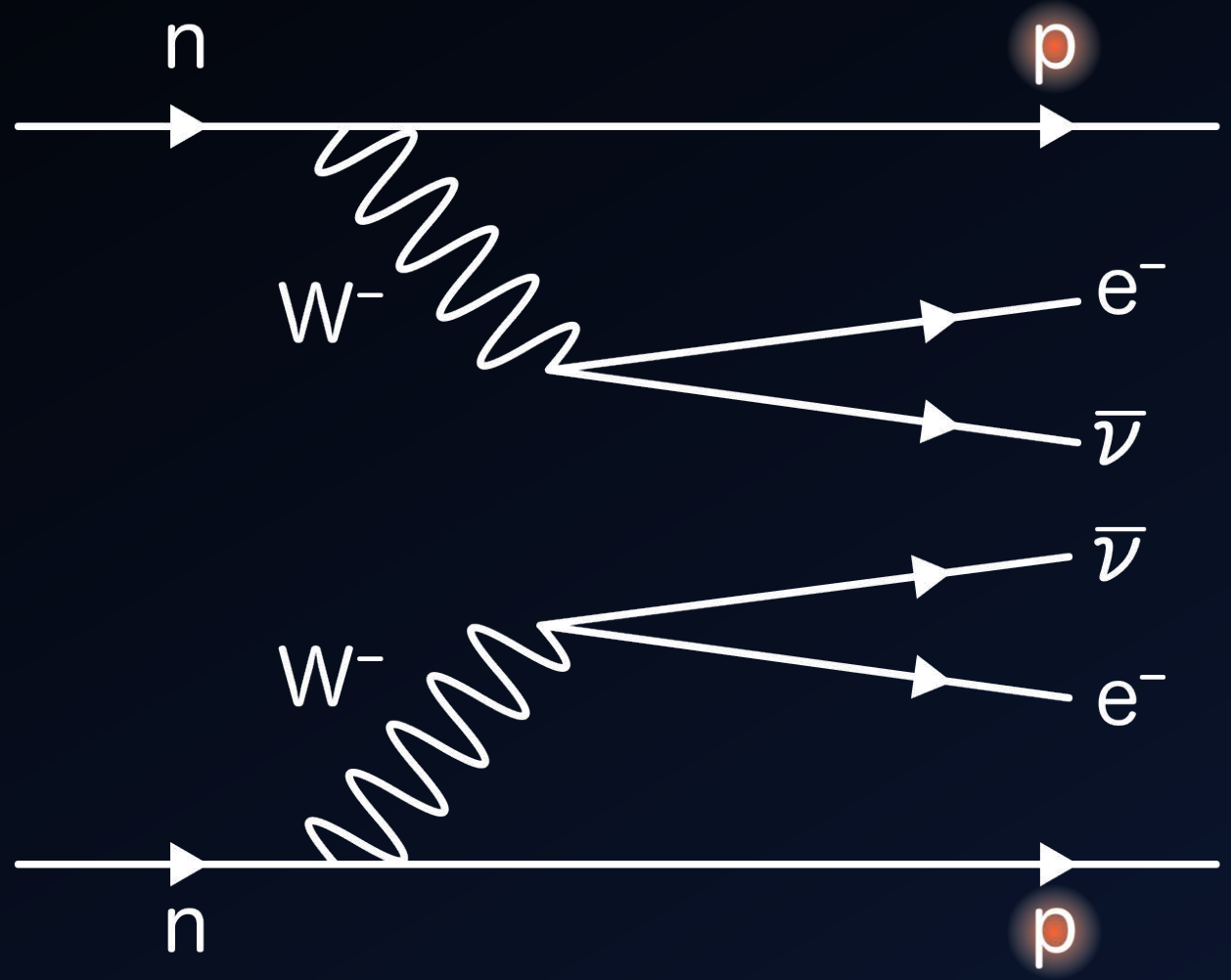

Yale

Double-beta decay

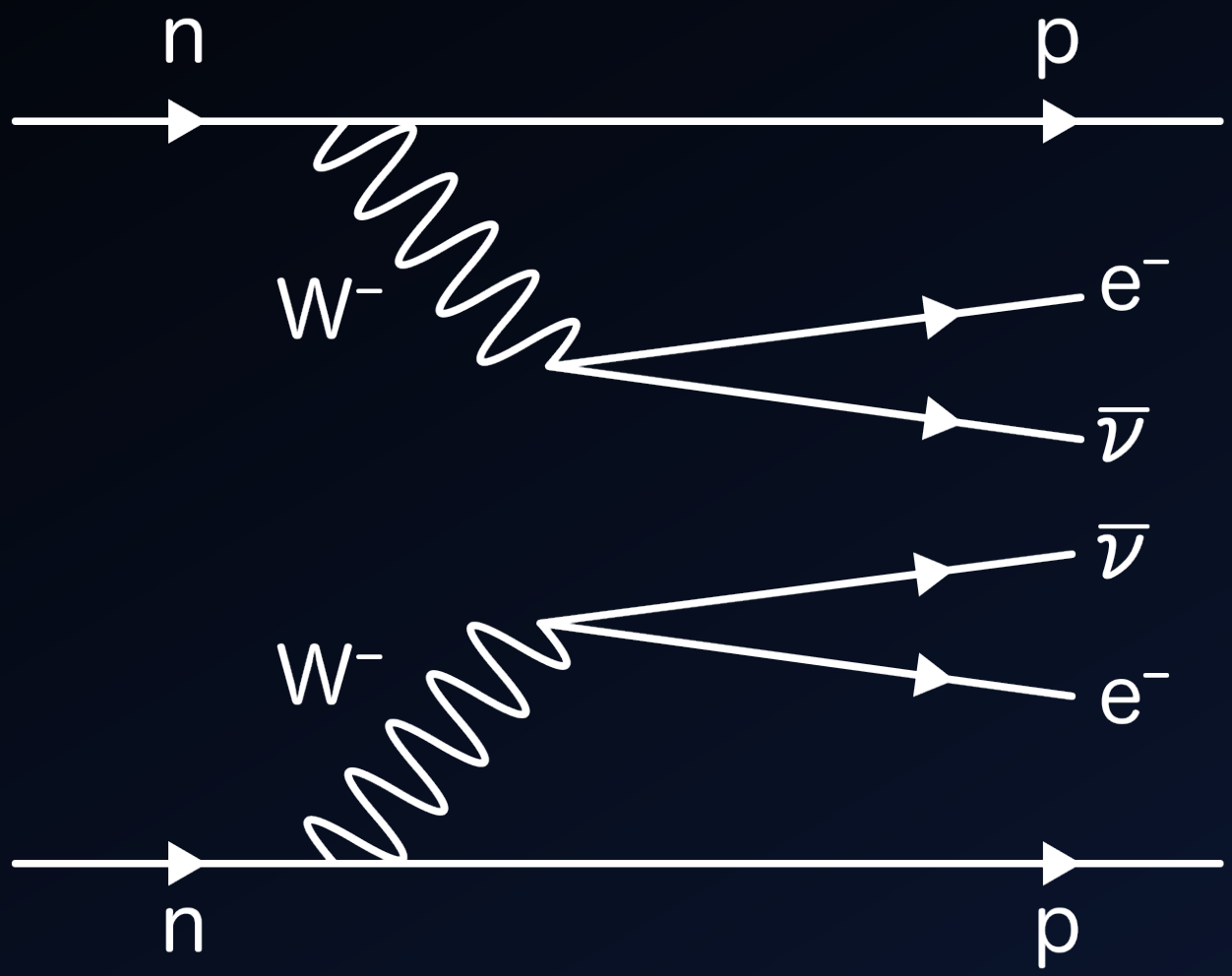

Yale

Double-beta decay

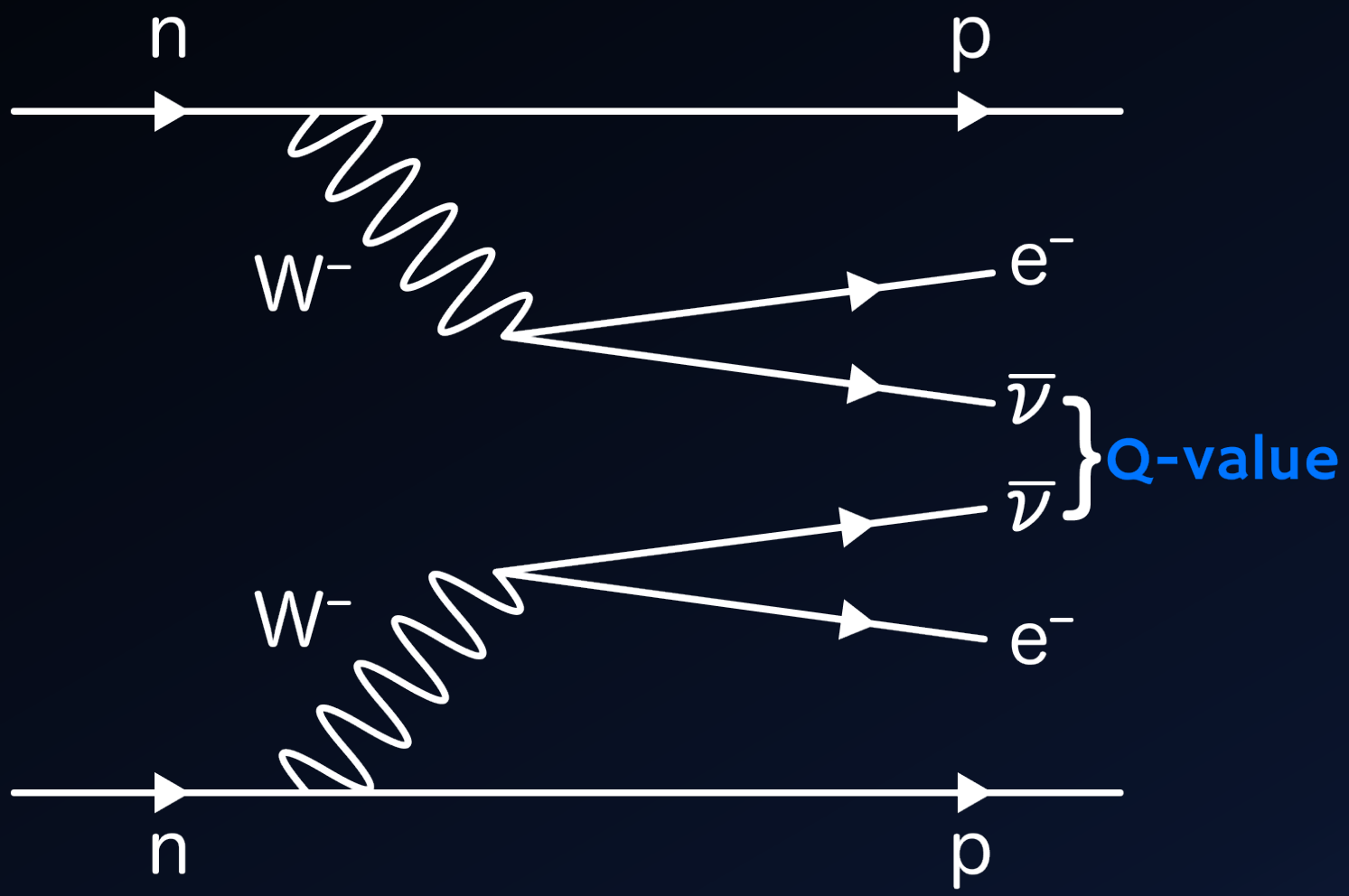

Yale

Double-beta decay

$$^{A}_{Z}X \rightarrow {}^{A}_{Z+2}X + 2e^{-} + 2\bar{\nu}_e$$

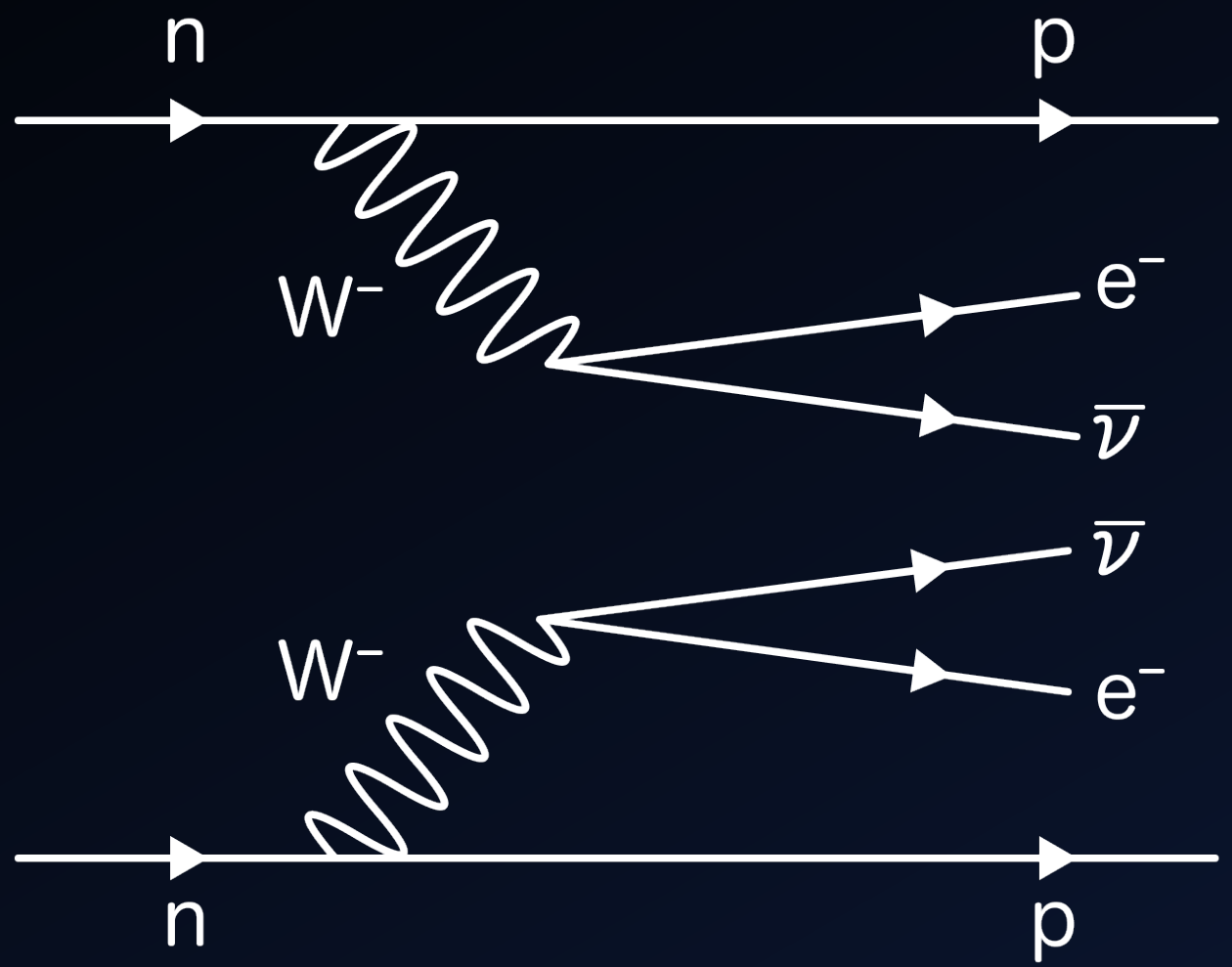

Yale

Double-beta decay

Yale

Double-beta decay

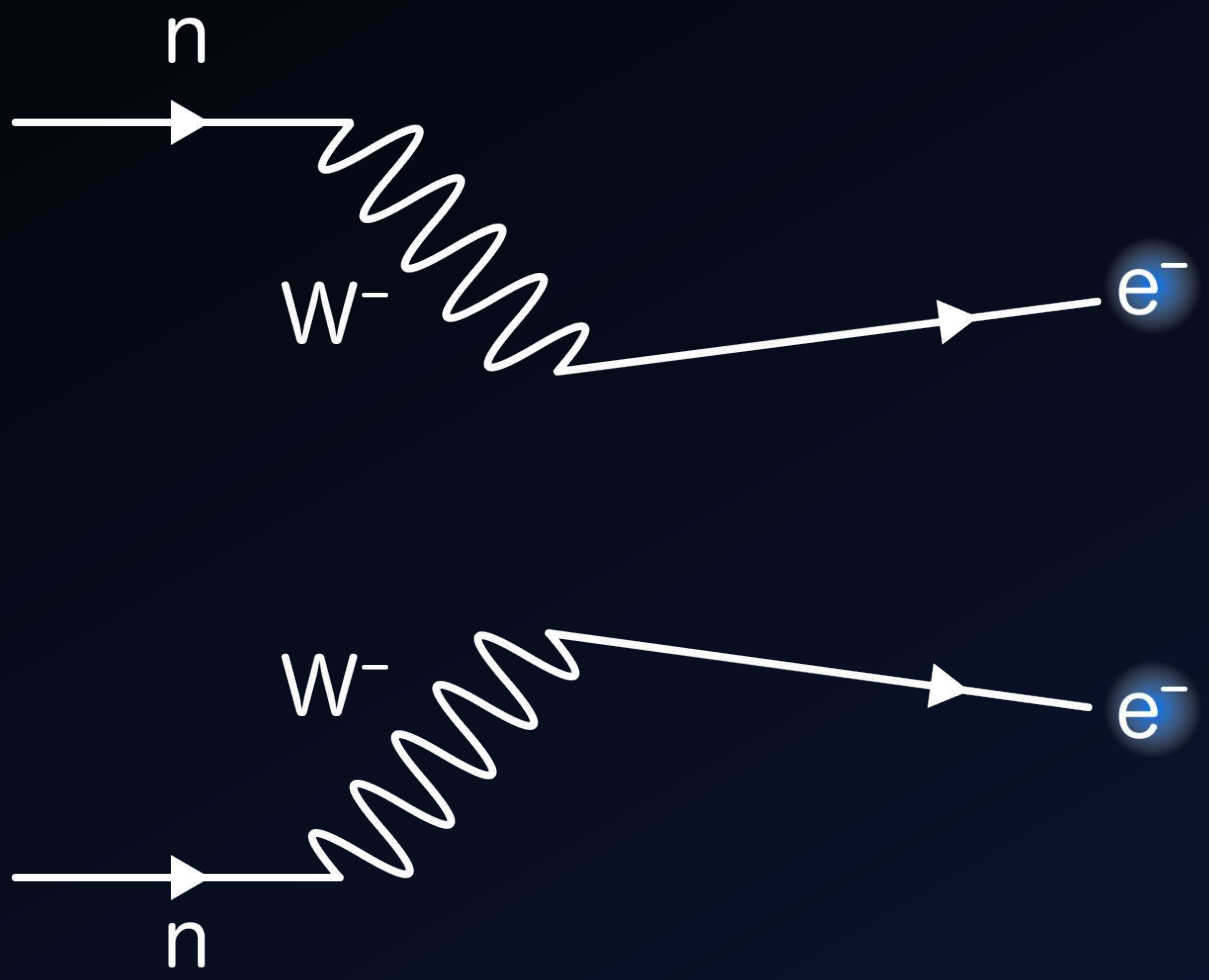

Yale

Double-beta decay

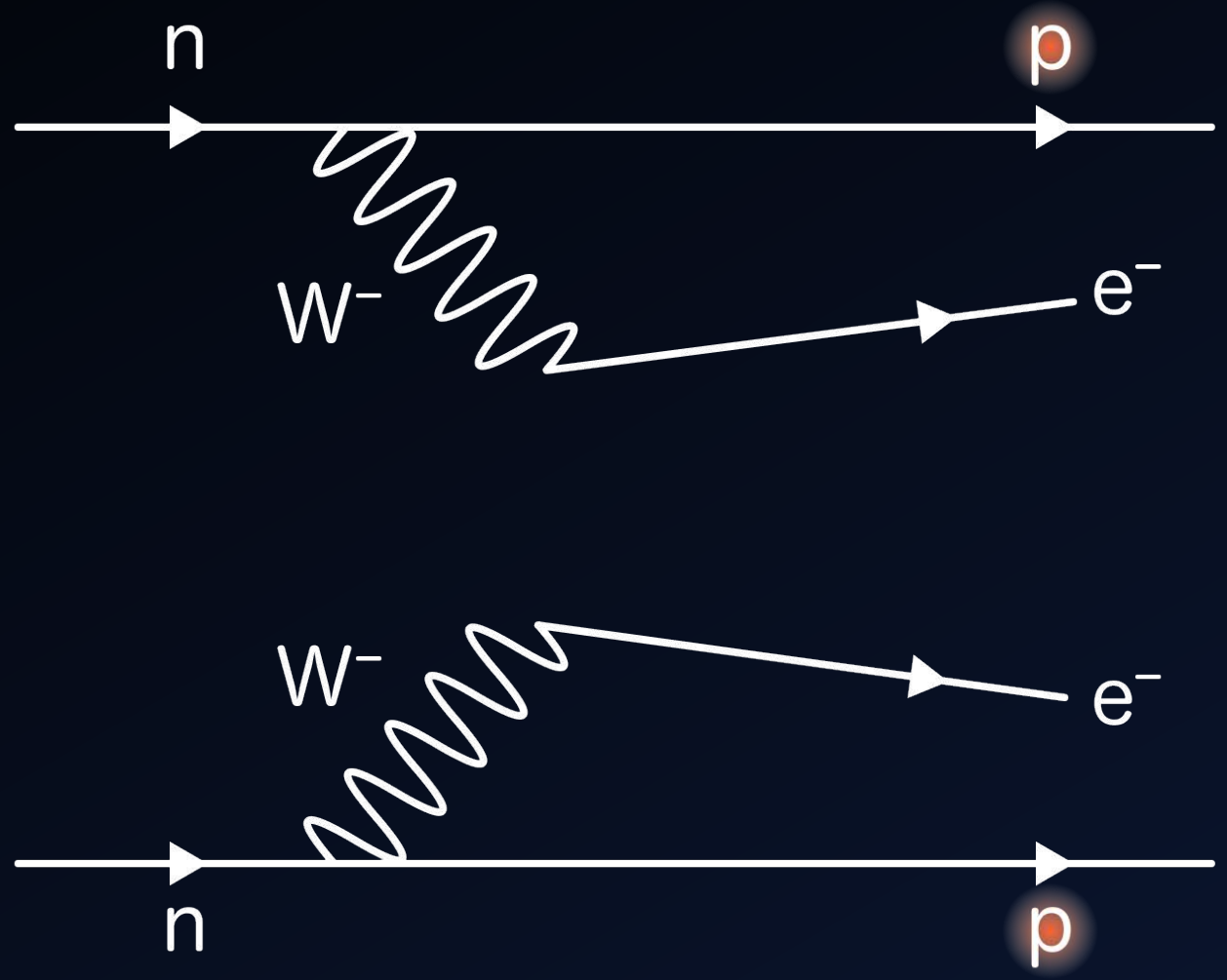

Yale

Neutrinoless double-beta decay

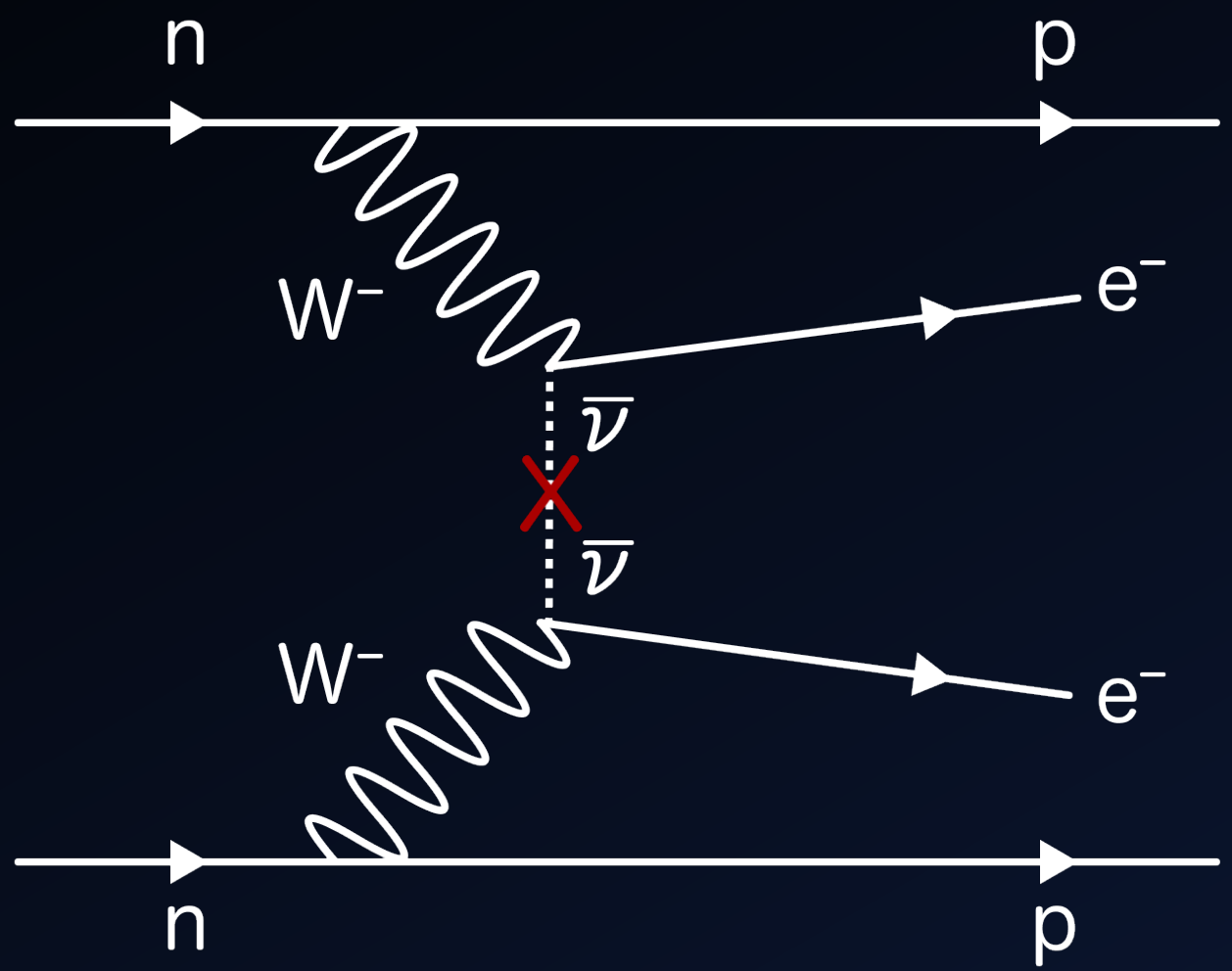

Yale

Neutrinoless double-beta decay

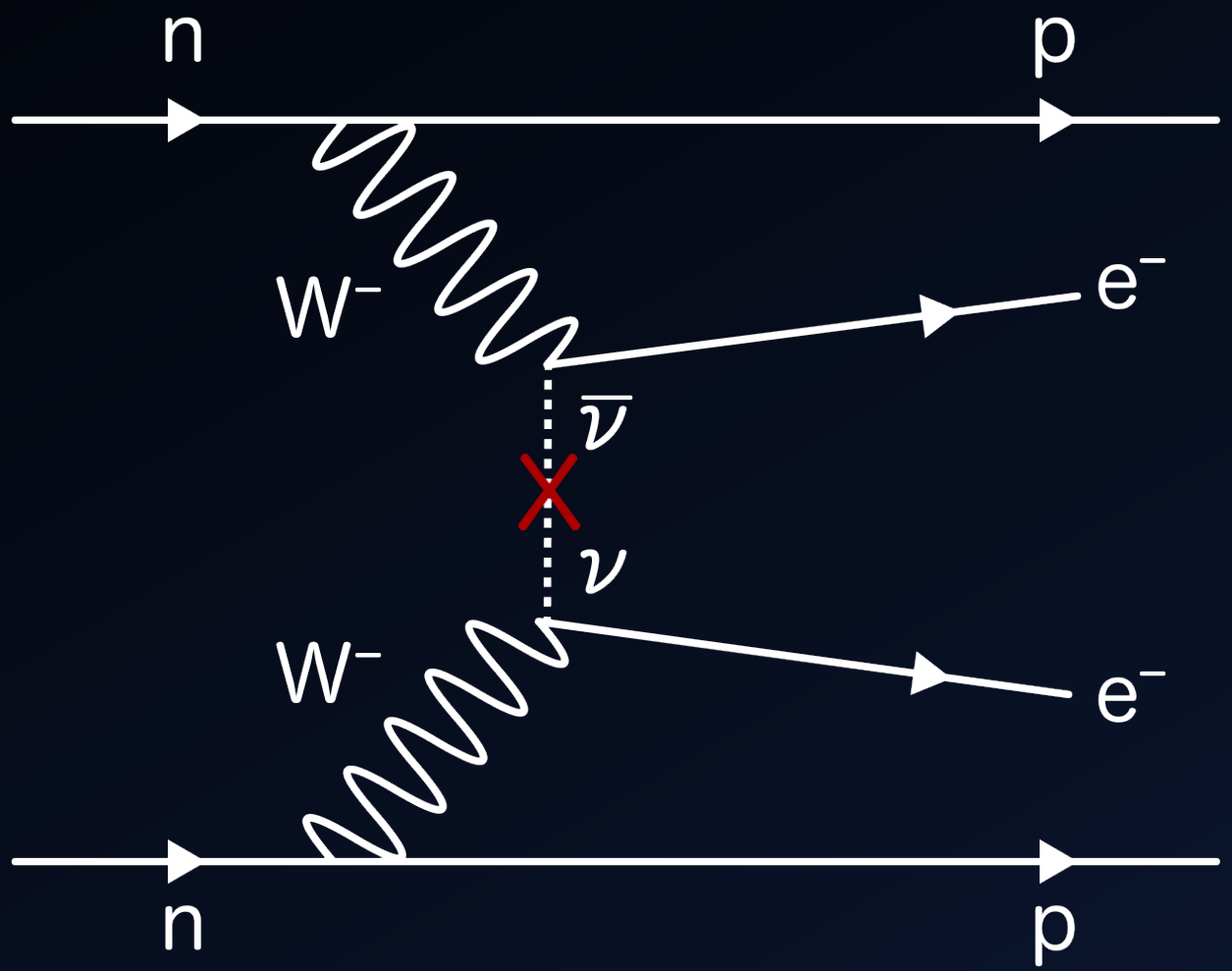

Yale

Neutrinoless double-beta decay

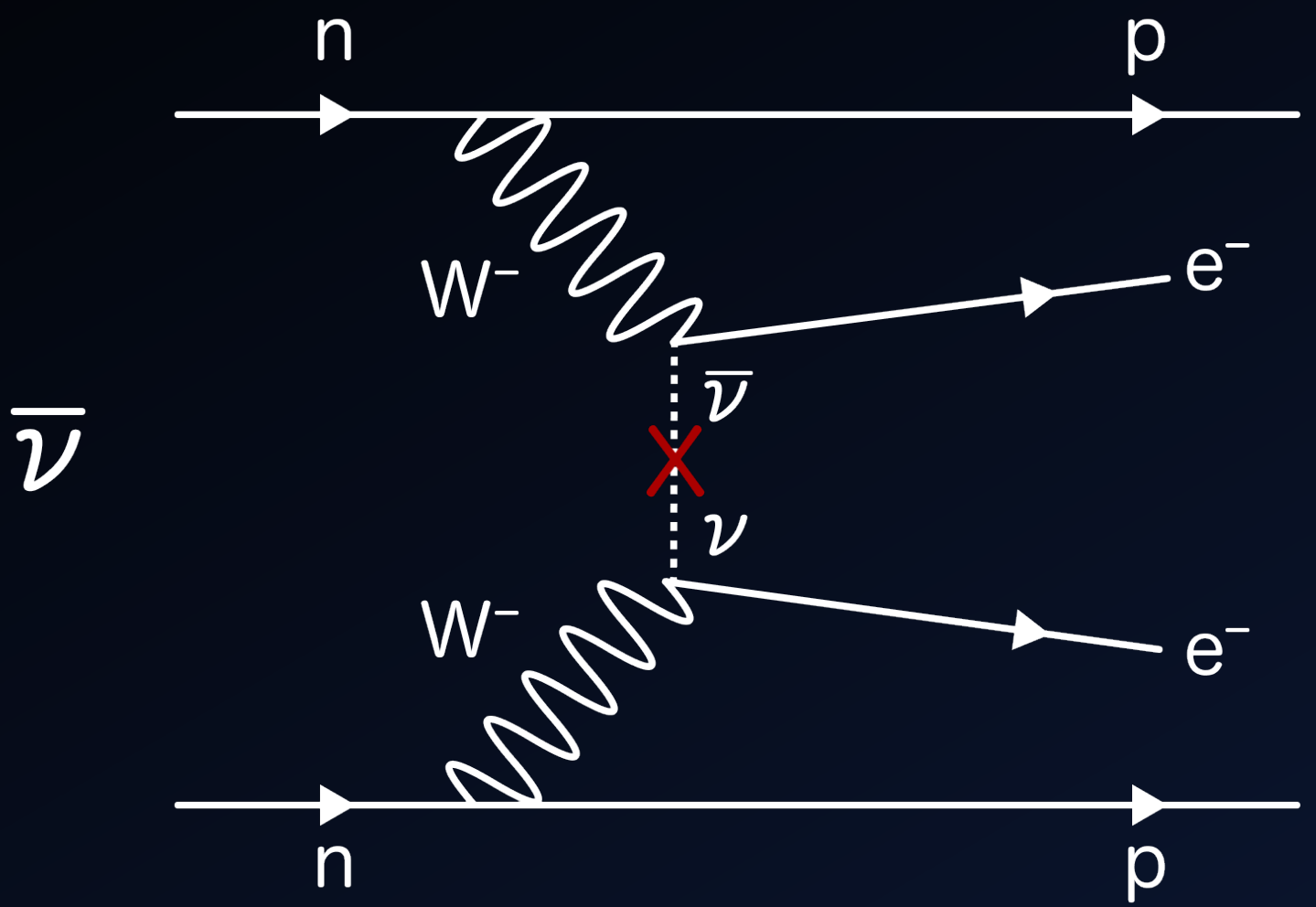

Yale

Neutrinoless double-beta decay

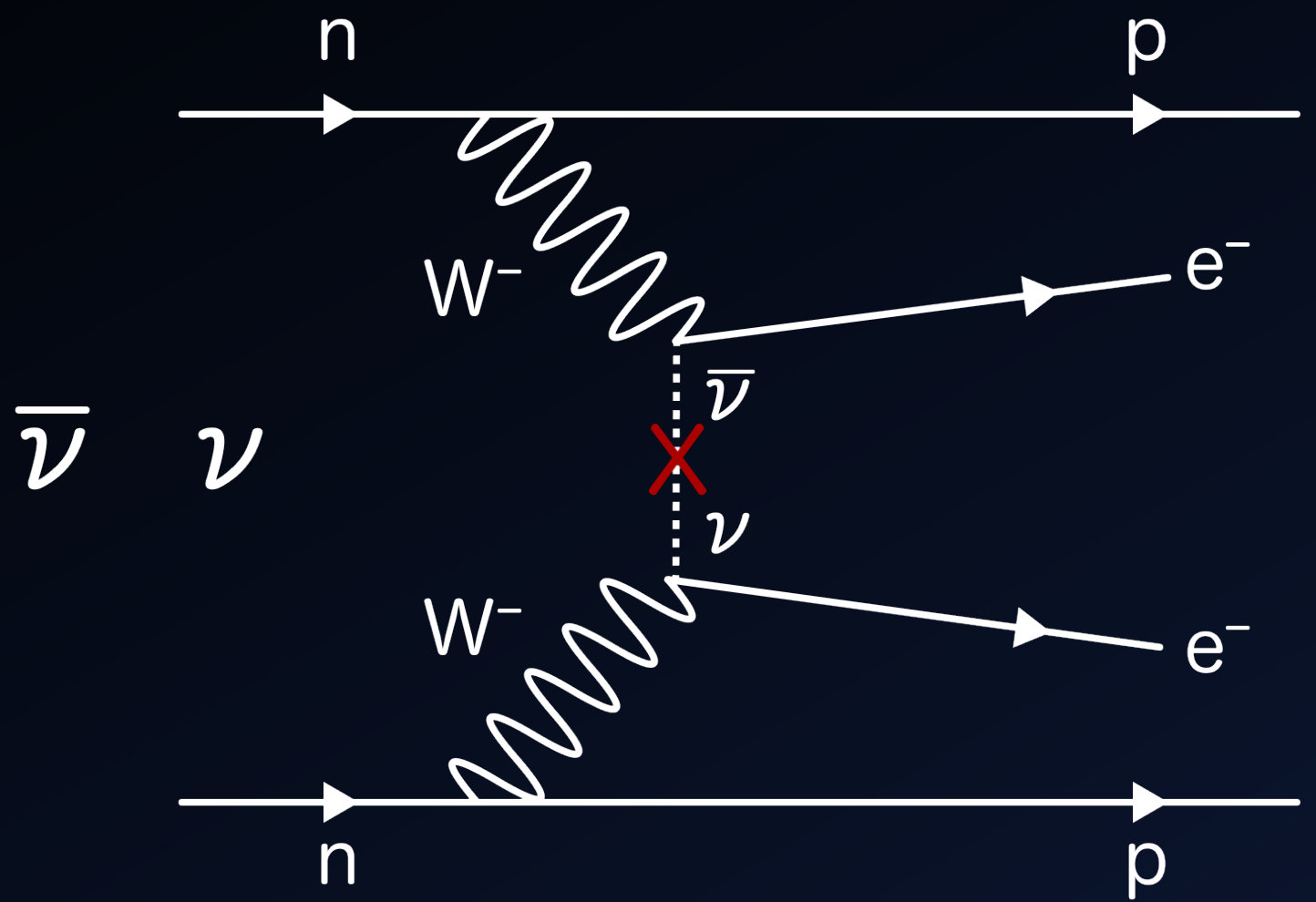

Yale

Neutrinoless double-beta decay

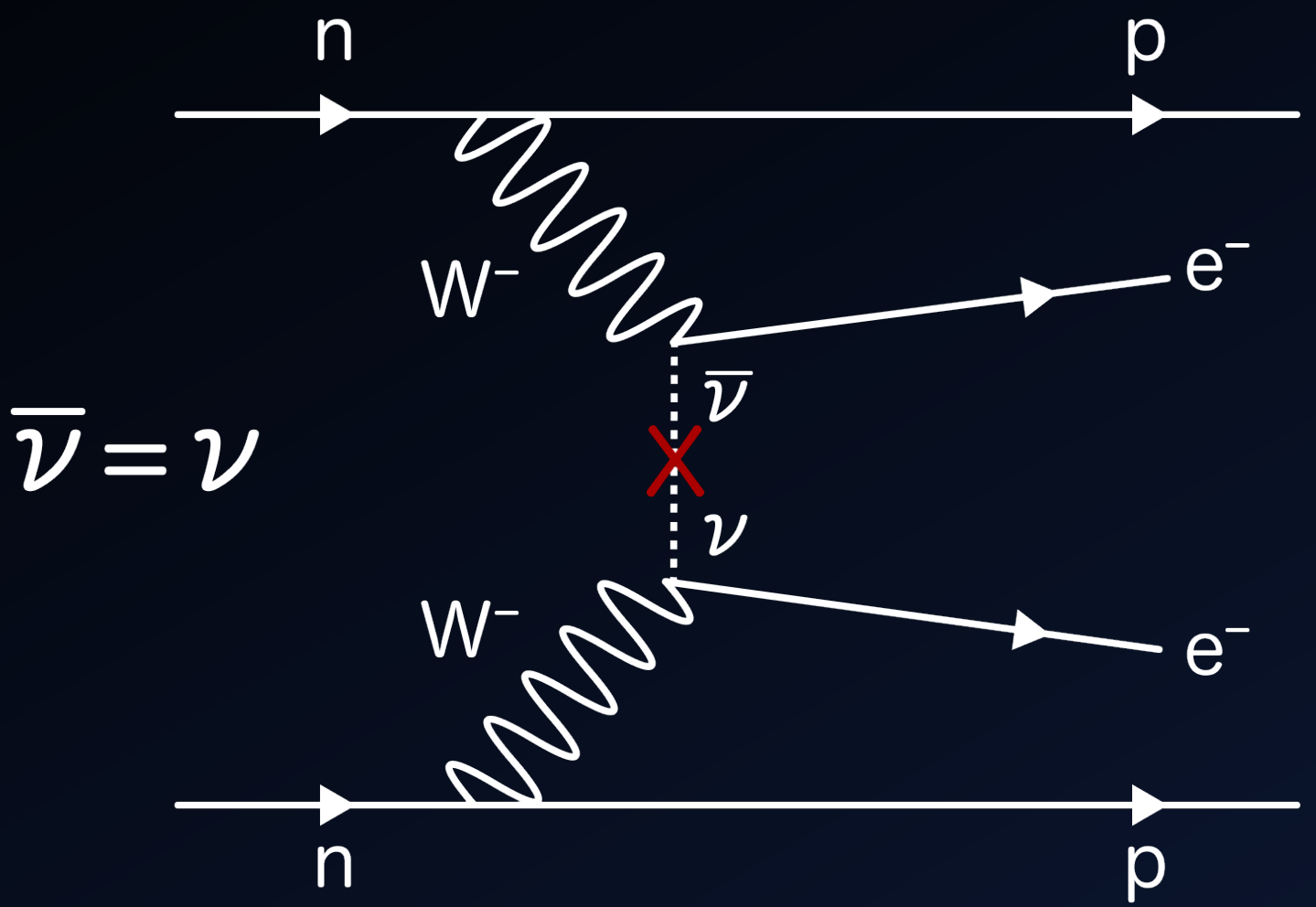

Yale

Neutrinoless double-beta decay

$$\overline{\nu} = \nu$$

Majorana Particles

Yale

Neutrinoless double-beta decay

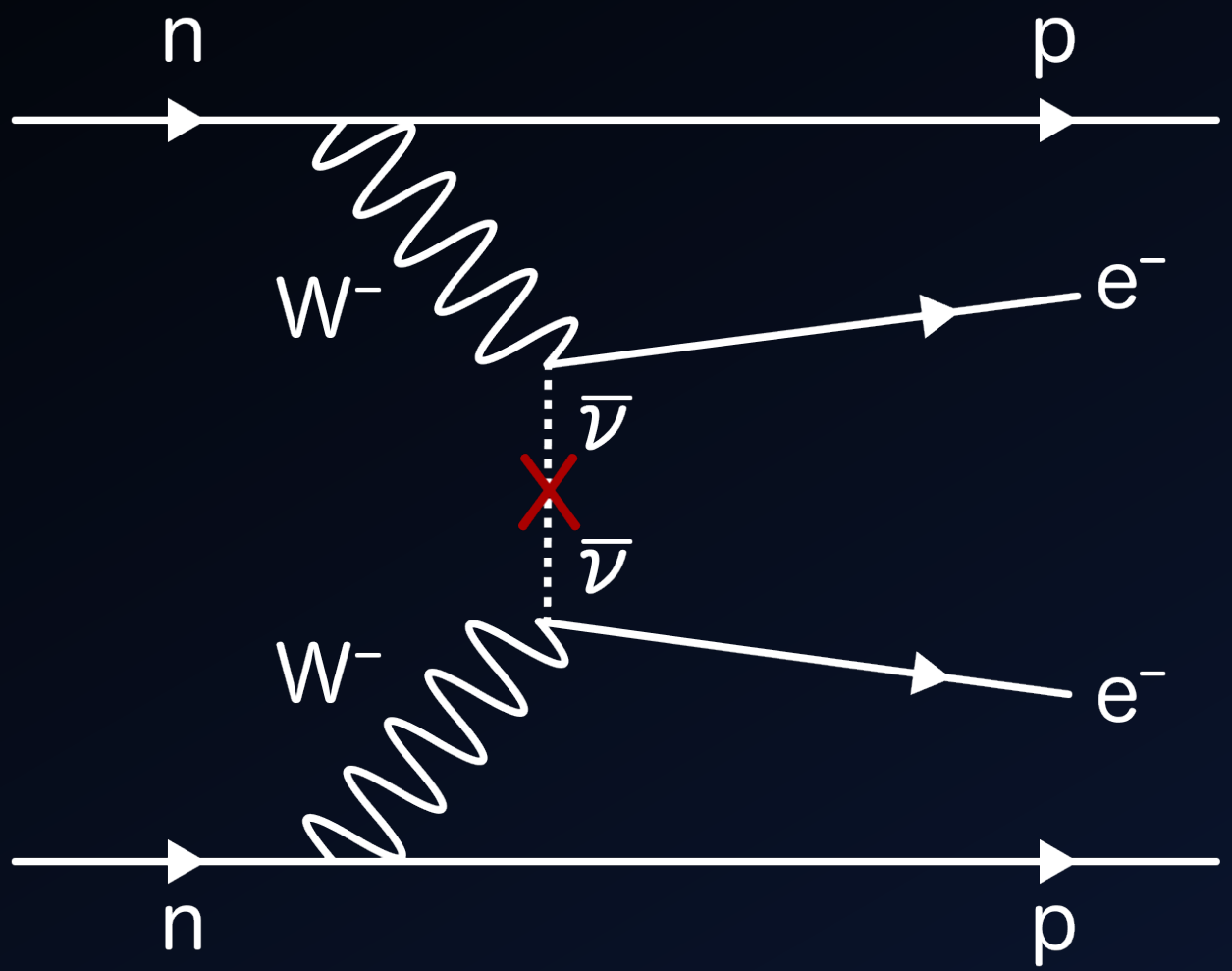

Yale

Neutrinoless double-beta decay

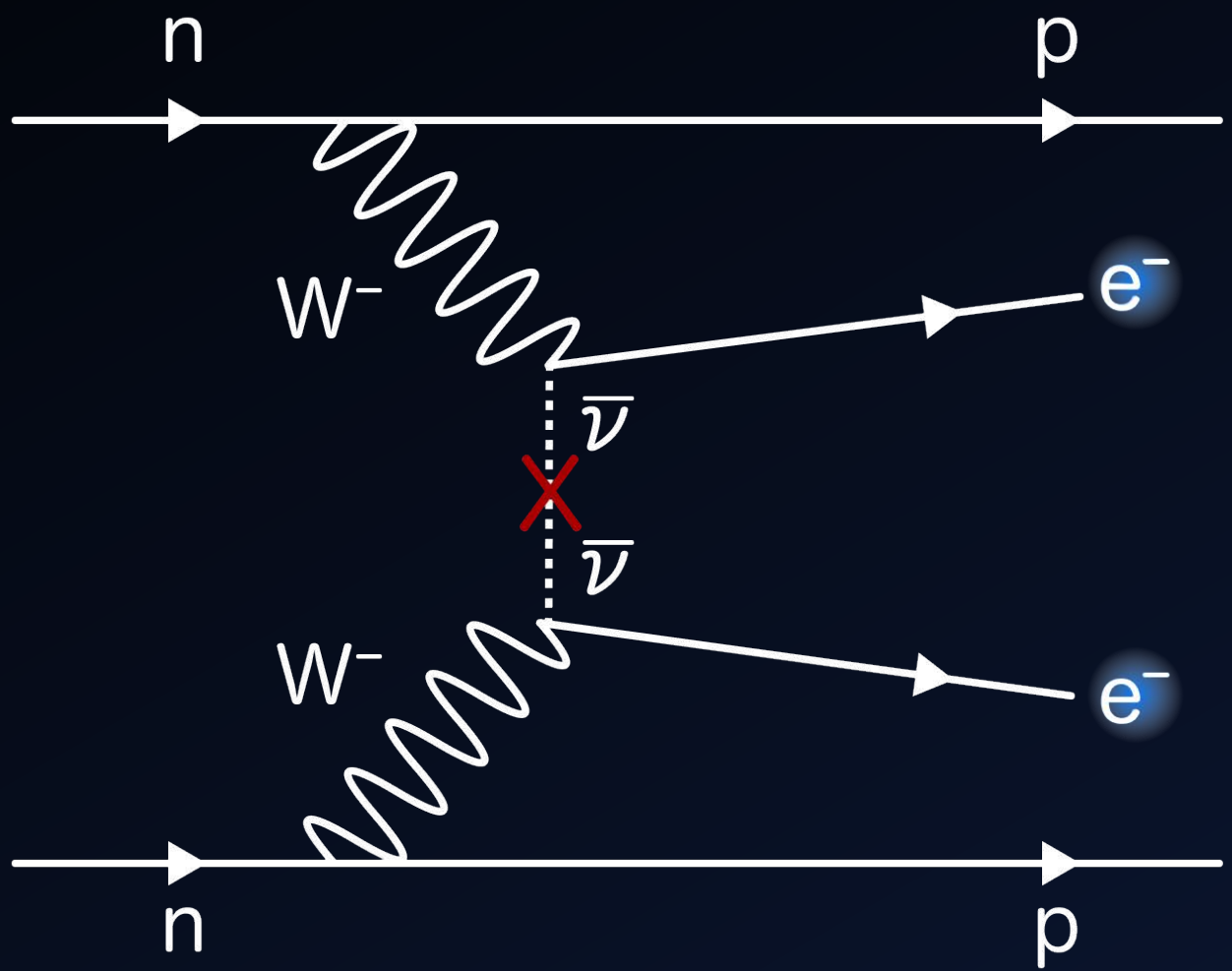

Yale

Neutrinoless double-beta decay

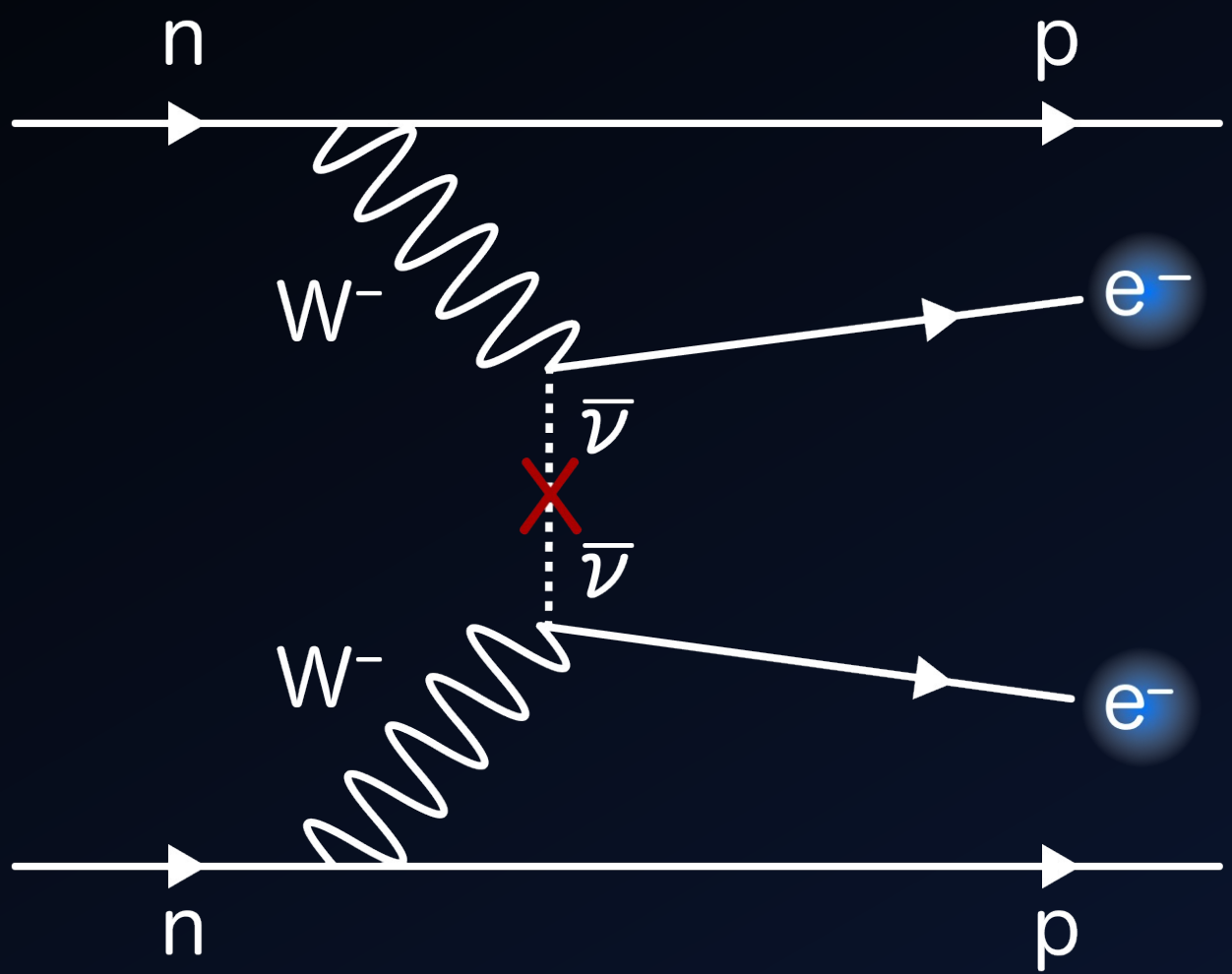

Yale

Detection of $0\nu\beta\beta$

Yale

nEXO

- next Enriched Xenon Observatory
  - Multi-tonne (5000kg LXe)
  - Low-background
- 90% Xe^{136} enriched liquid xenon
- Time Projection Chamber (TPC)
- SiPMs
- Anode consisting of charge collection tiles

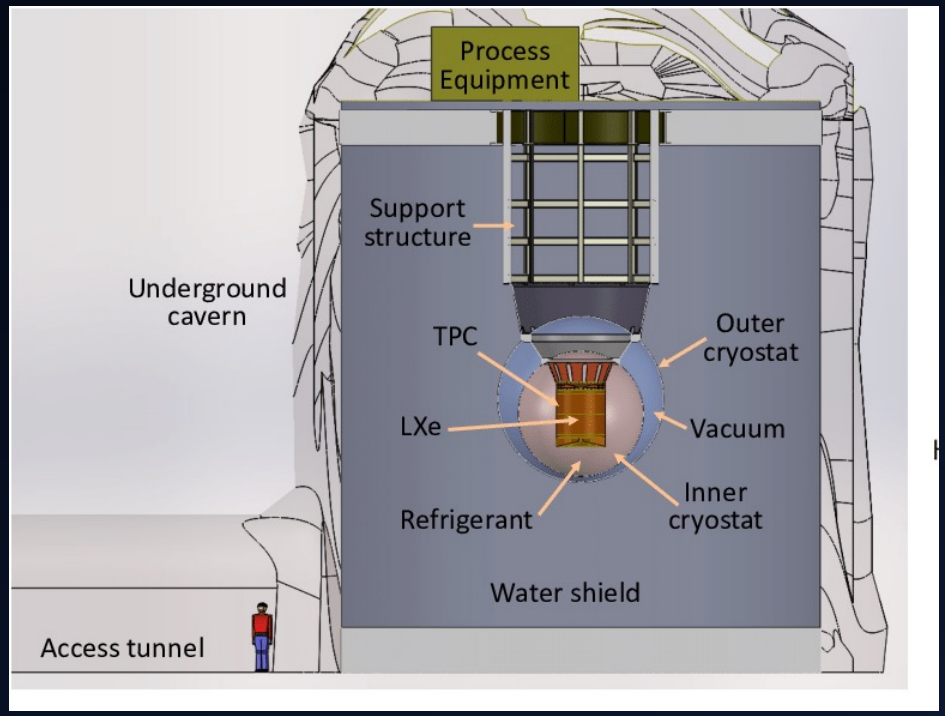

Yale

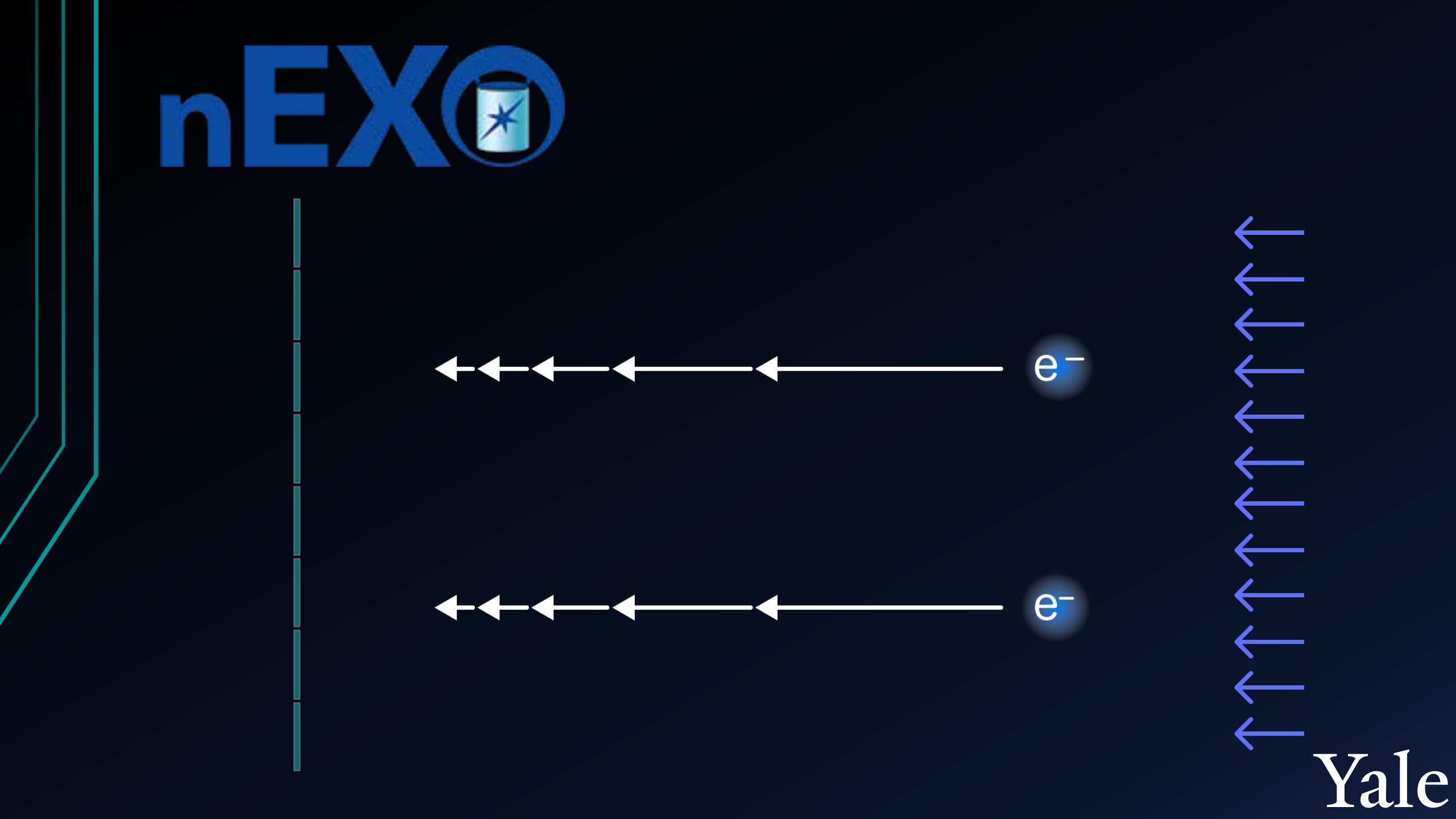
nEXO
e⁻
e⁻
Yale


nEXO
e⁻
e⁻
Yale

nEXO

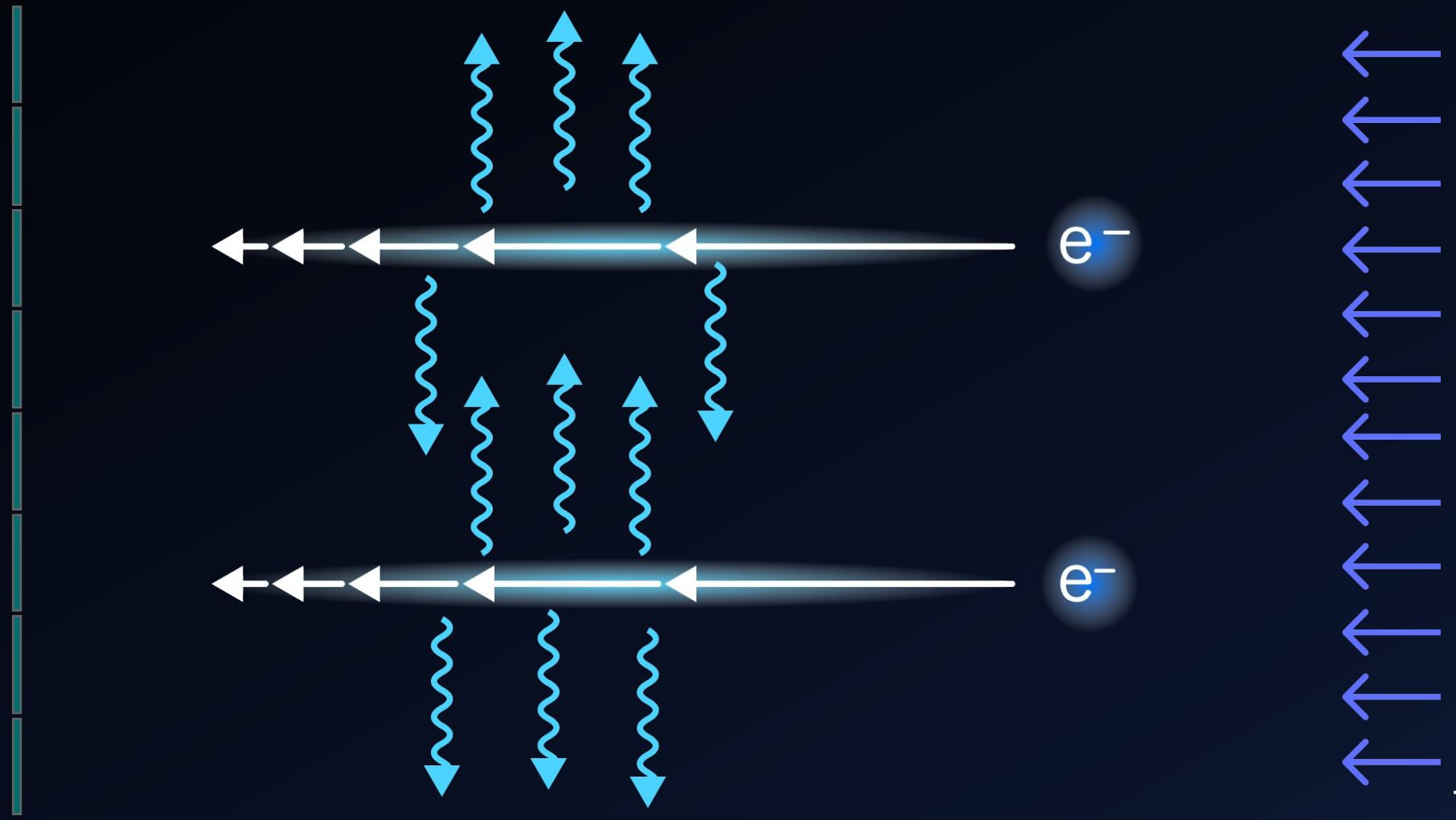

Yale

nEXO

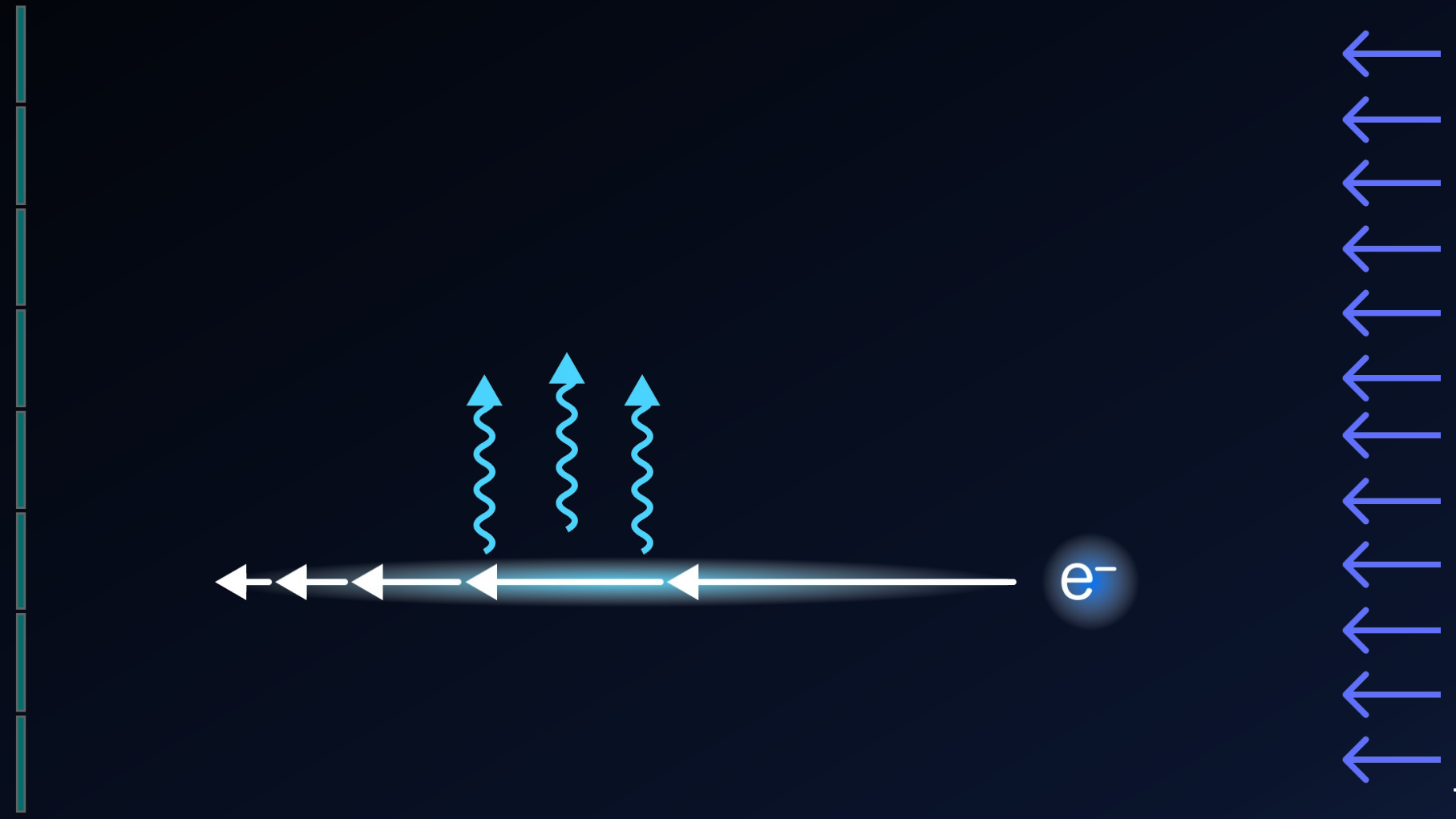

Yale

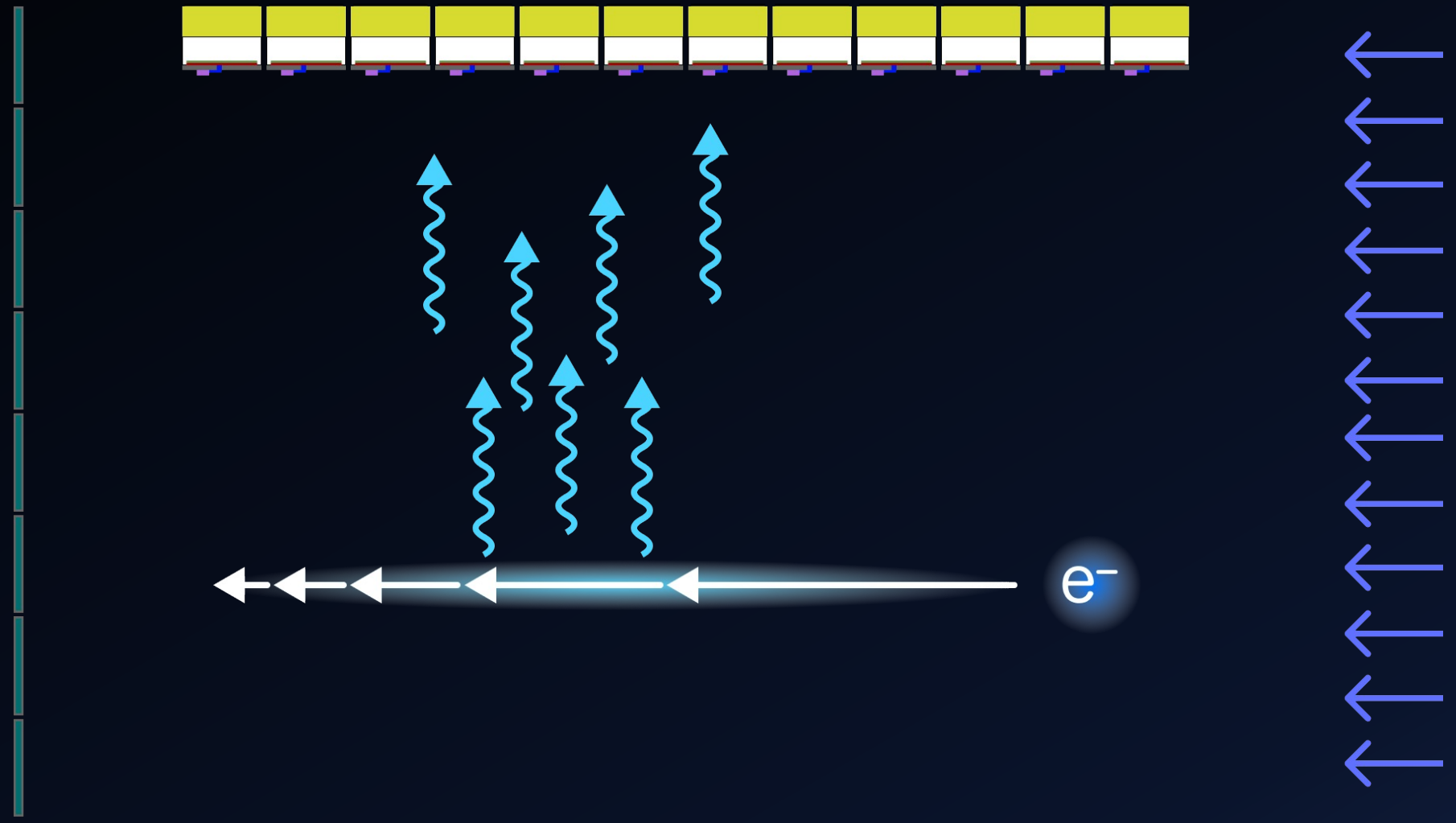

Yale

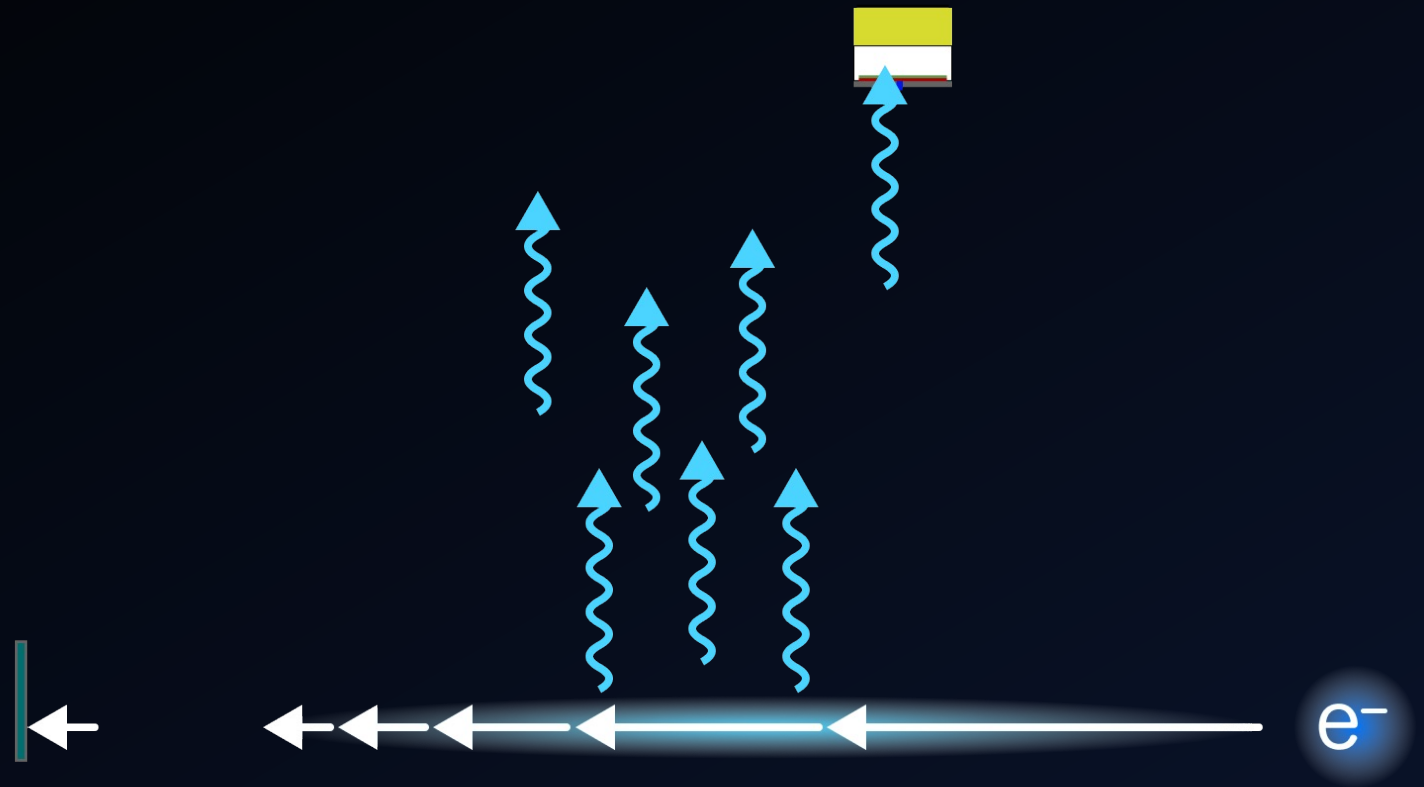

TIME PROJECTION CHAMBER (TPC)

Yale

Moore Lab at Yale

nEXO R&D

Yale

Moore Lab’s role in nEXO’s R&D

- Characterization of the SiPMs that will be used in nEXO
- Comparison of SiPMs manufactured by FBK and Hamamatsu
- Calibration of the SiPMs using radioactive-sources

Yale

Moore Lab's role in nEXO's R&D – what we look for

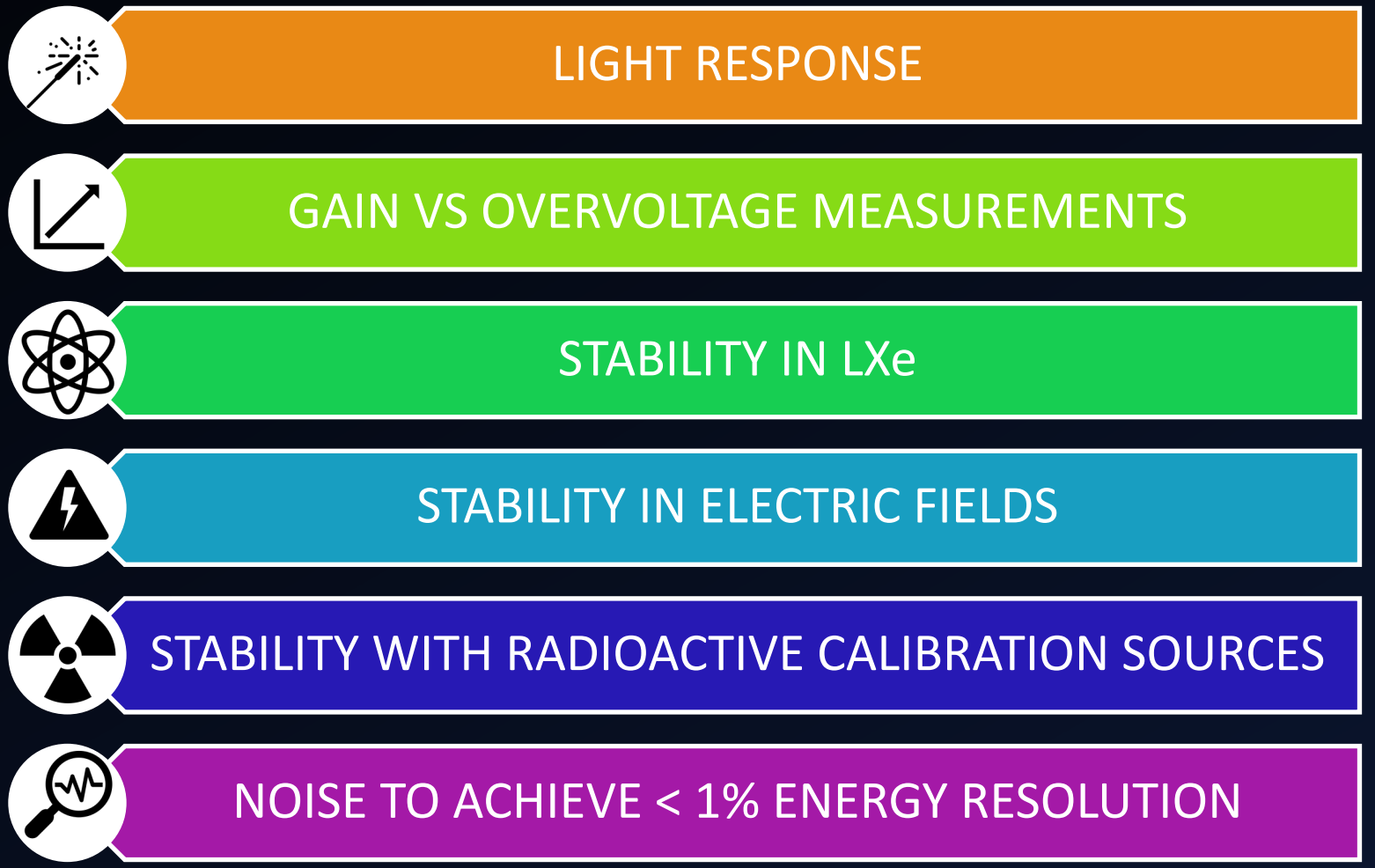

Yale

My role as a member of the team

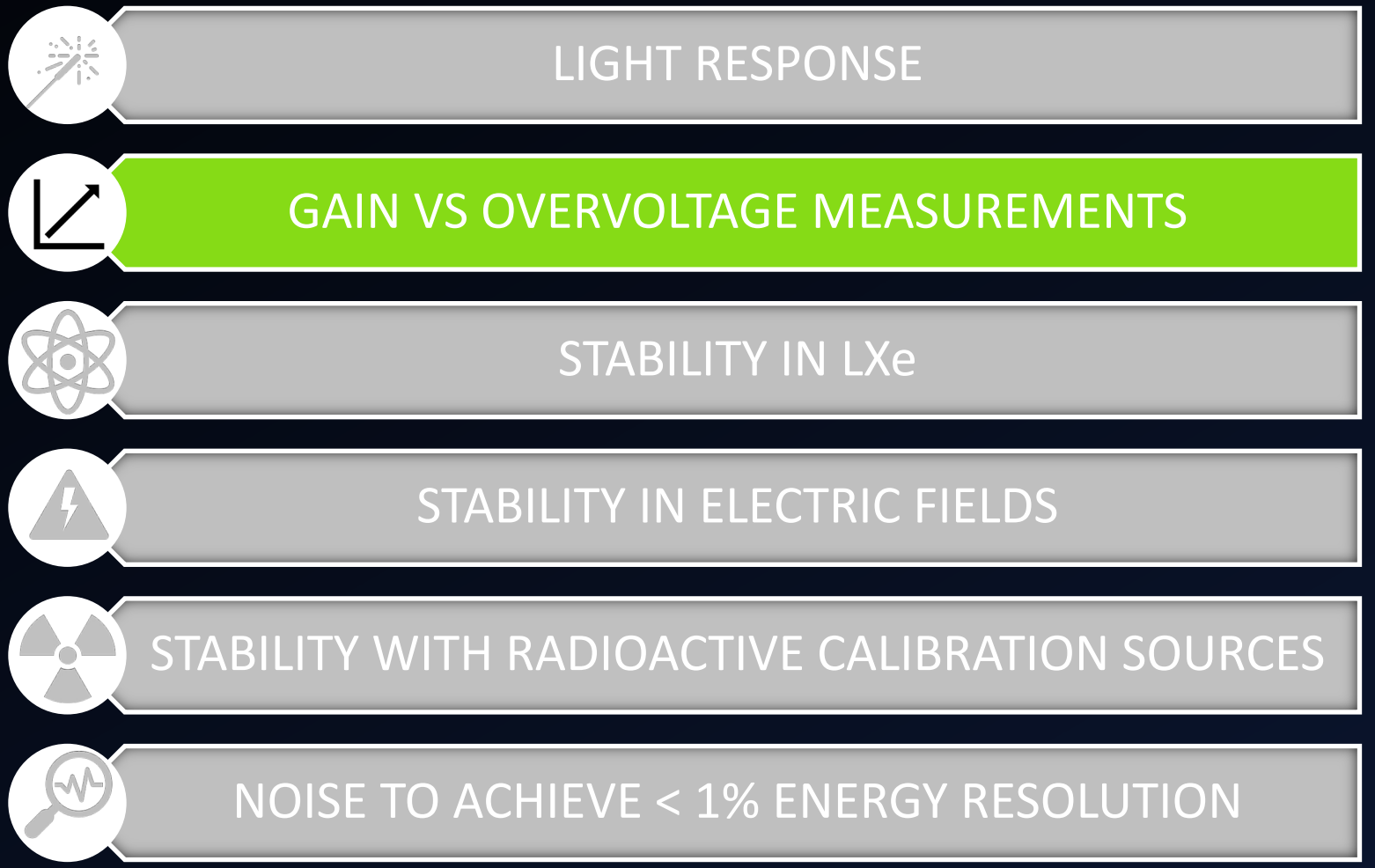

Yale

Moore Lab's setup for SiPM testing

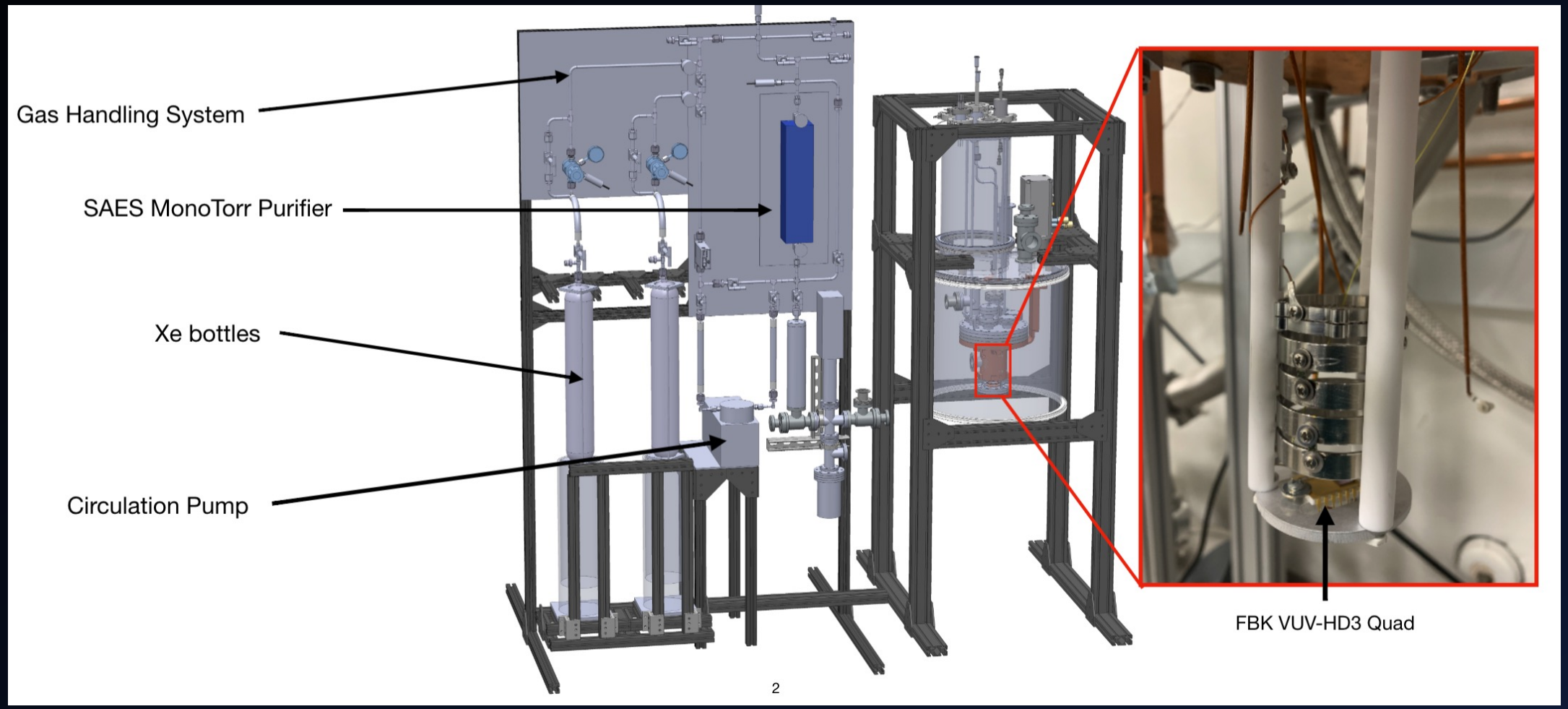

Yale

Moore Lab's setup for SiPM testing

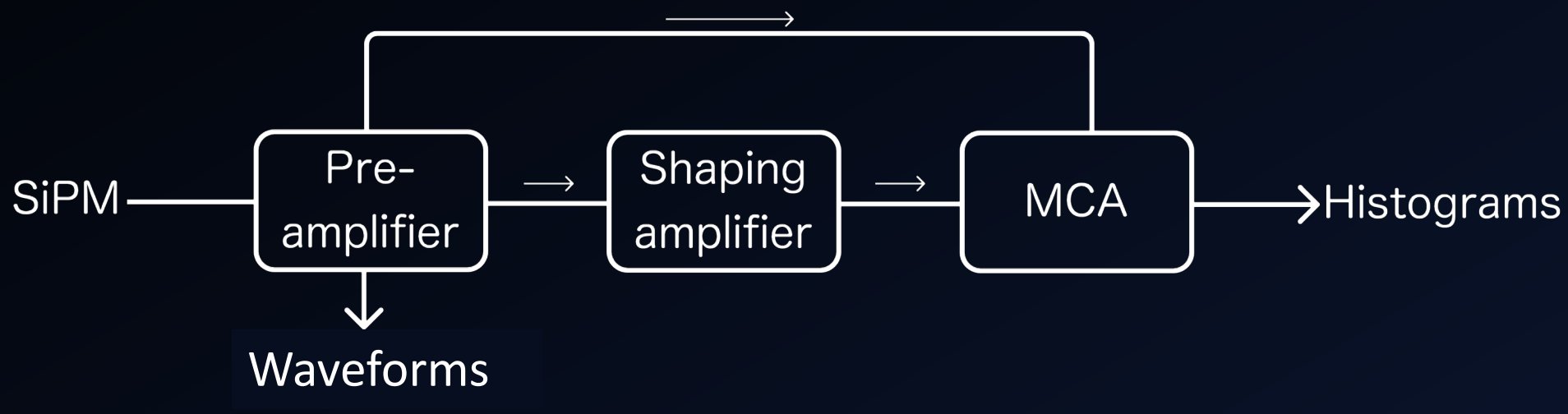

Yale

Multi-channel analyzer – data acquisition

Yale

Multi-channel analyzer

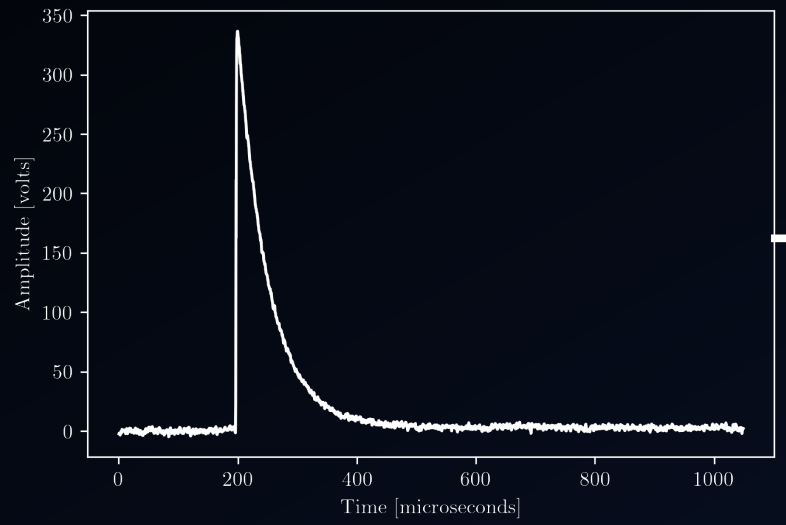

MCA

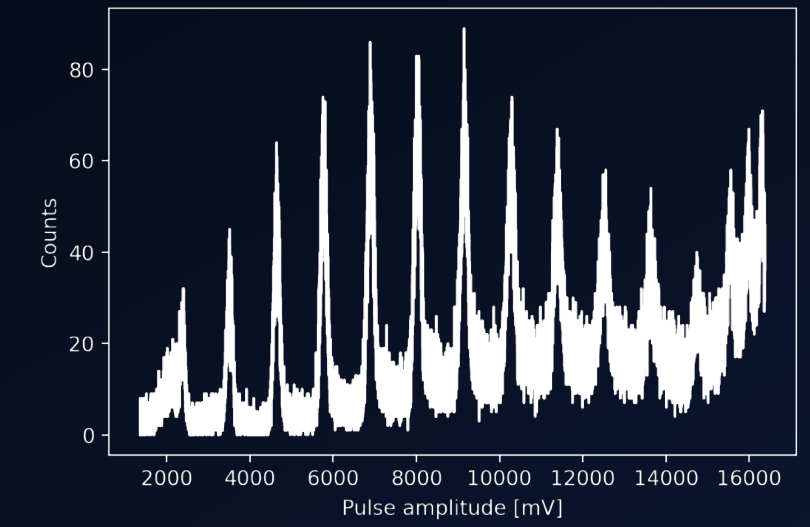

Yale

Multi-channel analyzer – data analysis

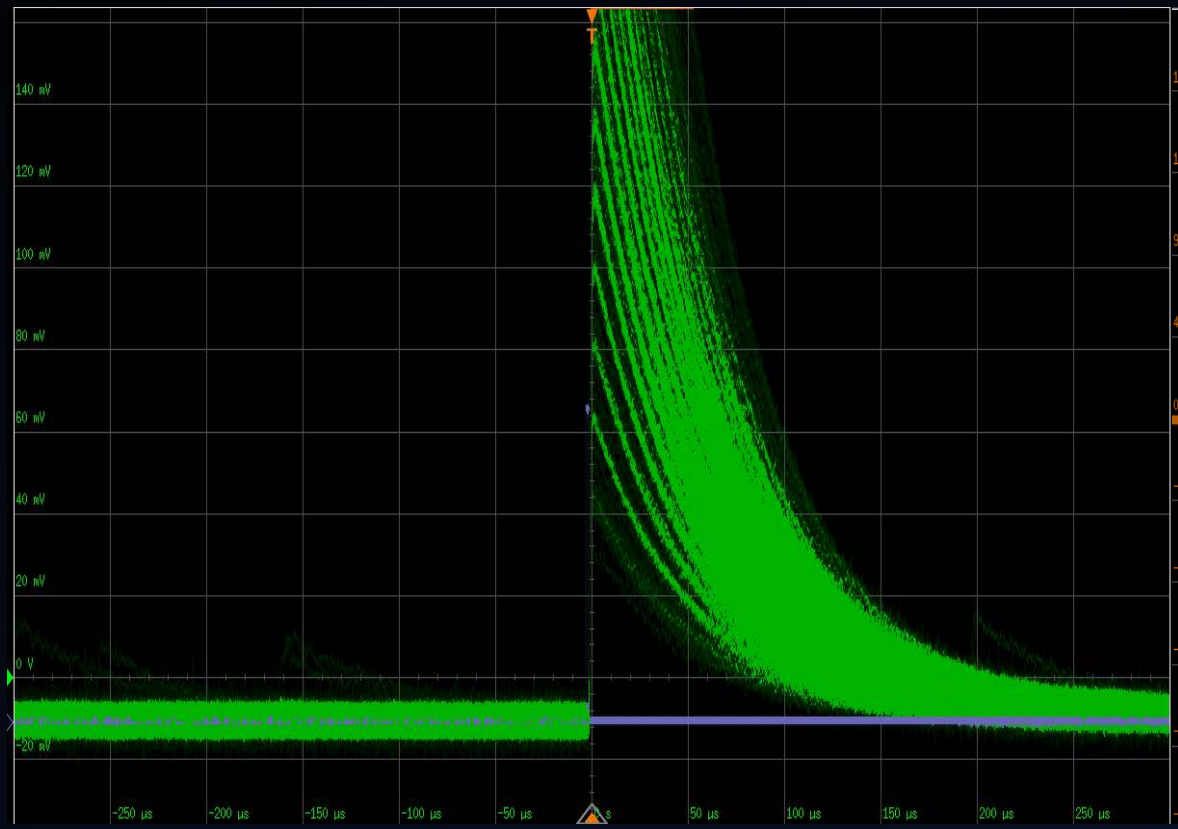

Pre-amplifier signal

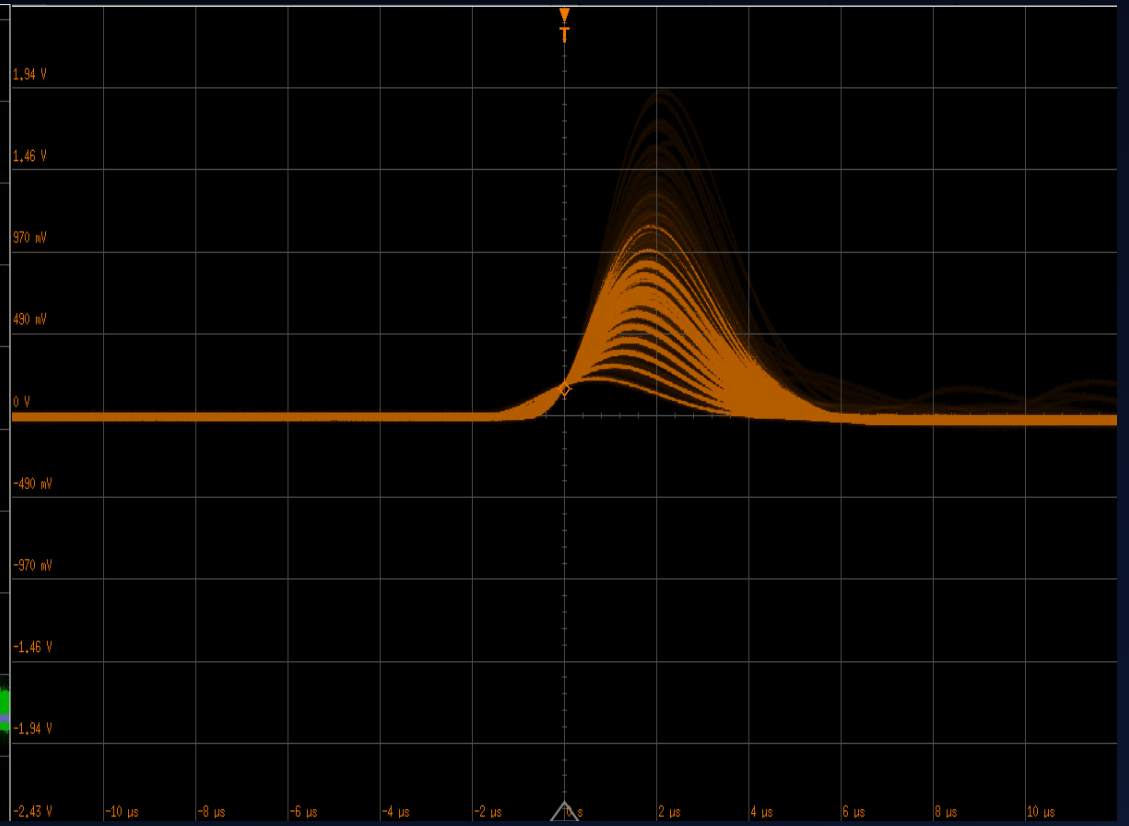

Shaping amplifier signal

Yale

Multi-channel analyzer – data analysis

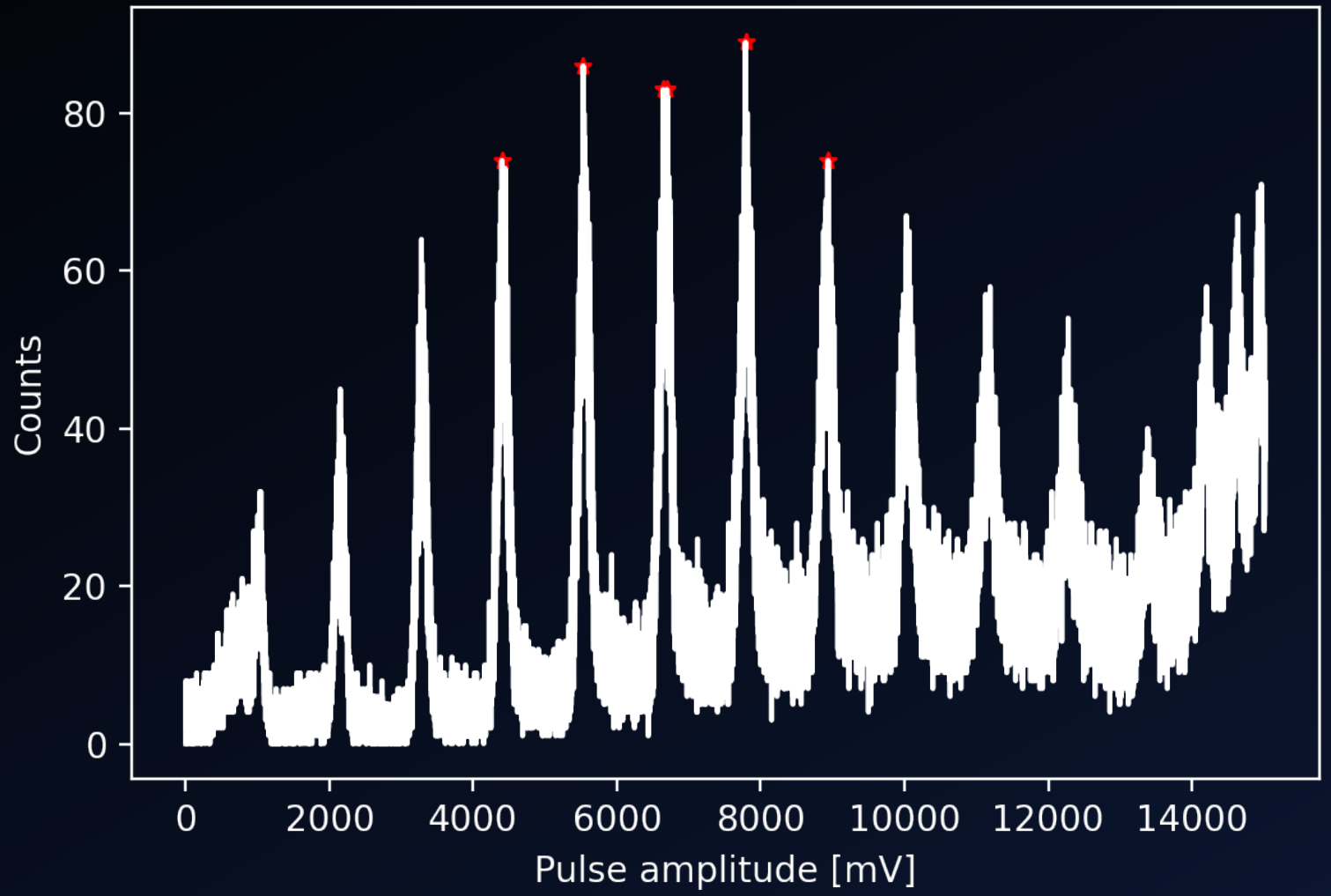

Yale

Multi-channel analyzer – data analysis

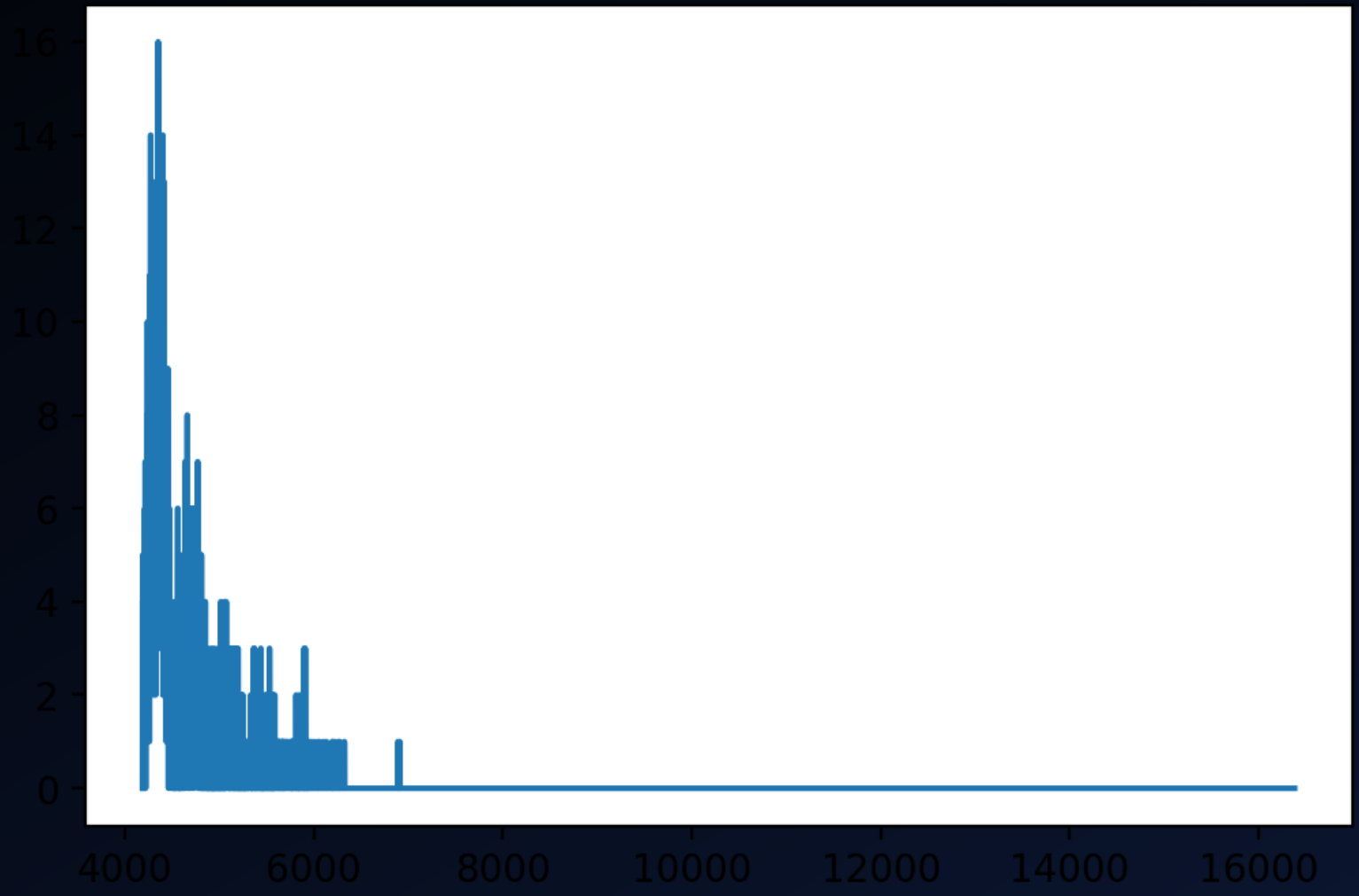

Yale

DIFFERENT DATA SETS NEED DIFFERENT FIT AND ADJUSTMENT PARAMETERS TO BE ANALYZED

Can we fit each waveform and each histogram manually?

SmartGAT
Gain Analysis Tool

Yale

SmartGAT

- Automatic raw MCA data trimming (pedestal and flat trail removal)
- Smart peak fitting
  - Automatic peak edges detection with parameters adjustements
  - Automatic edges correction when find_peaks fails to detect edges
  - Recognition of good vs bad peak fits -> ignore bad gaussian fits
- Automatic peak number and sequence selection for best results
  - Selection of best subgroup of peaks to obtain cleanest gain measurement
- Backup of data for faster further analysis

Yale

SmartGAT

- ***Multiprocessing*** (including on Grace High Power Computer)
  - Loading times greatly reduced by increasing number of cores
- Multithreading within multiprocessing

Yale

SmartGAT

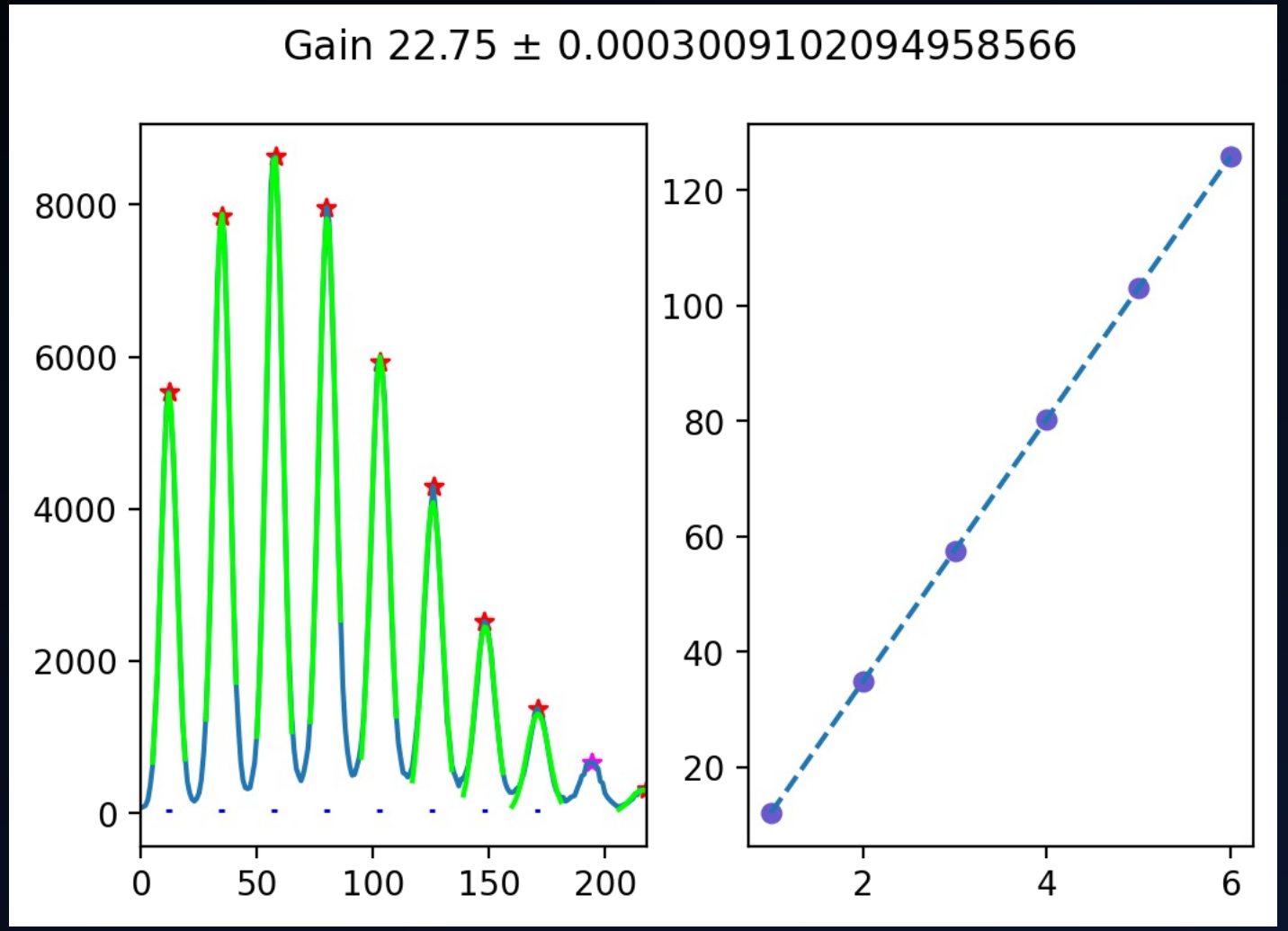

Yale

SmartGAT

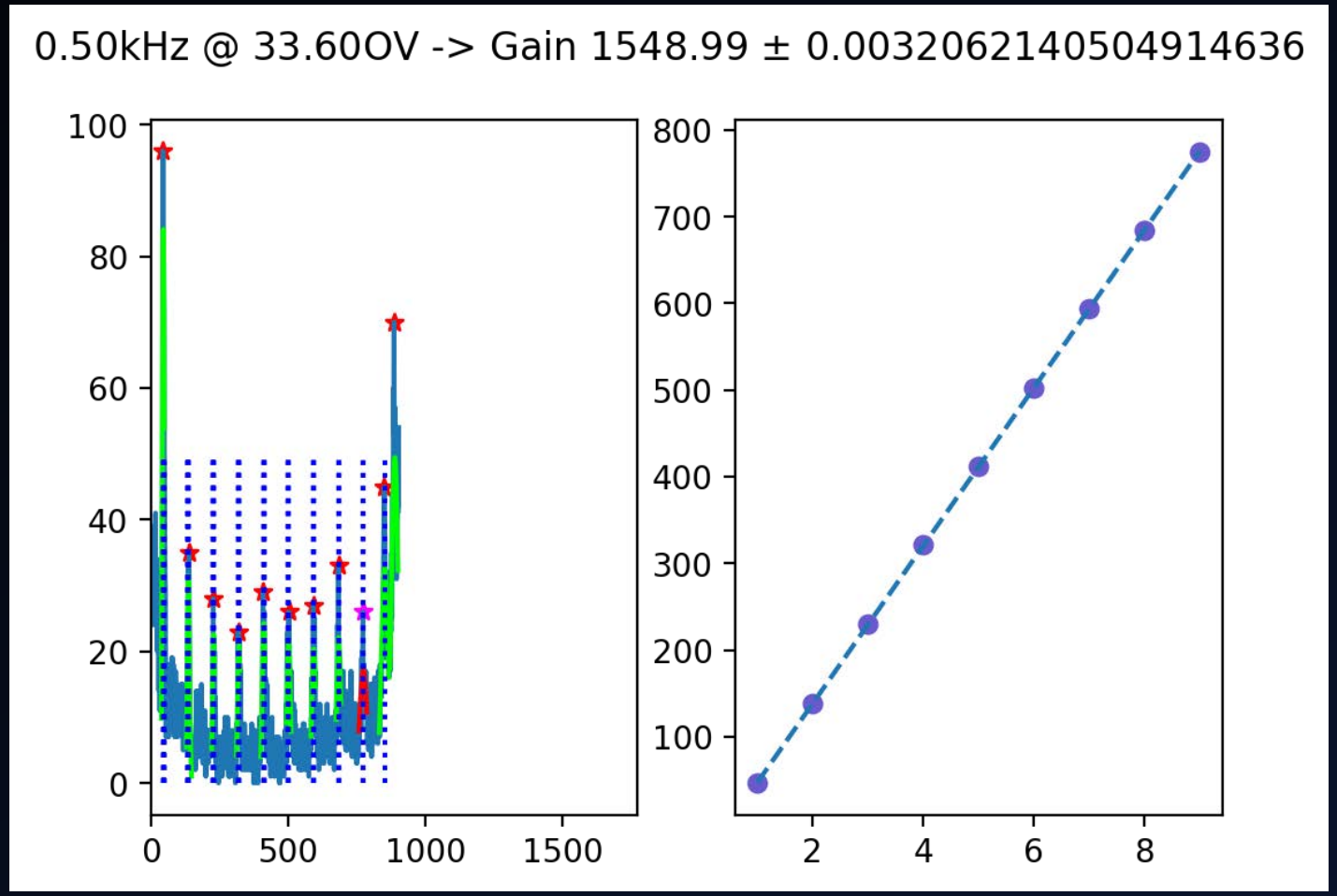

Yale

SmartGAT

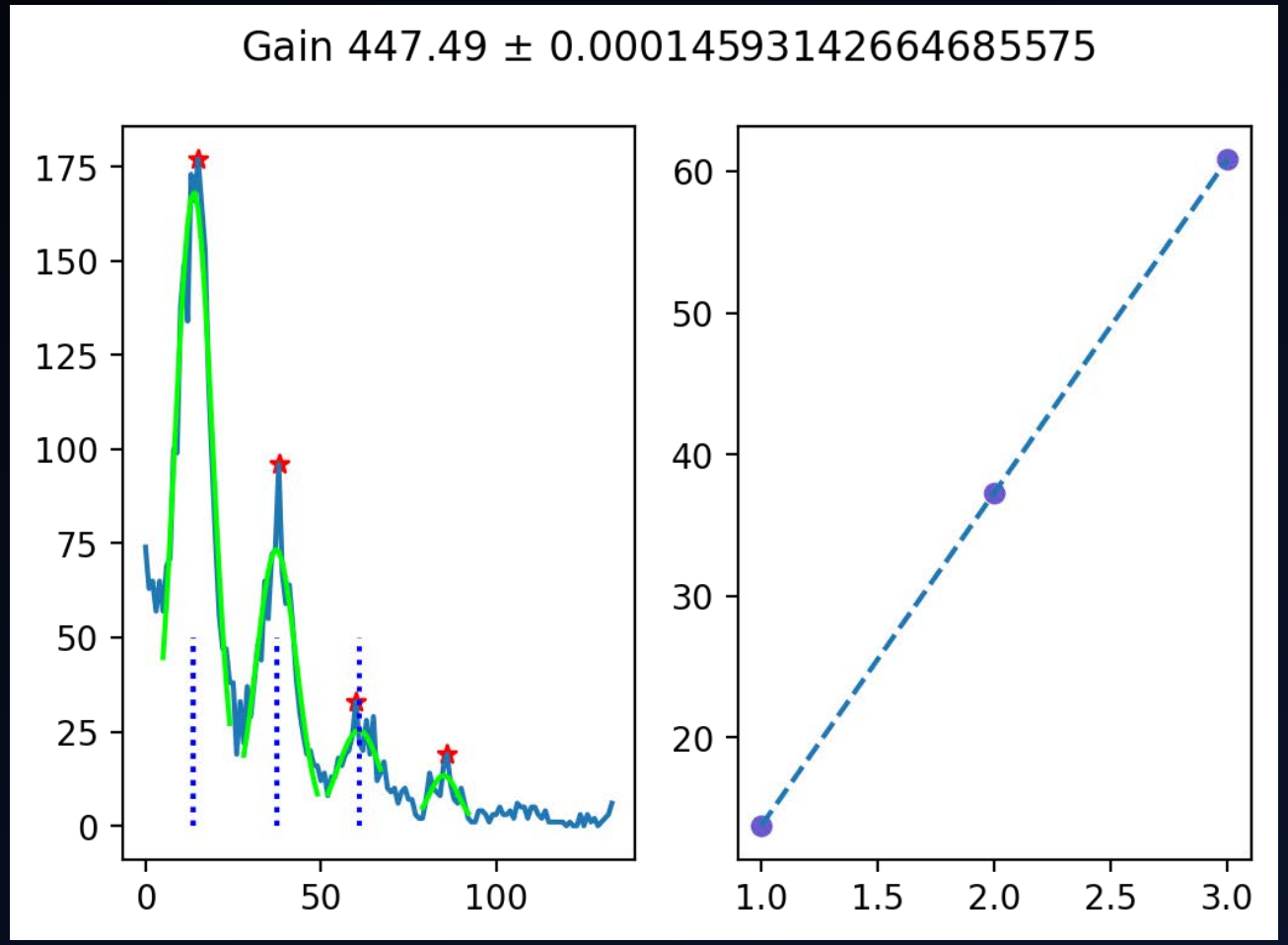

Yale

SmartGAT

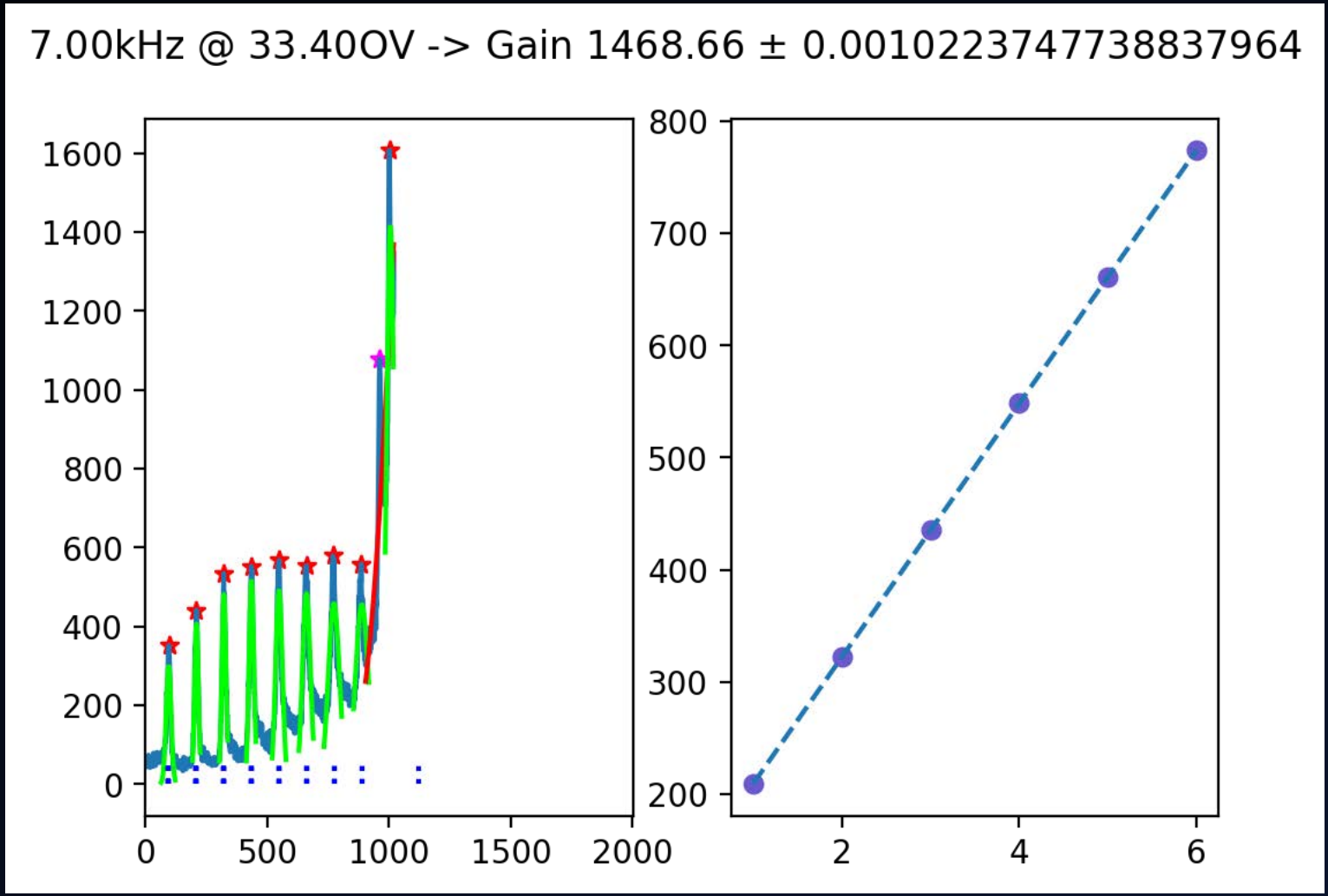

Yale

SmartGAT

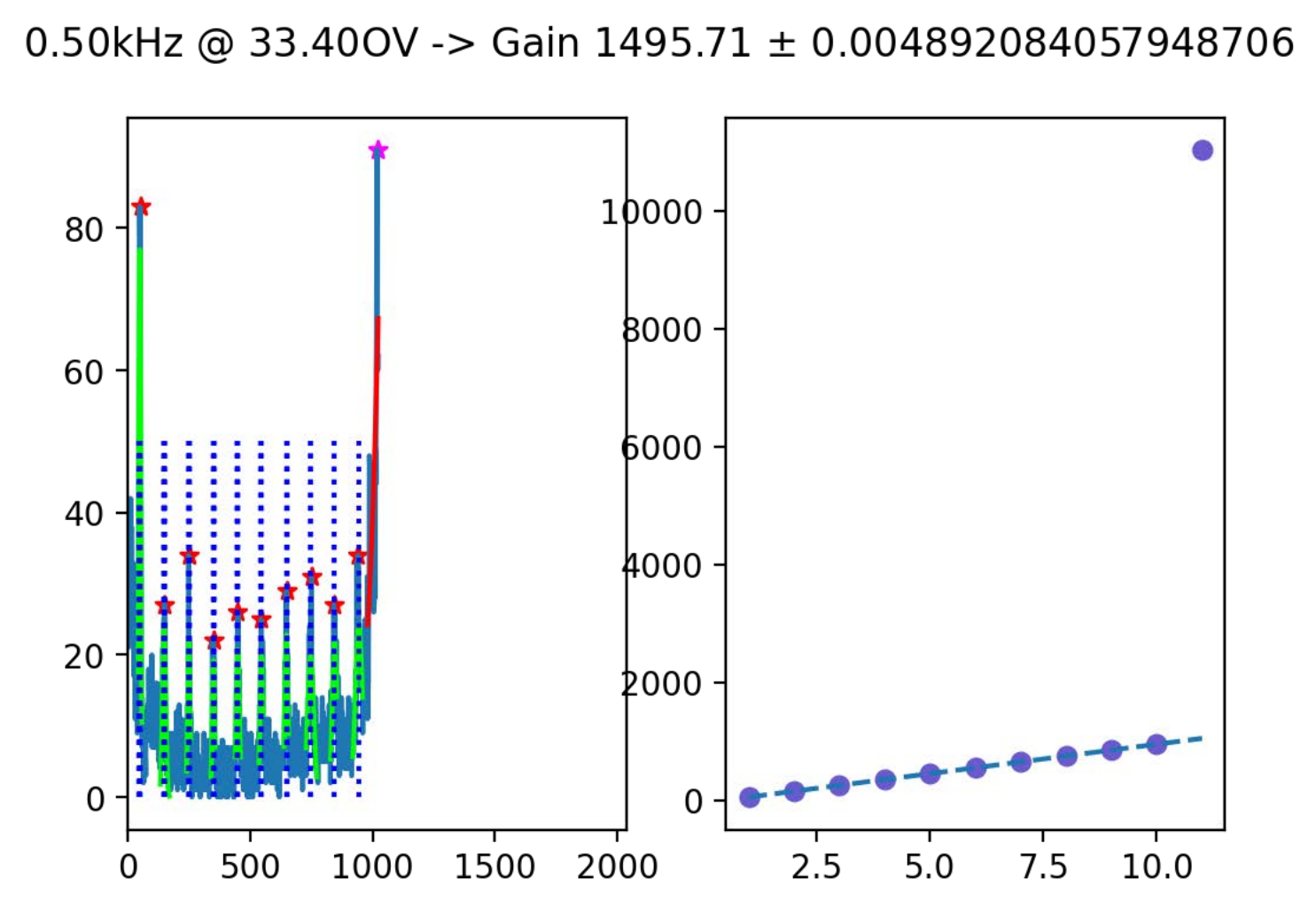

Yale

SmartGAT

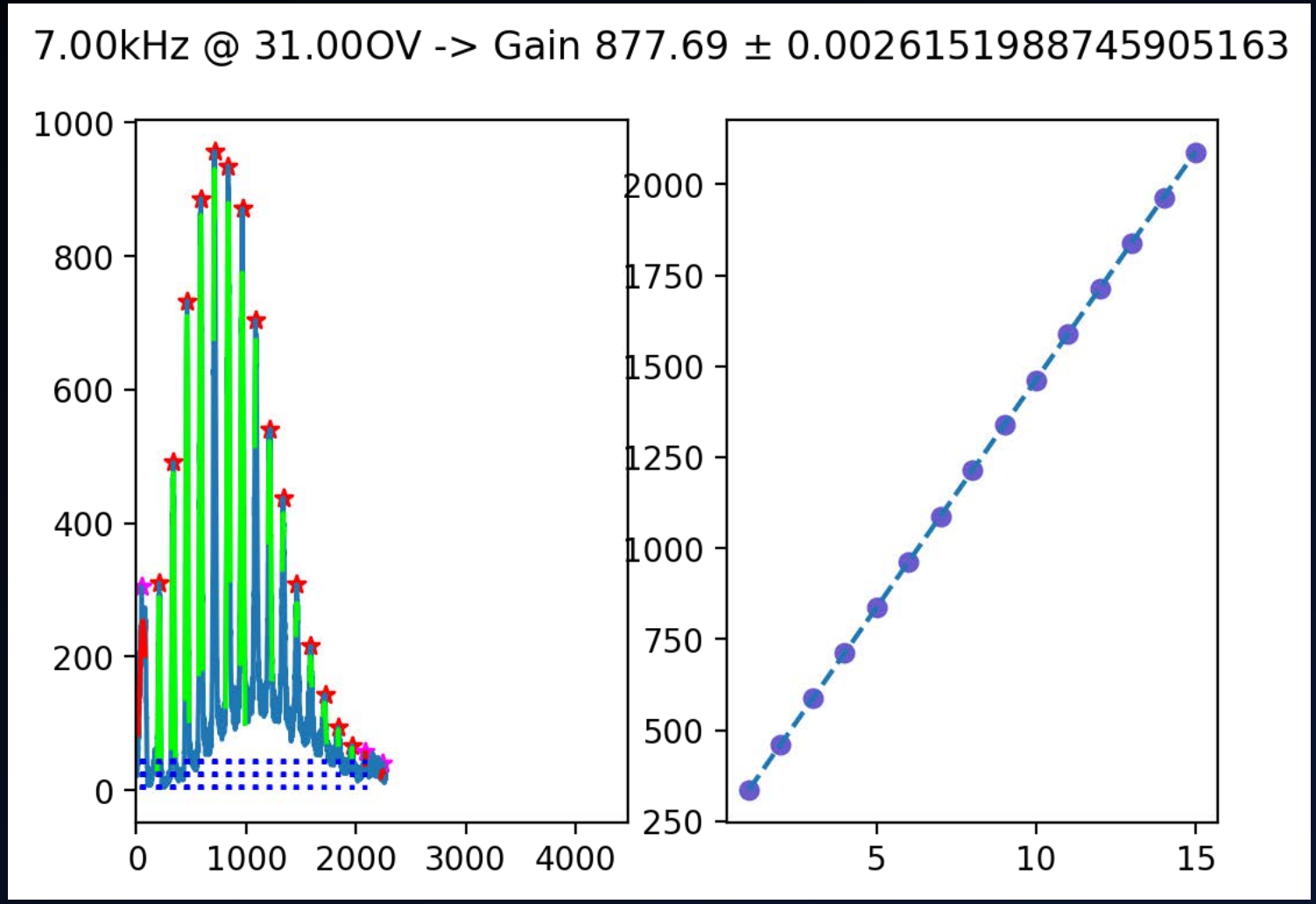

Yale

Waveform analysis

NEW STRATEGIES FOR GAIN CALCULATION

Yale

SmartGAT

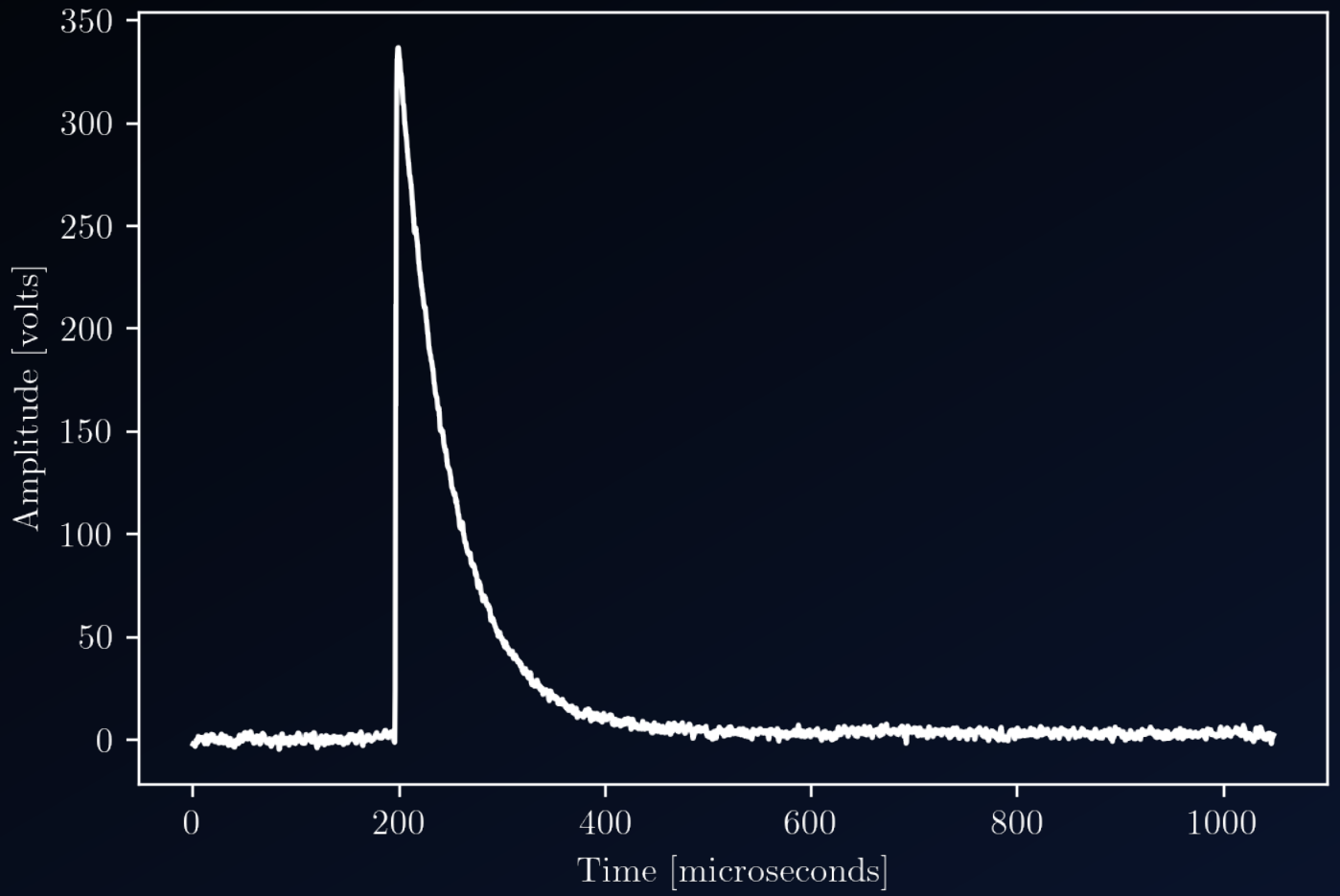

Yale

SmartGAT

```
from Gat import Gat as Gat     # Gain Analysis Tool

path = r'/home/tb829/sipm_data/202206[0-1]*/'

example = Gat(path, 'wave*',4.00,debug=False,force=False,notify=False)
```

Memory usage (traced): 79.65 MB

```
[01:50:49PM - __init__]:  56 files and 1 voltages loaded
```

Yale

SmartGAT

```
example.eval_gain(4.00,plot=False,find_best=True,fix_params=True)
```

```
[02:21:01PM - eval_waveform_func_fit]:  Loading from backup file

[02:21:01PM - __peak_filter]:  Average peak mu is 198.53943103967774 for 2275261.879714707 and 11460

[02:21:01PM - __find_best]:  Multiprocessing does not support progress bars.

Resulting peaks:
 * 151.5434322003957 ± 0.1024826880262279
 * 233.3873251316392 ± 0.1264417260768181
 * 315.1470115767167 ± 0.3374323933332382
 * 396.8200309403013 ± 0.2084546172419785
 * 478.9852437822216 ± 0.3005449807690225
[02:28:11PM - __gain_from_peaks]:  Gain: 69.74 ± 0.08
Memory usage: 478.643887 MB peak
```

Yale

SmartGAT

```
example.eval_gain(4.00,plot=False,find_best=True,fix_params=True)
```

```
[02:21:01PM - eval_waveform_func_fit]:  Loading from backup file

[02:21:01PM - __peak_filter]:  Average peak mu is 198.53943103967774 for 2275261.879714707 and 11460

[02:21:01PM - __find_best]:  Multiprocessing does not support progress bars.

Resulting peaks:
 * 151.5434322003957 ± 0.1024826880262279
 * 233.3873251316392 ± 0.1264417260768181
 * 315.1470115767167 ± 1.3374323933332382
 * 396.8200309403013 -> FIT FAILED
 * 478.9852437822216 ± 0.3005449807690225
```

Yale

SmartGAT

```
example.plot(hist=True, hist_fit=True)
```

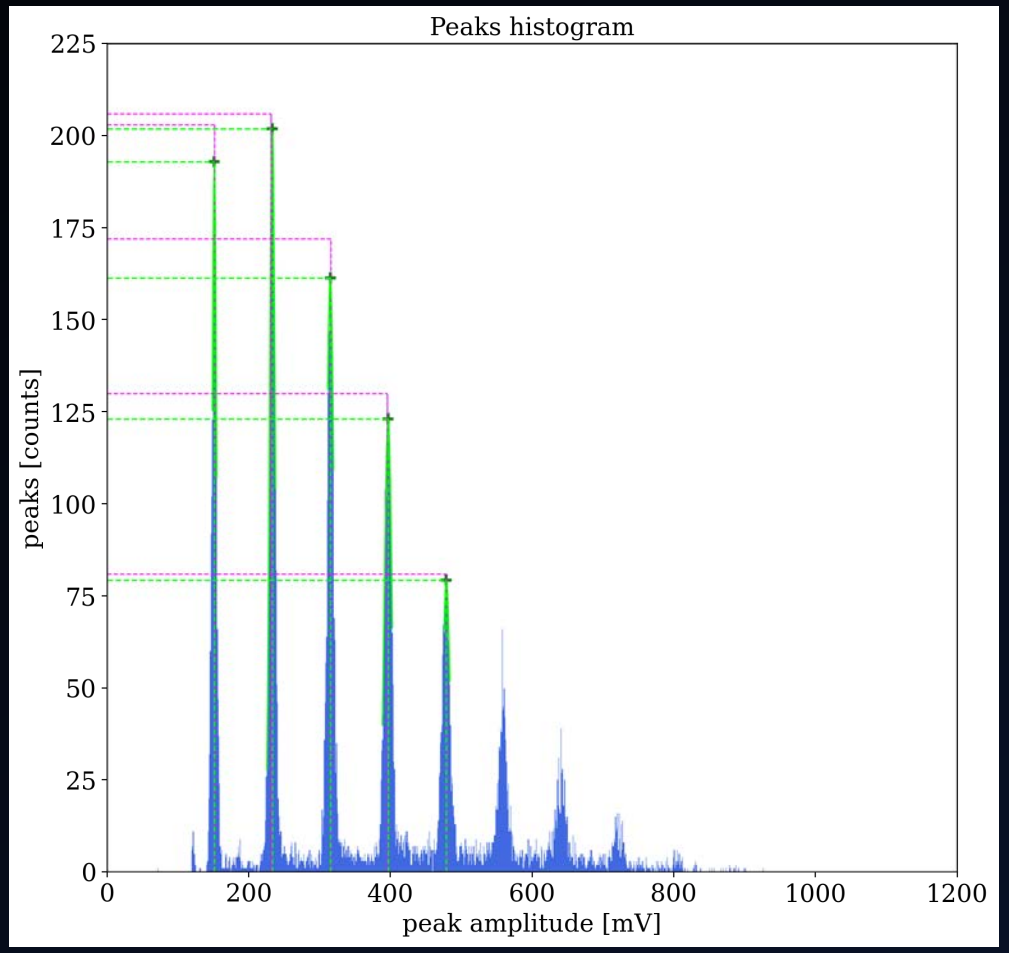

GOOD GAUSSIAN FIT

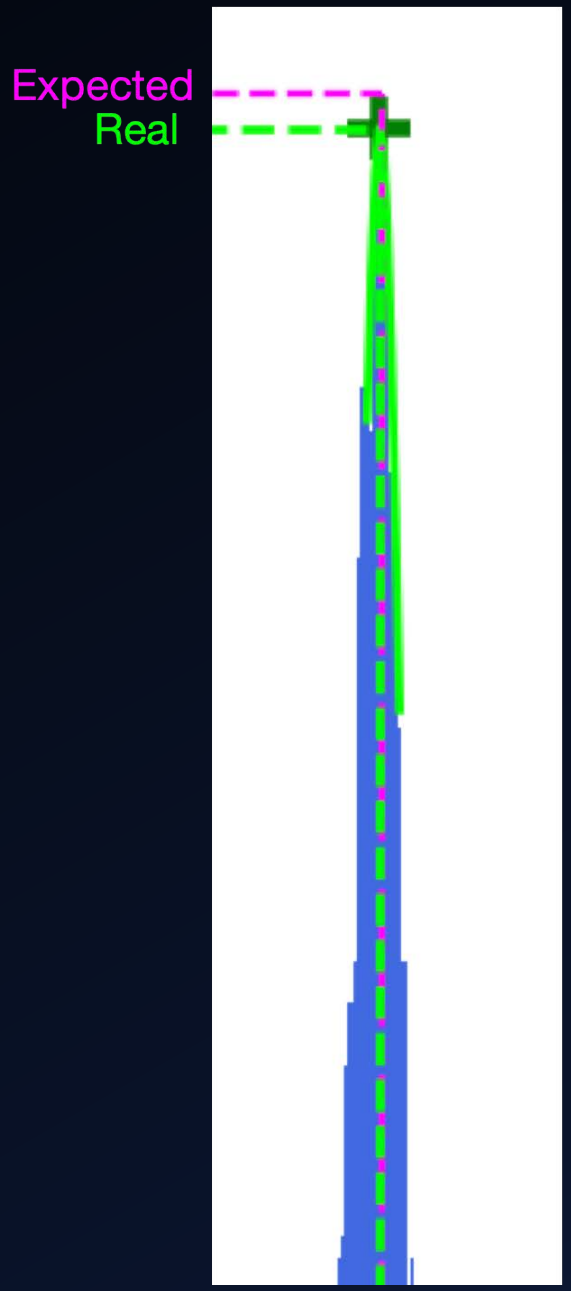

Yale

SmartGAT

```
example.plot(hist=True, gain=True, hist_fit=True)
```

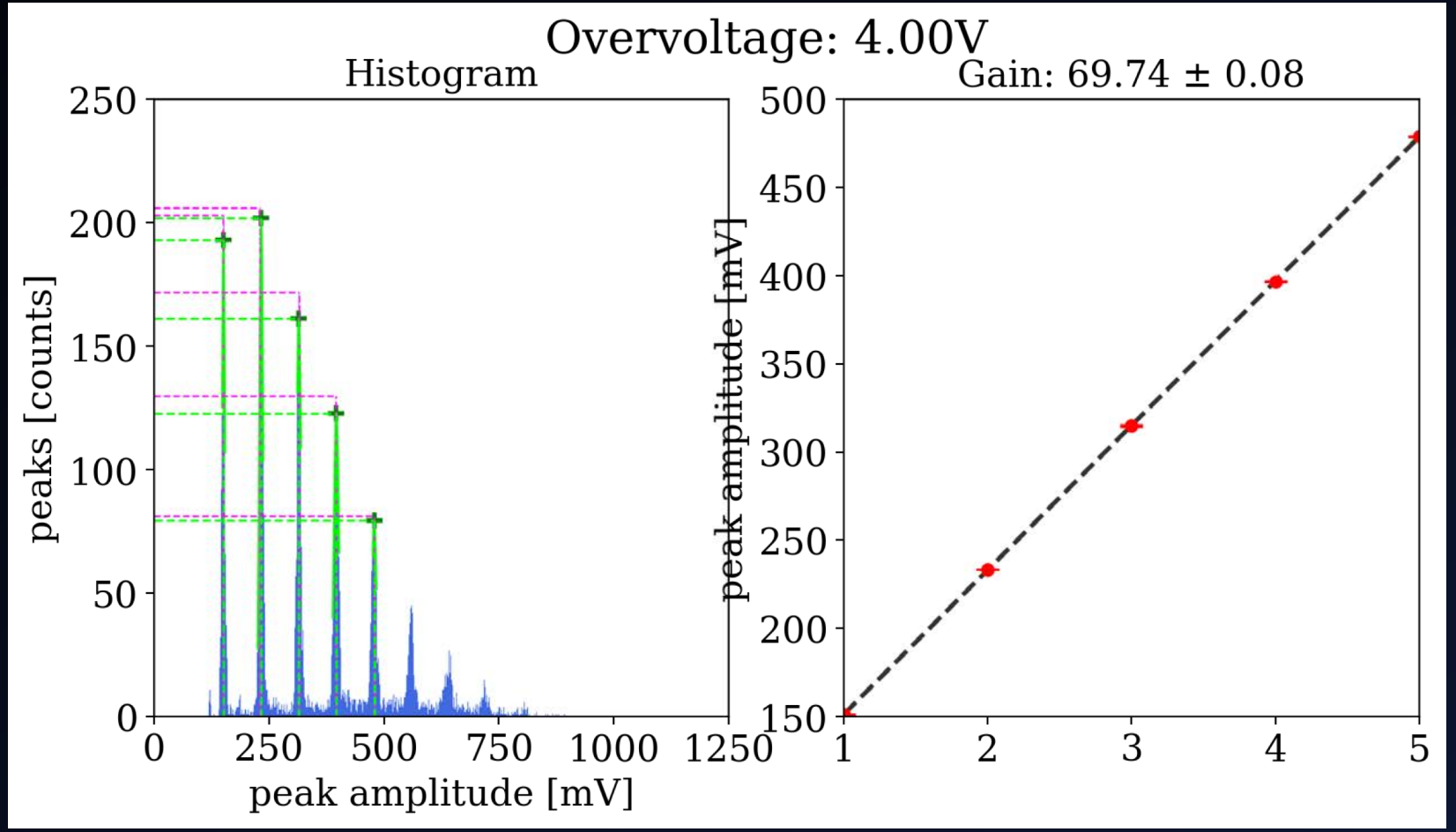

Yale

GAT

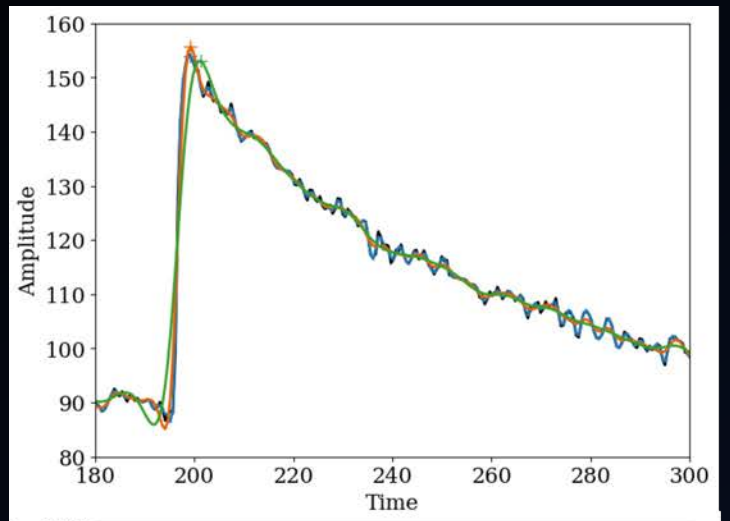
Amplitude
Time

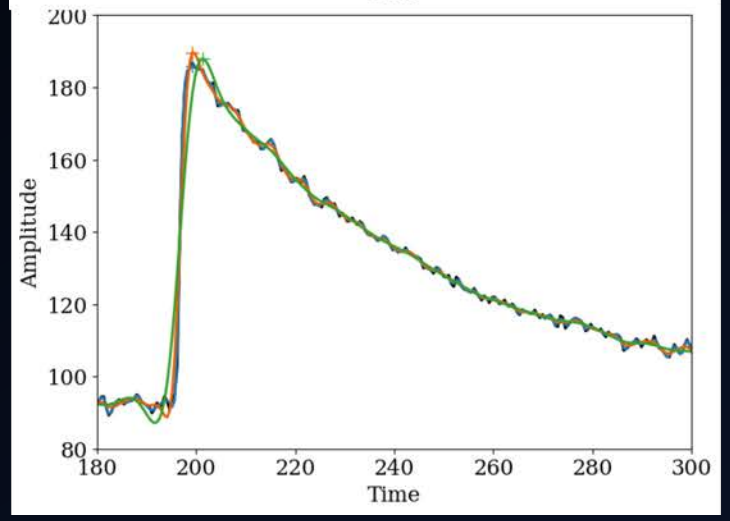
Amplitude
Time

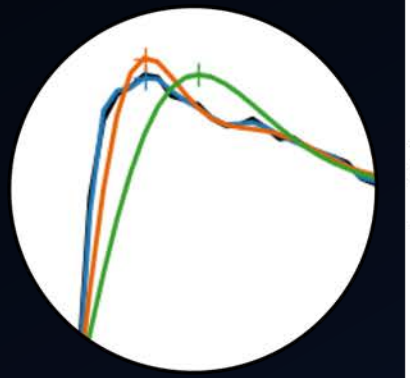

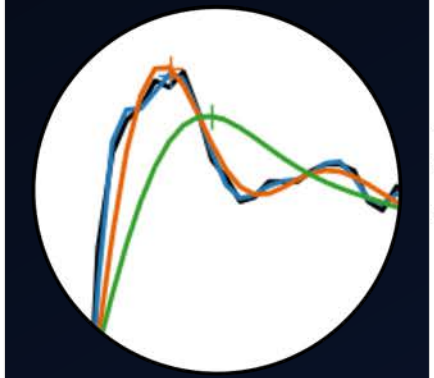

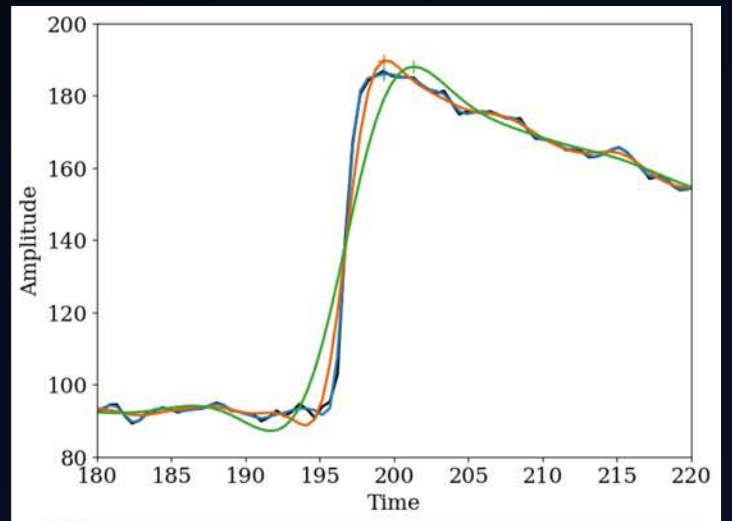
Amplitude
Time

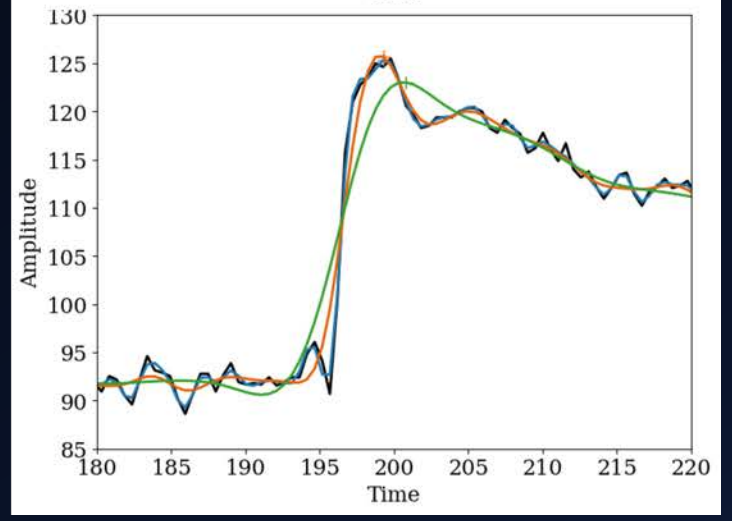
Amplitude
Time

Yale

GAT

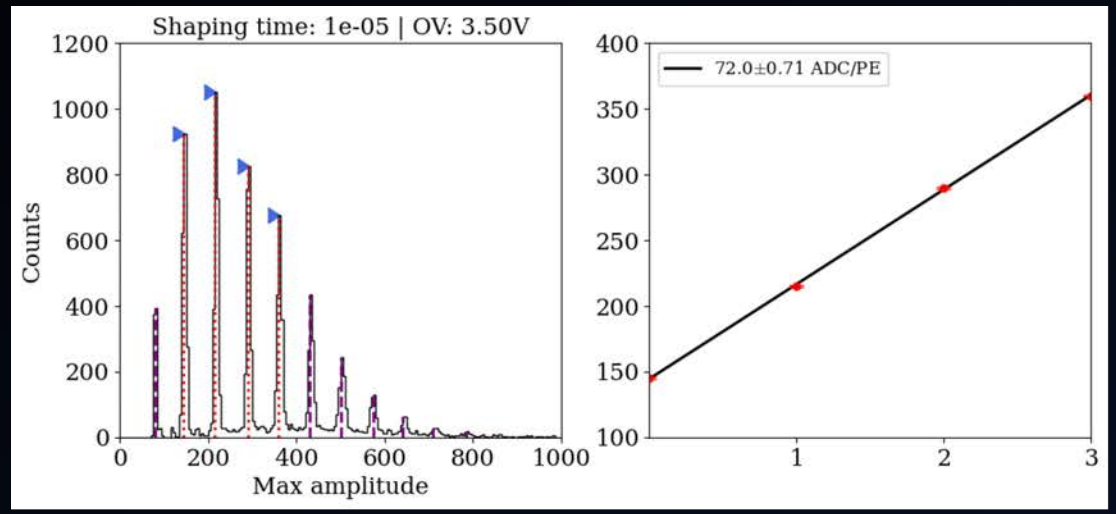
Shaping time: 1e-05 | OV: 3.50V
Counts
Max amplitude
72.0±0.71 ADC/PE

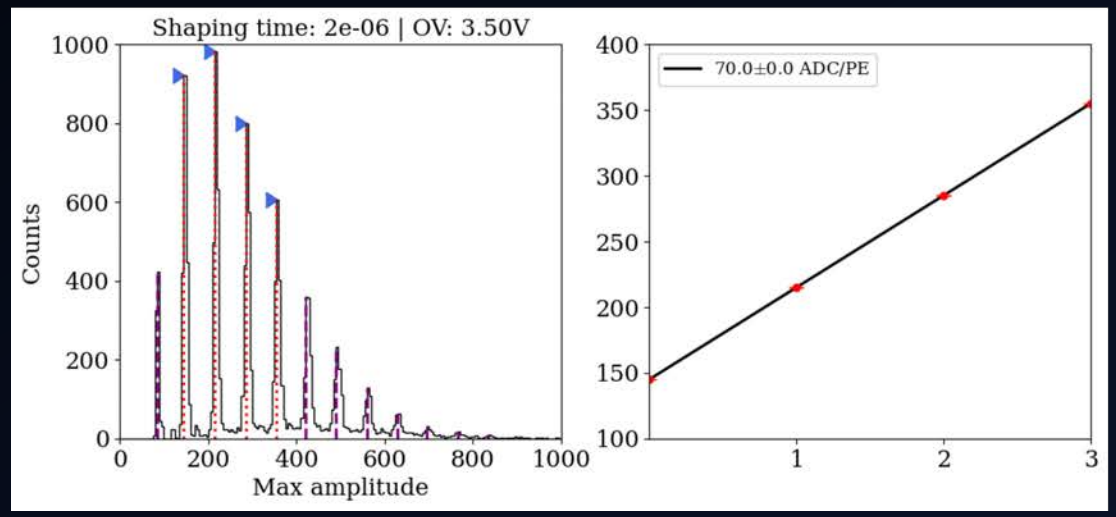
Shaping time: 2e-06 | OV: 3.50V
Counts
Max amplitude
70.0±0.0 ADC/PE

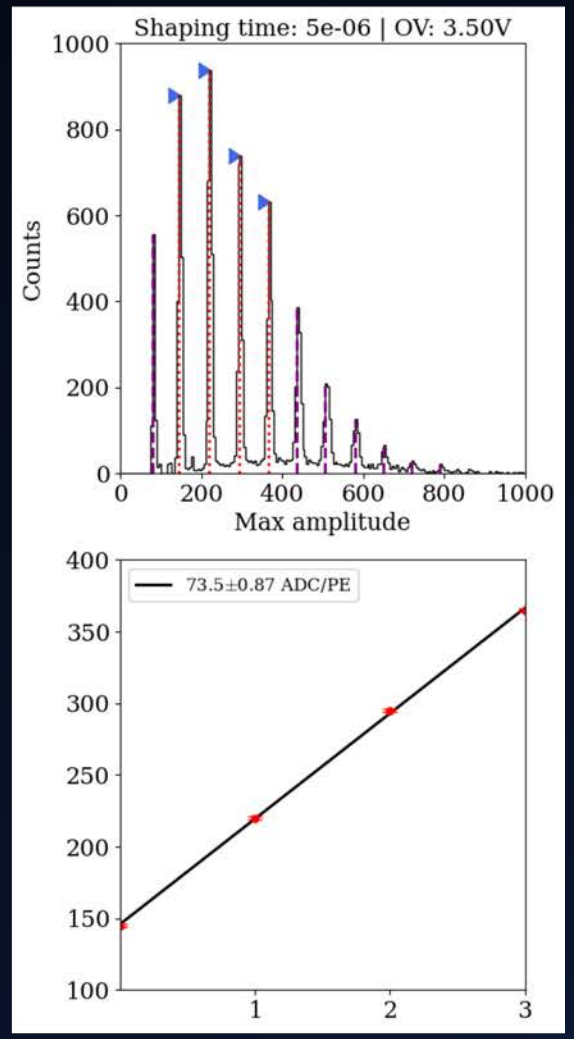
Shaping time: 5e-06 | OV: 3.50V
Counts
Max amplitude
73.5±0.87 ADC/PE

Yale

SmartGAT

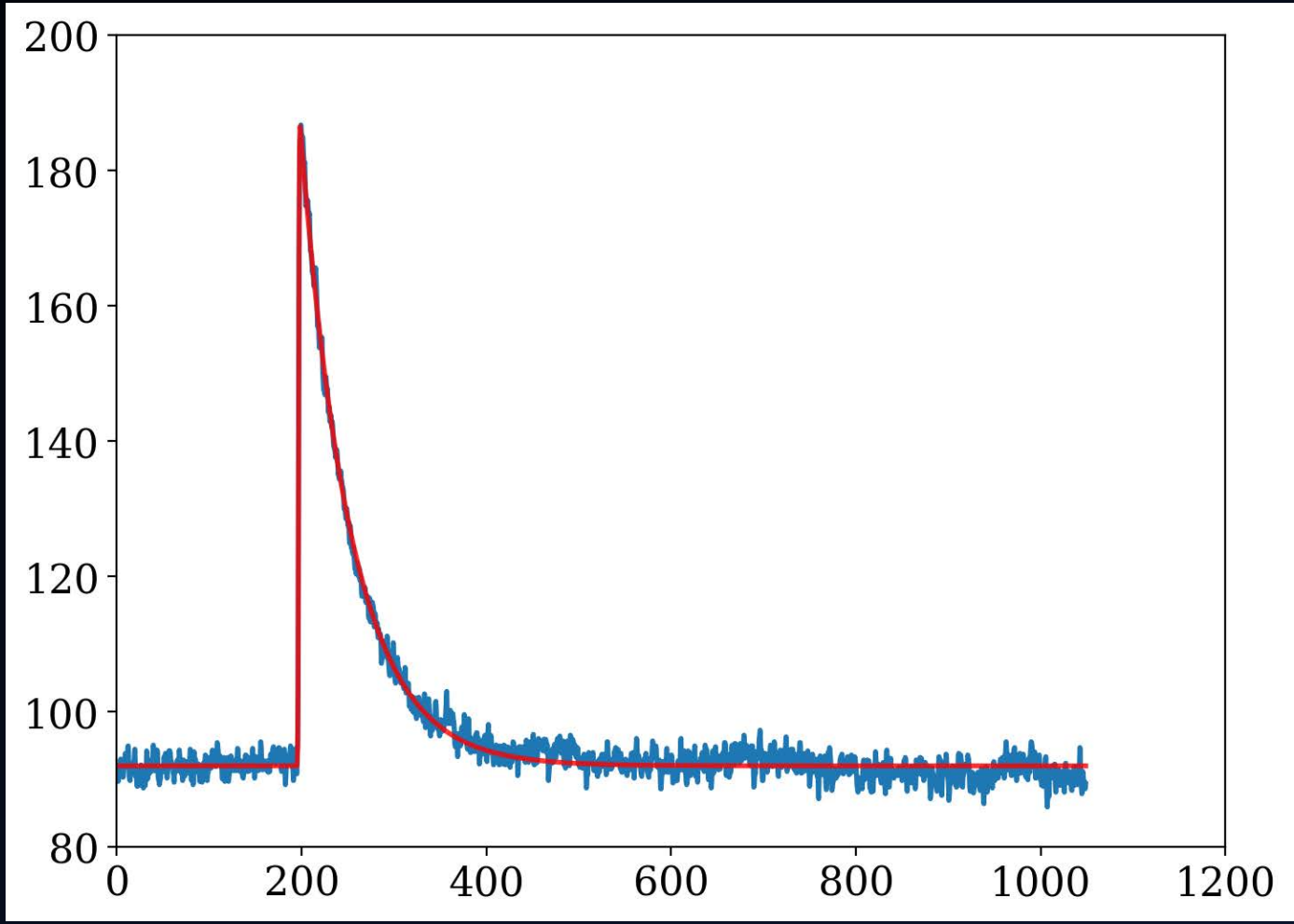

Yale

SmartGAT

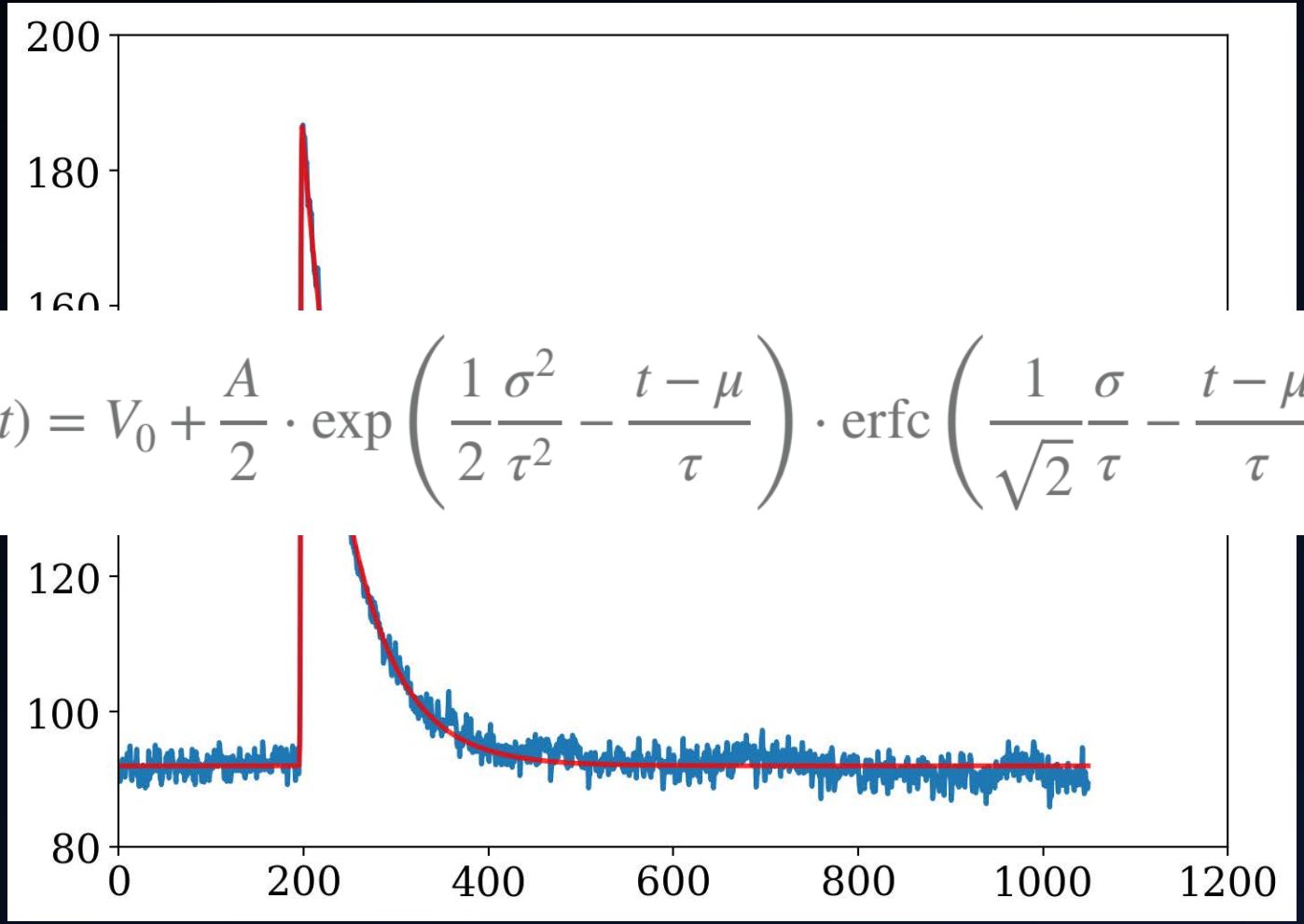

$$V(t) = V_0 + \frac{A}{2} \cdot \exp\left(\frac{1}{2}\frac{\sigma^2}{\tau^2} - \frac{t-\mu}{\tau}\right) \cdot \operatorname{erfc}\left(\frac{1}{\sqrt{2}}\frac{\sigma}{\tau} - \frac{t-\mu}{\tau}\right)$$

Fit function by Dr. Ako Jamil

Yale

SmartGAT

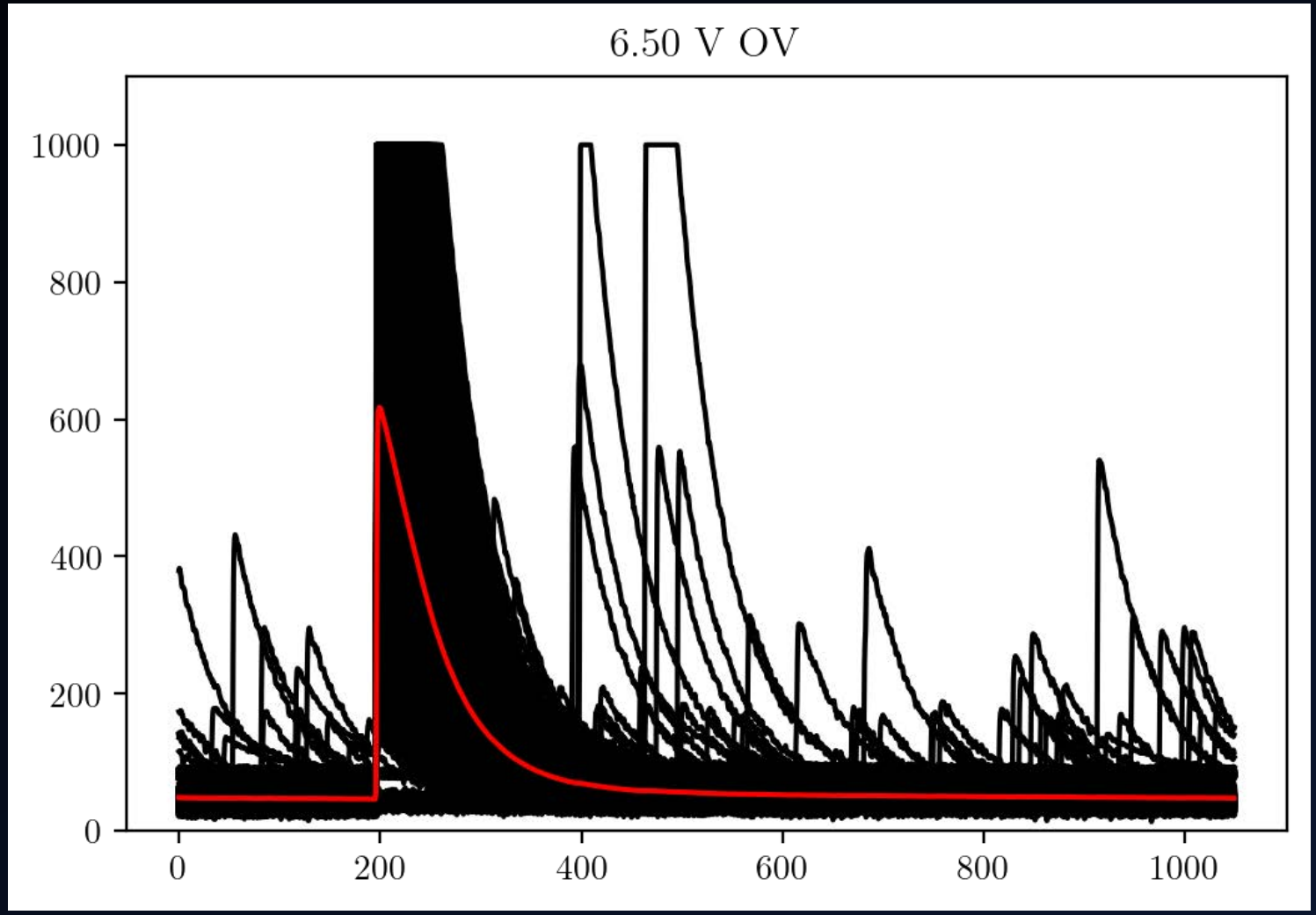

Yale

SmartGAT

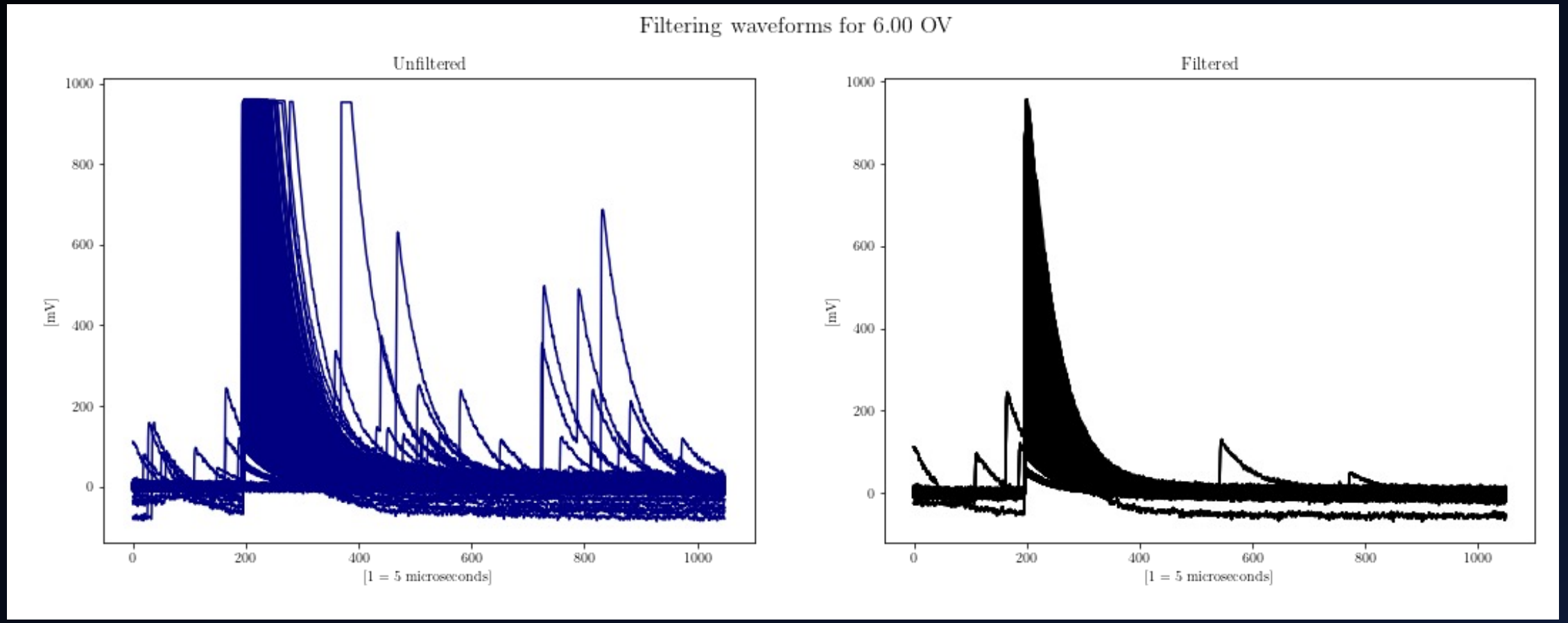

Yale

SmartGAT

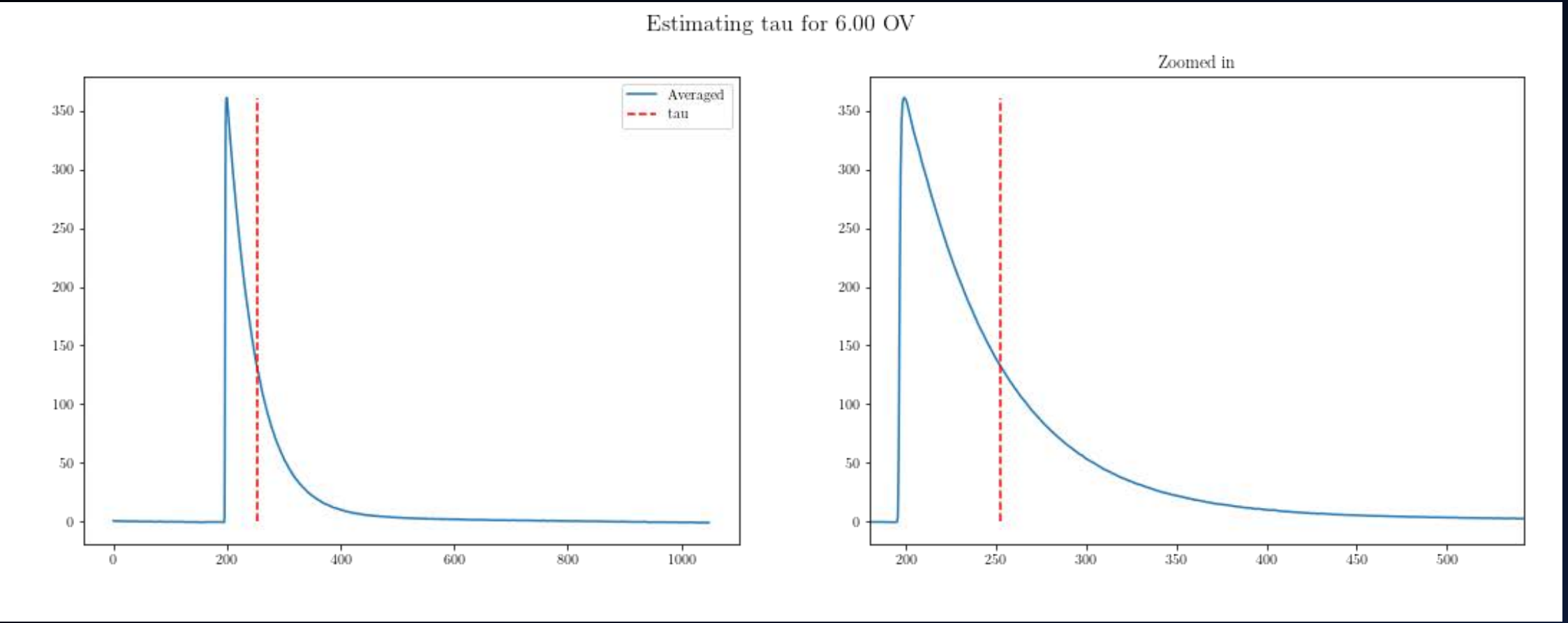

Yale

SmartGAT

$$V(t) = V_0 + \frac{A}{2} \cdot \exp\left(\frac{1}{2}\frac{\sigma^2}{\tau^2} - \frac{t-\mu}{\tau}\right) \cdot \operatorname{erfc}\left(\frac{1}{\sqrt{2}}\frac{\sigma}{\tau} - \frac{t-\mu}{\tau}\right)$$

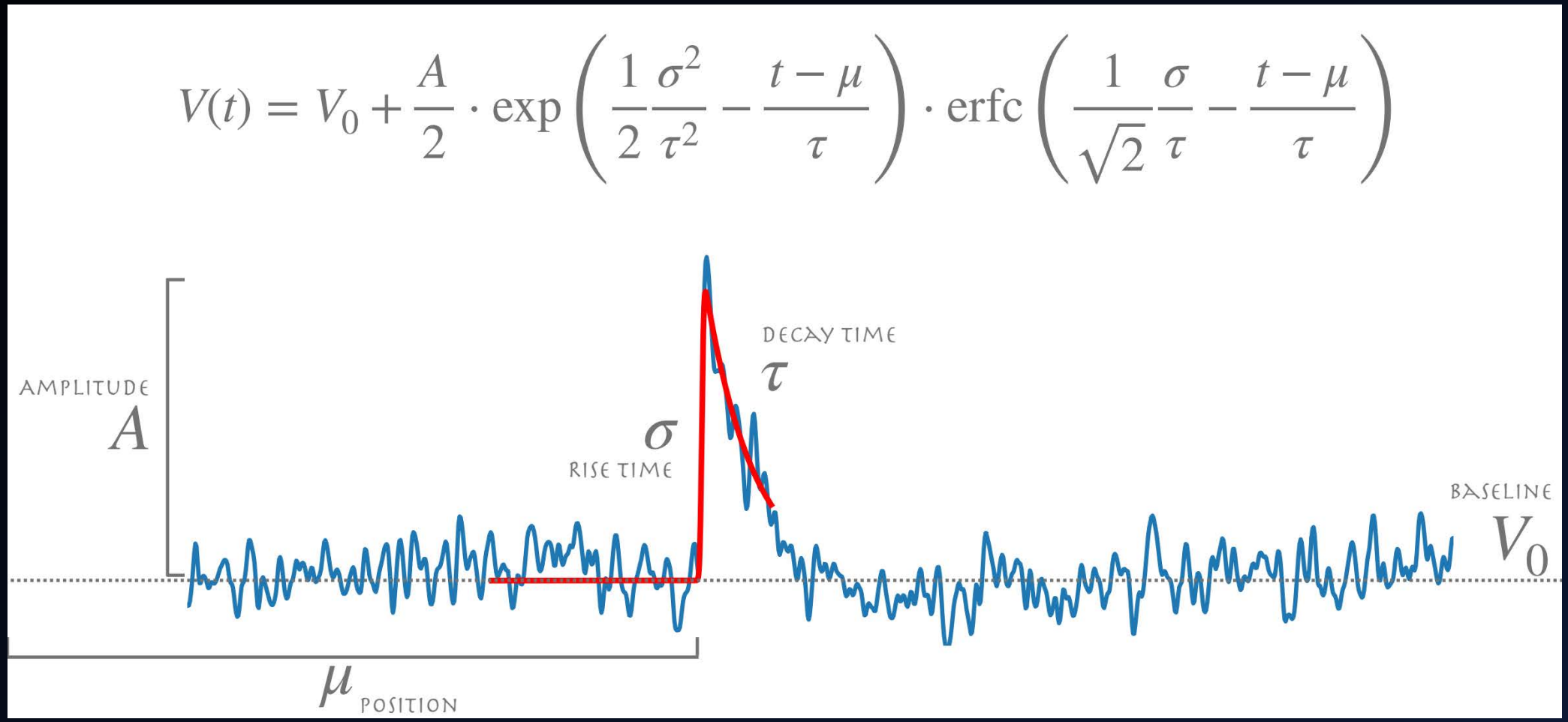

SiPM waveform fitting by Dr. Ako Jamil

Yale

Results

FROM SmartGAT

Yale

Gain vs Bias voltage analyis pre/post resistor change

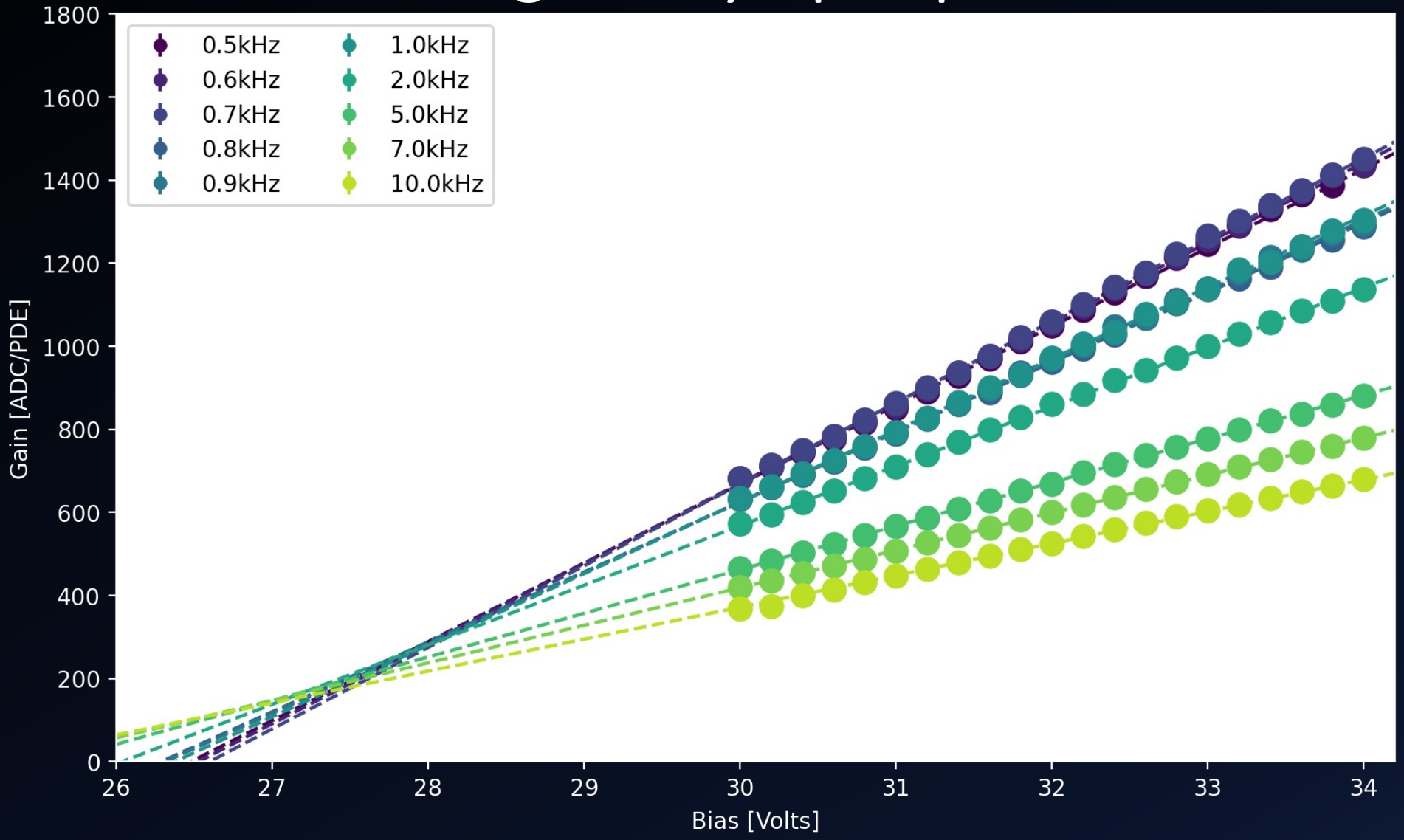

Yale

Gain vs Bias voltage analyis pre/post resistor change

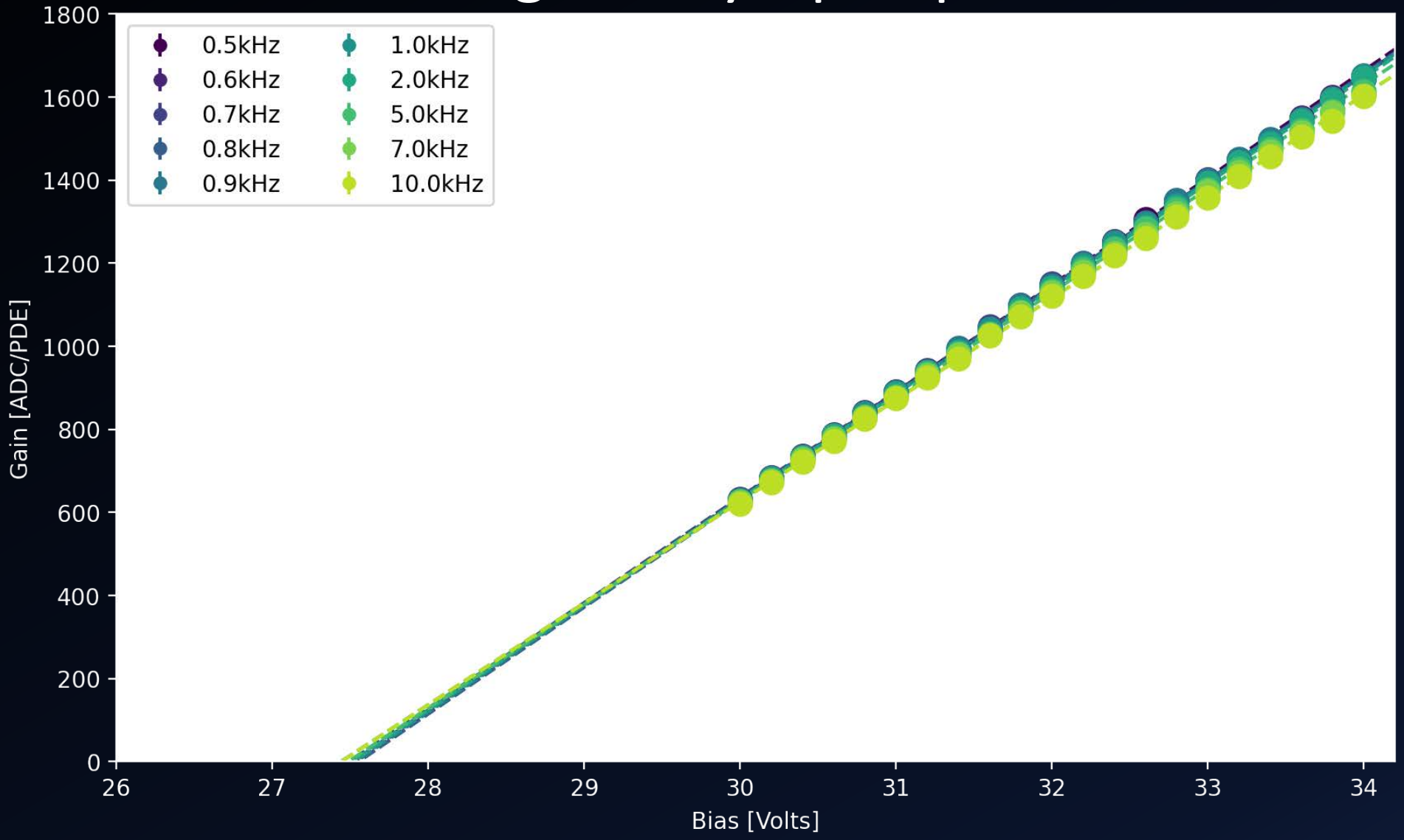

Yale

Summary and conclusions

- Created a Python class (SmartGAT) that utilizes a smart algorithm to distinguish between waveforms and histograms corresponding to SiPM PEs
- SmartGAT fits single PE histogram peaks from the MCA as well as from raw waveforms from the pre-amplifier
- This tool has enabled quick calculation of SiPM gain which will be utilized by Moore Lab for SiPM characterization such as stability in LXe, electric field as well as exposure to radioactive calibration sources

Yale

References

[1] *Sensitivity and Discovery Potential of nEXO to Neutrinoless Double Beta Decay - Scientific Figure on ResearchGate. Available from: https://www.researchgate.net/figure/Engineering-design-rendering-of-the-nEXO-experiment-concept-for-concreteness-drawn-in_fig1_320441791* [accessed 17 Aug, 2022]

[2] *Characterisation of Silicon Photomultipliers with Xenon Scintillation Light for the nEXO Experiment* by Tobias Ziegler (2016)

Yale

Acknowledgments

Prof. David Moore, PhD

Dr. Avinay Bhat, PhD

Glenn Richardson

Molly Watts

Sierra Wilde

Dr. Ako Jamil, PhD

Yale

A special thank you to the people who made this possible

Francesco Tavernese

Giorgio Coretti

Emanuela Pallotta

Paolo Giovenali

Prof. Antonio Ereditato, PhD

Victoria Misenti

Taylor Dunnigan

Wright Laboratory

Yale

'LET THERE BE LIGHT'

ANTONIO FERRALORO
Medical Student
University of Messina

ONAOSI-YALE
UNDERGRADUATE RESEARCH EXPERIENCE IN INSTRUMENTATION
Summer 2022

Wright Laboratory, Yale University
June 19th – August 20th

Wright Laboratory

FONDAZIONE ONAOSI

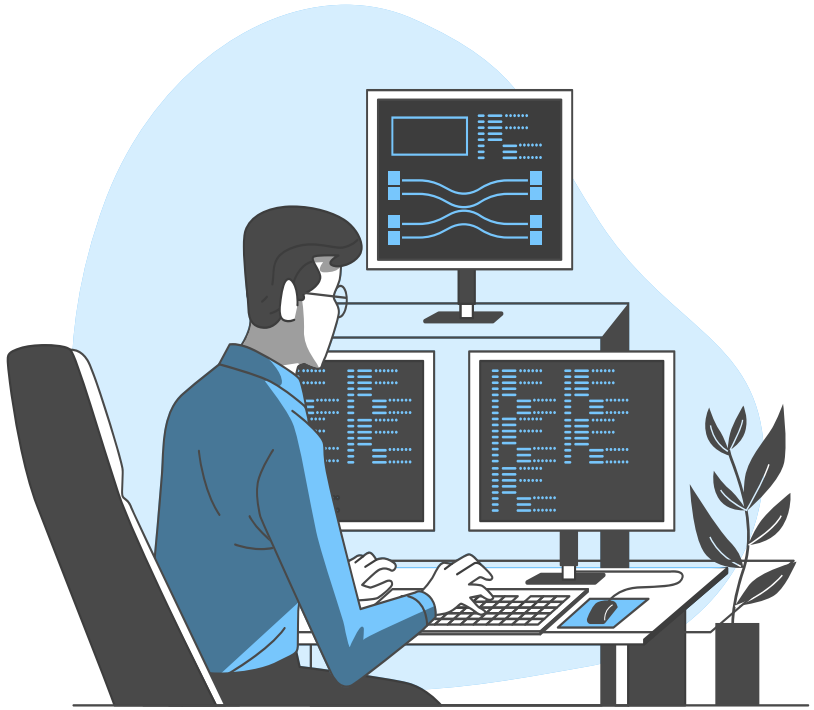

DUNE Experiment

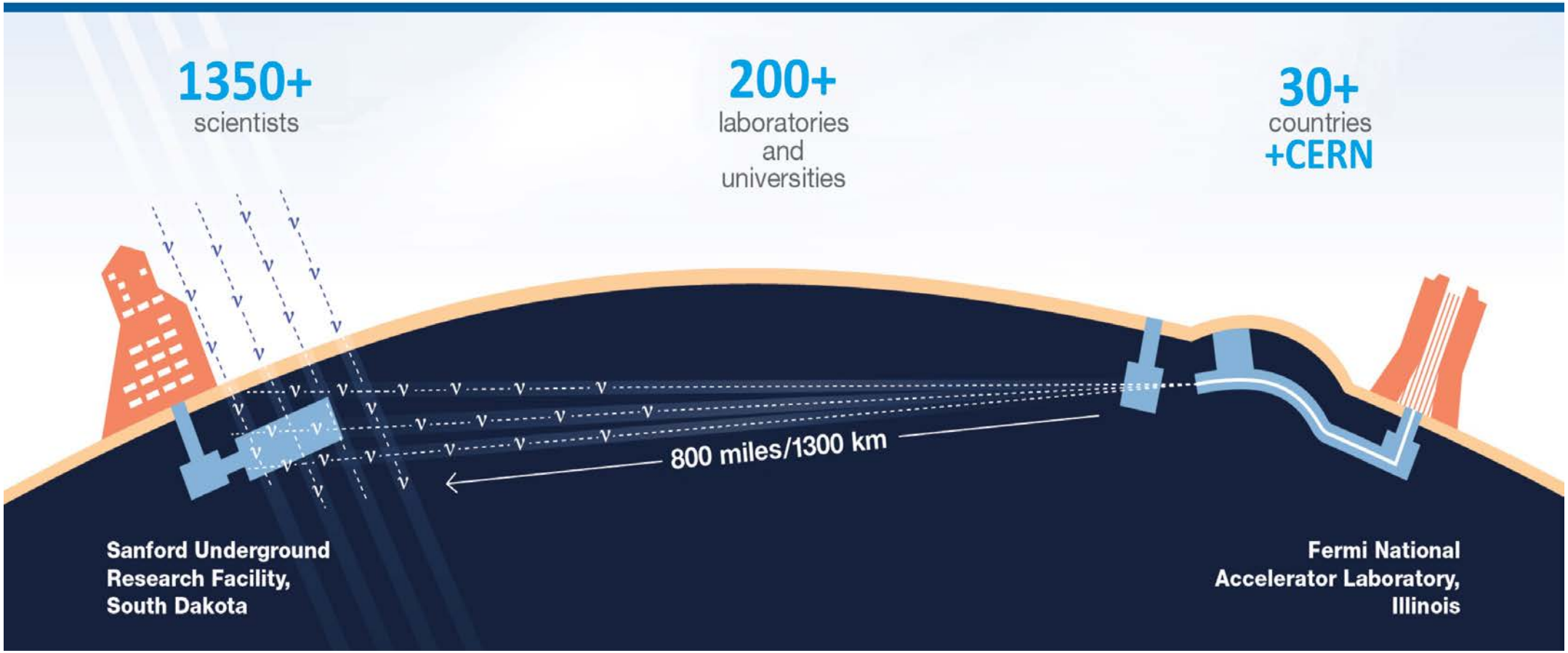

Near Detector

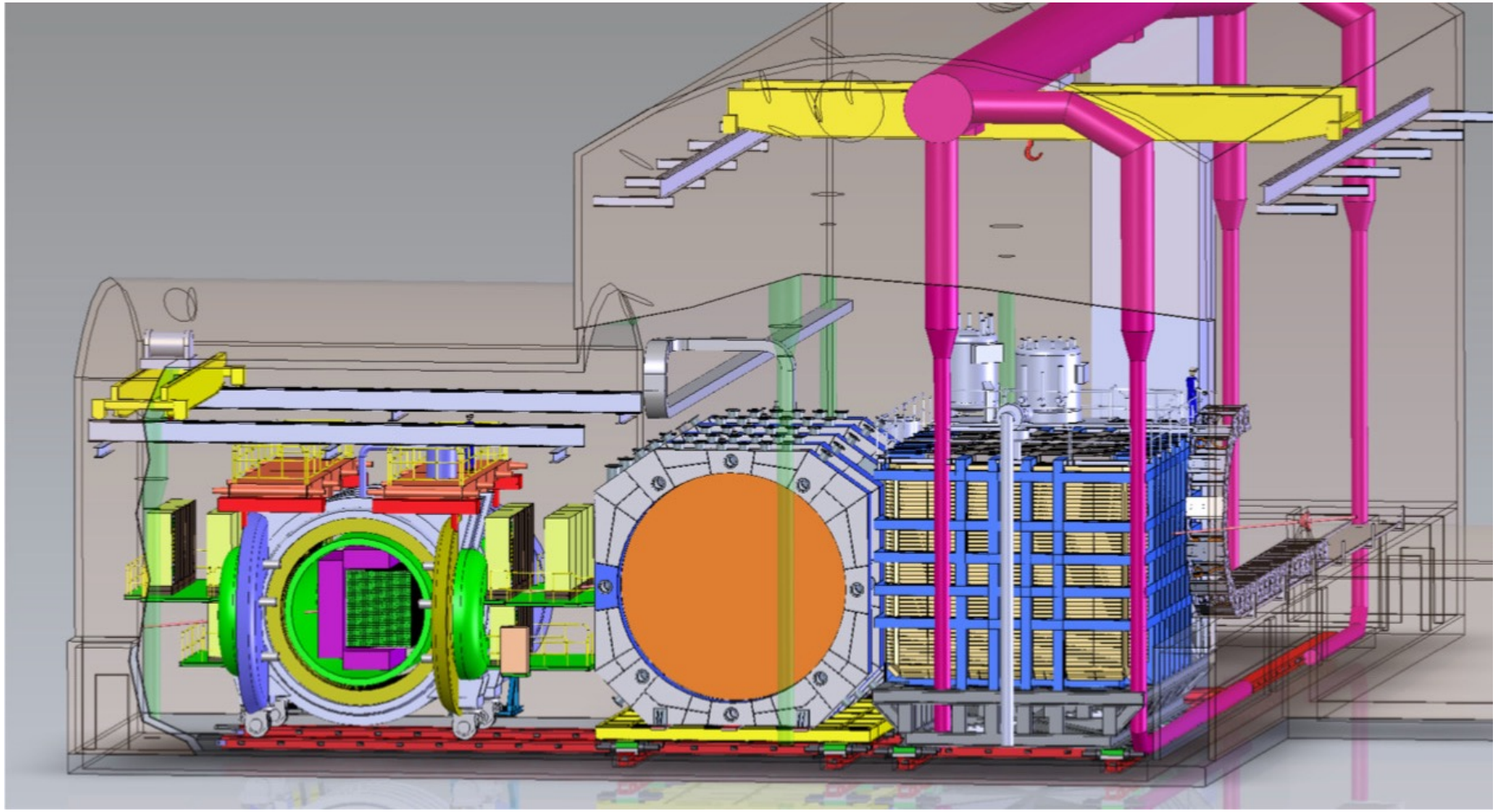

LArTPC

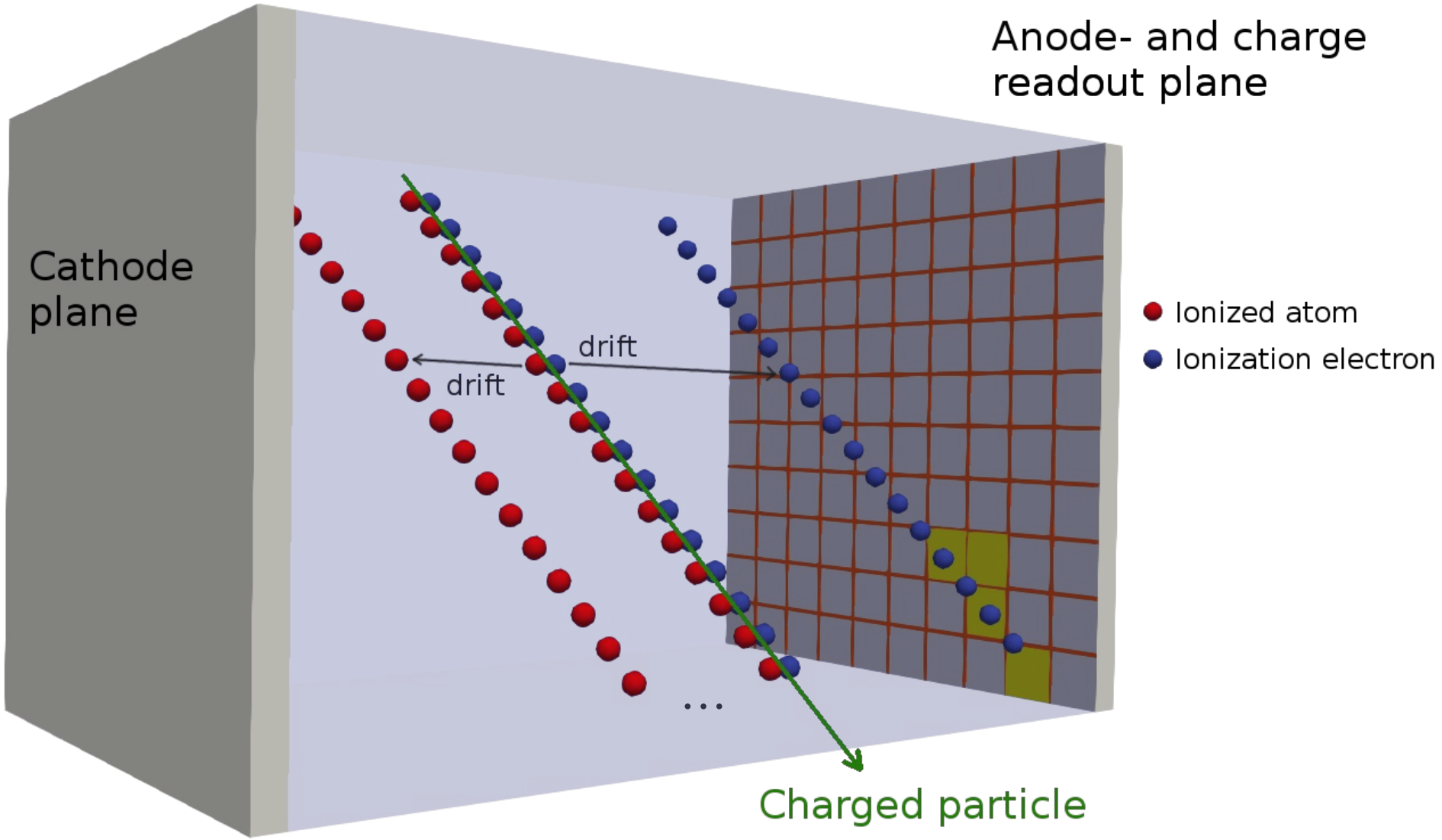
Anode- and charge readout plane
Cathode plane
drift
drift
Ionized atom
Ionization electron
Charged particle

What I focused on: LArTPC

Cryostat

Cryostat section

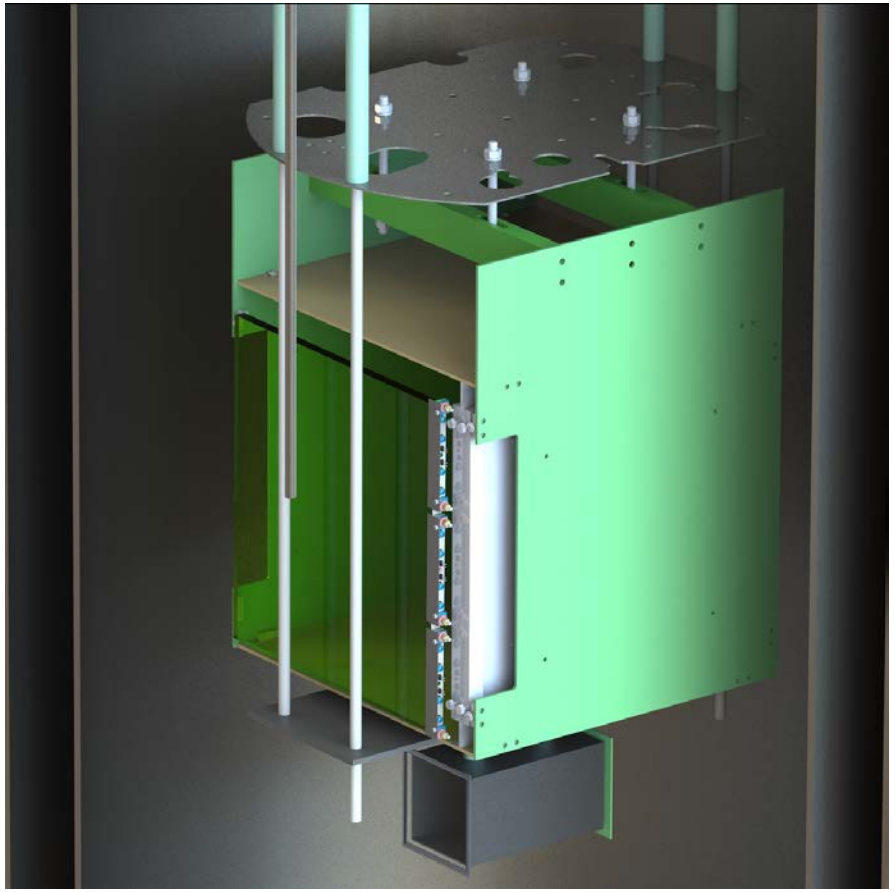

Single Cube

Slow Control

Key components:

- Temperature sensors
- Pressure gauges
- Pressure valve control
- LAr purity, level and control sensors
- Arduino and LabView Main Display

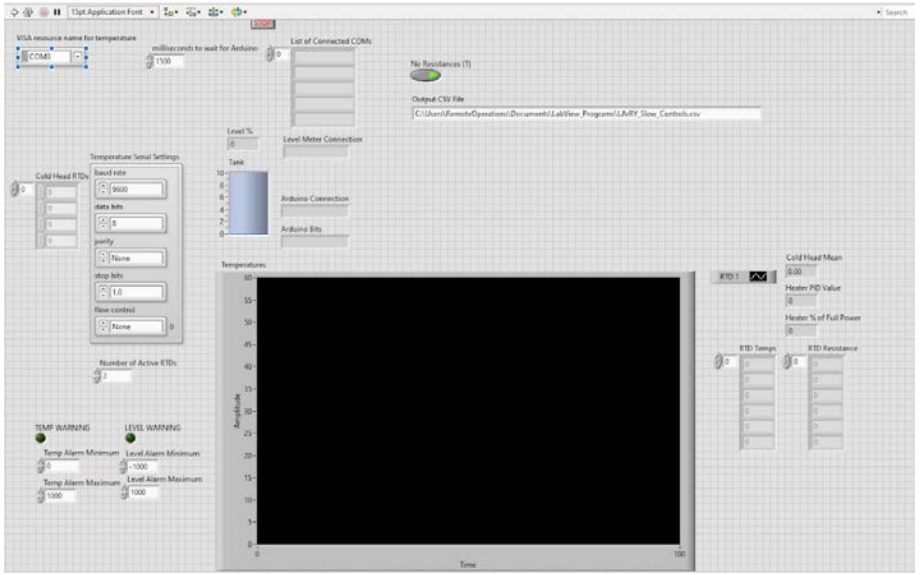

LabView Main Display
Poshu Ng

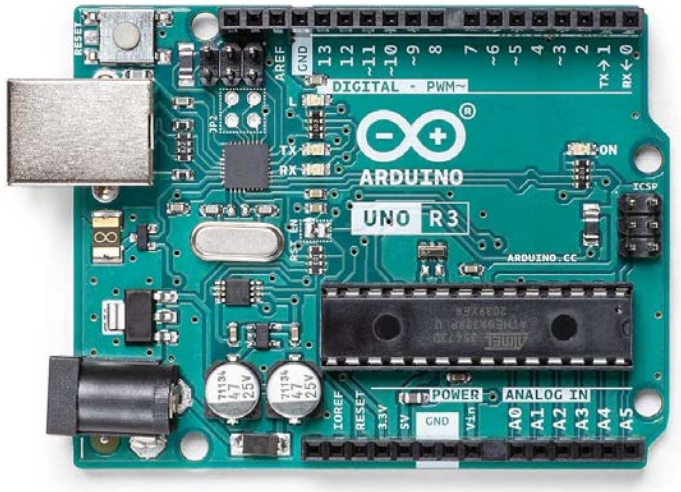

Arduino
UNO REV3 A0006

RTDs

Pressure Gauge

RTDs?

Resistance/Temperature detectors: detect temperature through a change in resistivity of certain materials.

$$\rho(T) = \rho_0 \cdot [1 + \alpha(T - T_0)]$$

Resistivity/Temperature linear relation
Wikipedia

Image of an RTD
labfacility.com

RTDs Calibration Experiment

PURPOSES

- RTDs for calibration
- Arduino connections .
- Level sensor.

MATERIALS

- Ice-filled Cooler
- Insulative material
- Wiring for all 5 RTDs
- Thin, non-permeable bags.
- Thermometre

"RTDs Calibration Experiment Setup"
Poshu Ng

RTDs Calibration Experiment Results

Consistency vs Accuracy

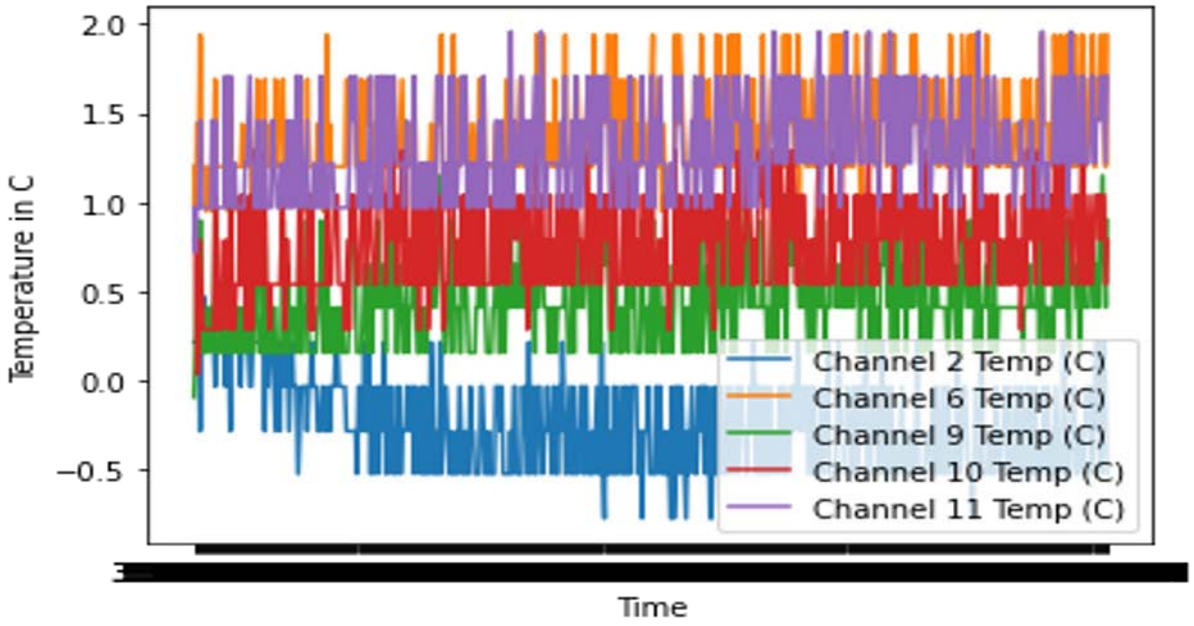

"Temperature over time for 4 RTDs"
Matt King

230 Ohm with 0.0128V offset		Arduino	Difference
2	229	229.79	-0.79
3	228.54	228.36	0.18
4	228.62	228.44	0.18
5	228.56	228.38	0.18
9	228.15	227.97	0.18
			-0.014

"Test Resistances w/ Voltage Offset"
Poshu Ng

Light Detection System

Key components:

- ArcLight
- Multi-Pixel Photon Counter (SiPM
- Multi-Channel Front-End Board for SIPM Readout

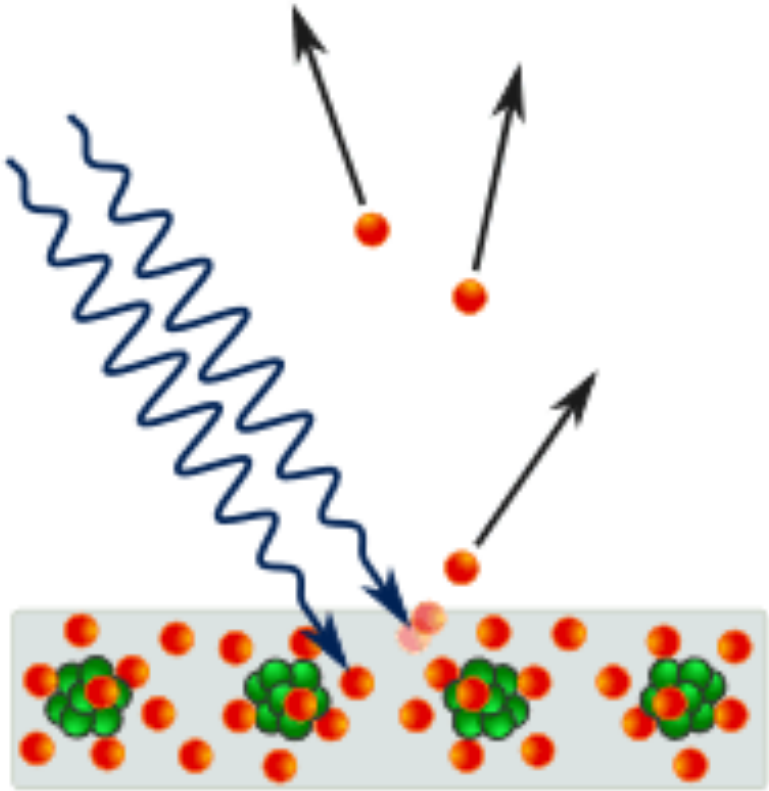

ArCLight

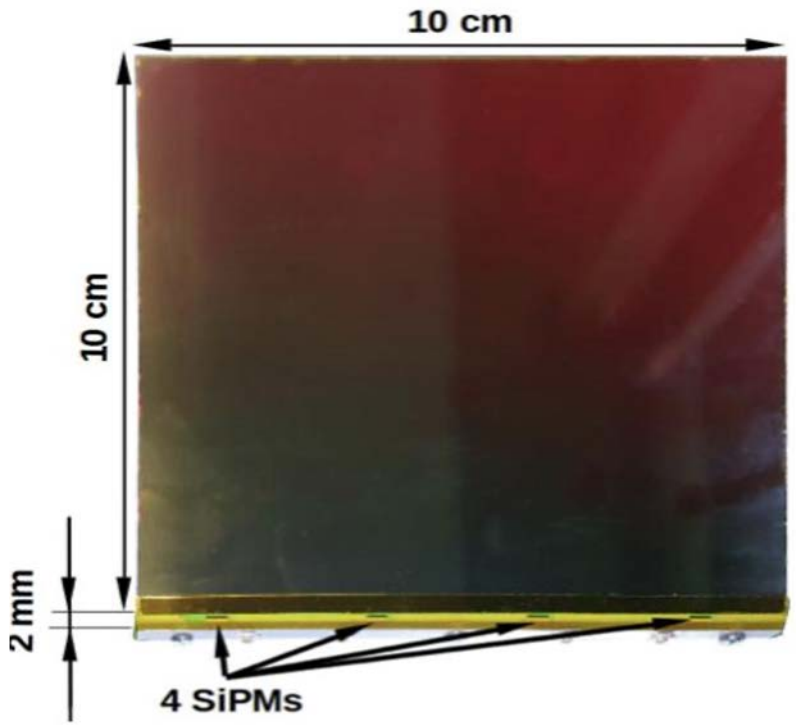

Front image of ArCLight [I]

- A 4mm EJ280 WLS with reflective films
- A dichroic film transparent in blue and reflective in green
- A dielectric specular reflector foil with a 98% reflectance in the visible spectrum [1]

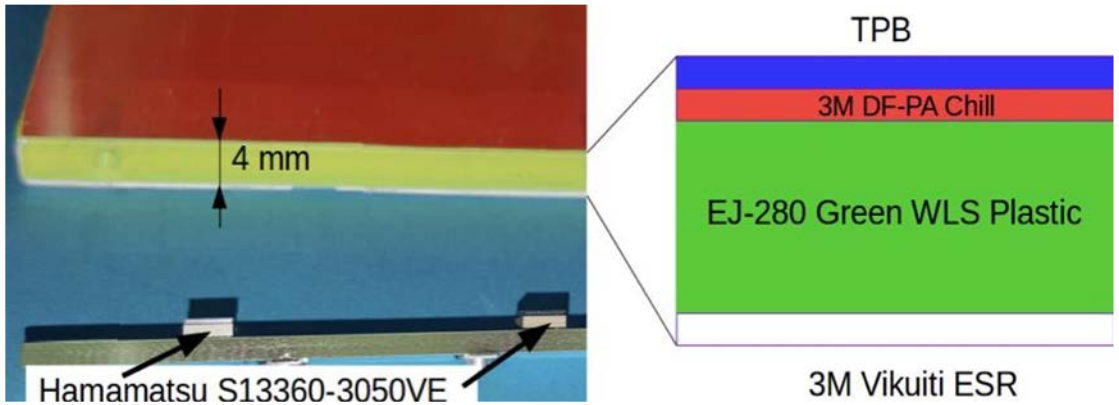

ArCLight Layers [II]

Multi-Pixel Photon Counter

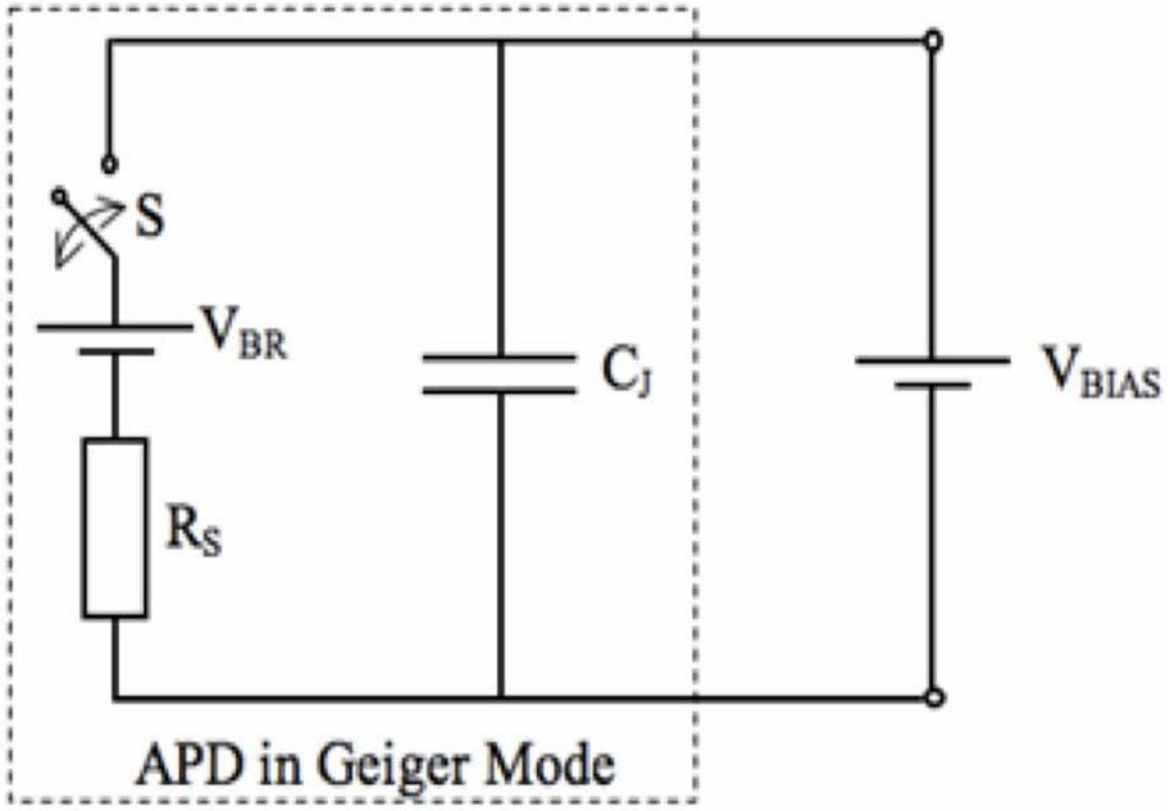

Equivalent circuit of an APD operating in Geiger mode. [III]

Geiger mode[2]

- Switch is open
- Cj is charged to bias voltage
- Bias voltage > Breakdown voltage.
- No current flowing

Front-End Board

Some of its functions are [3]**:**

- Amplifies and perform shaping of mppc output on each channel
- Performs digitization of signal amplitude for 32 channels
- Provides basic coincidence of signals from each pair of adjacent channels

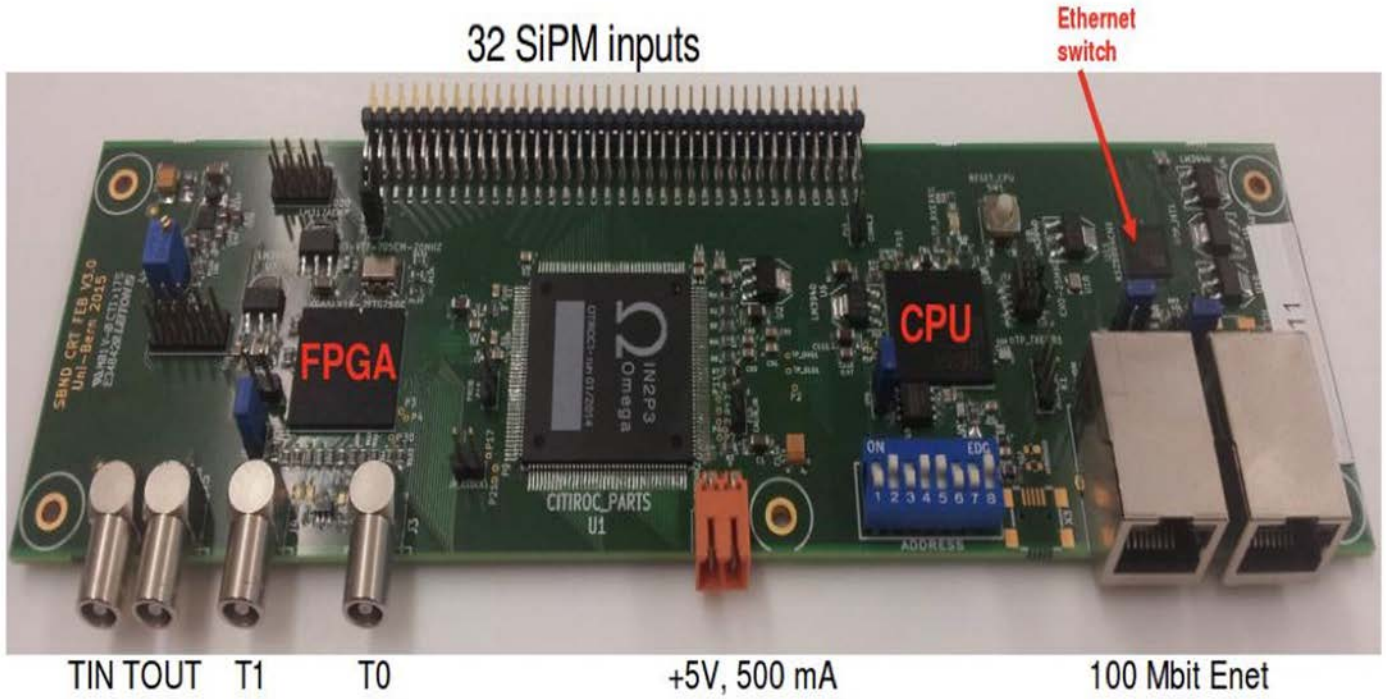

General View of the Front-End Board [IV]

DATA COLLECTION AND LIGHT DETECTION TESTS

- Ensure diodes are functioning for all SiPMs
- Create a baseline for all SiPMs
- Collect data for all SiPMs in dark conditions and with light
- Repeat all the steps increasing the bias voltage by 0.1V

LED Driver

Front-End Board

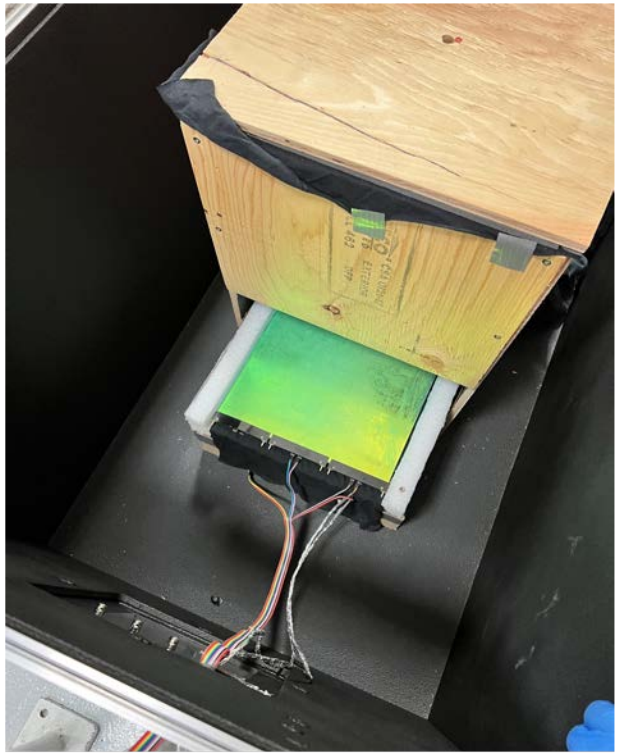

ArCLight

Light Detection Graph

Lorentzian fit to light peaks

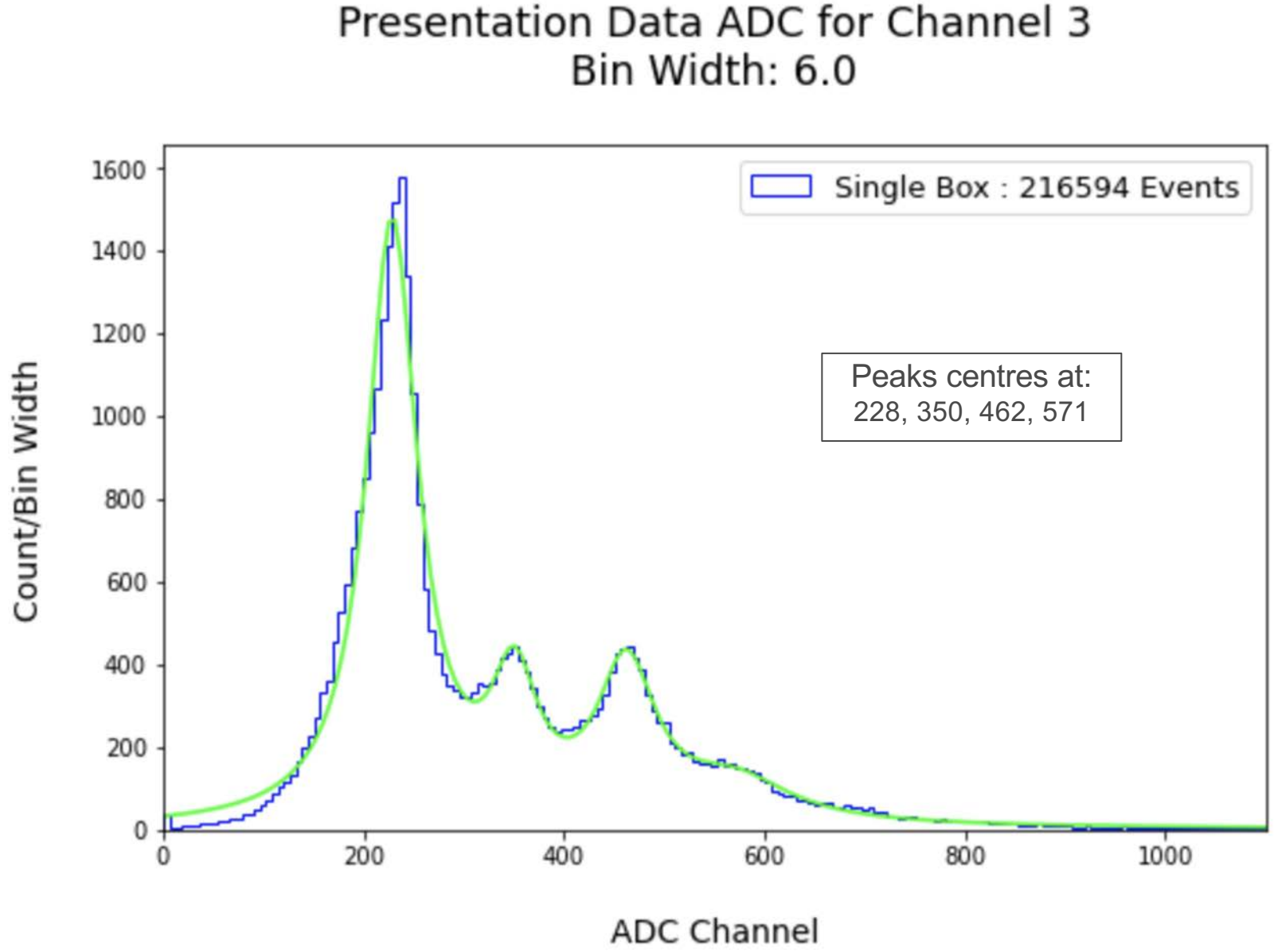

Data Analysis and Curve fitting Code

```
!pip install scipy
import scipy
from astropy.modeling.models import Lorentz1D
from scipy.optimize import curve_fit
```

✓ 8.2s

```
Requirement already satisfied: scipy in /opt/anaconda3/lib/python3.9/site-packages (1.7.3)
Requirement already satisfied: numpy<1.23.0,>=1.16.5 in /opt/anaconda3/lib/python3.9/site-packages (from scipy) (1.21.5)
```

```
filepath_l = "./light_1660242630_Light_56_8V.root"
filepath_nl = "./light_1660242376_NoLight_56_8V.root"
filepath_lt= "./light_1660242841_LightTrig_56_8V.root"

content_nl = uproot.open(filepath_nl)
content_l = uproot.open(filepath_l)
content_lt=uproot.open(filepath_lt)
print(content_nl.keys())
```

✓ 0.1s

```
['mppc;1']
```

```
data_nl = content_nl["mppc"]
data_l = content_l["mppc"]
data_lt= content_lt["mppc"]
data_nl.show()
```

✓ 0.8s

```
def _2Lorentzian(x, amp1, cen1, wid1, amp2,cen2,wid2,amp3, cen3, wid3,amp4,cen4,wid4):
    return (amp1*wid1**2/((x-cen1)**2+wid1**2)) +\
           (amp2*wid2**2/((x-cen2)**2+wid2**2)) +\
           (amp3*wid3**2/((x-cen3)**2+wid3**2))+\
              (amp4*wid4**2/((x-cen4)**2+wid4**2))

channel_names = [3, 30]
guess=[ 1600, 210, 10, 400, 370, 15, 400,470, 15,200,580,30]
for i in range(0, 2):
    bins = np.linspace(0, 3000, 500)
    counts, bins = np.histogram(nl_channels[i], bins= bins)
    bin_width = bins[2] - bins[1]
    fig = plt.figure(figsize=(8,6))
    y, b_x,z = plt.hist(bins[:-1], bins, weights=counts/bin_width, histtype="step", color='blue', label='Single Box : '+str(len(nl_channels[i]))+" Events")

    #counts, bins = np.histogram(nl_channels[i], bins=bins)
    #plt.hist(bins[:-1], bins, weights=counts/bin_width, histtype="step", color='b', label='Double Box: '+str(len(nl_channels[i]))+" Events")

    bin_centres = np.array((b_x[:-1] + b_x[1:])/2)

    plt.xlabel('\nADC Channel', fontsize=14)
    plt.ylabel('Count/Bin Width\n', fontsize=14)
    plt.title('Presentation Data ADC for Channel '+str(channel_names[i])+'\nBin Width: '+str(round(bin_width,1))+'\n', fontsize=18)
    plt.legend(loc='upper right', fontsize=13)
    plt.tight_layout()
    plt.xlim(0, 1100)
    #plt.yscale('log')


    coefficients, var = curve_fit(_2Lorentzian, bin_centres,y,p0= guess, maxfev=2000000)
    print(coefficients)
    print(np.sqrt(np.diag(var))[1])
    lorentzian = _2Lorentzian(bin_centres, *coefficients)
    plt.plot(bin_centres,lorentzian,color='lime')
    plt.show()
```

What I've gained from the lab experience

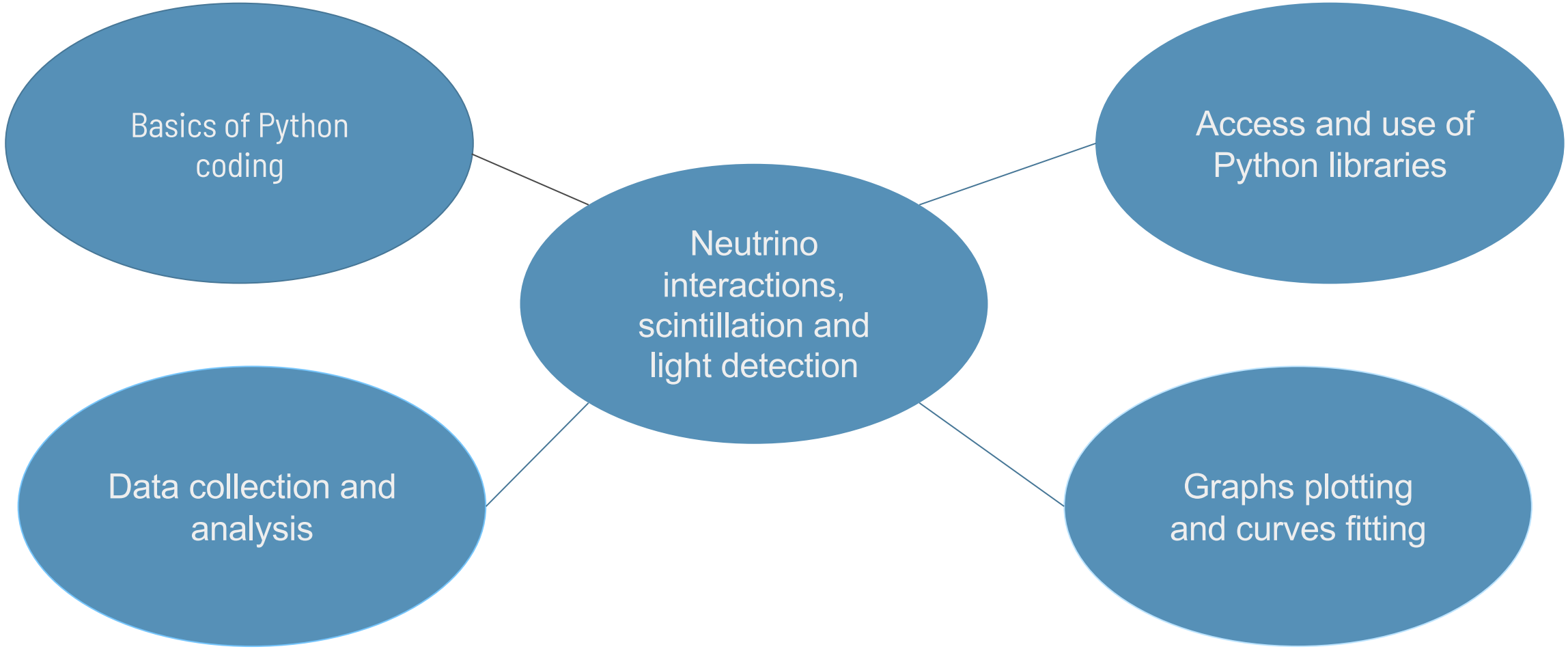

Acknowledgements

- ***Professor A. Ereditato***, Visiting Professor at Yale University
- ***ONAOSI Foundation***
- ***Domenico Franco***, Research Scientist at Yale University
- ***Angela White*** and ***Matt King***, Phd students at Yale University
- **Poshu Ng**, High School Intern
- The ONAOSI-YALE Programme **Students**

Onaosi-Yale Programme Students

FONDAZIONE ONAOSI

Yale University

Bibliography

1: Arclight- a compact dielectric Large-Area Photon Detector: M.Auger, Y. Chen, A.Ereditato, D. Goeldi, I. Kreslo, D. Lorca, M. Luethi, T. Mettler, J. R. Sinclair, and M.S. Weber
2: Measuring the electrical and optical properties of silicon multipliers
3: Multi-channel front-endboard for SiPM readout: M.Auger, A.Ereditato, D. Goeldi, I. Kreslo, M. Luethi, T. Mettler, C. Rudolf von Rohr, J. R. Sinclair, and M.S. Weber

Images

I: Arclight- a compact dielectric Large-Area Photon Detector: M.Auger, Y. Chen, A.Ereditato, D. Goeldi, I. Kreslo, D. Lorca, M. Luethi, T. Mettler, J. R. Sinclair, and M.S. Weber
II: Arclight- a compact dielectric Large-Area Photon Detector: M.Auger, Y. Chen, A.Ereditato, D. Goeldi, I. Kreslo, D. Lorca, M. Luethi, T. Mettler, J. R. Sinclair, and M.S. Weber
III: Measuring the electrical and optical properties of silicon multipliers
IV: Multi-channel front-endboard for SiPM readout: M.Auger, A.Ereditato, D. Goeldi, I. Kreslo, M. Luethi, T. Mettler, C. Rudolf von Rohr, J. R. Sinclair, and M.S. Weber

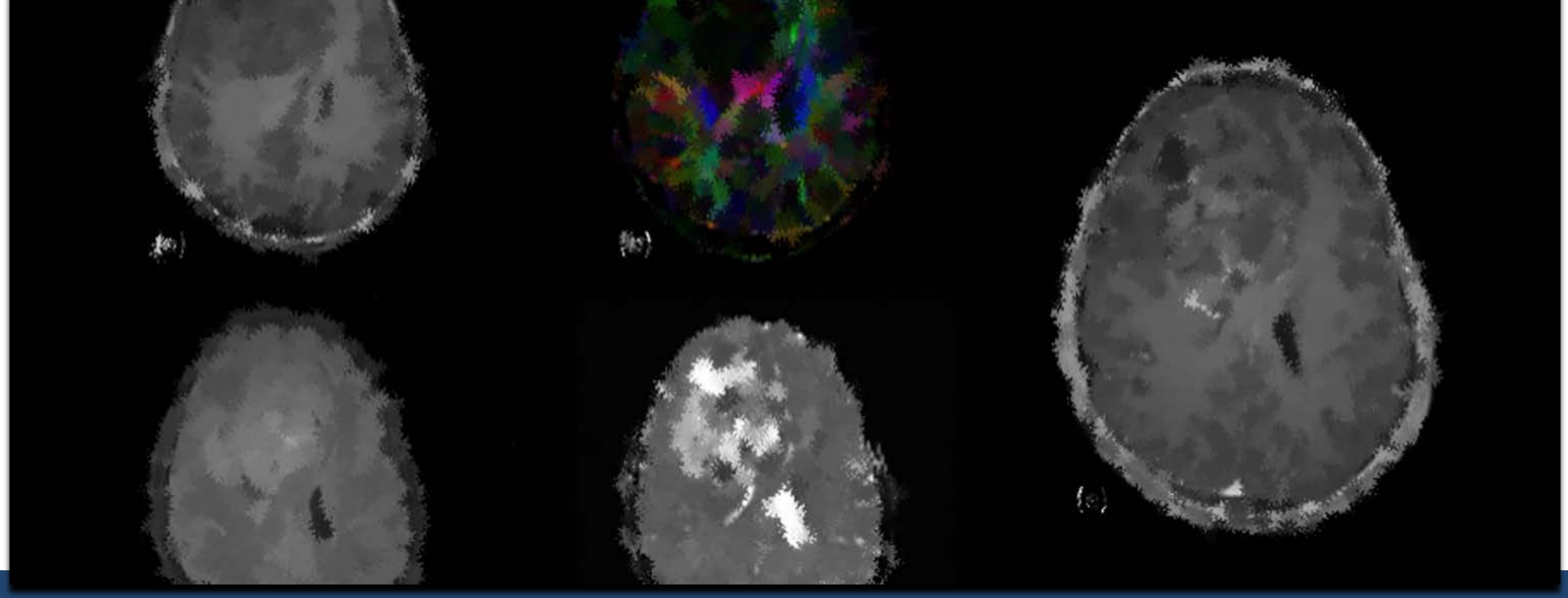

Advanced Imaging of Brain Tumors

Lodovico Balzoni, Department of Neuroradiology and Nuclear Medicine

August 18th, 2022

Yale SCHOOL OF MEDICINE

Types of classifications

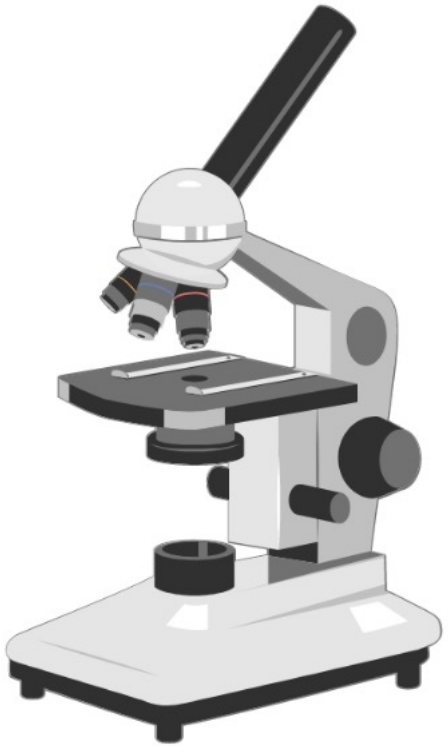

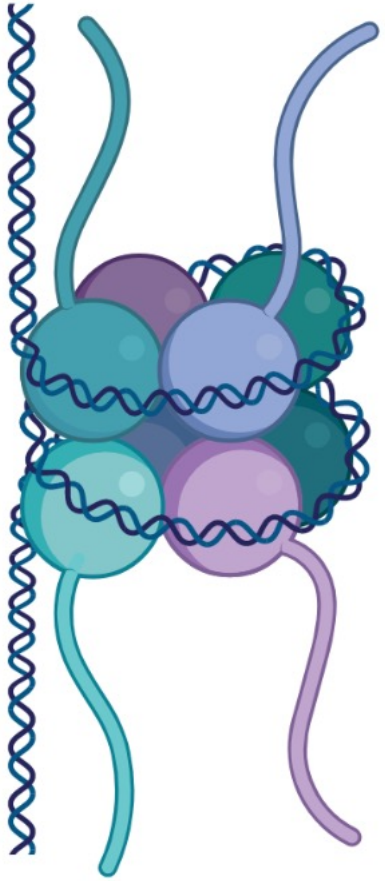

PNETs

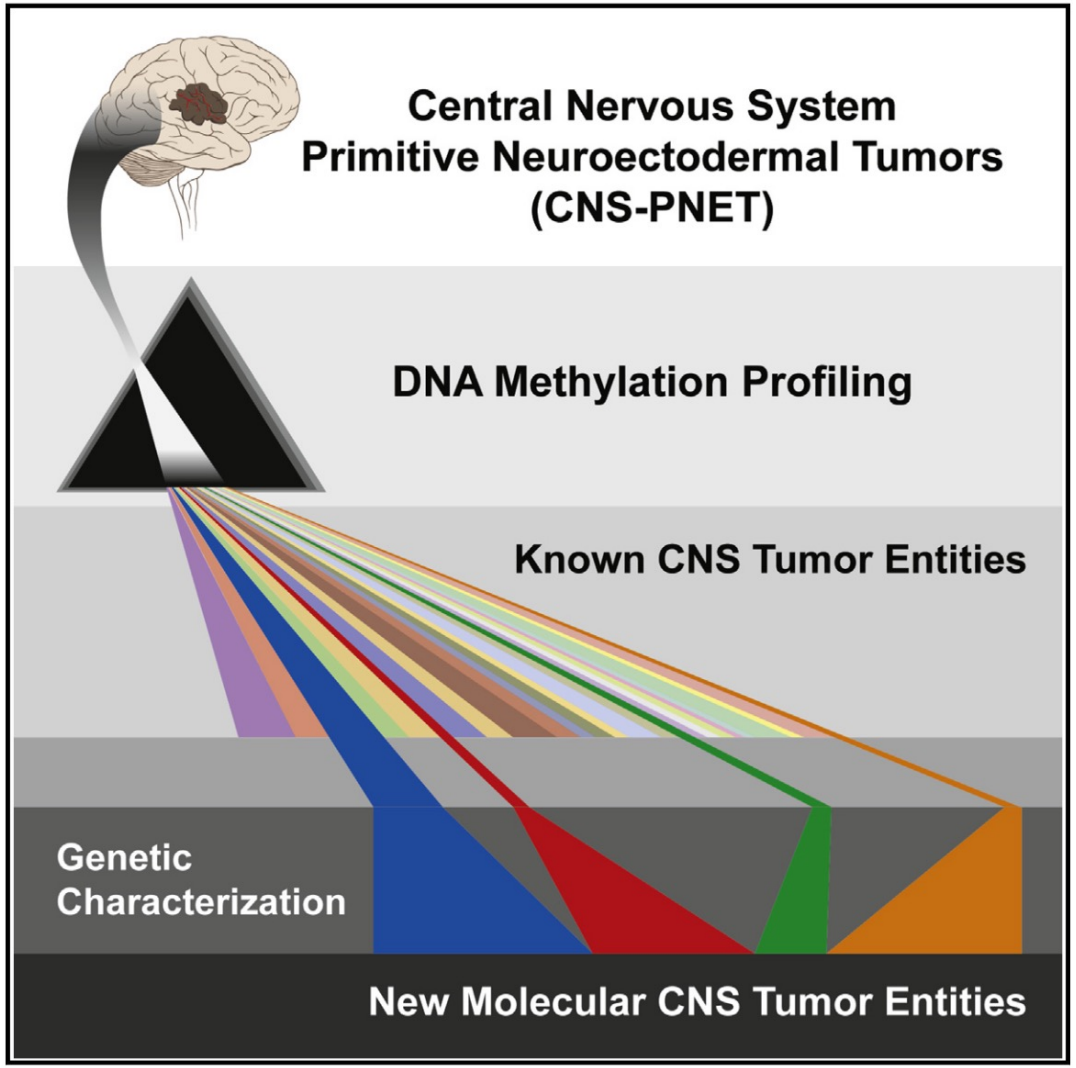

Sturm D, Orr BA, Toprak UH, Hovestadt V, Jones DTW, Capper D, et al. New Brain Tumor Entities Emerge from Molecular Classification of CNS-PNETs. Cell. 2016;164:1060-72.

MRI physics

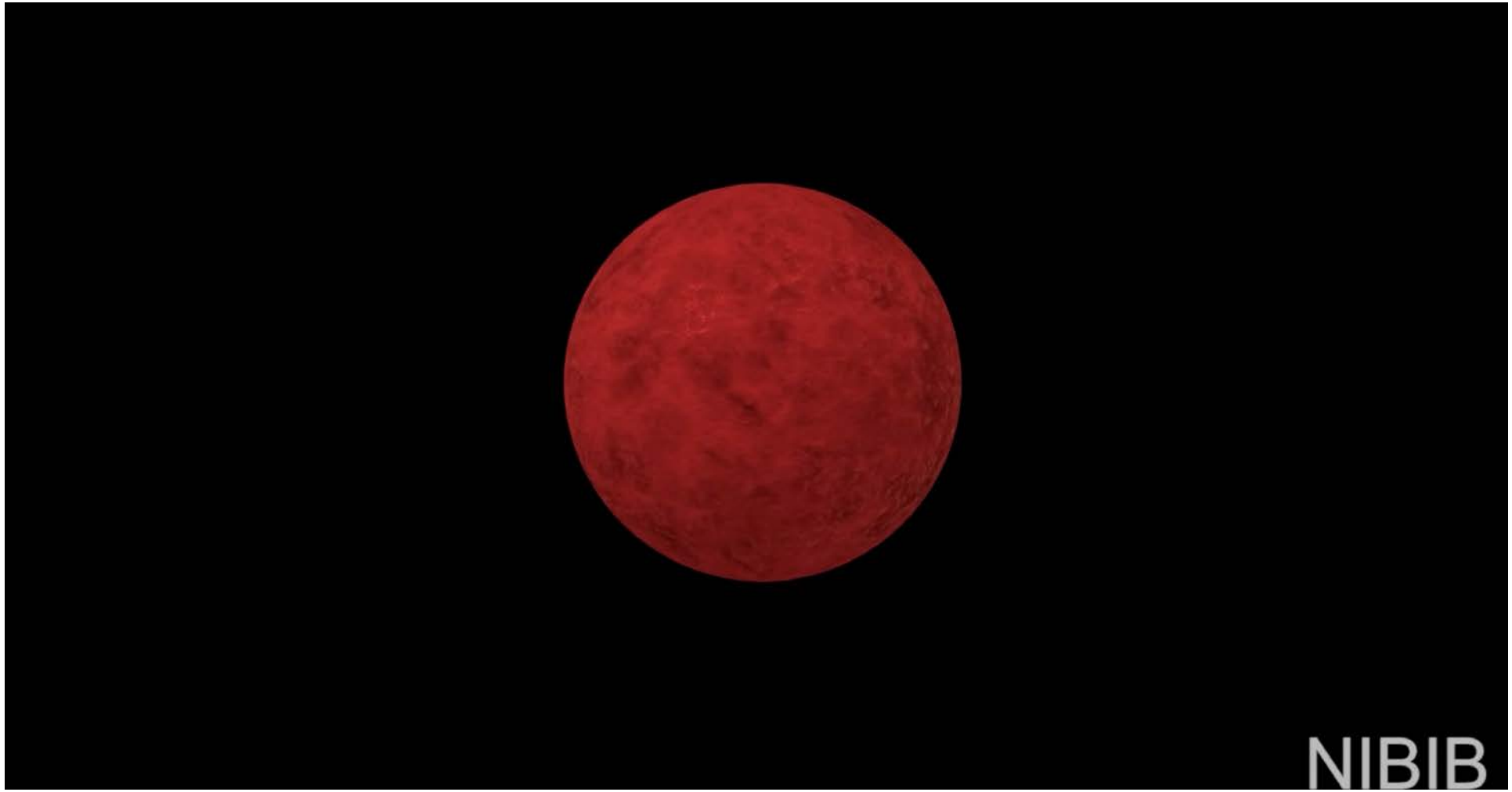

MN1-mutated astroblastoma: case presentation

Healthy,

9 y.o. girl

T1 is used for:

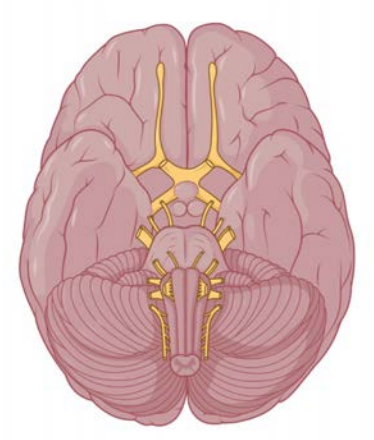

Anatomic details

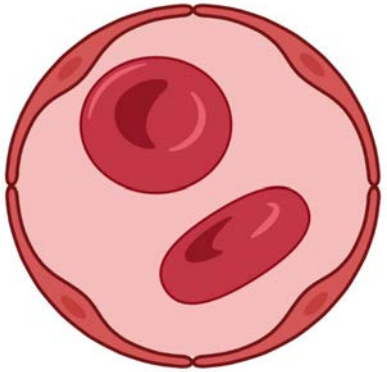

Vascular changes

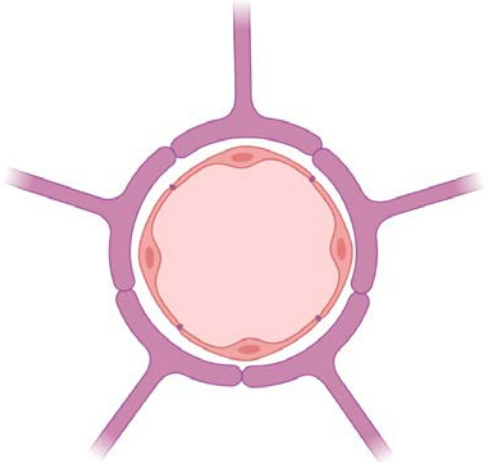

Blood brain barrier disurption

With contrast

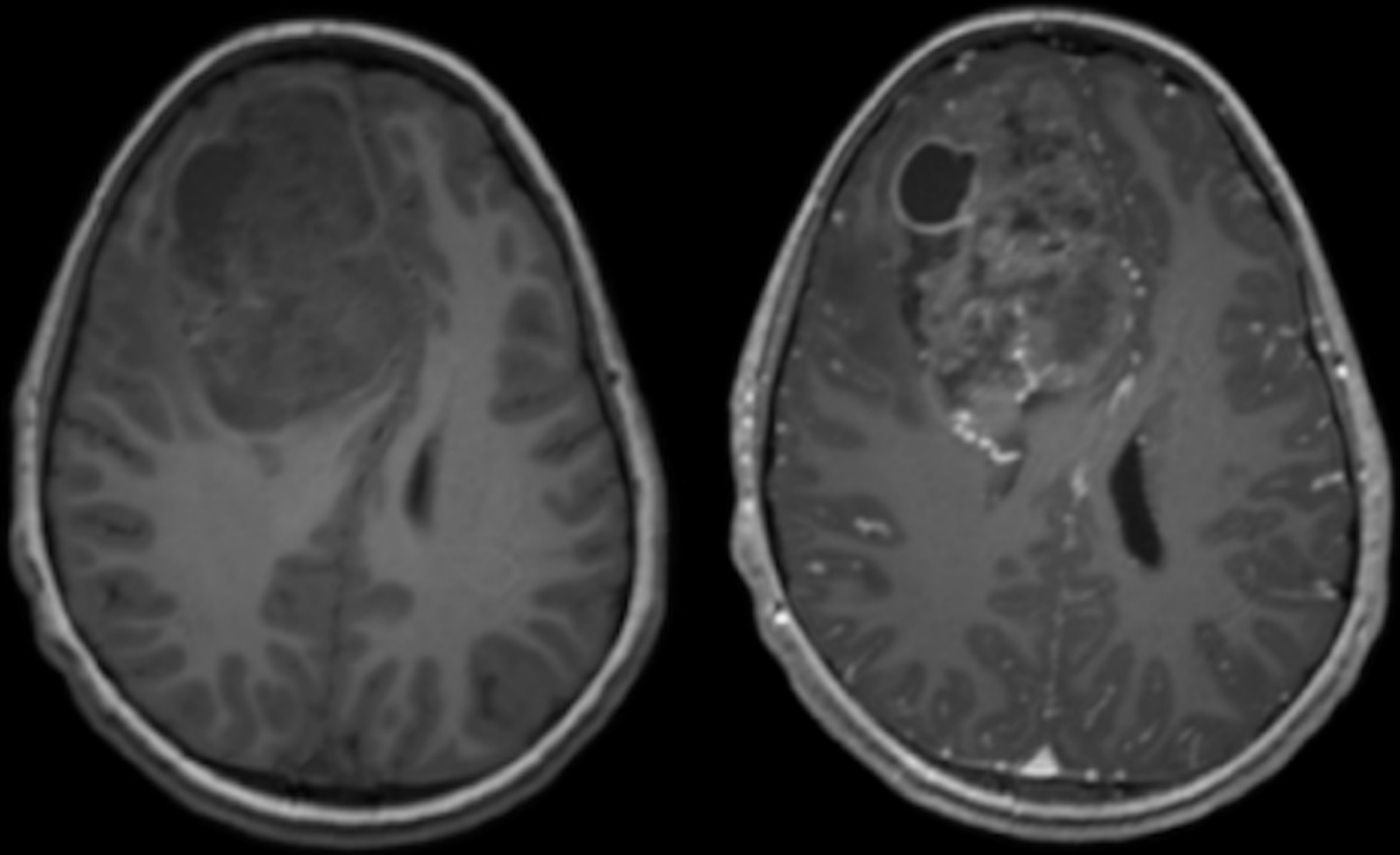

T1

Gadolinium-enhanced T1

T2 is used for:

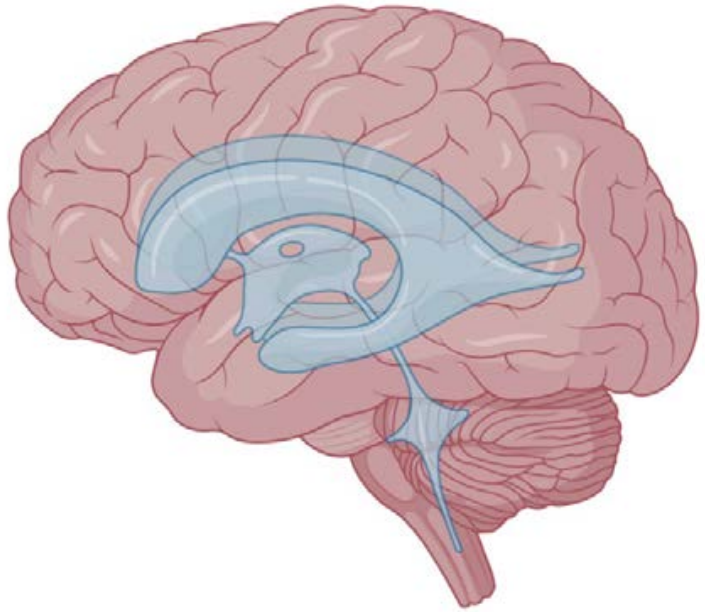

Anatomic details (CSF)

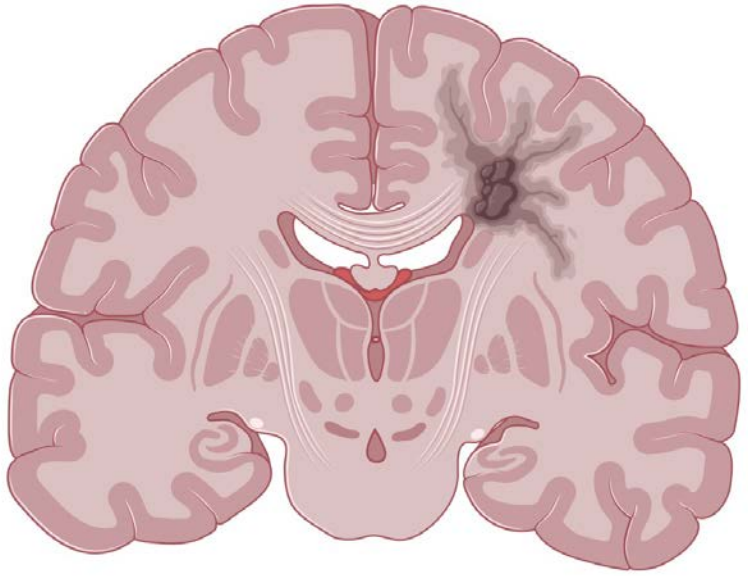

Most lesions

But it cannot distinguish lesions from CSF

FLAIR is used for:

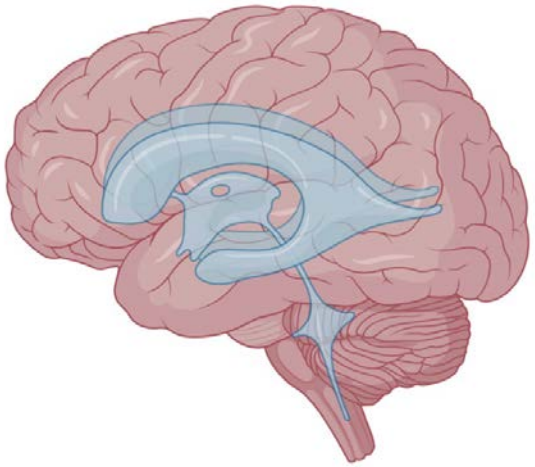

Lesions near ventricles

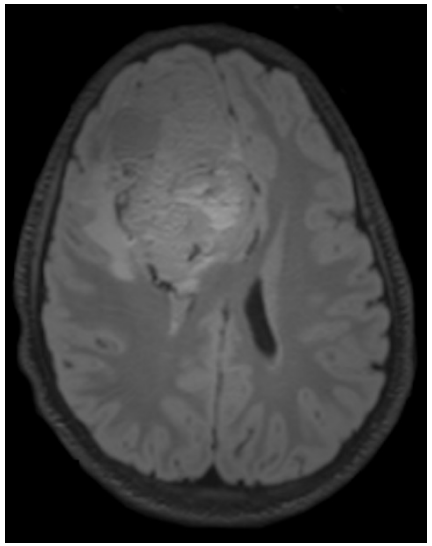

Edema

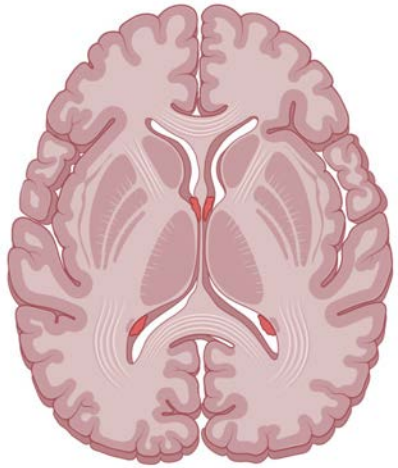

Grey white matter differentiation

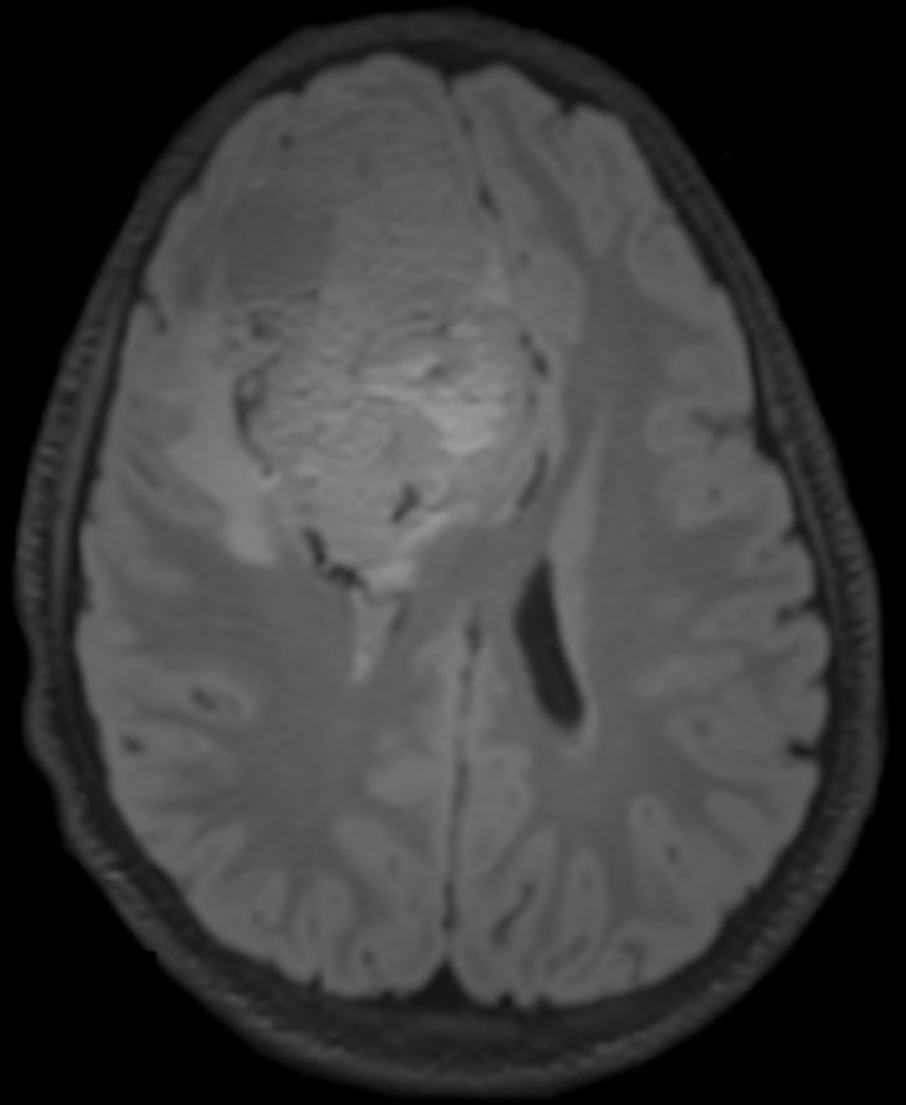

FLAIR

What makes it difficult for water to move?

Packed cells from a highly cellular tumor

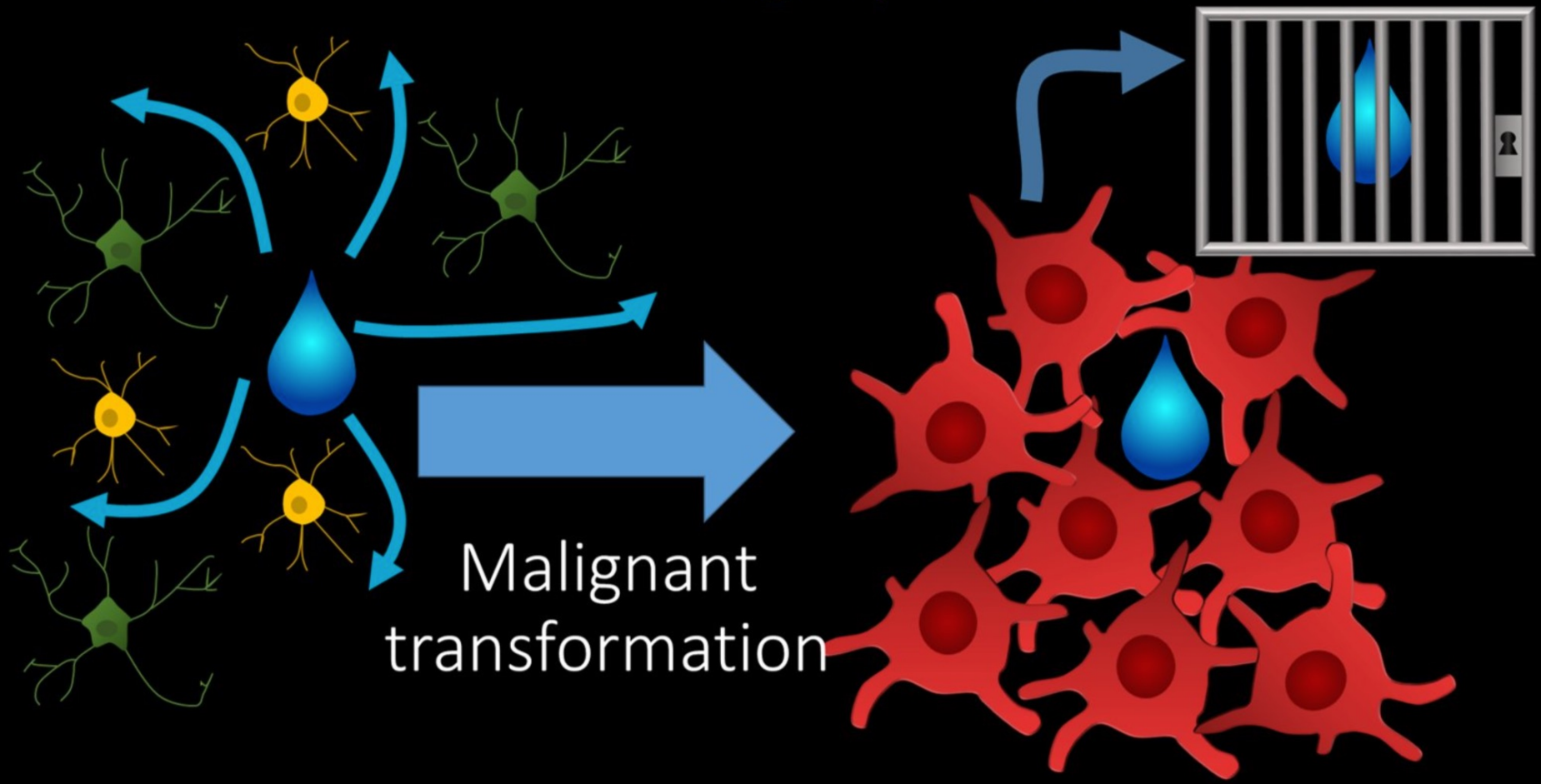

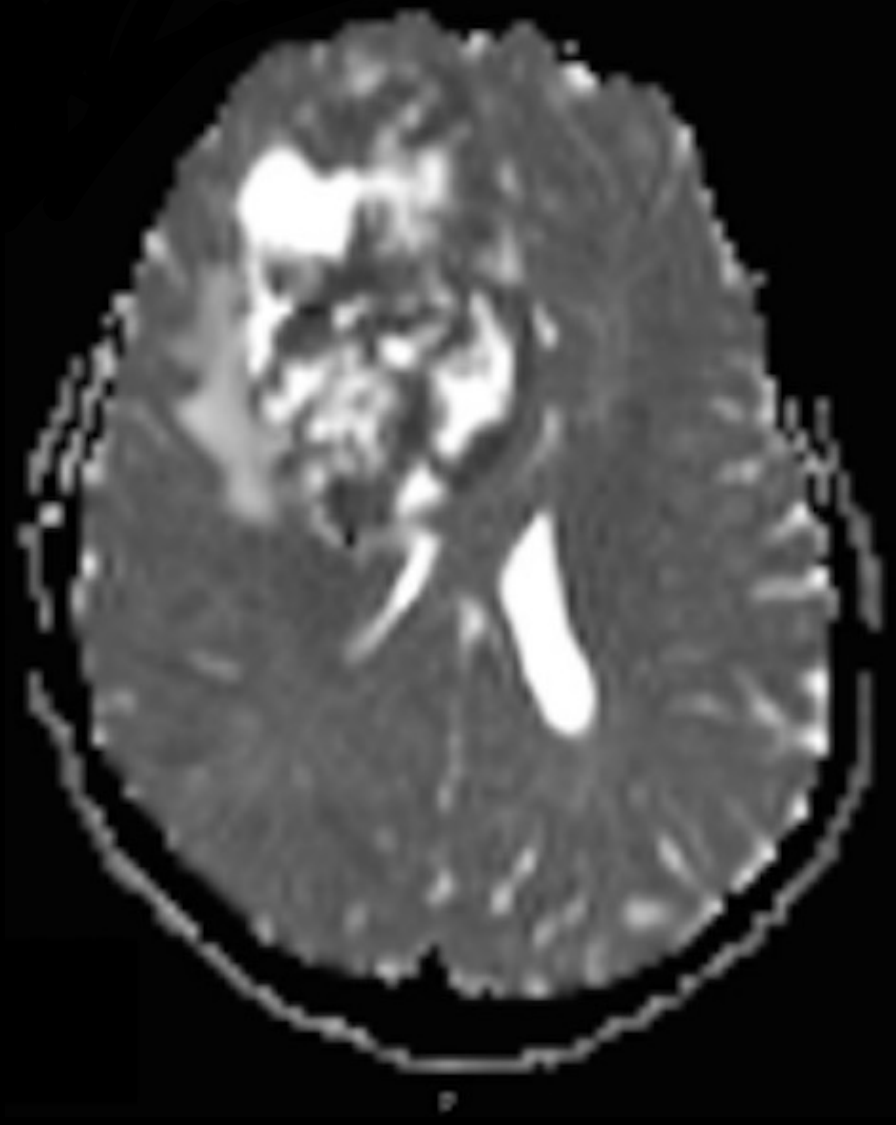

DWI-ADC

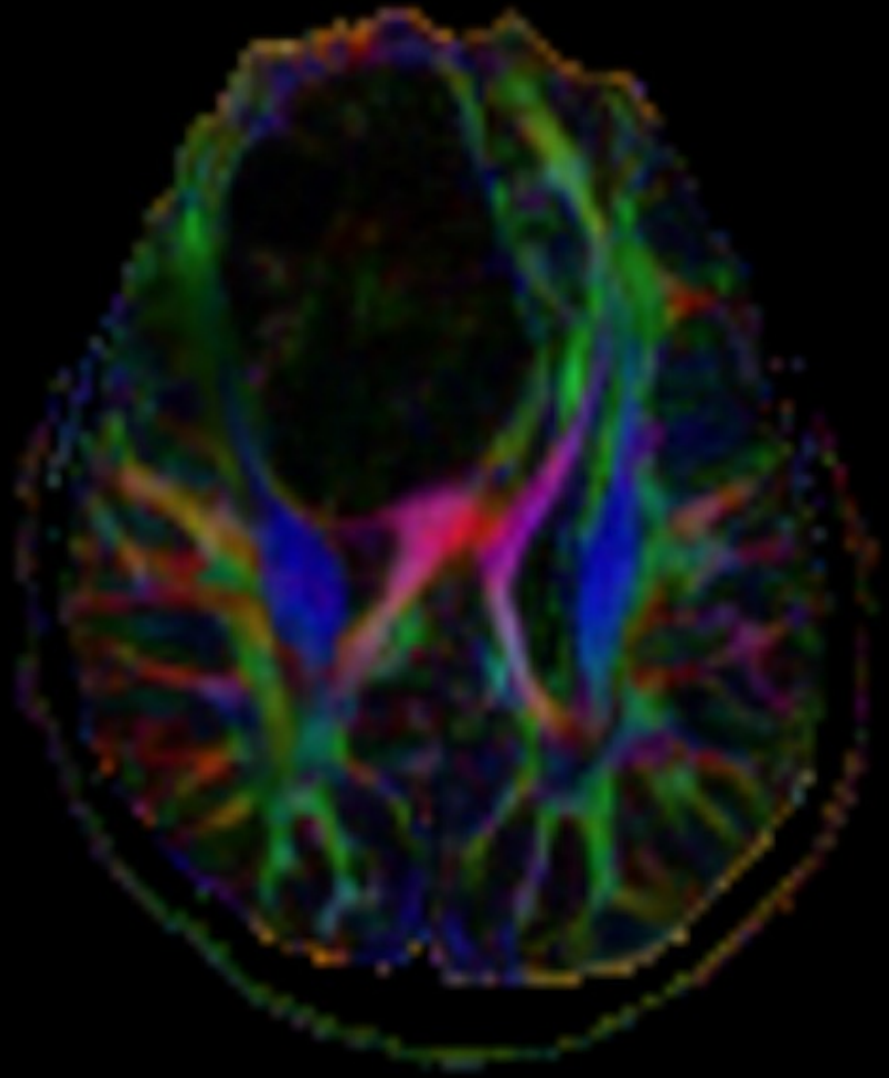

Tractography

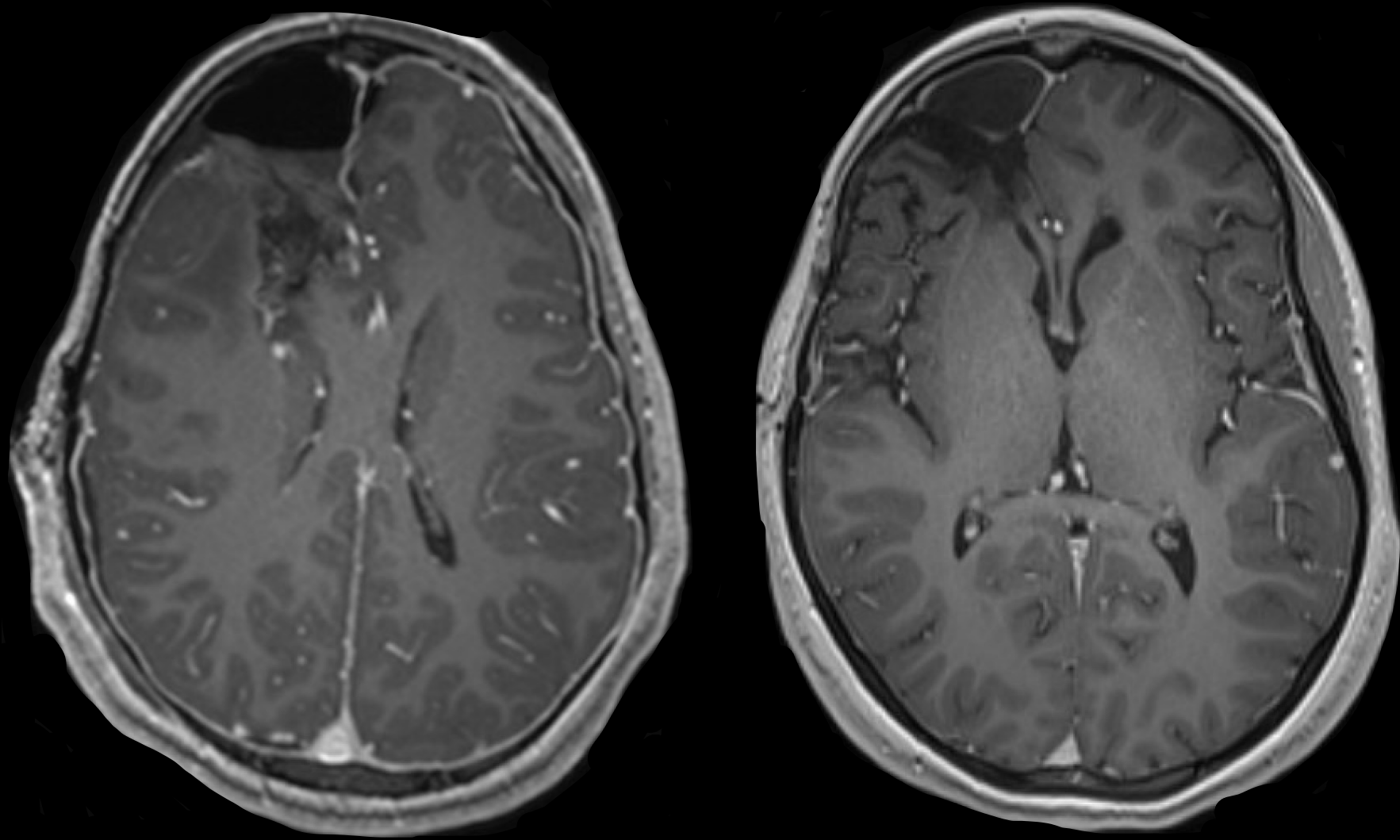

Right after surgery

3 years and 6 months
after diagnosis

Conclusions and future perspectives

Aggressive features do not necessarily correlate with aggressive behavior.

Histologic and imaging features combined with molecular and epigenetic profiles would allow more clear classification and prognosis, thus favoring individualized therapy.

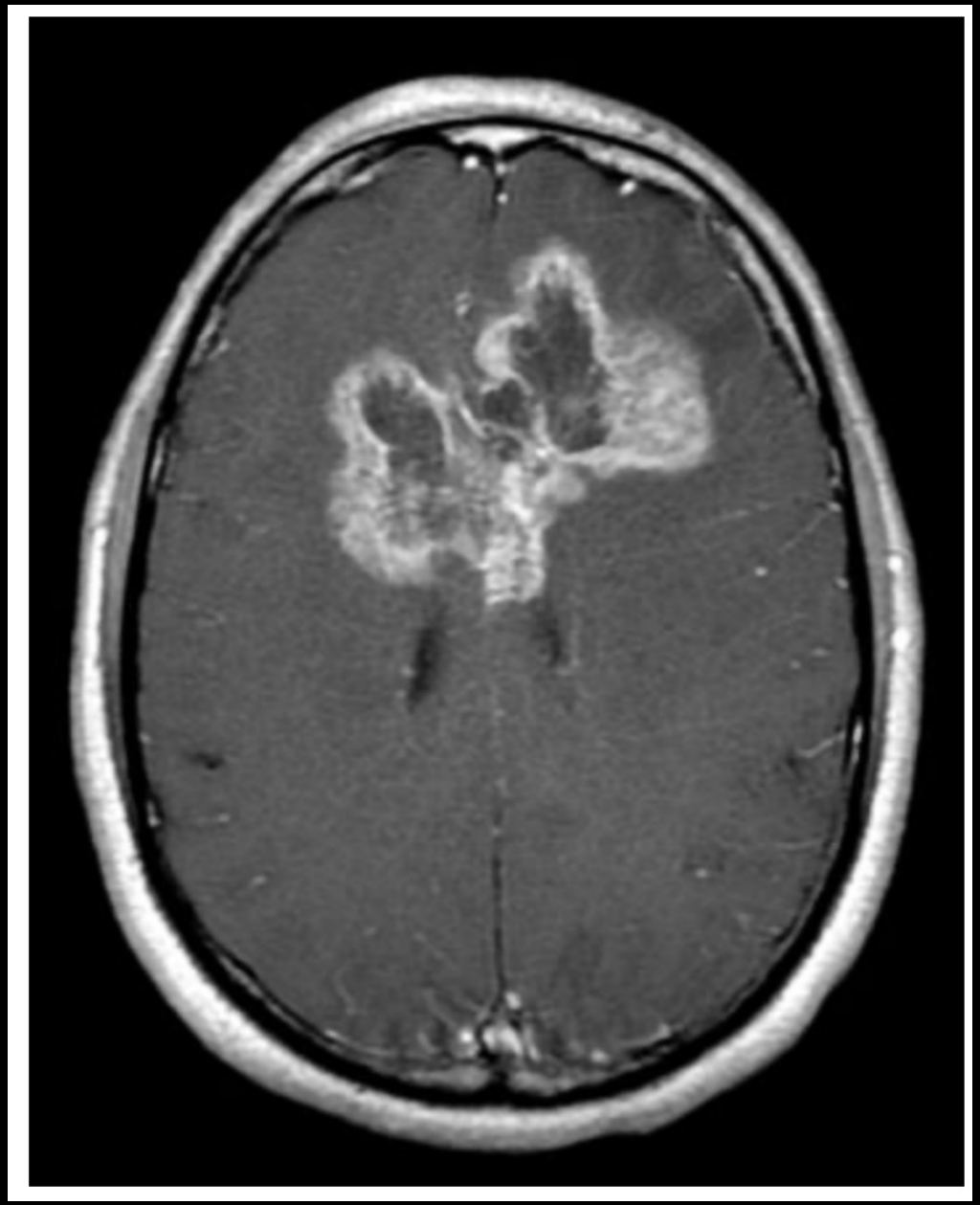

Case 1

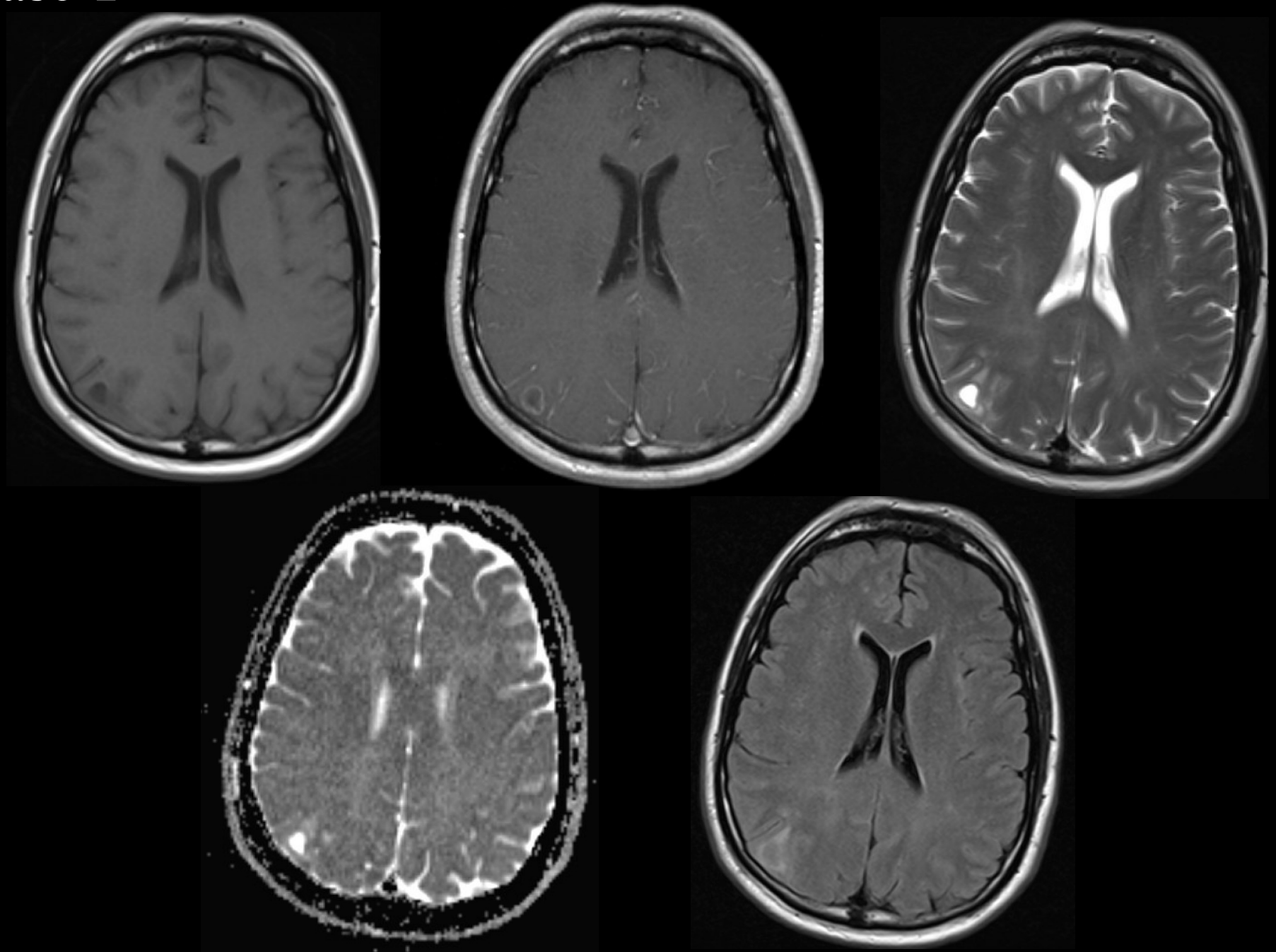

Last followup case 1

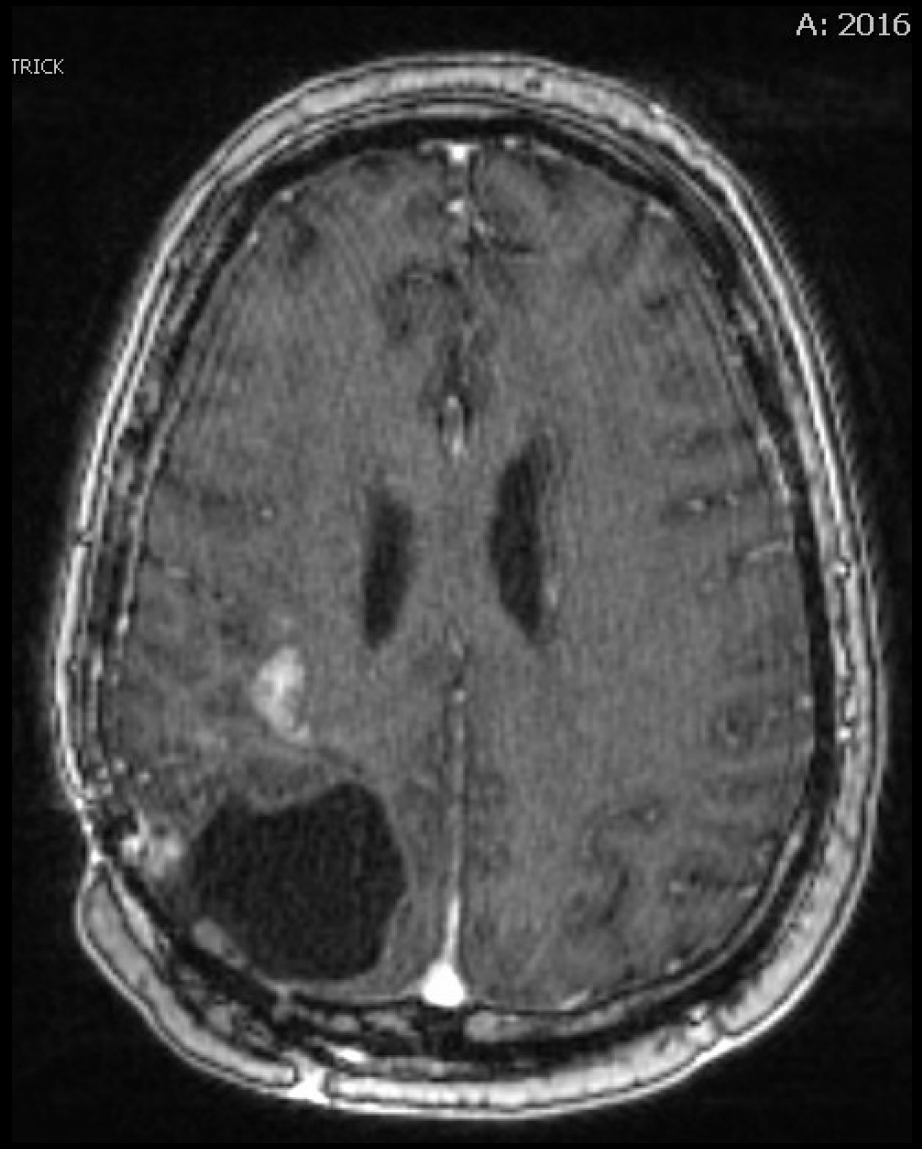

Case 2

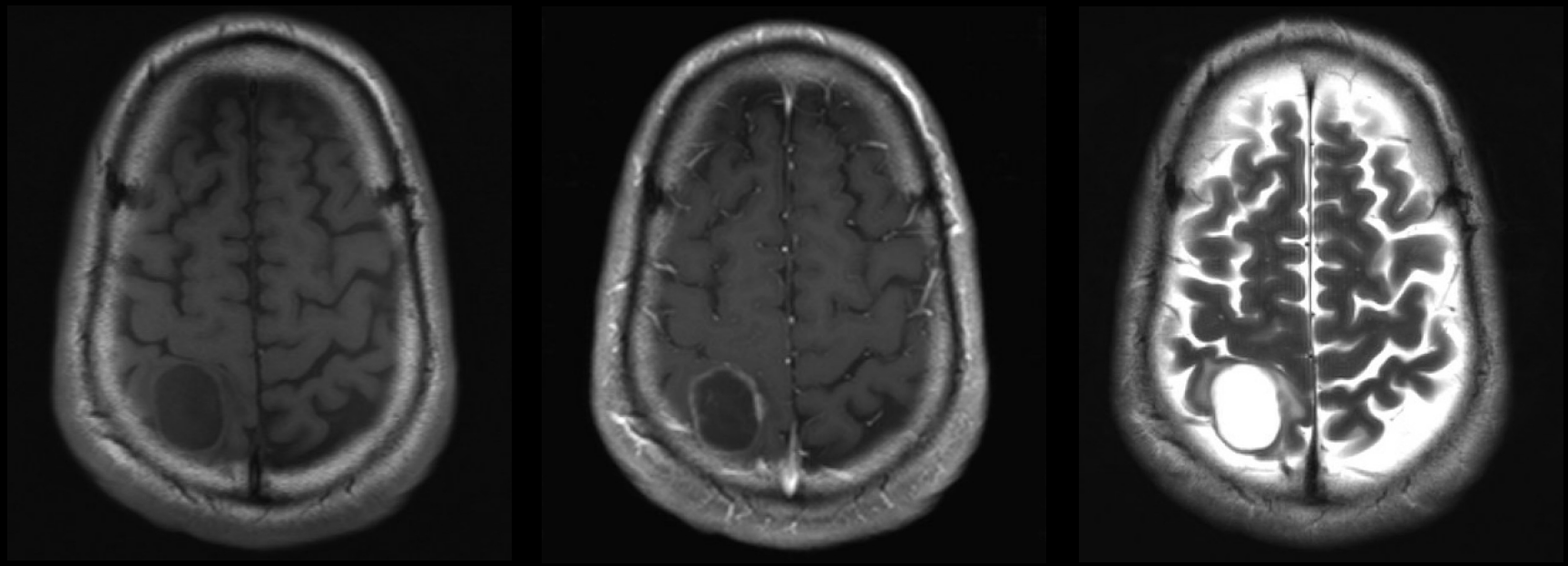

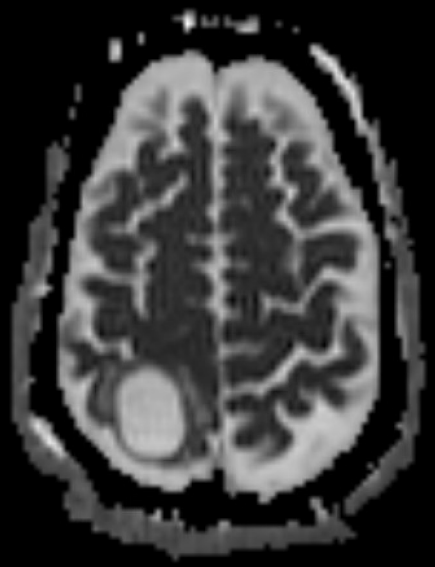

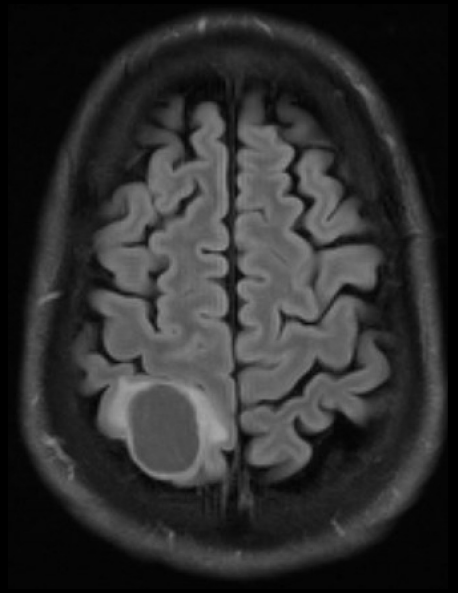

Last followup case 2

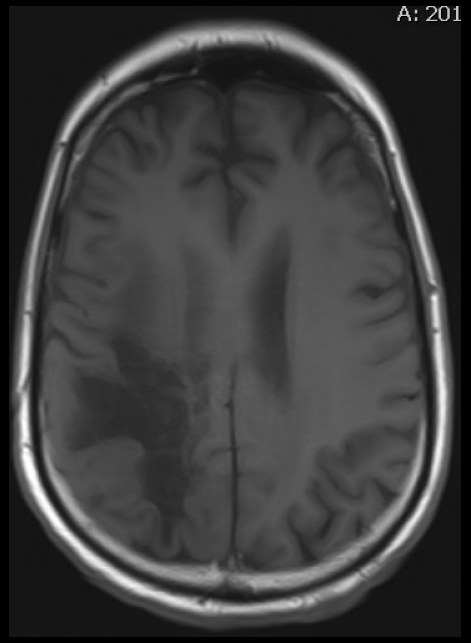

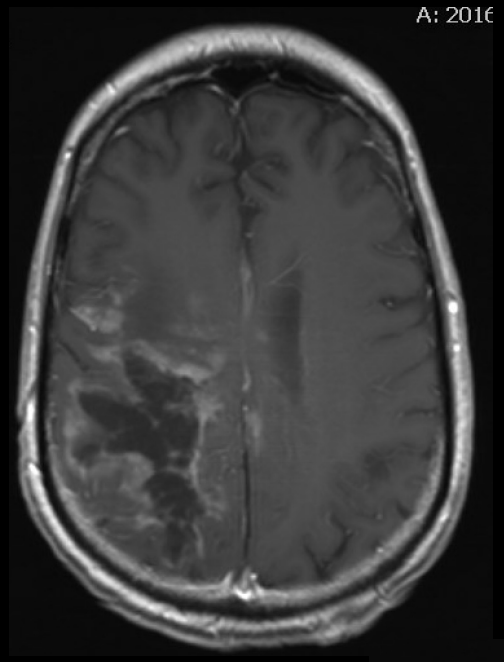

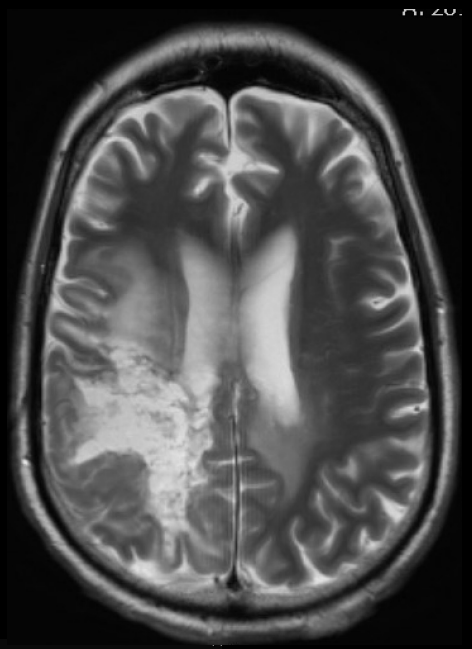

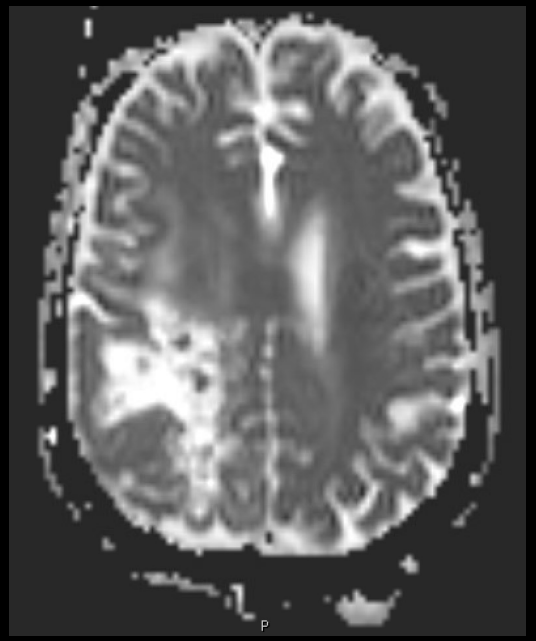

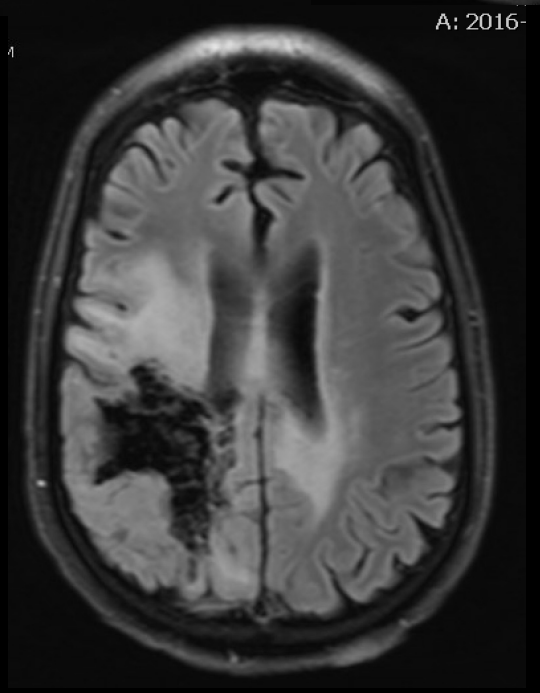

Case 3

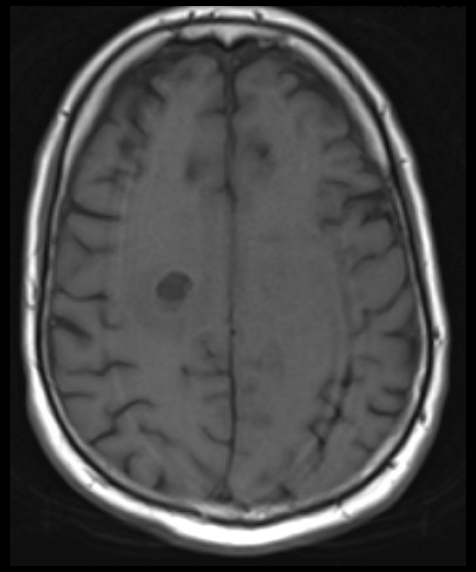
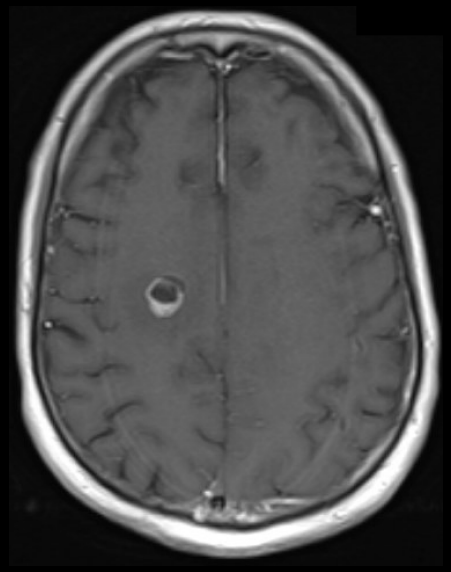
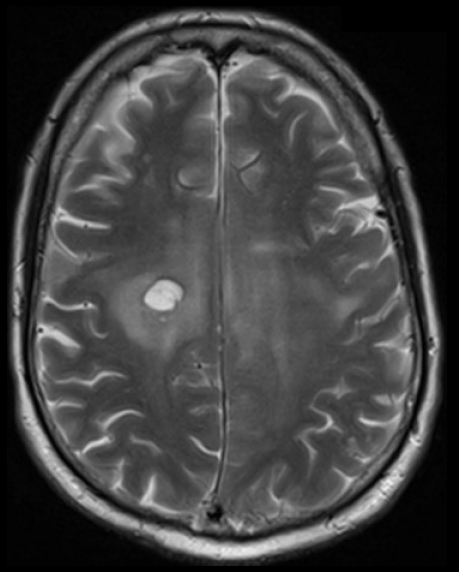
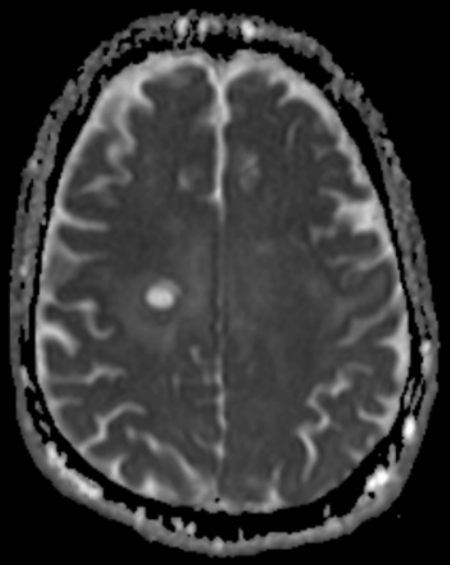
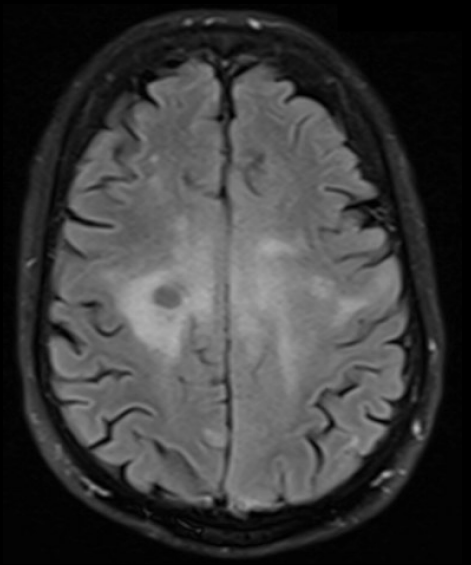

Last followup case 3

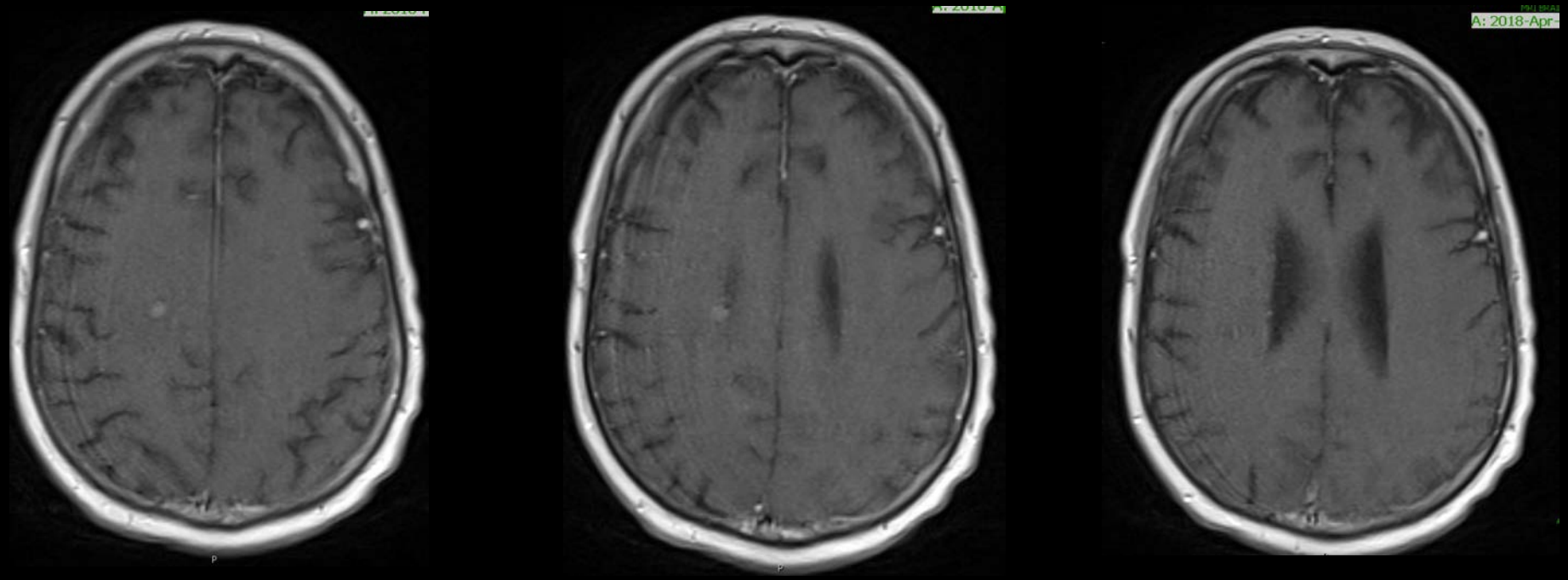

Case 4

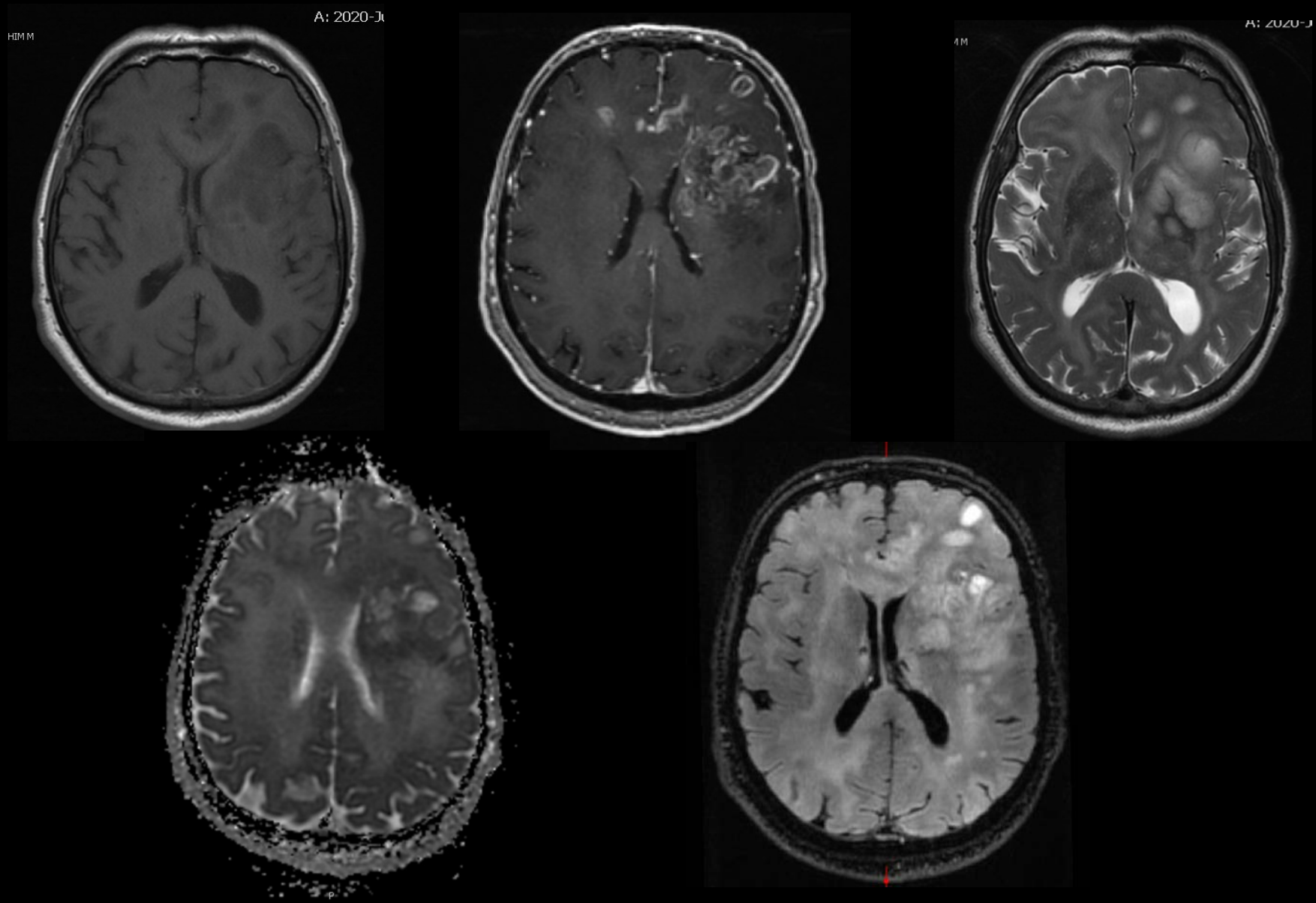

Case 5

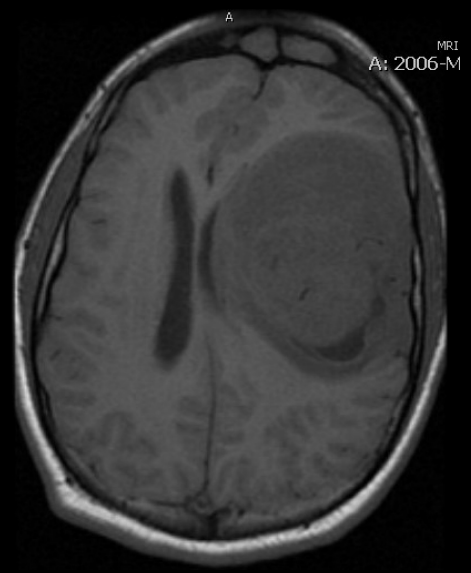

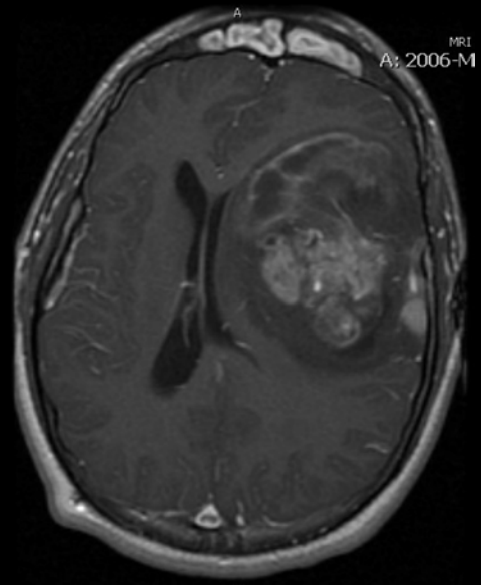

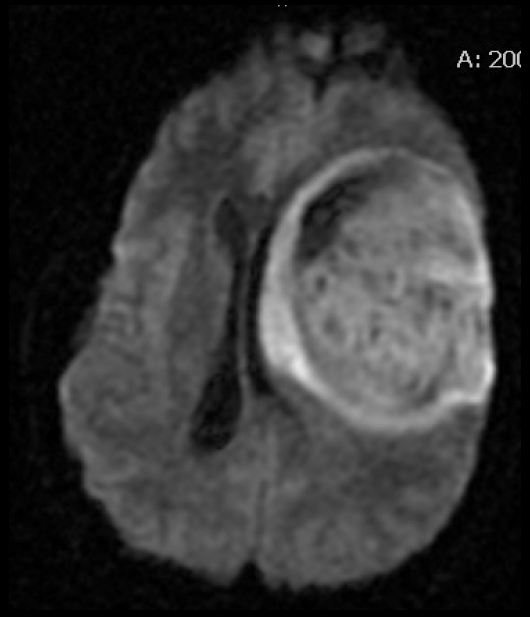

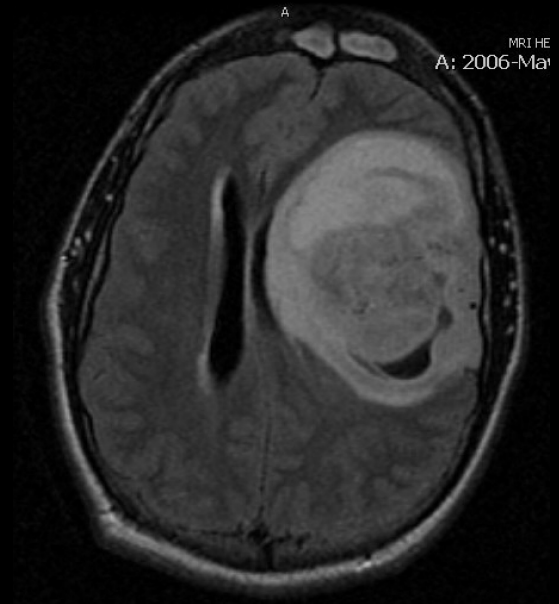

Last followup case 5

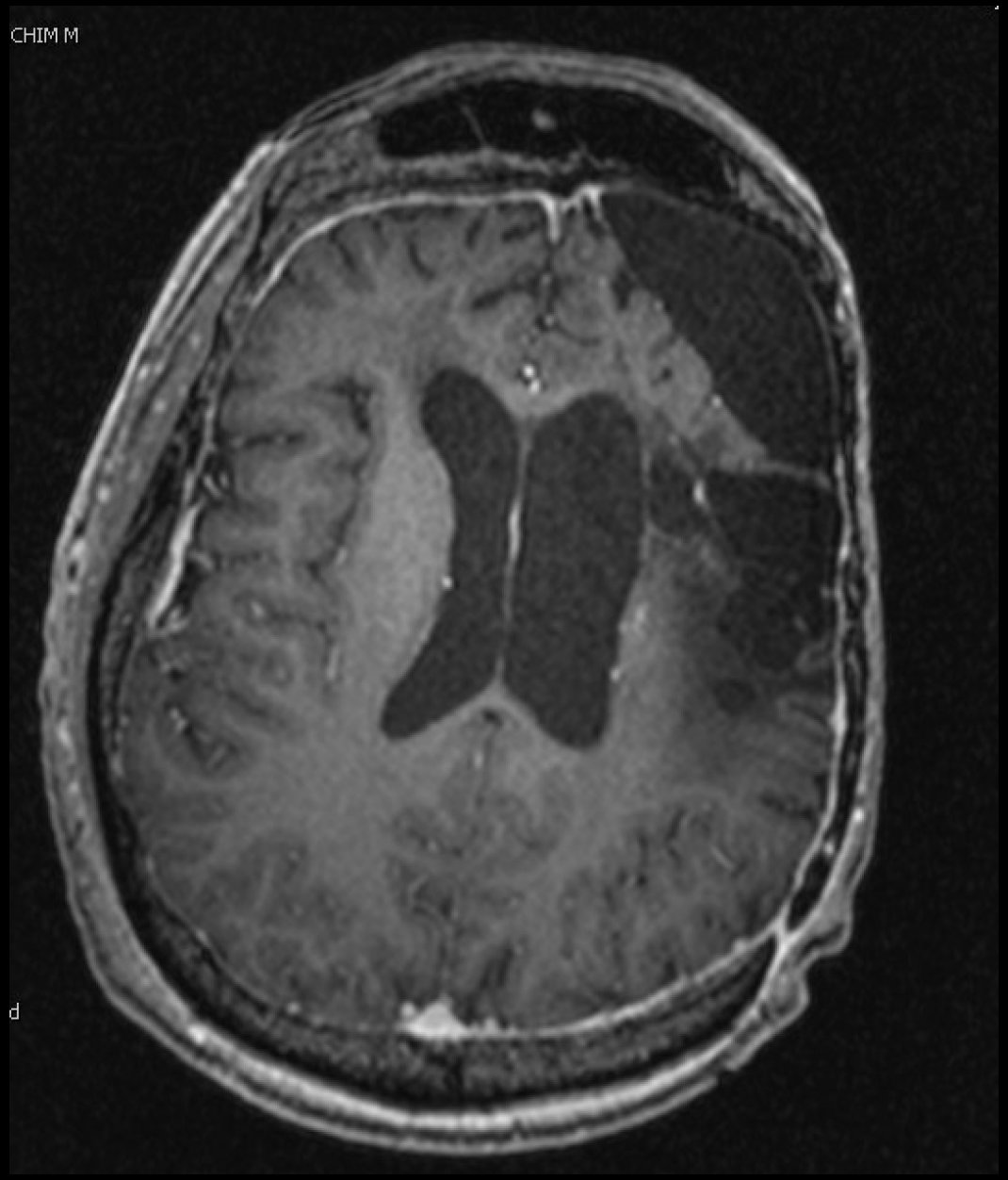

Conclusions

- Not all PNETs are the same and current classification of brain tumors requires better understanding of imaging features;
- PNETs are a specific subtype of brain tumors that are now classified based on epigenetic modficination but mutations play a role in classes such MN1 mutation;
- GBMs with PNET features have specific imaging features which may help in suggesting diagnosis;
- Gross total resection is the most important factor in predicting prognosis.

Introduction to Synthetic MRI

In brief:

In synthetic MRI, images are generated from quantitative tissue properties, which are derived from one single acquisition.

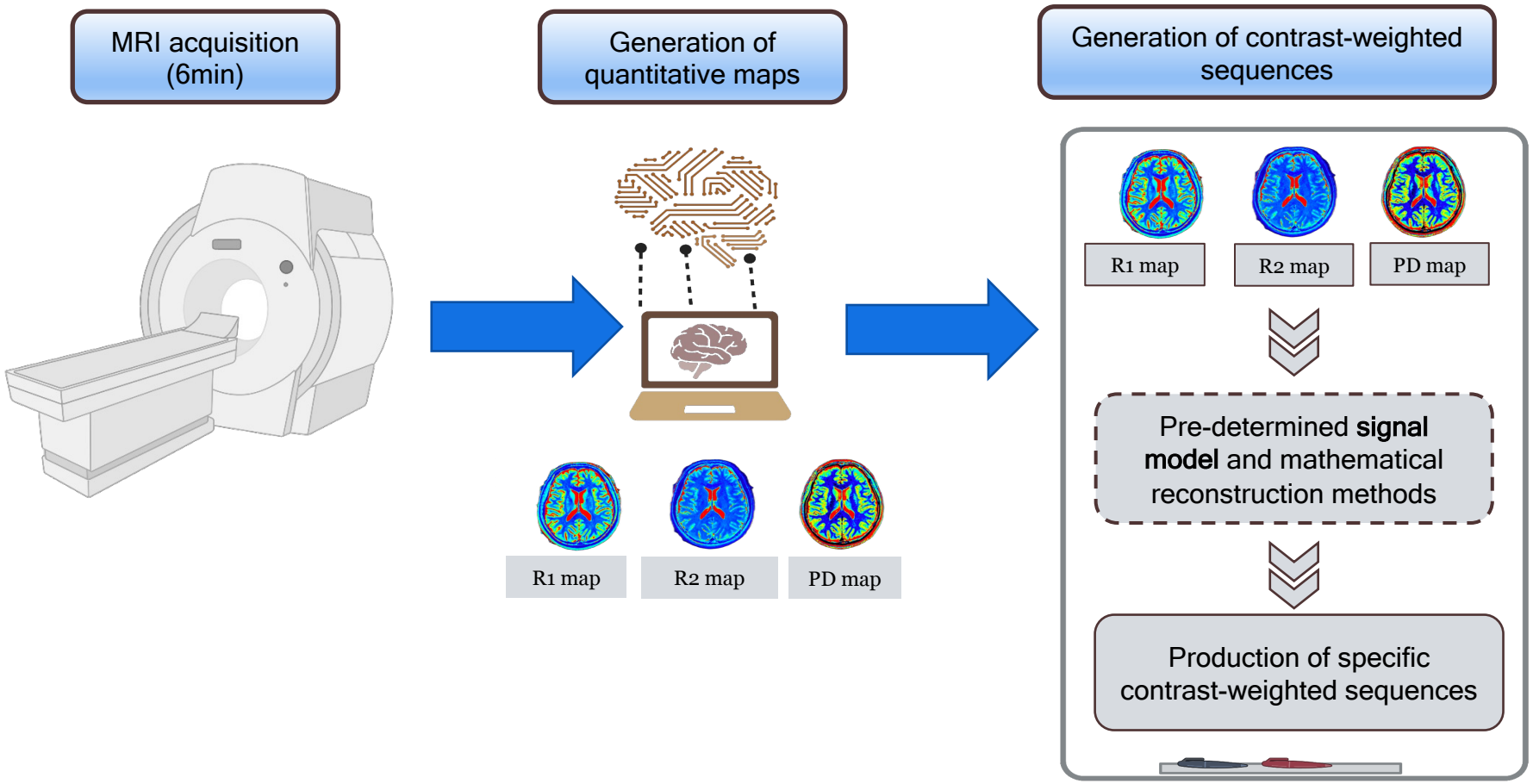

Figures adapted from:

Gonçalves, F. G., Serai, S. D., & Zuccoli, G. (2018). Synthetic brain MRI: Review of current concepts and future directions. In Topics in Magnetic Resonance Imaging (Vol. 27, Issue 6, pp. 387–393). Lippincott Williams and Wilkins.

Ji, S., Yang, D., Lee, J., Choi, S. H., Kim, H., & Kang, K. M. (2020). Synthetic MRI: Technologies and Applications in Neuroradiology. In *Journal of Magnetic Resonance Imaging*. John Wiley and Sons Inc.

Data analysis

	Standard sequences	STAGE sequences
Number of cases where Swallow tail sign is visible	2/18 bilateral 2/18 unilateral	17/21 2/21 bilateral
Number of cases where Subthalamic nucleus is visible	3/18	19/21
Number of cases where T1 sequence was preferred	8/21	13/21
Number of cases where T2 sequence was preferred	21/21	0/21
Number of cases where SWI sequences was preferred	0/21	21/21
Number of microbleeds reported	3/21	21/21

Conclusions

Patients need uniform and rapid imaging protocols for standardization of features extraction:

- Highly variable protocols in clinical practice prevent innovation in fields such as AI;
- STAGE is a consistent and rapid way of acquiring sequences, although improvements are necessary to allow clinical use.

References (1)

1. Burel-Vandenbos F, Pierron G, Thomas C, Reynaud S, Gregoire V, Duhil de Benaze G, et al. A polyphenotypic malignant paediatric brain tumour presenting a MN1-PATZ1 fusion, no epigenetic similarities with CNS High-Grade Neuroepithelial Tumour with MN1 Alteration (CNS HGNET-MN1) and related to PATZ1-fused sarcomas. Neuropathol Appl Neurobiol. 2020;46:506-9.
2. Sturm D, Orr BA, Toprak UH, Hovestadt V, Jones DTW, Capper D, et al. New Brain Tumor Entities Emerge from Molecular Classification of CNS-PNETs. Cell. 2016;164:1060-72.
3. Louis DN, Perry A, Wesseling P, Brat DJ, Cree IA, Figarella-Branger D, et al. The 2021 WHO Classification of Tumors of the Central Nervous System: a summary. Neuro-Oncol. 2021;23:1231-51.
4. Ujihara M, Mishima K, Sasaki A, Adach J-I, Shirahata M, Suzuki T, et al. Unique pathological findings of astroblastoma with MN1 alteration in a patient with late recurrence. Brain Tumor Pathol. 2021;38:243-9.
5. Tauziède-Espariat A, Pagès M, Roux A, Siegfried A, Uro-Coste E, Nicaise Y, et al. Pediatric methylation class HGNET-MN1: unresolved issues with terminology and grading. Acta Neuropathol Commun. 2019;7:176.
6. Horbinski C, Nikiforova MN, Hagenkord JM, Hamilton RL, Pollack IF. Interplay among BRAF, p16, p53, and MIB1 in pediatric low-grade gliomas. Neuro-Oncol. 2012;14:777-89.
7. Lassaletta A, Zapotocky M, Mistry M, Ramaswamy V, Honnorat M, Krishnatry R, et al. Therapeutic and Prognostic Implications of BRAF V600E in Pediatric Low-Grade Gliomas. J Clin Oncol Off J Am Soc Clin Oncol. 2017;35:2934-41.
8. Dias-Santagata D, Lam Q, Vernovsky K, Vena N, Lennerz JK, Borger DR, et al. BRAF V600E mutations are common in pleomorphic xanthoastrocytoma: diagnostic and therapeutic implications. PloS One. 2011;6:e17948.
9. Jones DTW, Kocialkowski S, Liu L, Pearson DM, Bäcklund LM, Ichimura K, et al. Tandem duplication producing a novel oncogenic BRAF fusion gene defines the majority of pilocytic astrocytomas. Cancer Res. 2008;68:8673-7.
10. Hawkins C, Walker E, Mohamed N, Zhang C, Jacob K, Shirinian M, et al. BRAF-KIAA1549 fusion predicts better clinical outcome in pediatric low-grade astrocytoma. Clin Cancer Res Off J Am Assoc Cancer Res. 2011;17:4790-8.
11. Capper D, Jones DTW, Sill M, Hovestadt V, Schrimpf D, Sturm D, et al. DNA methylation-based classification of central nervous system tumours. Nature. 2018;555:469-74.
12. Louis DN, Perry A, Reifenberger G, von Deimling A, Figarella-Branger D, Cavenee WK, et al. The 2016 World Health Organization Classification of Tumors of the Central Nervous System: a summary. Acta Neuropathol (Berl). 2016;131:803-20.
13. Zülch, K., Histologic Typing of Tumours of the Central Nervous System. Geneva: World Health Organization; 1979.
14. Hirose T, Nobusawa S, Sugiyama K, Amatya VJ, Fujimoto N, Sasaki A, et al. Astroblastoma: a distinct tumor entity characterized by alterations of the X chromosome and MN1 rearrangement. Brain Pathol Zurich Switz. 2018;28:684-94.
15. Bale TA, Abedalthagafi M, Bi WL, Kang YJ, Merrill P, Dunn IF, et al. Genomic characterization of recurrent high-grade astroblastoma. Cancer Genet. 2016;209:321-30.
16. Janz C, Buhl R. Astroblastoma: report of two cases with unexpected clinical behavior and review of the literature. Clin Neurol Neurosurg. 2014;125:114-24.
17. Brat DJ, Hirose Y, Cohen KJ, Feuerstein BG, Burger PC. Astroblastoma: clinicopathologic features and chromosomal abnormalities defined by comparative genomic hybridization. Brain Pathol Zurich Switz. 2000;10:342-52.
18. Lehman NL, Hattab EM, Mobley BC, Usubalieva A, Schniederjan MJ, McLendon RE, et al. Morphological and molecular features of astroblastoma, including BRAFV600E mutations, suggest an ontological relationship to other cortical-based gliomas of children and young adults. Neuro-Oncol. 2017;19:31-42.
19. Asha U, Mahadevan A, Sathiyabama D, Ravindra T, Sagar BKC, Bhat DI, et al. Lack of IDH1 mutation in astroblastomas suggests putative origin from ependymoglial cells? Neuropathol Off J Jpn Soc Neuropathol. 2015;35:303-11.
20. Wood MD, Tihan T, Perry A, Chacko G, Turner C, Pu C, et al. Multimodal molecular analysis of astroblastoma enables reclassification of most cases into more specific molecular entities. Brain Pathol Zurich Switz. 2018;28:192-202.
21. Burford A, Mackay A, Popov S, Vinci M, Carvalho D, Clarke M, et al. The ten-year evolutionary trajectory of a highly recurrent paediatric high grade neuroepithelial tumour with MN1:BEND2 fusion. Sci Rep. 2018;8:1032.

References (2)

22. Mhatre R, Sugur HS, Nandeesh BN, Chickabasaviah Y, Saini J, Santosh V. MN1 rearrangement in astroblastoma: study of eight cases and review of literature. Brain Tumor Pathol. 2019;36:112-20.
23. Fudaba H, Momii Y, Kawasaki Y, Goto H, Nobusawa S, Fujiki M. Well-differentiated Astroblastoma with Both Focal Anaplastic Features and a Meningioma 1 Gene Alteration. NMC Case Rep J. 2020;7:205-10.
24. Chen W, Soon YY, Pratiseyo PD, Sutanto R, Hendriansyah L, Kuick CH, et al. Central nervous system neuroepithelial tumors with MN1-alteration: an individual patient data meta-analysis of 73 cases. Brain Tumor Pathol. 2020;37:145-53.
25. Kashgari A, Al Otaibi R, Al Sufiani F, Azzubi M. A rare cerebellar vermis high-grade neuroepithelial tumor: Radiological-pathological correlation. Int J Pediatr Adolesc Med. 2021;8:264-7.
26. Chadda KR, Holland K, Scoffings D, Dean A, Pickles JC, Behjati S, et al. A rare case of paediatric astroblastoma with concomitant MN1-GTSE1 and EWSR1-PATZ1 gene fusions altering management. Neuropathol Appl Neurobiol. 2021;47:882-8.
27. Port JD, Brat DJ, Burger PC, Pomper MG. Astroblastoma: Radiologic-Pathologic Correlation and Distinction from Ependymoma. 2002;5.
28. Jeon C, Kim B, Choi JW. Clinicoradiological and histopathological characteristics and treatment outcomes of cerebral astroblastoma in children: a single-institution experience. J Neurosurg Pediatr. 2022;1-7.
29. Barakat MI, Ammar MG, Salama HM, Abuhashem S. Astroblastoma: Case Report and Review of Literature. Turk Neurosurg. 2016;26:790-4.
30. Mallick S, Benson R, Venkatesulu B, Melgandi W, Rath GK. Patterns of care and survival outcomes in patients with astroblastoma: an individual patient data analysis of 152 cases. Childs Nerv Syst ChNS Off J Int Soc Pediatr Neurosurg. 2017;33:1295-302.
31. Merfeld EC, Dahiya S, Perkins SM. Patterns of care and treatment outcomes of patients with astroblastoma: a National Cancer Database analysis. CNS Oncol. 2018;7:CNS13.
32. Yapıcıer Ö, Demir MK, Özdamarlar U, Kılıç D, Akakın A, Kılıç T. Posterior fossa astroblastoma in a child: a case report and a review of the literature. Childs Nerv Syst ChNS Off J Int Soc Pediatr Neurosurg. 2019;35:1251-5.
Icons are taken from https://biorender.com

MRI physics video is taken from: https://www.nibib.nih.gov/science-education/science-topics/magnetic-resonance-imaging-mri
Papilledema picture is taken from: https://www.ophthalmologyreview.org/articles/papilledema
Brain images are taken from: https://radiopaedia.org

Acknowledgments

Mariam Aboian
Leon Jekel
Jan Lost
Divya Ramakrishnan
Matthew Sala
Niklas Tillmanns
Marc Von Reppert

Tiziano Buzzigoli
Giulia Colonna
Francesca Conti
Andrea De Simone
Antonio Ferraloro
Margherita Montavoci

Giorgio Coretti
Paolo Giovenali
Antonio Ereditato
Emanuela Pallotta
Francesco Tavernese

Tayor Dunningan
Victoria Misenti


YALE

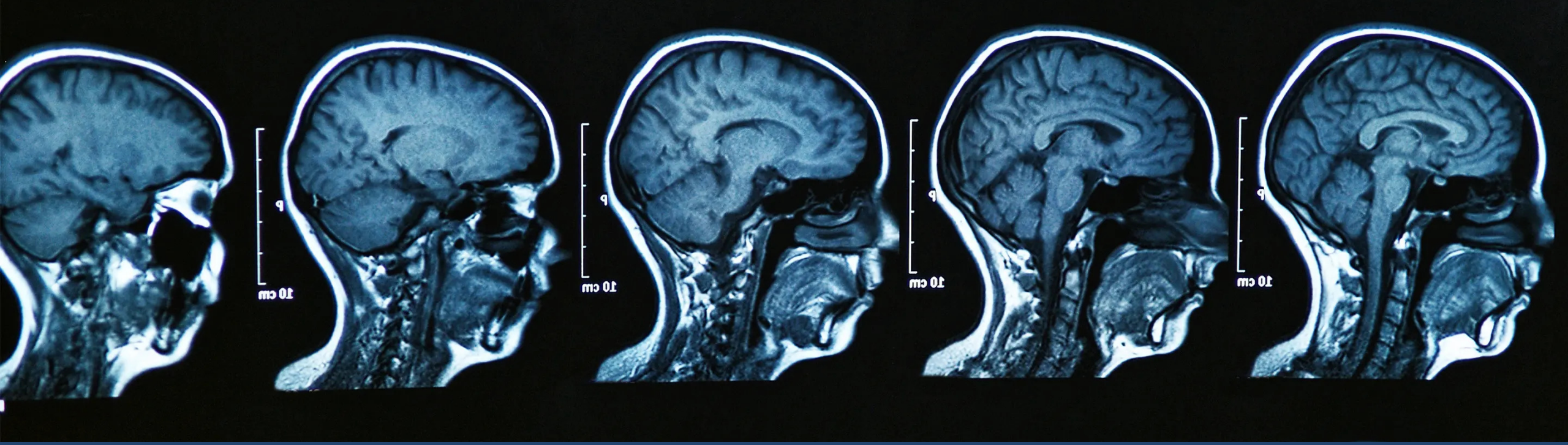

New Frontiers in CNS neoplasms classification and diagnosis: The Role of Neuro-Imaging

Francesca Conti, Department of Neuroradiology and Nuclear Medicine

August 18th, 2022

Yale SCHOOL OF MEDICINE

WHO Classification of Tumours of the Central Nervous System

2007

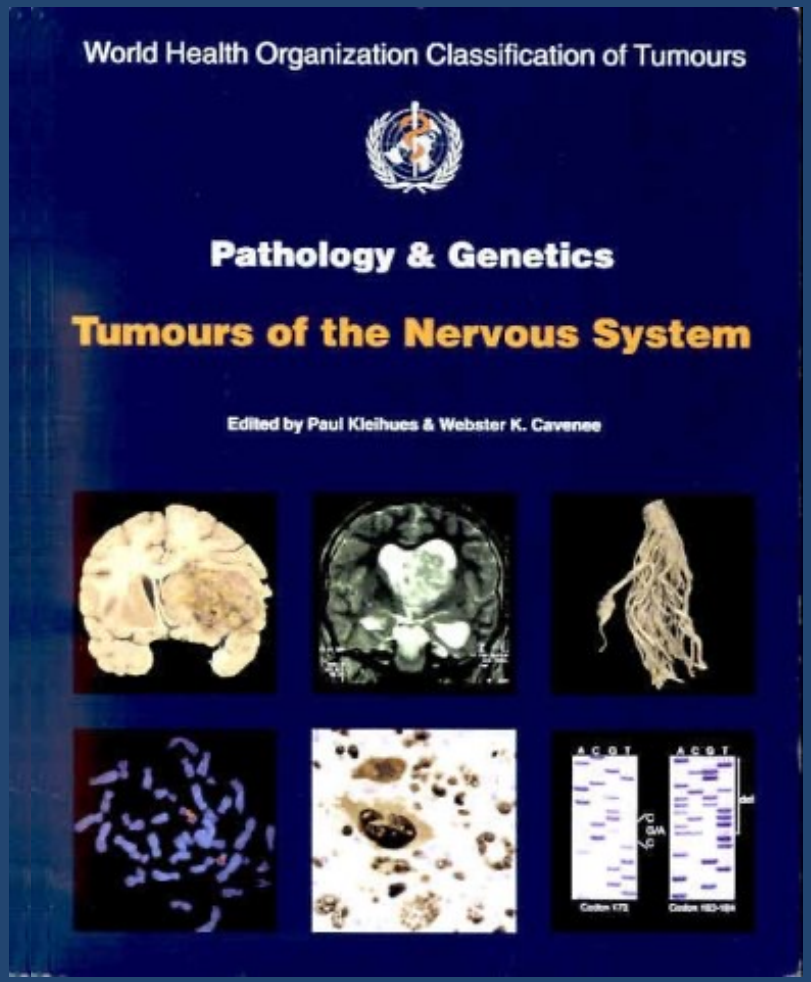

2016

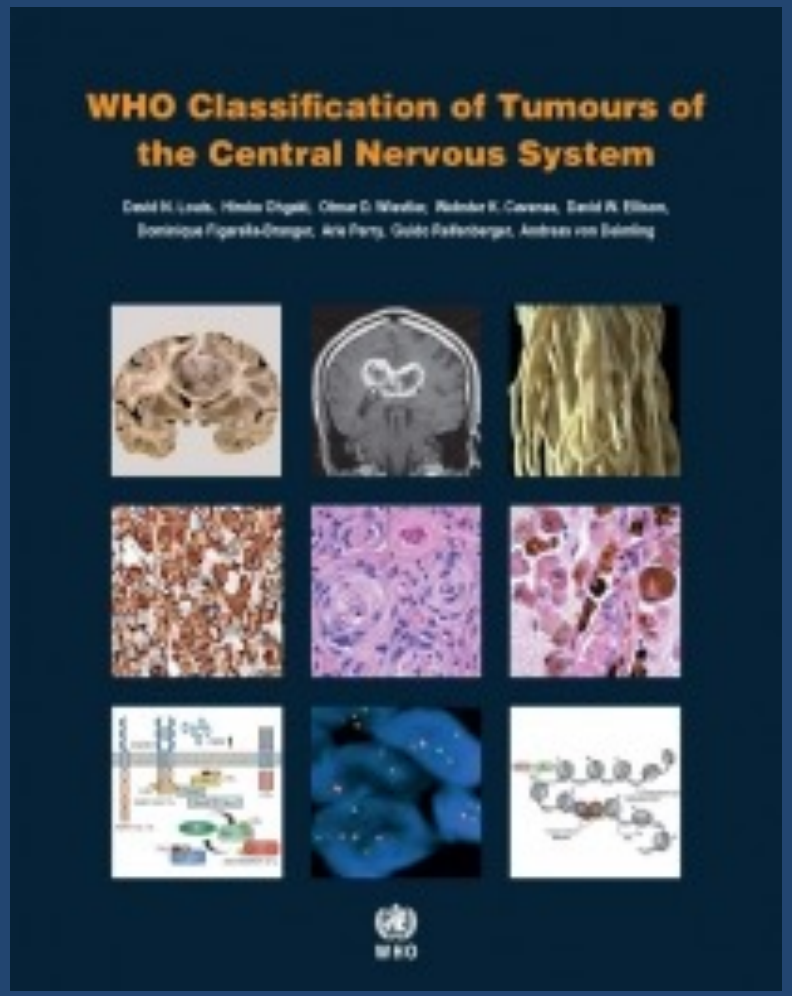

2021

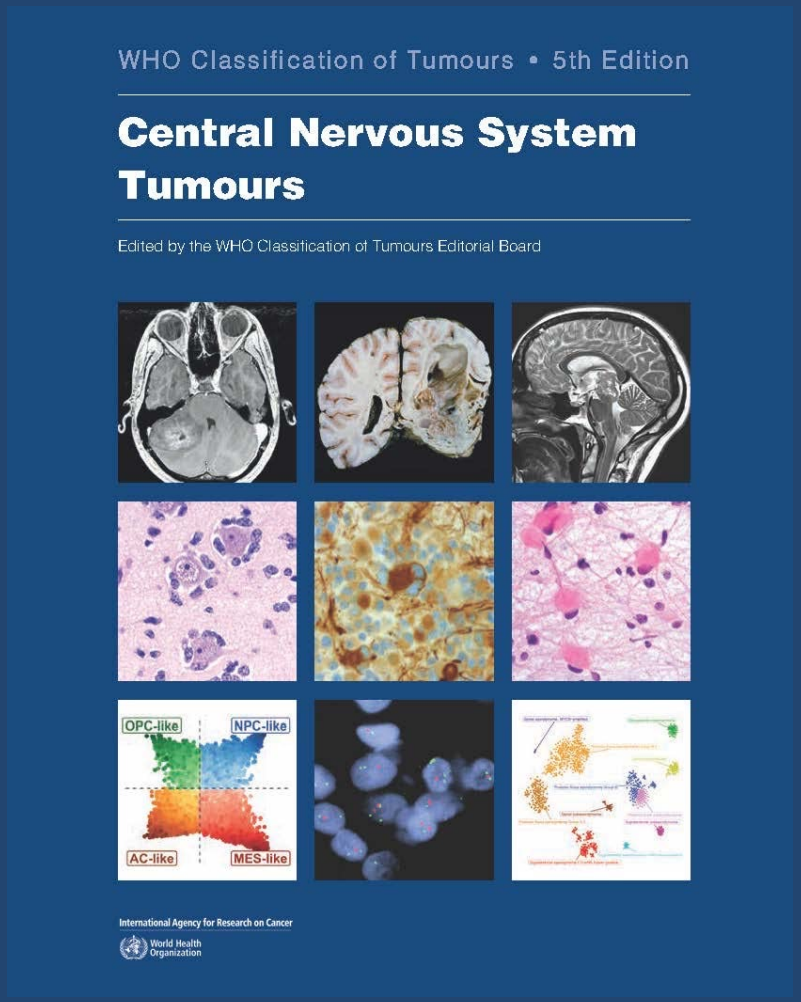

Can Neuro-Imaging provide a better understanding of CNS tumors?

Case Report

- Analysis of a rare brain tumor case
- Search for unique imaging features that could help in diagnosis and classification

Image – Based Search

- Development of an algorithm that permits an image-based search in the hospital database
- Creation of tumor clusters based on imaging
- Analysis of results

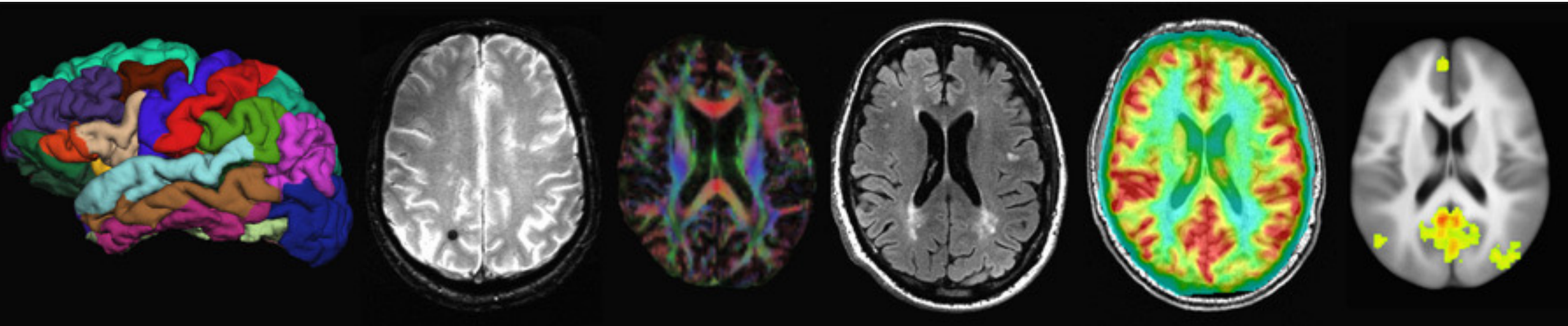

Lymphomatoid Granulomatosis

- Lymphomatoid Granulomatosis (LYG) is a rare lymphoproliferative disease.
- While details behind the pathogenesis of LYG remain unknown[2], it has been proven to follow a previous EBV infection[3].
- The pathological damage is caused by rapid expansion of lymphocyte clones, most frequently of a B-cell phenotype[3-5].
- A T-cell phenotype is also possible, particularly in HIV-infected patients[3-5].

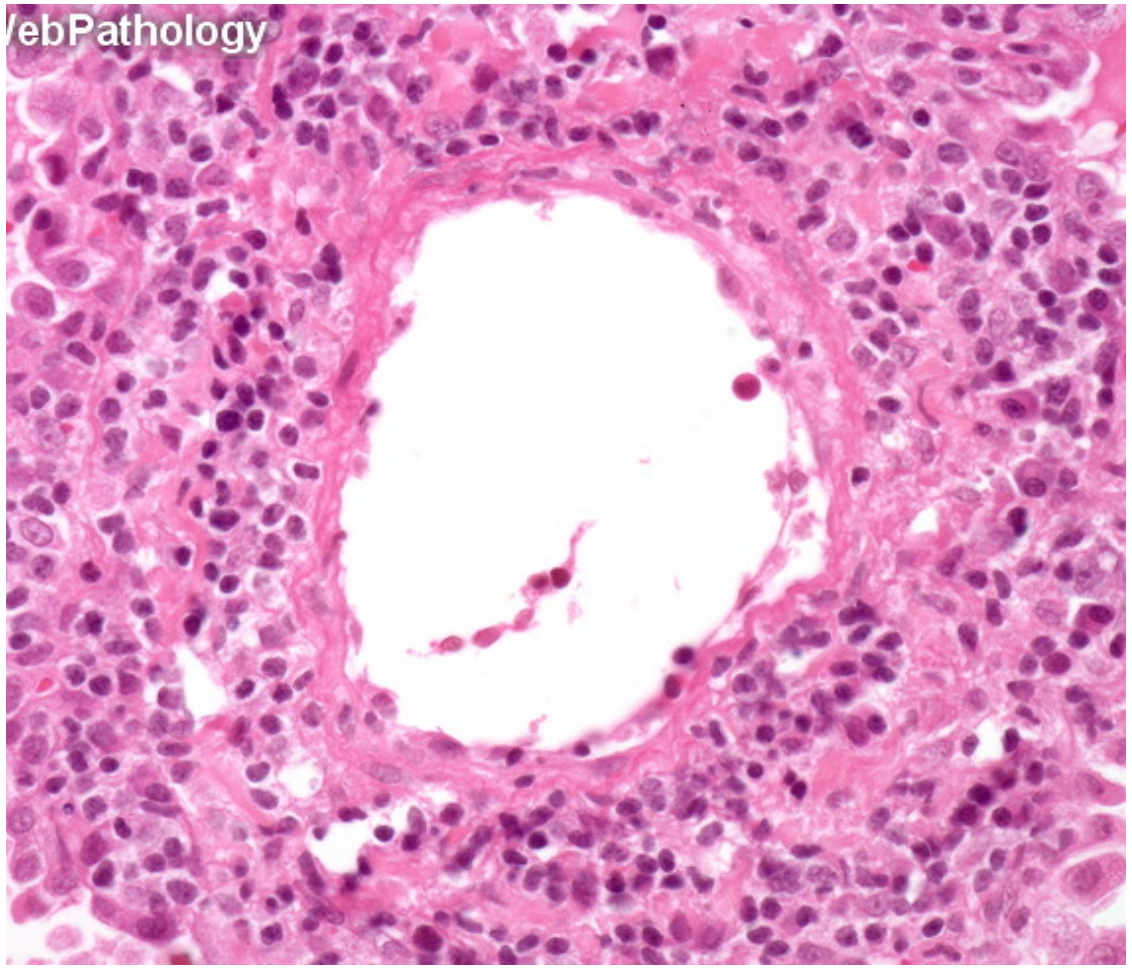

LYG most commonly originates in the lungs with subsequent systemic involvement of skin and CNS[1,2,4-6].

Rare instances of primary CNS LYG have also been documented in the literature[2-4,7-10].

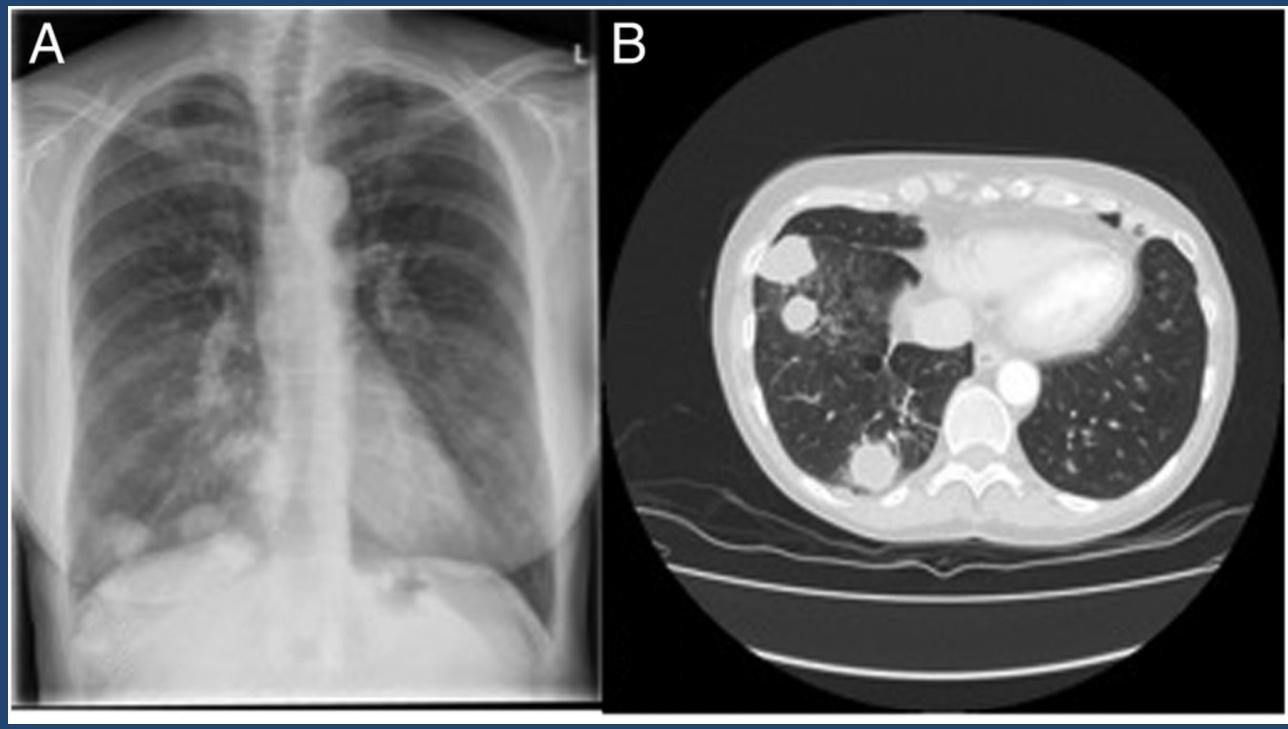

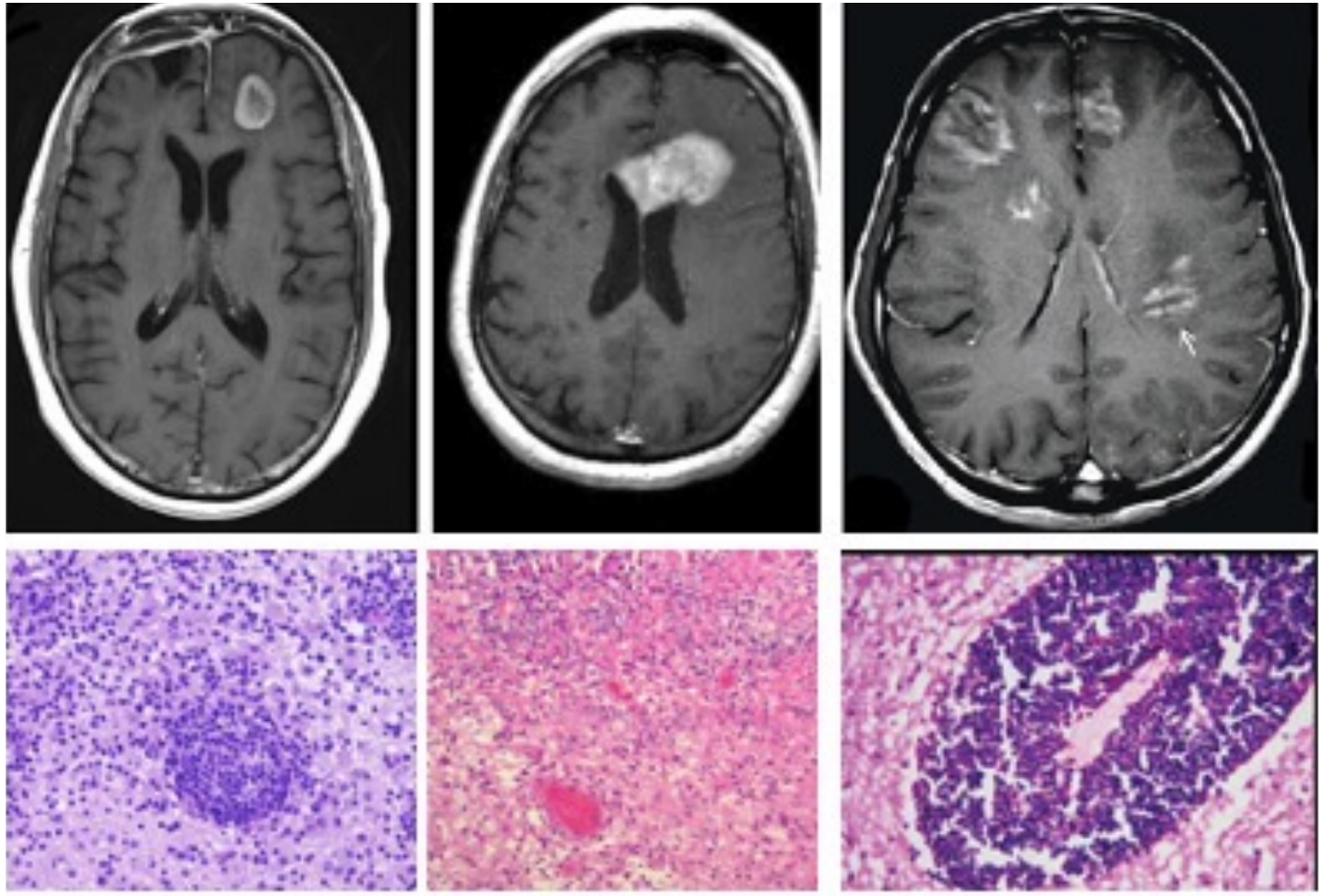

LYG Lymphoma Vasculitis

Primary differential diagnosis[3,8,11]:

- Primary CNS Lymphoma
- CNS vasculitis

Neurological symptoms at presentation[3,6,8,11]:

- dizziness
- dysarthria
- lower limb numbness
- involuntary movement
- headaches
- parkinsonism

LYG grading is based on the predominant lymphocyte phenotype, the amount of necrosis and the amount of EBV infected cells.

The higher the number of EBV+ cells, necrosis and proliferation, the higher the grade of LYG will be.

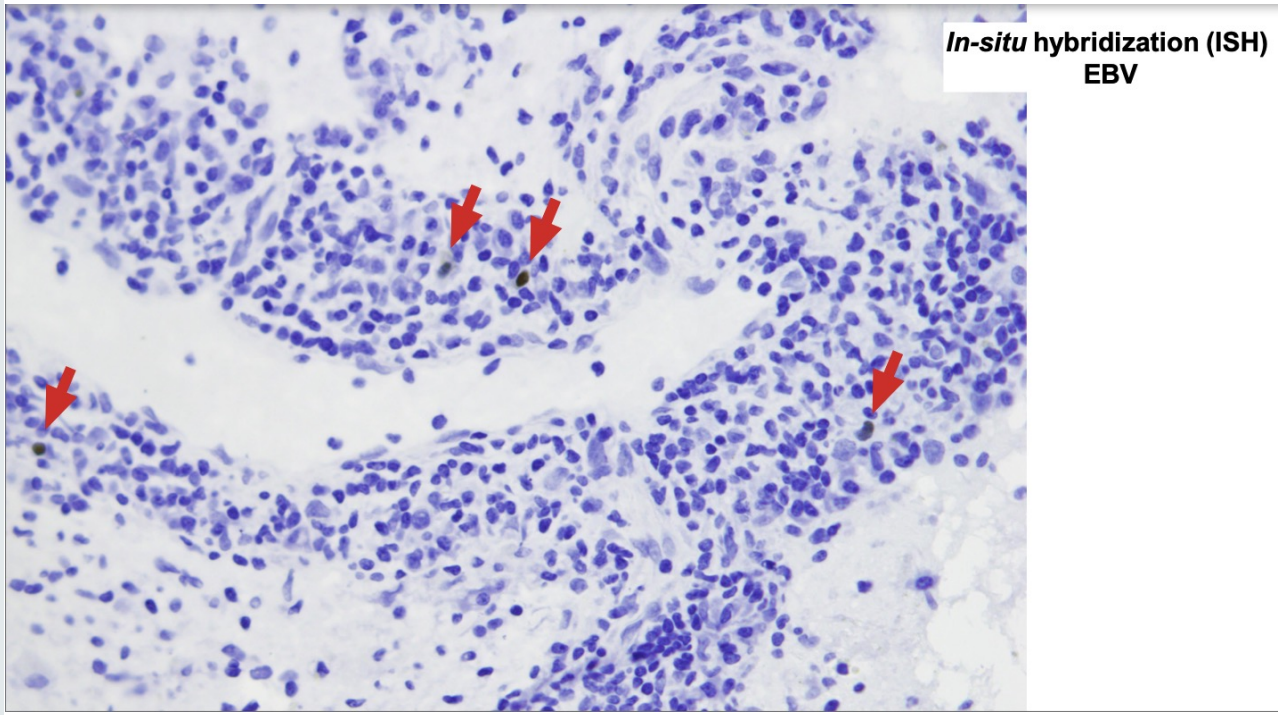

Common treatment options for CNS LYG include chemotherapy, radiotherapy, steroids, surgical resections and anti-retroviral treatment for HIV patients; however, a standardized treatment scheme has not yet been developed[2,3,10,14].

.

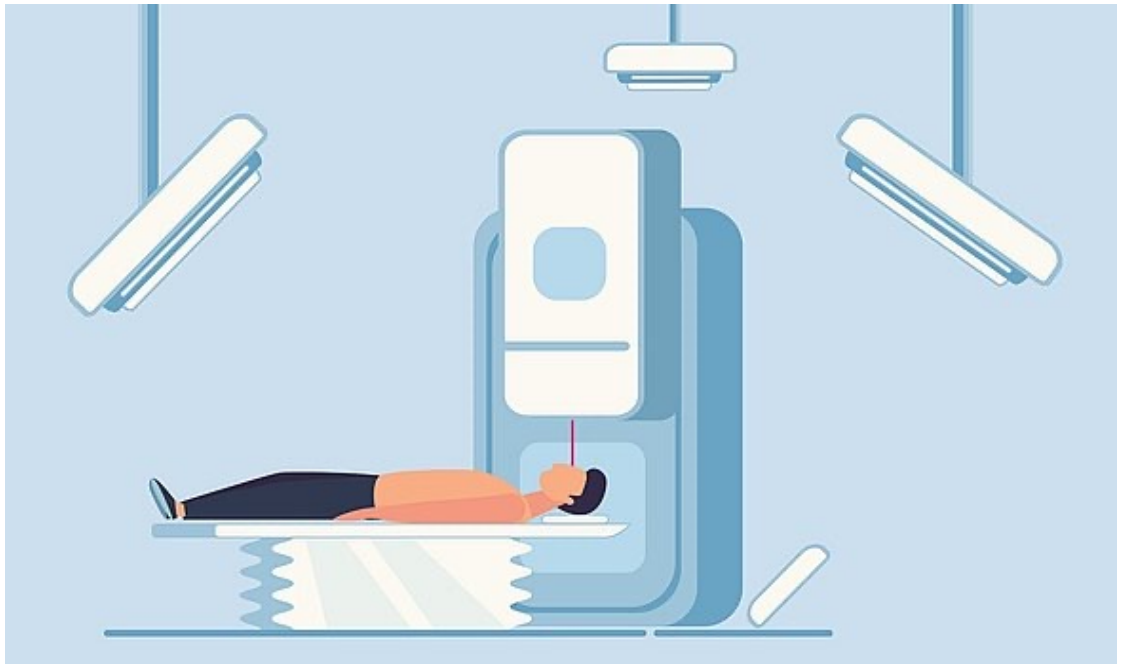

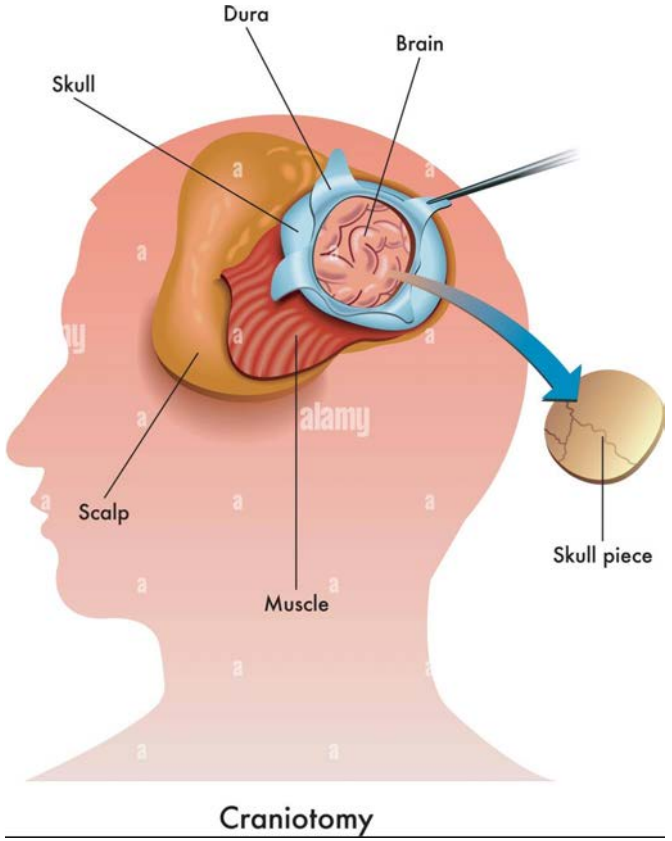

Our cohort of LYG patients consisted of more than 90 patients. Five of them had central nervous system involvement.

We built a case report of one of those cases.

Primary CNS Lymphomatoid Granulomatosis

The patient is a 48 year-old man, HIV and HBV positive, with poly-substance abuse history. He was admitted because of refractory seizures and was started with fosphenytoin and Keppra, but the seizures continued with progressive decline in mental status despite treatment.

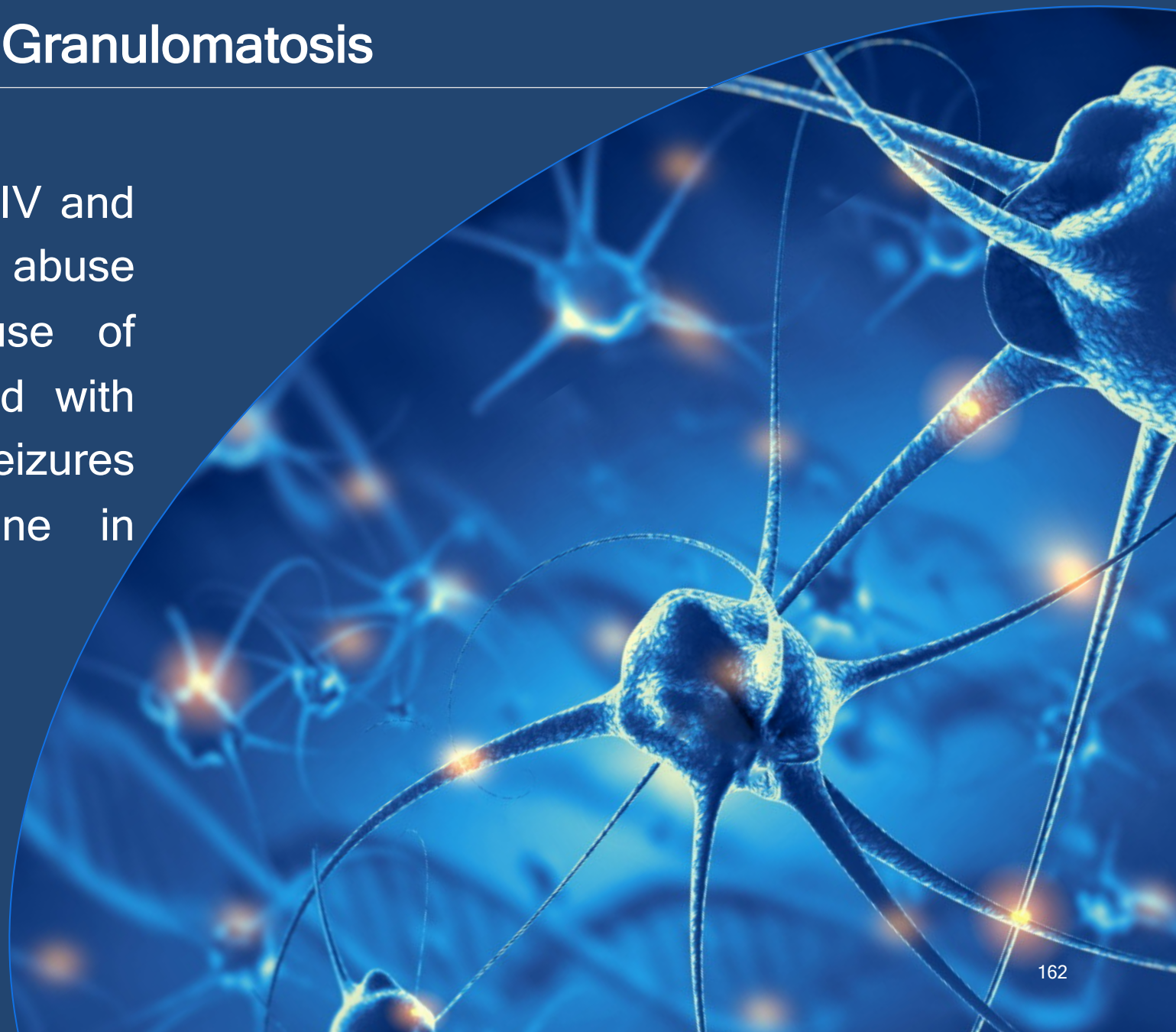

Imaging – First Set of Scan from an Outside Facility

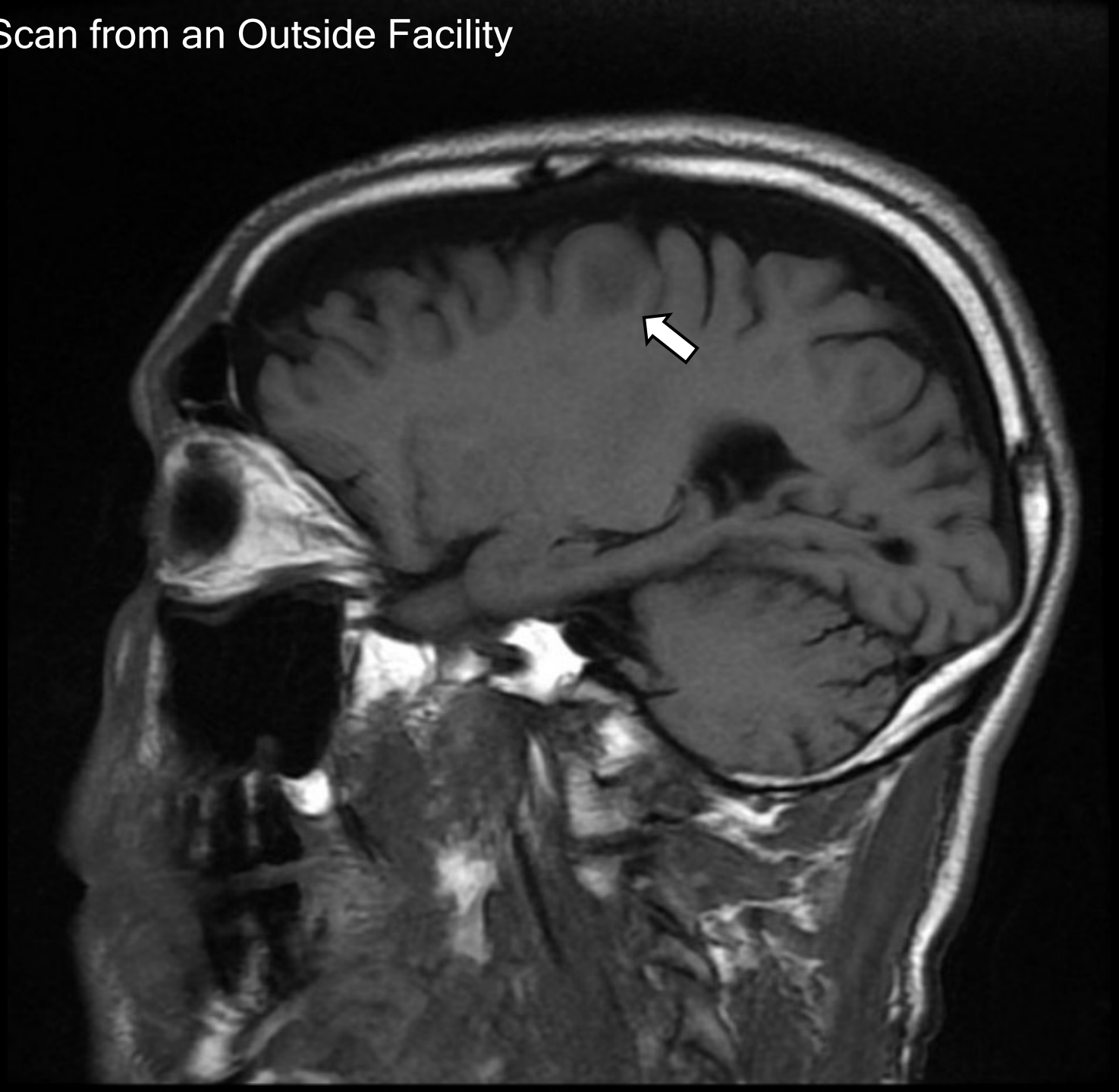

T1

Imaging – First Set of Scan from an Outside Facility

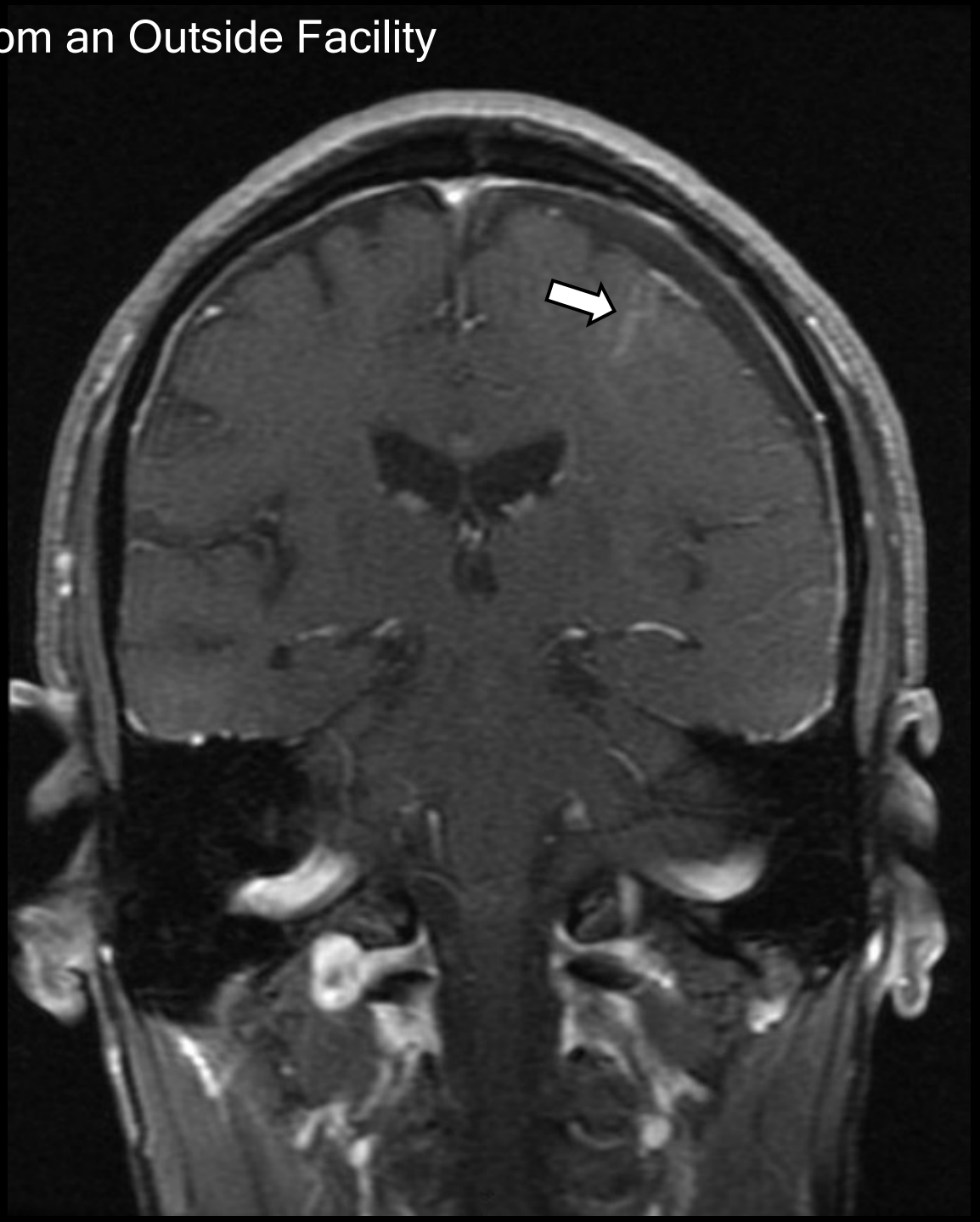

Gadolinium – enhancing T1

Imaging - First Set of Scan from an Outside Facility

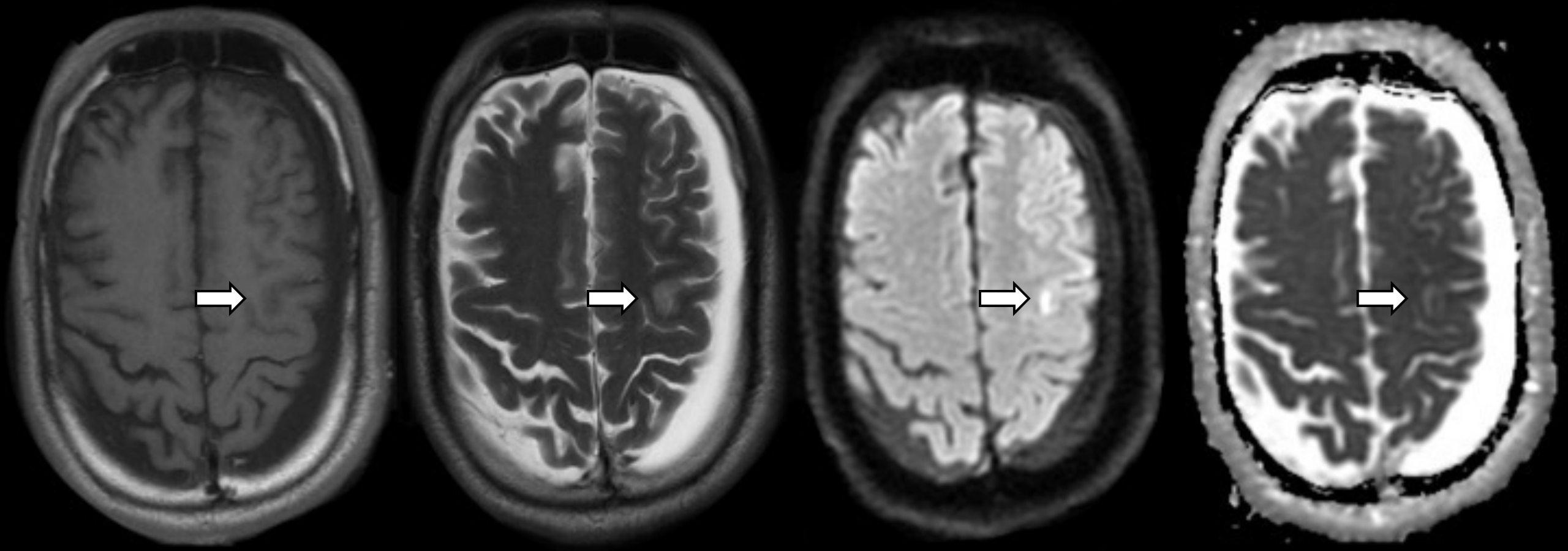

Imaging – Follow up Scan from Yale Health

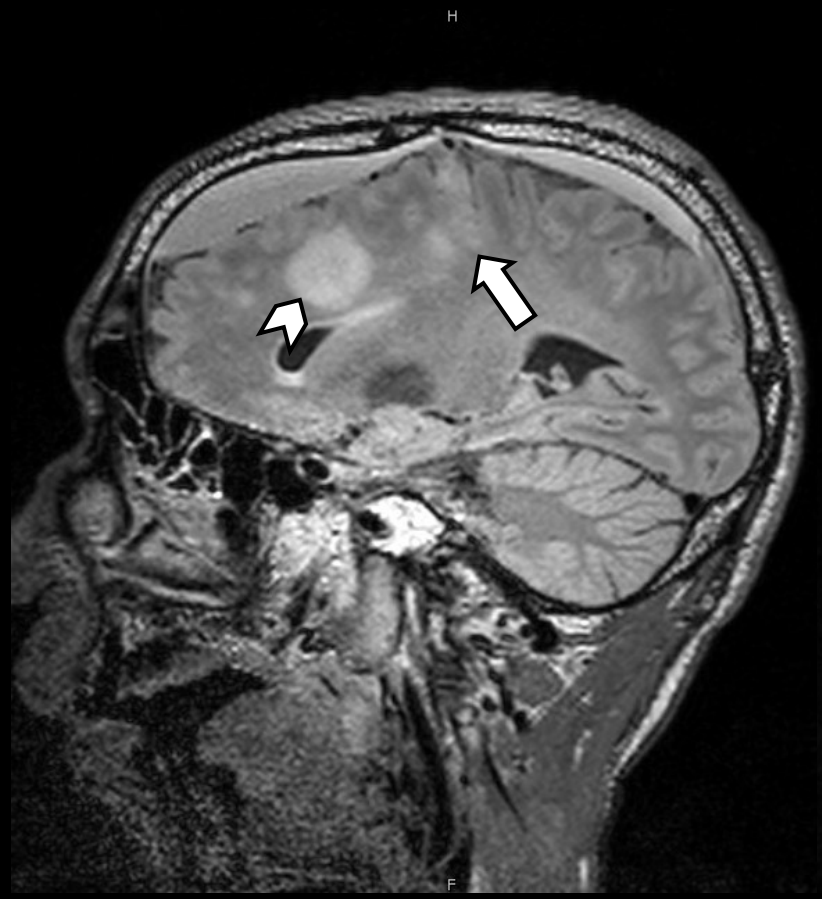

FLAIR

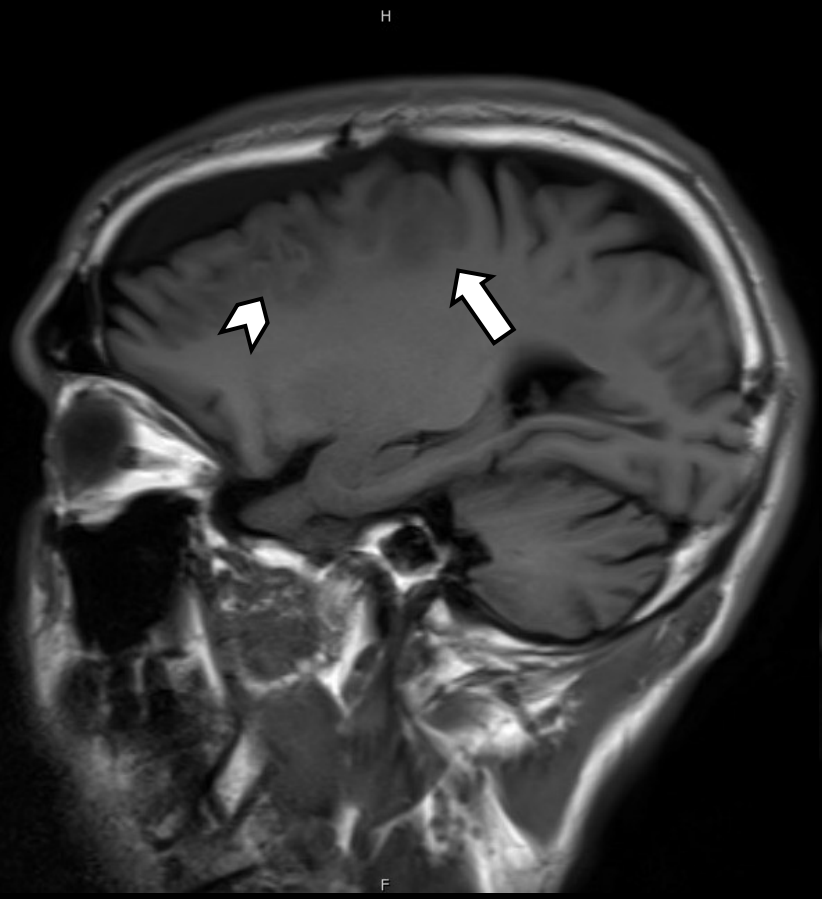

T1

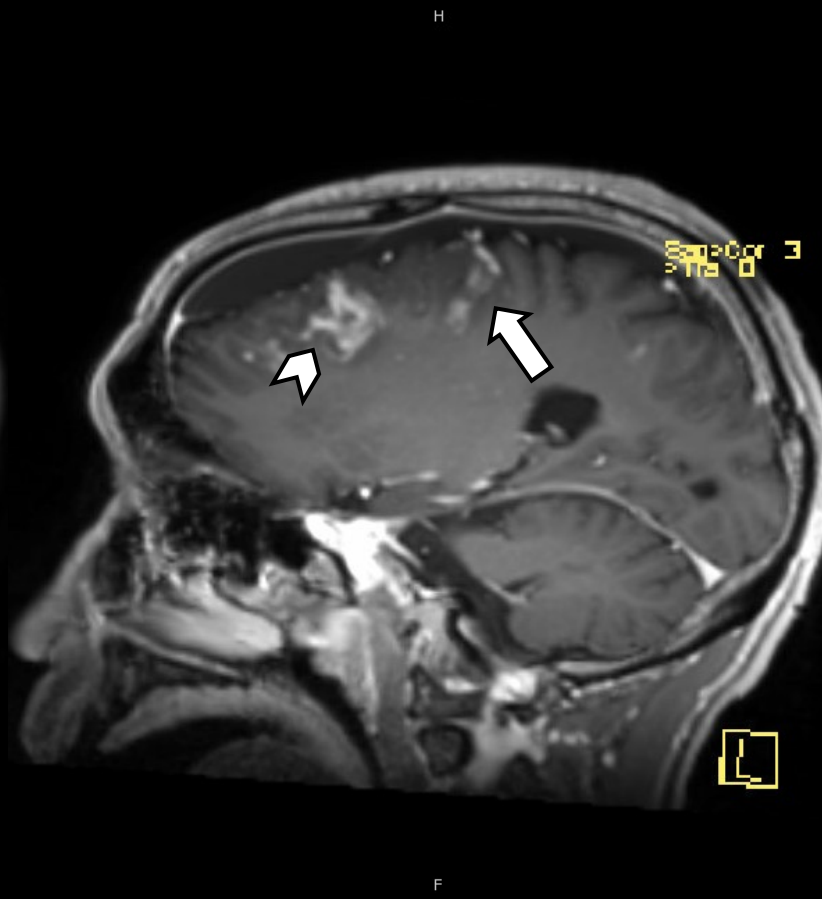

Gadolinium – enhancing T1

Imaging – Follow up Scan from Yale Health

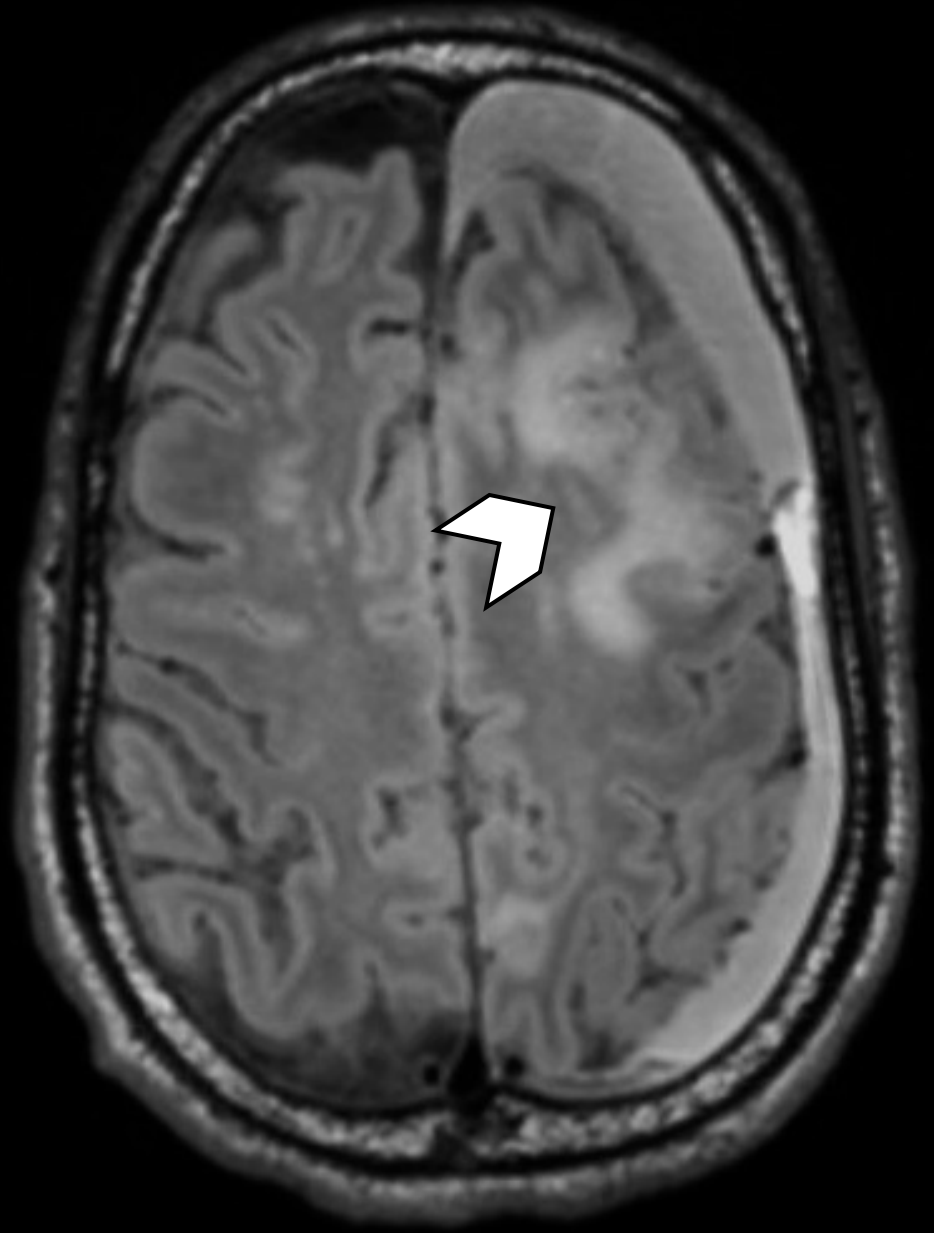

FLAIR

Imaging – Follow up Scan from Yale Health

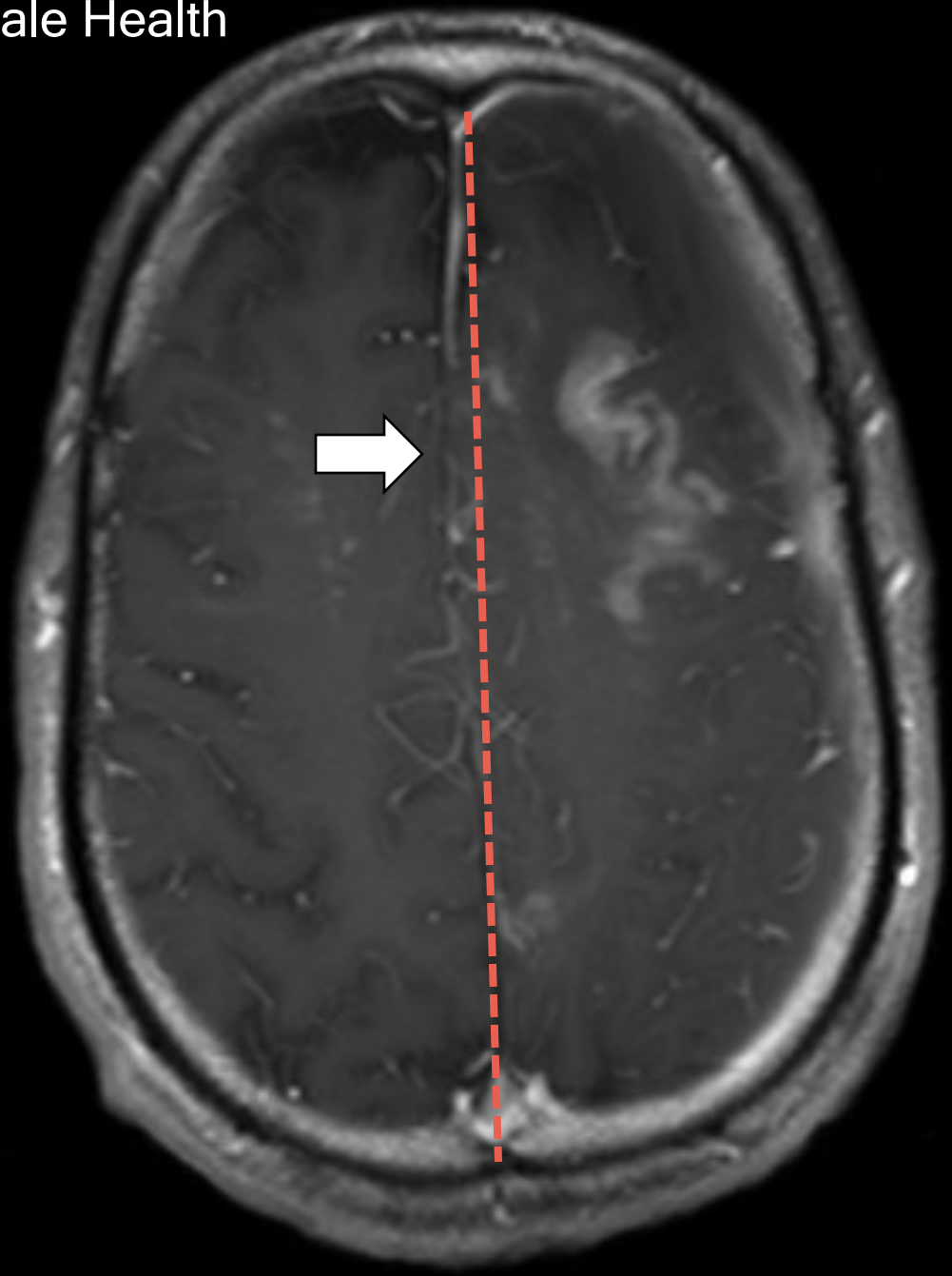

Imaging – Follow up Scan from Yale Health

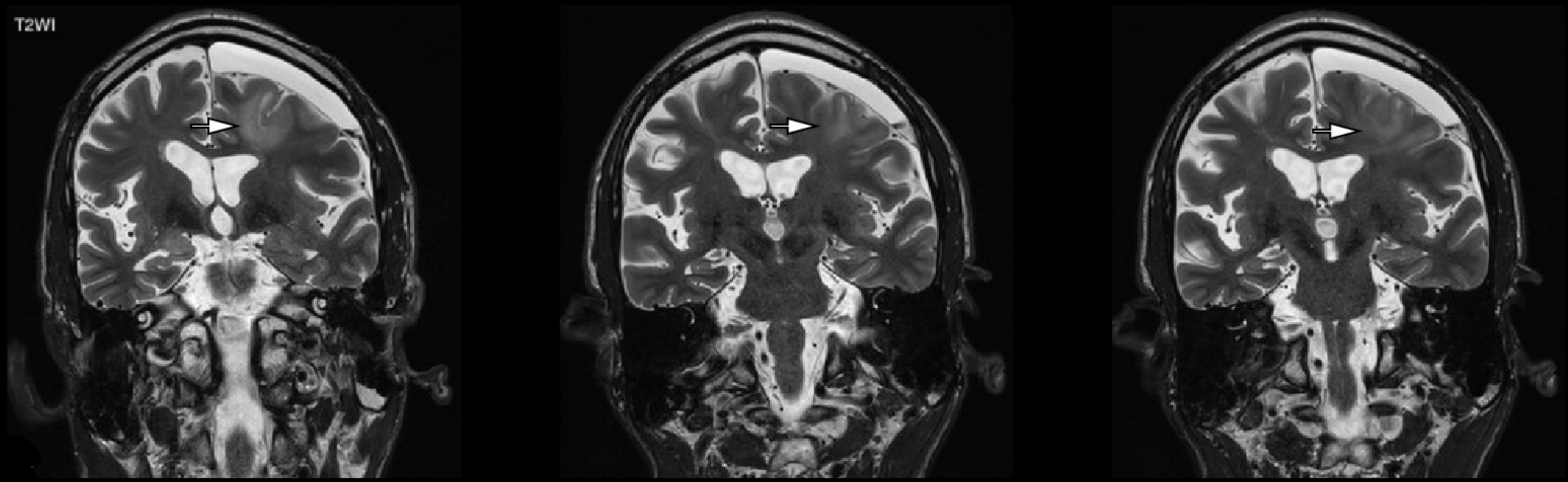

T2

Histopathology

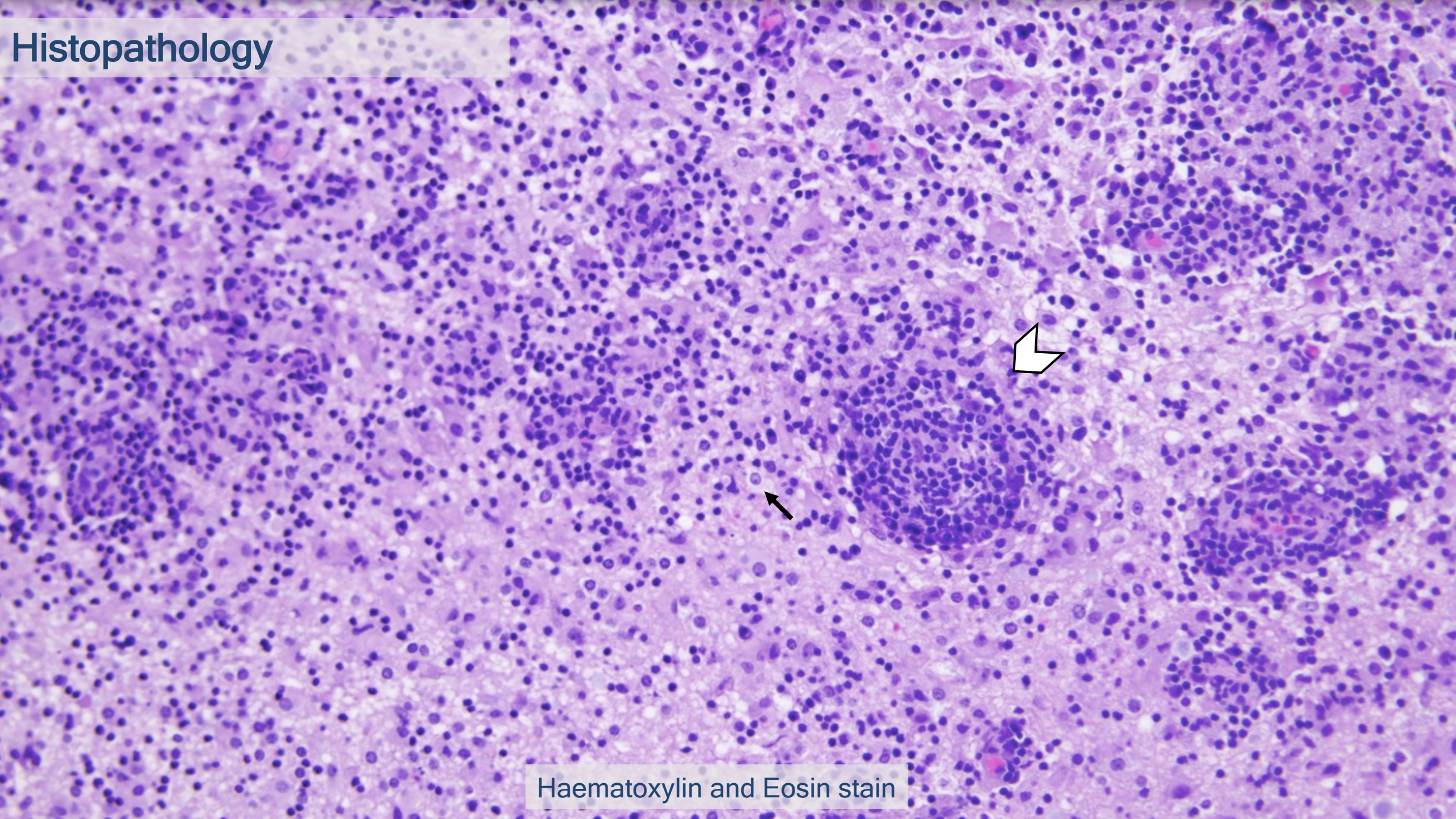

Haematoxylin and Eosin stain

In-situ hybridization (ISH)
EBV

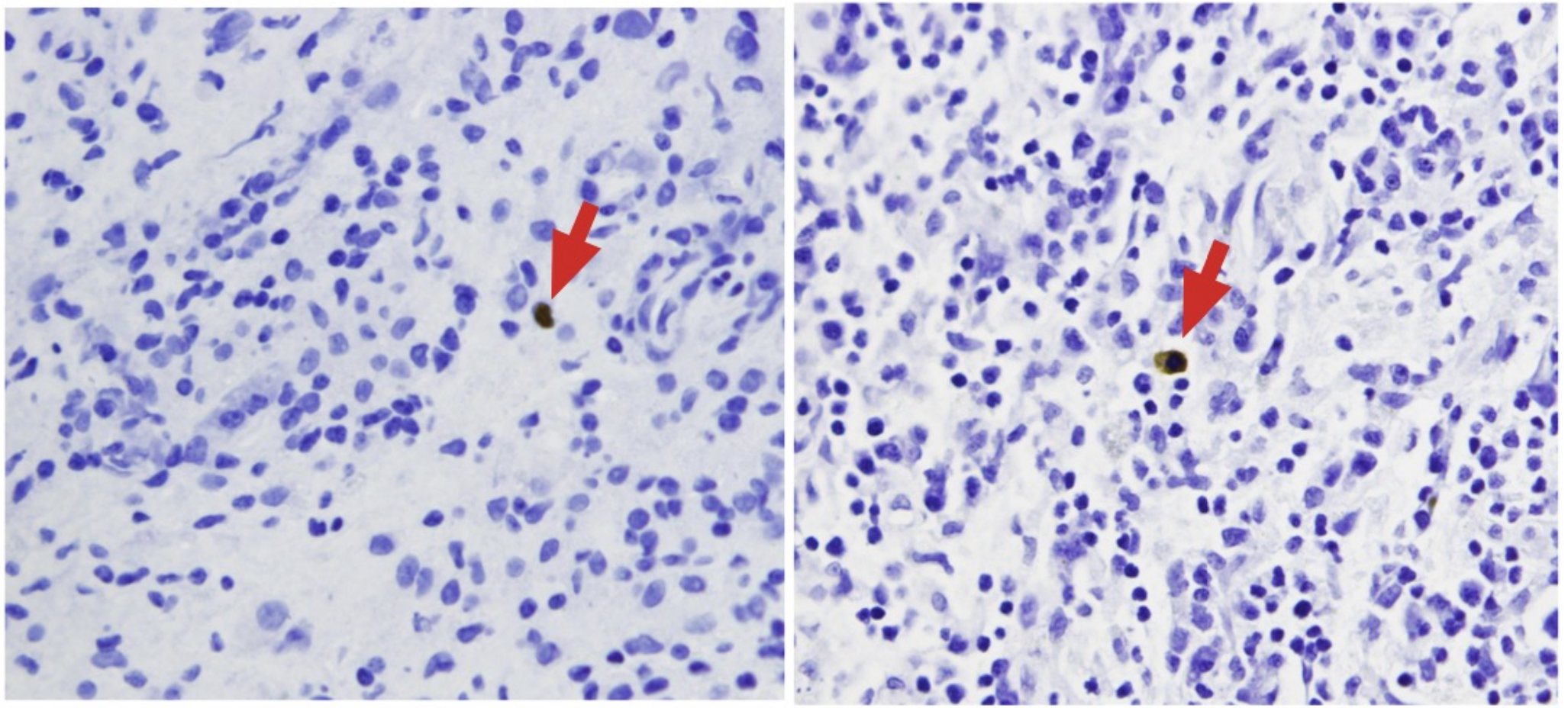

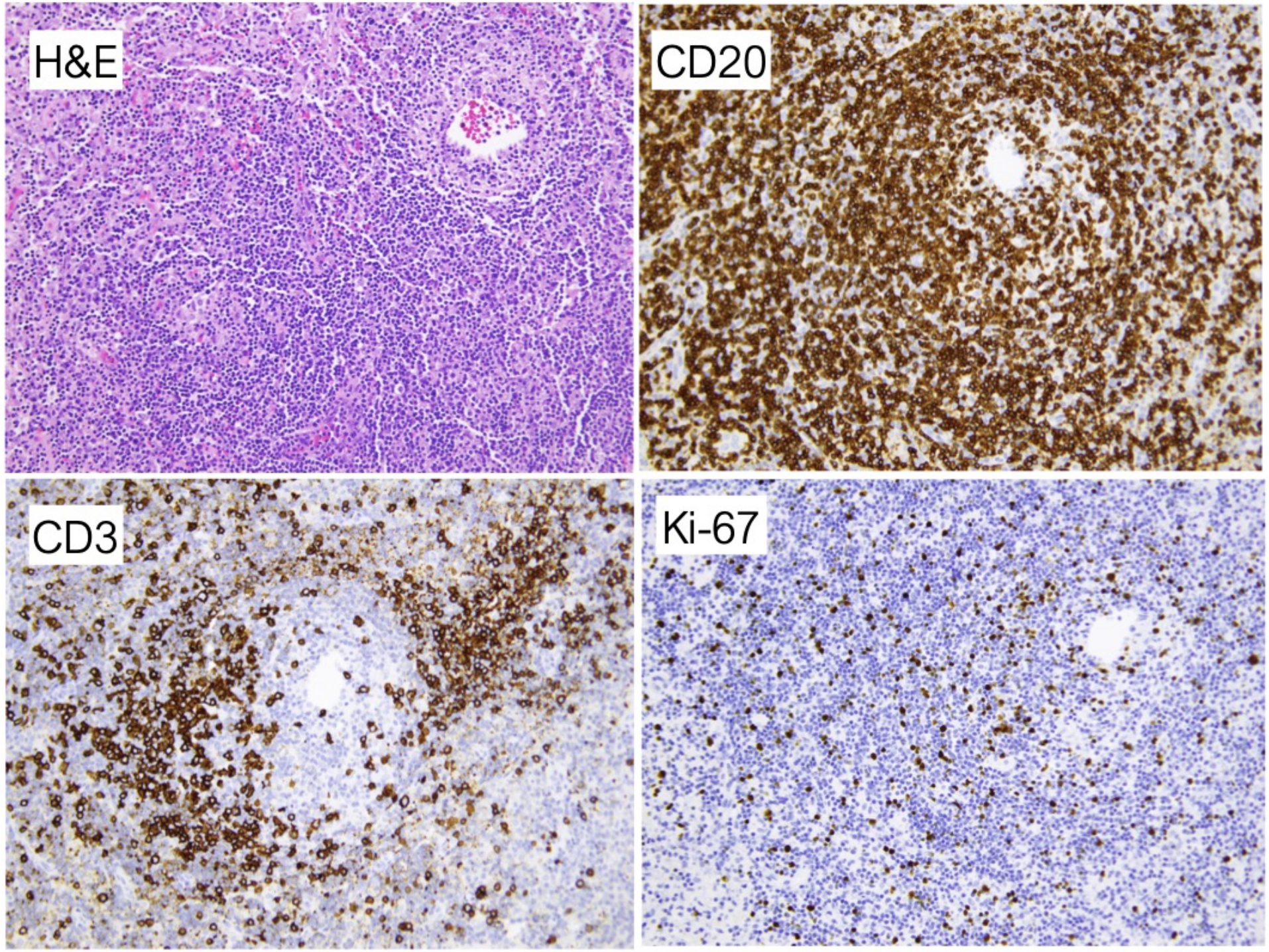
H&E
CD20
CD3
Ki-67

EBV role

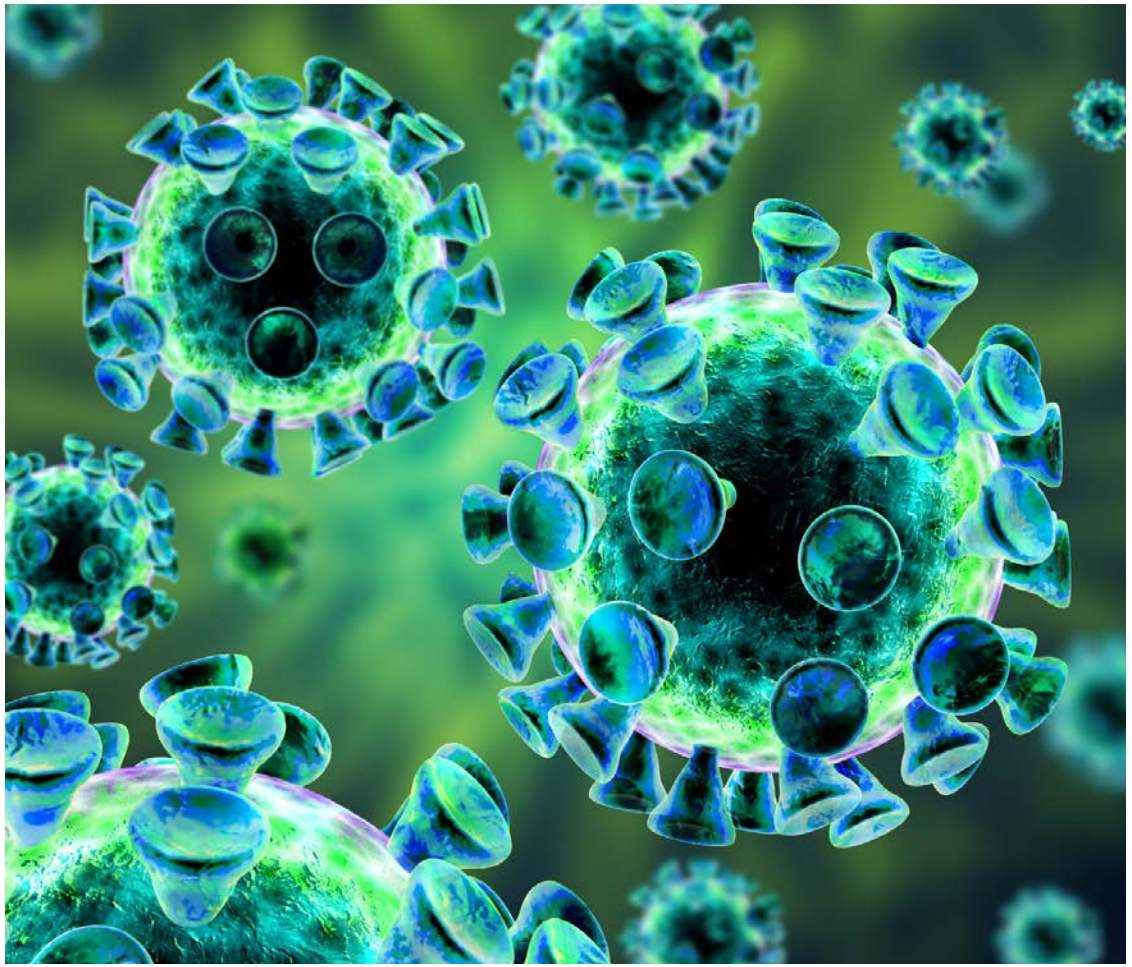

- First encounter and primary infection
- Primary infection resolution
- Latency inside B lymphocytes
- T-cells (CD4+/CD8+) control B-cell proliferation
- Immunocompromised status can lead to EBV+ cells proliferation
- Possible malignant transformation

HIV and immunodeficiency role

- HIV targets CD4+ T-cells
- HIV+ patients have a higher chance to develop lymphoproliferative diseases
- CNS-LYG HIV+ patients show a predominant T-cell infiltrate
- In HIV+ patients, the disease is more aggressive

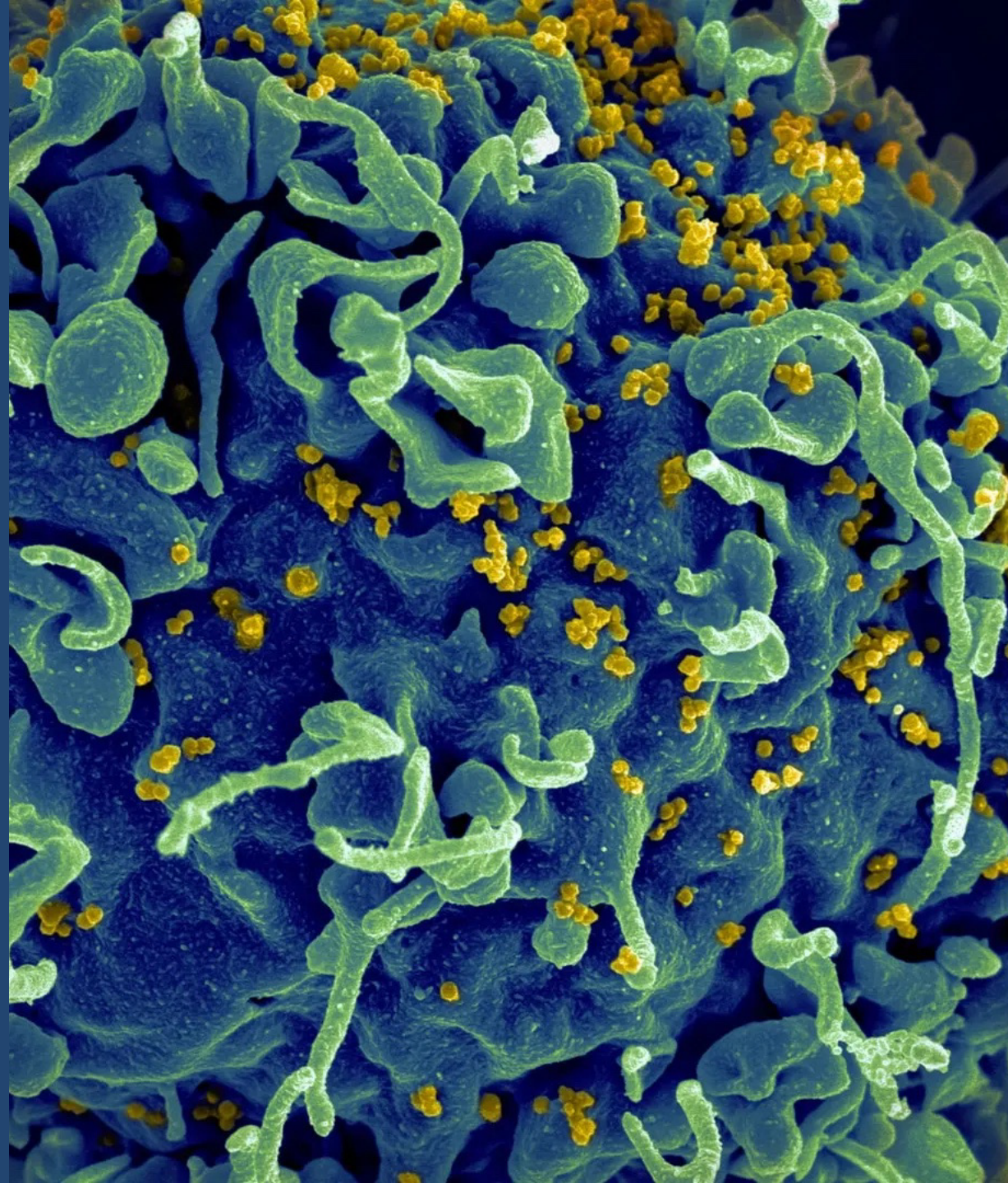

Imaging at diagnosis

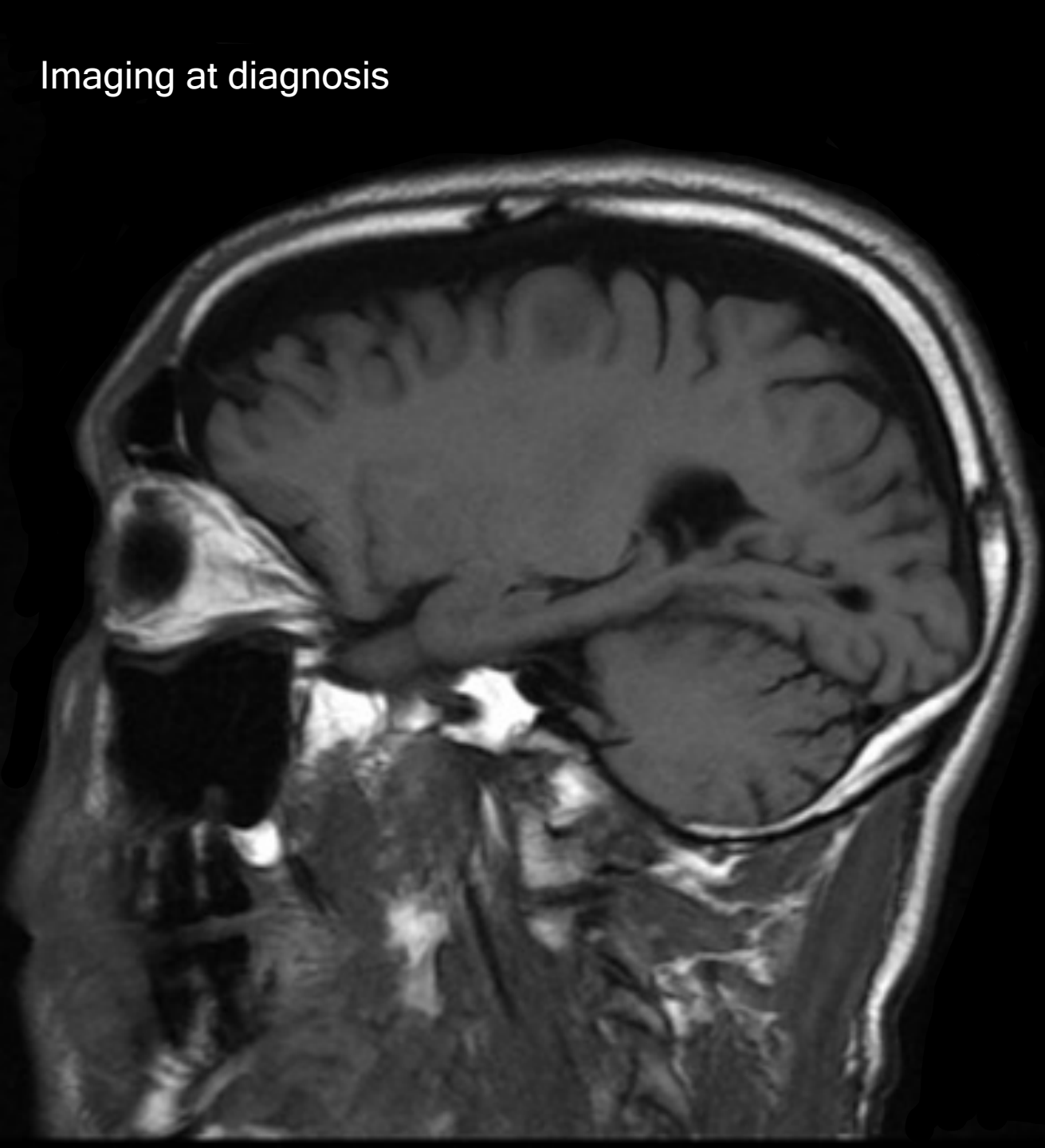

Follow-up diagnosis

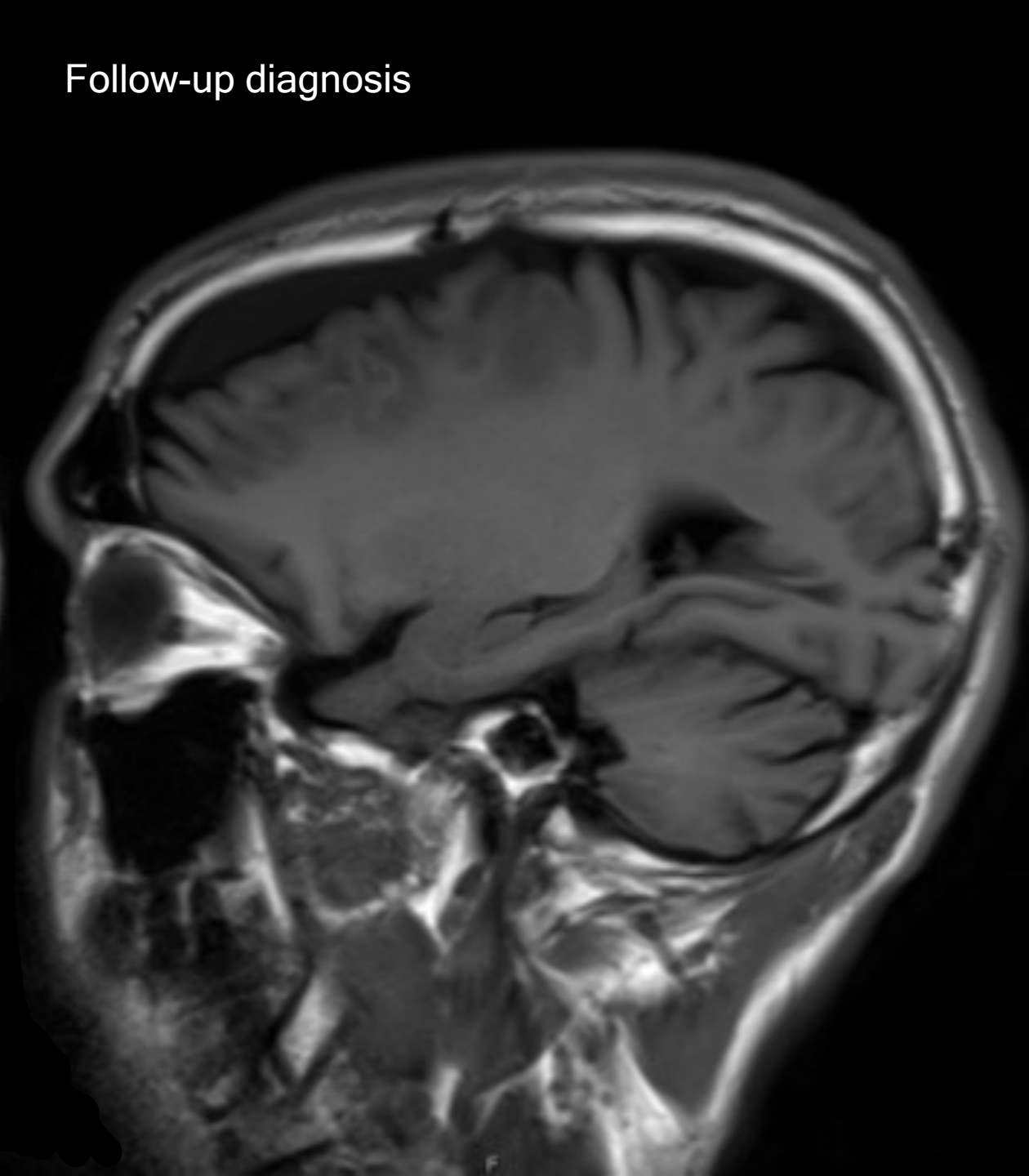

Therapy

- HAART Therapy (Dolutegravir and TRUVADA)
- Dexamethasone: 4 milligrams every 8 hours for two weeks
- Discharged
- Lost at follow-up

Prognosis

- Median survival rate of 2 years[16]
- Systemic LYG without CNS involvement has a 66% mortality rate at 14 months[7]
- Systemic LYG with CNS involvement has a median mortality rate of 86% at 14 months[7]
- Primary CNS LYG correlates with a better life expectancy than systemic LYG[3,7,9]

Image - Based Search

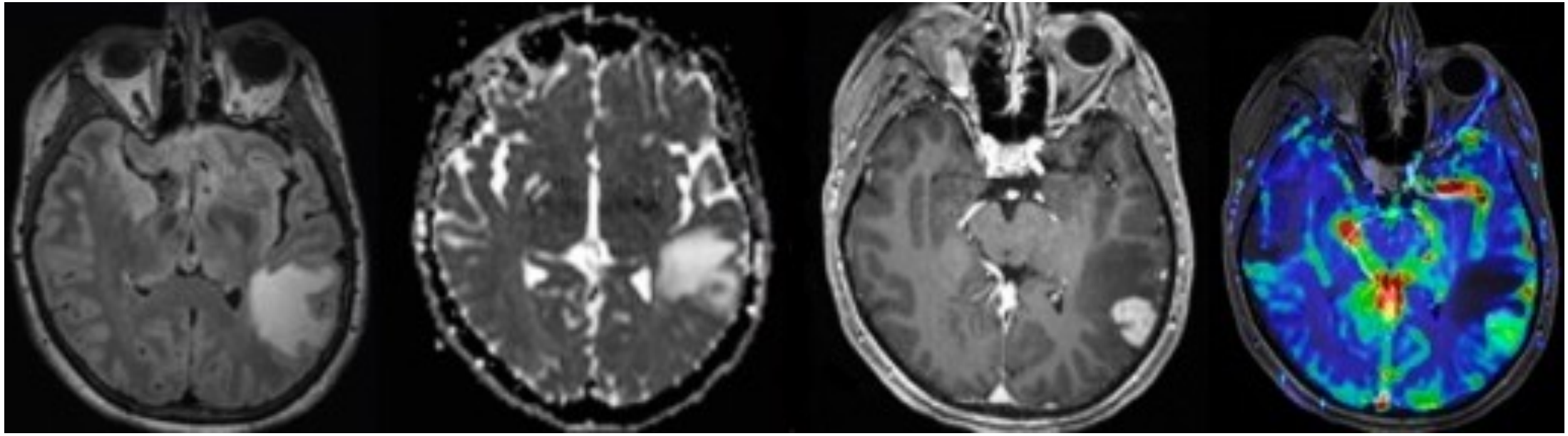

What happens when radiologist are unsure about a diagnosis?

Radiopaedia

Colleagues

Literature

Textbooks

Internet

What if we used the hospital dataset?

- The Picture Archiving and Communication System (PACS) in large hospitals contain thousands of cancer images associated with valuable clinical and pathology data.
- When reading a new patient with brain tumor, finding similar images within PACS can help to generate a differential diagnosis.

We propose an 'image-based' search workflow that uses autosegmentation and automated feature extraction to serve as diagnostic aid

We developed tools to automatically segment tumors and extract features in user interfaces that work within our PACS

How does it work?

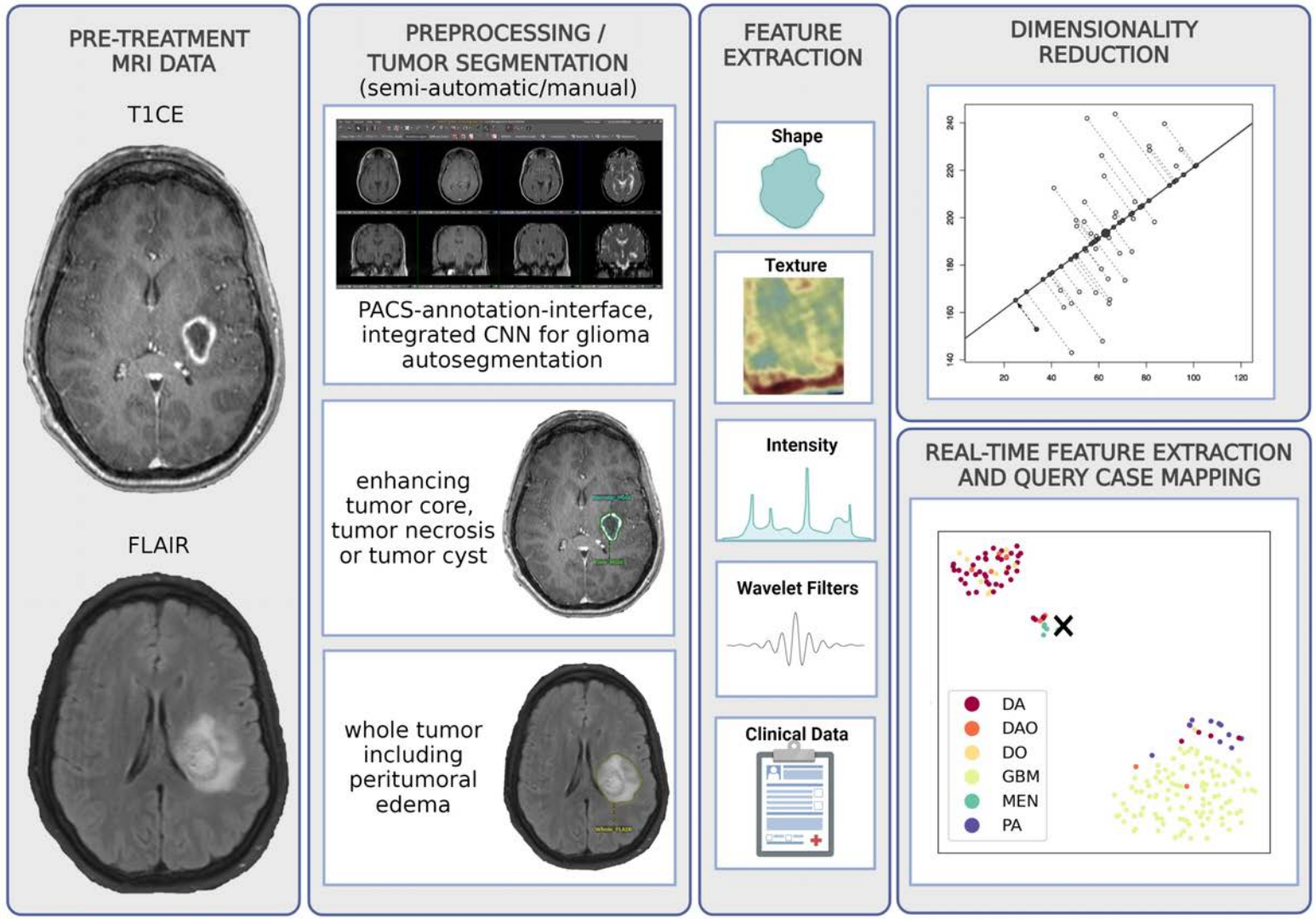

- Unknown or unclear case
- Anonymous accession number
- Query
- Clustering of tumors based on imaging features
- Retrieval of the closest/most similar cases

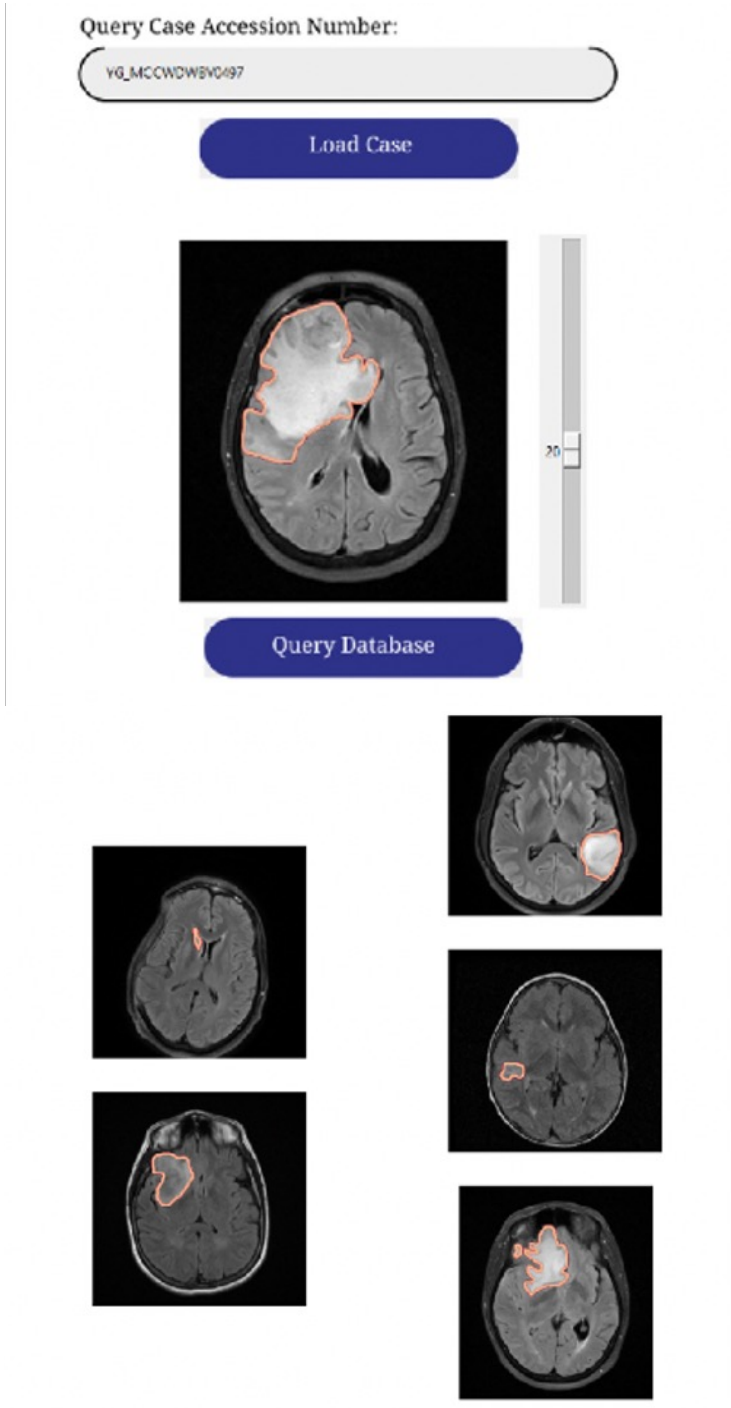

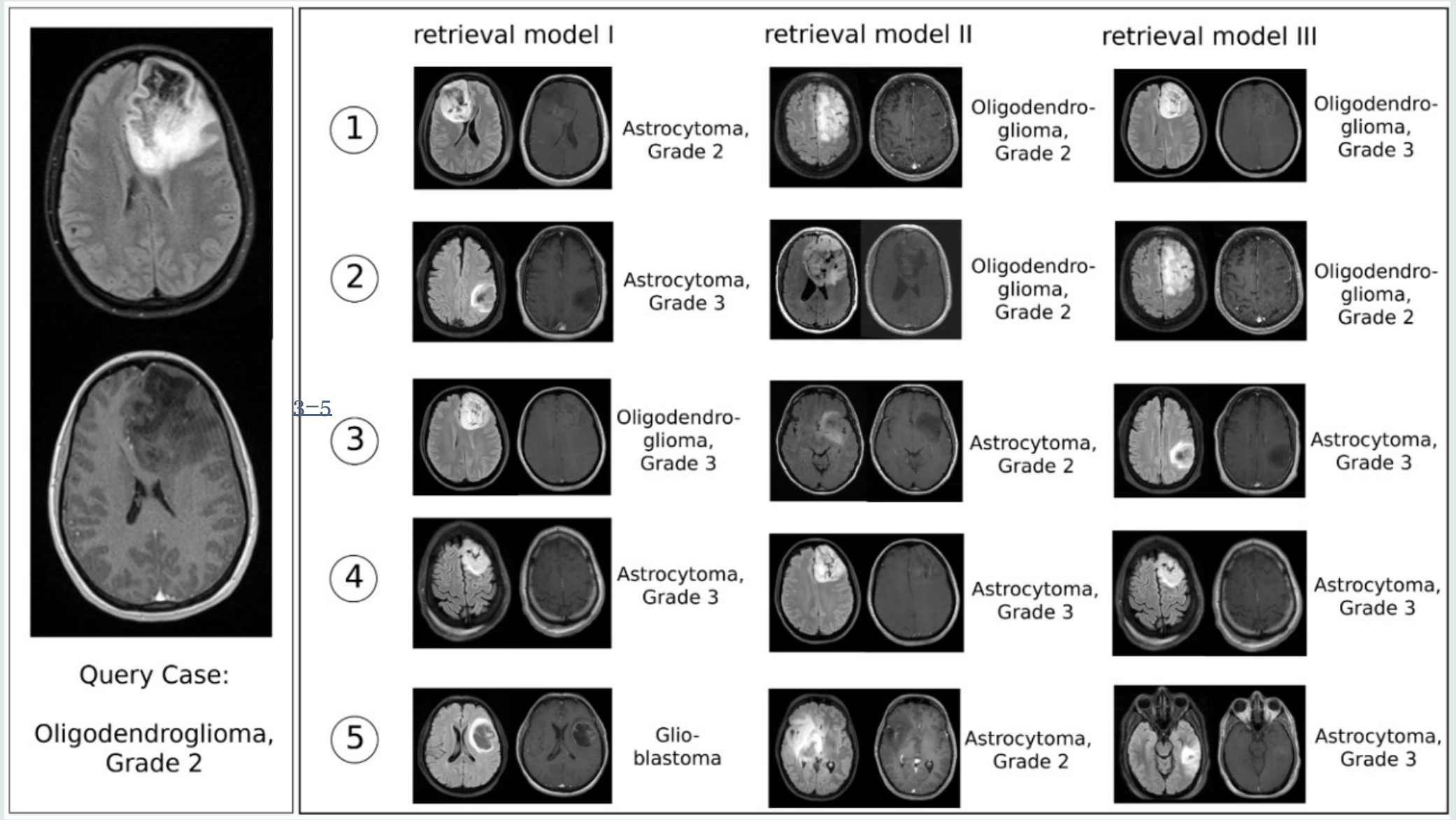
retrieval model I
retrieval model II
retrieval model III
1
Astrocytoma, Grade 2
Oligodendro-glioma, Grade 2
Oligodendro-glioma, Grade 3
2
Astrocytoma, Grade 3
Oligodendro-glioma, Grade 2
Oligodendro-glioma, Grade 2
3
Oligodendro-glioma, Grade 3
Astrocytoma, Grade 2
Astrocytoma, Grade 3
4
Astrocytoma, Grade 3
Astrocytoma, Grade 3
Astrocytoma, Grade 3
5
Glio-blastoma
Astrocytoma, Grade 2
Astrocytoma, Grade 3
Query Case:
Oligodendroglioma, Grade 2

3–5

Meningiomas

- Case retrieval from 2020 and 2021 tumor boards
- Manual segmentation
- Creation of the different cohorts:
  - Typical meningiomas
  - Atypical meningiomas

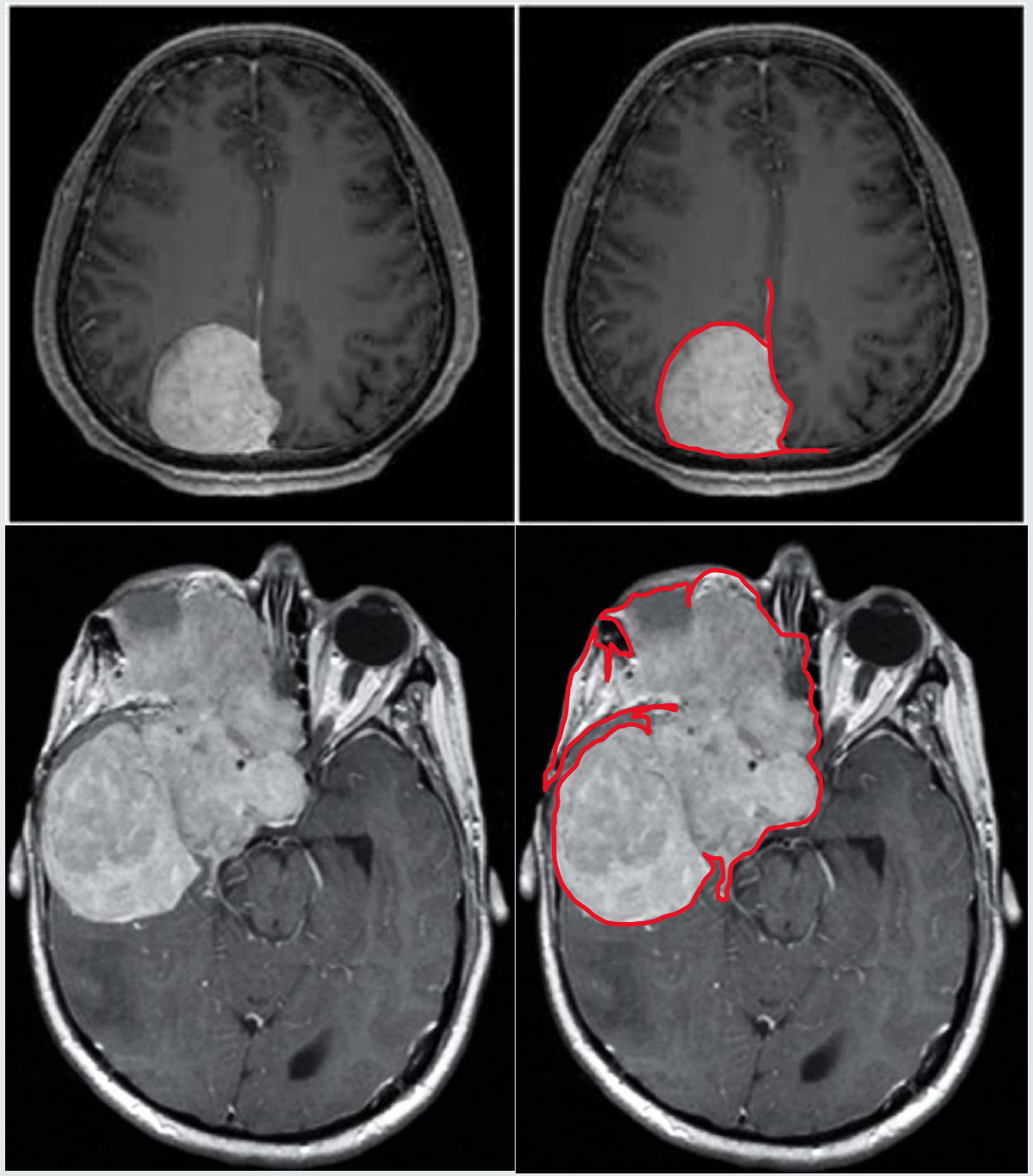

Outcomes

- Differential diagnosis assistance
- Annotation of imaging data to build databases
- Radiology Education
- Image based tumor classification

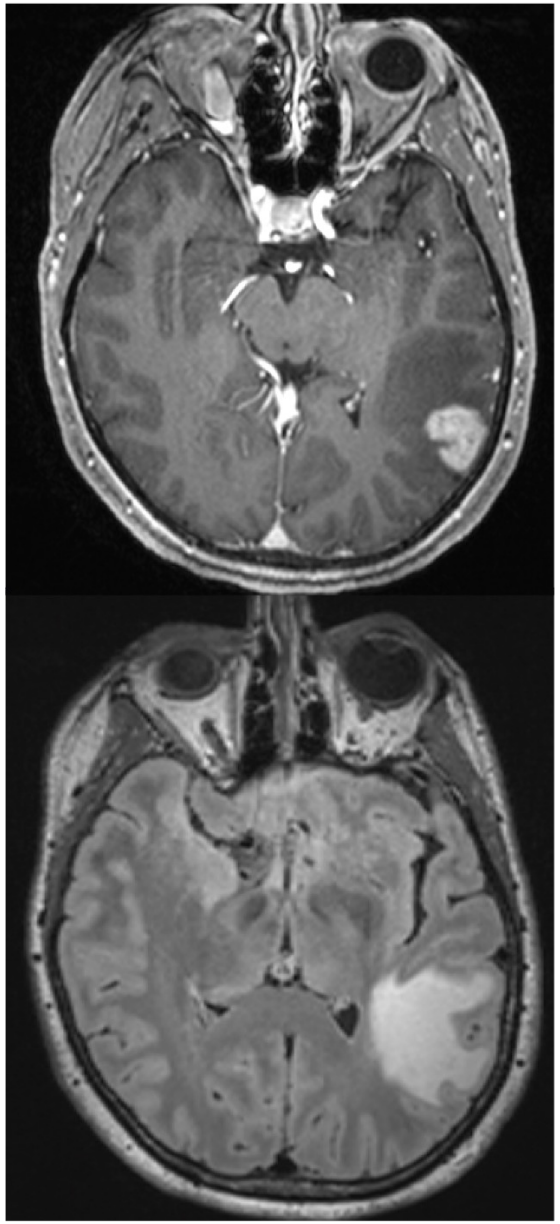

References

1. Liebow AA, Carrington CRB, Friedman PJ. Lymphomatoid granulomatosis. Hum Pathol. 1972;3(4):457-558. doi: 10.1016/S0046-8177(72)80005-4.

2. Quinones E, Potes L, Silva N, Lobato-Polo J. Lymphomatoid granulomatosis of the brain: A case report. Surg Neurol Int. 2016;7(24):612. doi: 10.4103/2152-7806.189732.

3. Xiang Y, Liu C, Xue Y, et al. Primary Central Nervous System Lymphomatoid Granulomatosis: Systemic Review. Front Neurol. 2020;11:901. doi: 10.3389/fneur.2020.00901.

4. Gonzalez-Valcarcel J, Corral I, Quereda C, et al. Primary cerebral lymphomatoid granulomatosis as an immune reconstitution inflammatory syndrome in AIDS. J Neurol. 2010;257(12):2106-2108. doi: 10.1007/s00415-010-5669-2.

5. Kano Y, Kodaira M, Ushiki A, et al. The Complete Remission of Acquired Immunodeficiency Syndrome-associated Isolated Central Nervous System Lymphomatoid Granulomatosis: A Case Report and Review of the Literature. Intern Med. 2017;56(18):2497-2501. doi: 10.2169/internalmedicine.8776-16.

6. Katzenstein A-LA, Doxtader E, Narendra S. Lymphomatoid Granulomatosis: Insights Gained Over 4 Decades. Am J Surg Pathol. 2010;34(12):e35-e48. doi: 10.1097/PAS.0b013e3181fd8781.

7. Lucantoni C, De Bonis P, Doglietto F, et al. Primary cerebral lymphomatoid granulomatosis: report of four cases and literature review. J Neurooncol. 2009;94(2):235-242. doi: 10.1007/s11060-009-9834-3.

8. Patil AK, Alexander M, Nair B, Chacko G, Mani S, Sudhakar S. Clinical, imaging and histopathological features of isolated CNS lymphomatoid granulomatosis. Indian J Radiol Imaging. 2015;25(01):56-59. doi: 10.4103/0971-3026.150149.

9. Takeishi G, Moroki K, Kawasoe T, et al. Spontaneous Regression and Regrowth of Central Nervous System Lymphomatoid Granulomatosis -Case Report-: –Case Report–. Neurol Med Chir (Tokyo). 2011;51(11):801-804. doi: 10.2176/nmc.51.801.

10. He C, Wang Y, Zhang L, et al. Isolated lymphomatoid granulomatosis of the central nervous system: A case report and literature review. Neuropathology. 2019;39(6):479-488. doi: 10.1111/neup.12605.

11. Srivali N, Thongprayoon C, Cheungpasitporn W, Ungprasert P. Lymphomatoid granulomatosis mimicking vasculitis. Ann Hematol. 2016;95(2):345-346. doi: 10.1007/s00277-015-2507-8.

12. Sabattini E, Bacci F, Sagramoso C, Pileri SA. WHO classification of tumours of haematopoietic and lymphoid tissues in 2008: an overview. Pathologica. 2010;102(3):83-87.

13. Zhang Y-X, Ding M-P, Zhang T, et al. Lymphomatoid Granulomatosis with CNS Involvement can Lead to Spontaneous Remission: Case Study. CNS Neurosci Ther. 2013;19(7):536-538. doi: 10.1111/cns.12109.

14. Harada S, Ando J, Ando M, et al. High-grade Primary Central Nervous System Lymphomatoid Granulomatosis: Successful Rituximab Monotherapy. Intern Med. 2021;60(23):3795-3799. doi: 10.2169/internalmedicine.7232-21.

15. Dunleavy K, Roschewski M, Wilson WH. Lymphomatoid Granulomatosis and Other Epstein-Barr Virus Associated Lymphoproliferative Processes. Curr Hematol Malig Rep. 2012;7(3):208-215. doi: 10.1007/s11899-012-0132-3.

16. Cetin B, Benekli M, Akyurek N, et al. Isolated Primary Lymphomatoid Granulomatosis of Central Nervous System. Indian J Hematol Blood Transfus. 2013;29(1):39-42. doi: 10.1007/s12288-011-0123-x.

Acknowledgements

ImagineQuant Lab
Dr. Mariam Aboian MD/PhD
Marc Von Reppert
Leon Jekel
Niklas Tilmann
Jan Lost
Matthew Sala
Divya Ramakrishnan

Wright Lab
Prof. Dr. Antonio Ereditato PhD
Prof. Bonnie Fleming PhD
Victoria Misenti
Taylor Dunnigan

Onaosi
Dr. Emanuela Pallotta
Dr. Paolo Giovenali
Dr. Francesco Tavernese

Onaosi – Yale Experience Team
Lodovico Maria Balzoni
Tiziano Buzzigoli
Giulia Colonna
Andrea De Simone
Antonio Ferraloro
Margherita Montavoci

Thank you!

ImmunoPET: Towards non-invasive selection of lung cancer patients for antibody therapies

Margherita Montavoci

Marquez-Nostra Laboratory of Cancer Imaging and Therapeutics

18th August 2022

Projects

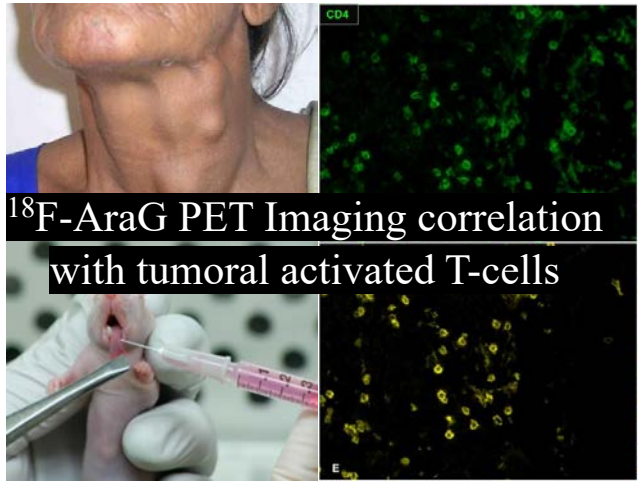

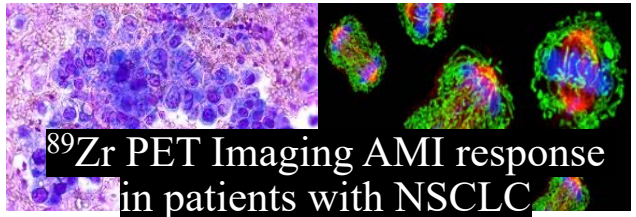

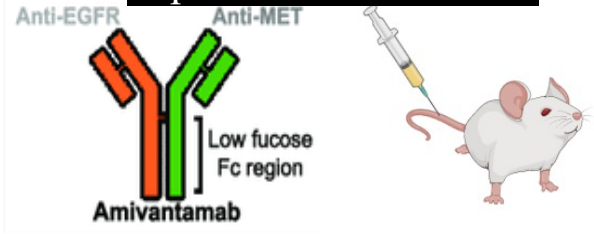

CIT

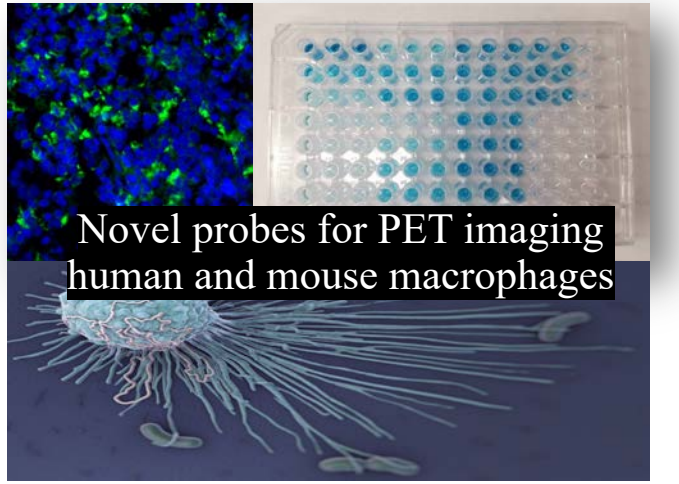

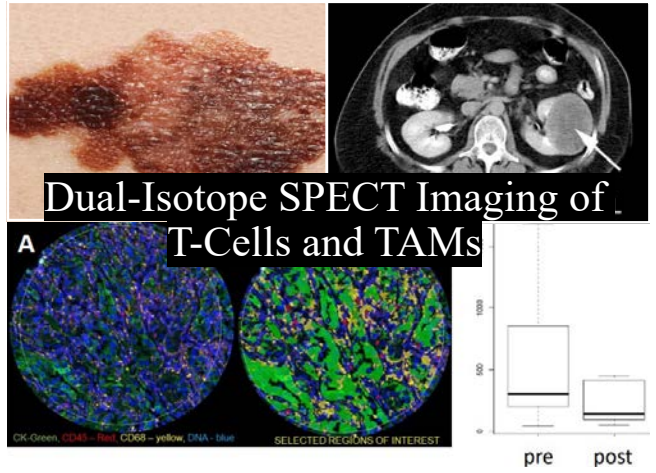

Yale University

Wright Laboratory

HOOL OF MEDICINE

Background Information: Unmet Need

Non-small Cell Lung Cancer

- Epidemiology
  - 2,206,771 lung cancer diagnoses in 2020
  - 82% is NSCLC
- Current therapeutics
  - EGFR-targeted drugs
  - Develop resistance after 1 year

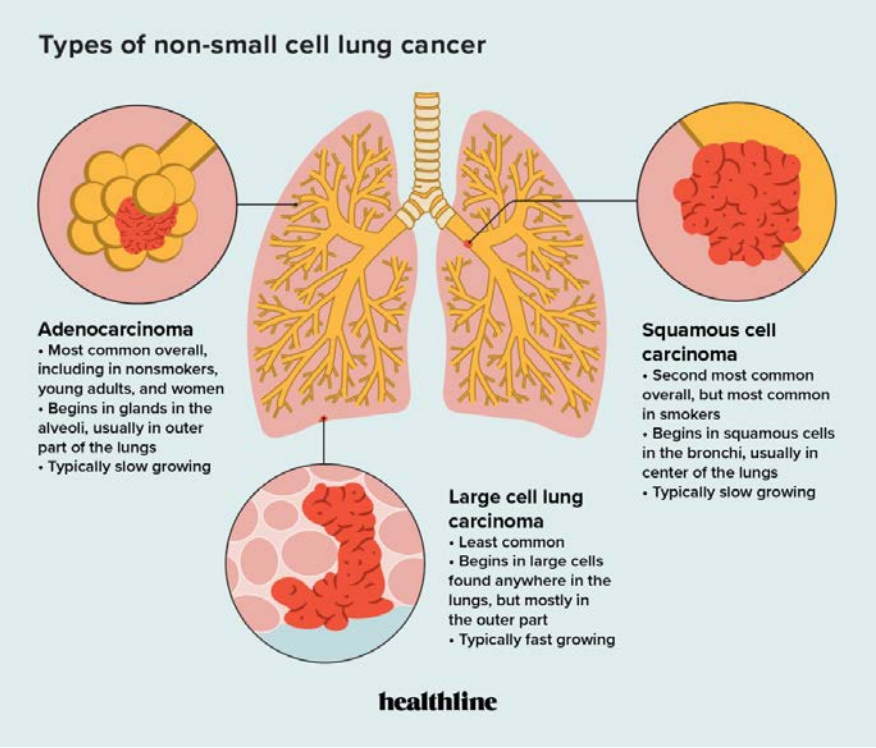

Lung Cancer - Non-Small Cell - Statistics https://www.cancer.net/cancer-types/lung-cancer-non-small-cell/statistics
Illustration available from: Types of Non-Small Cell Lung Cancer: Causes, Treatment, and Outlook https://www.healthline.com/health/lung-cancer/types-of-non-small-cell-lung-cancer

Background Information: Treatment regimes

FDA-approved Amivantamab (targets Epidermal Growth Factor Receptor and cytoplasmic Mesenchymal Epithelial Transition)

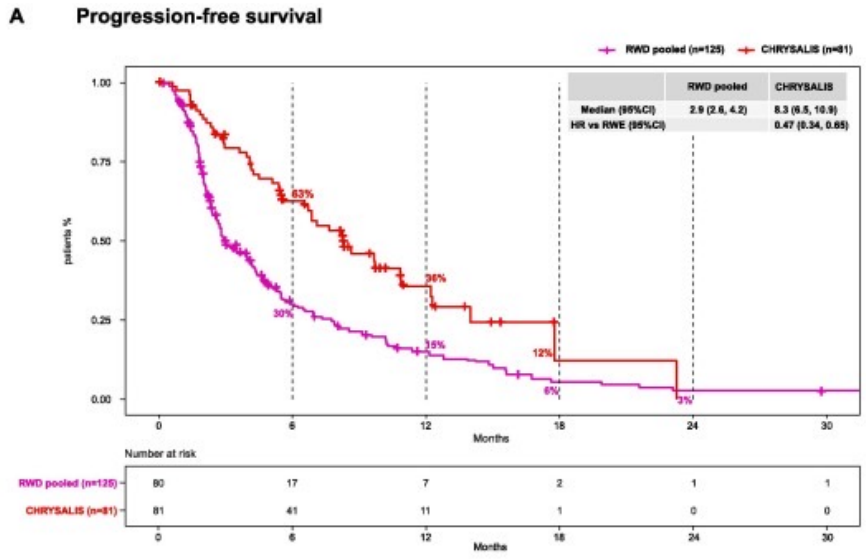

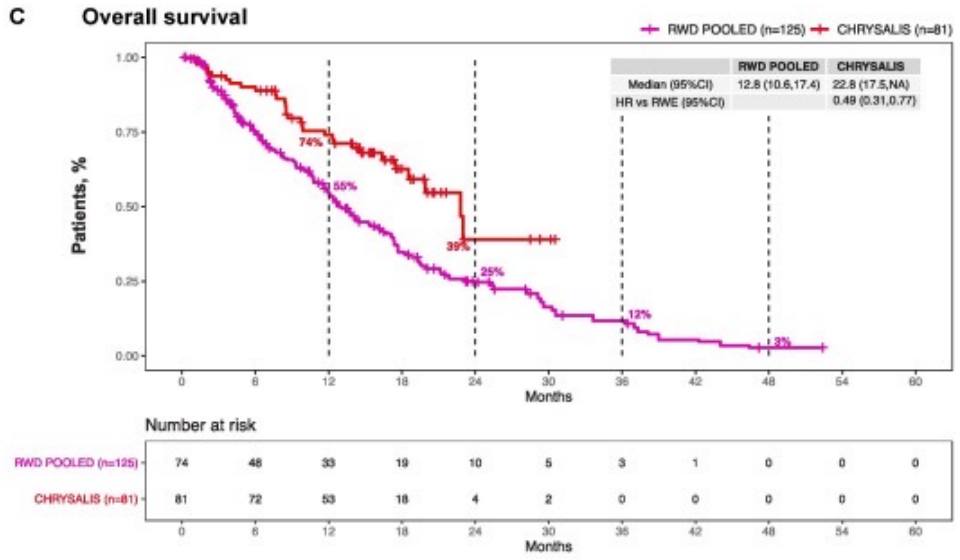

The overall response rate is 40%.

Minchom, A.; Viteri, S.; Bazhenova, L.; Gadgeel, S. M.; Ou, S.-H. I.; Trigo, J.; Bauml, J. M.; Backenroth, D.; Bhattacharya, A.; Li, T.; Mahadevia, P.; Girard, N. Amivantamab Compared with Real-World Therapies in Patients with Advanced Non-Small Cell Lung Cancer Harboring EGFR Exon 20 Insertion Mutations Who Progressed after Platinum-Based Chemotherapy. *Lung Cancer* **2022**, *168*, 74–82. https://doi.org/10.1016/j.lungcan.2022.03.005.

Current Selection Methods

- Biopsy
  - Immunohistochemistry (IHC)
  - Fluorescence In Situ Hybridization (FISH)
  - Gene Mutation Testing
- Limitations of tissue-based analysis:
  - Small sampling
  - Difficult to quantify heterogeneity
- Need a **whole-body assessment**

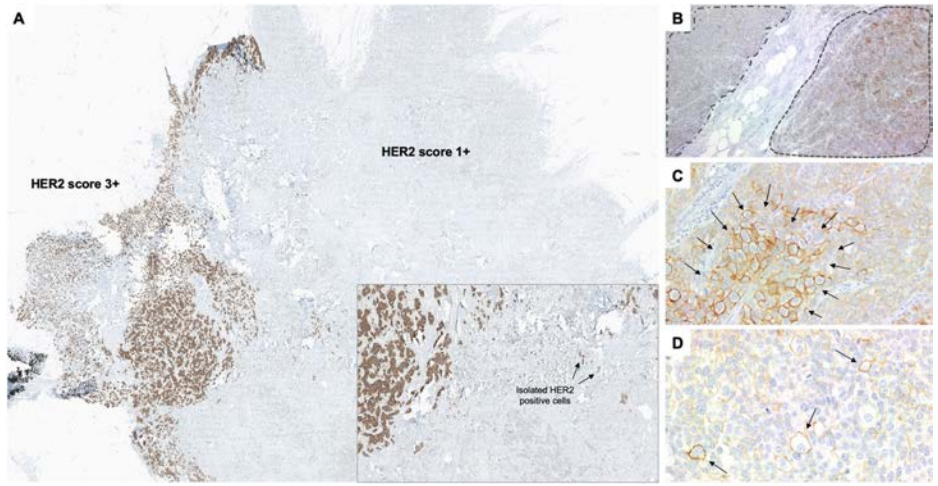

Marchio C. et al. 2020. *Seminars in Cancer Biology*

Positron Emission Tomography (PET)

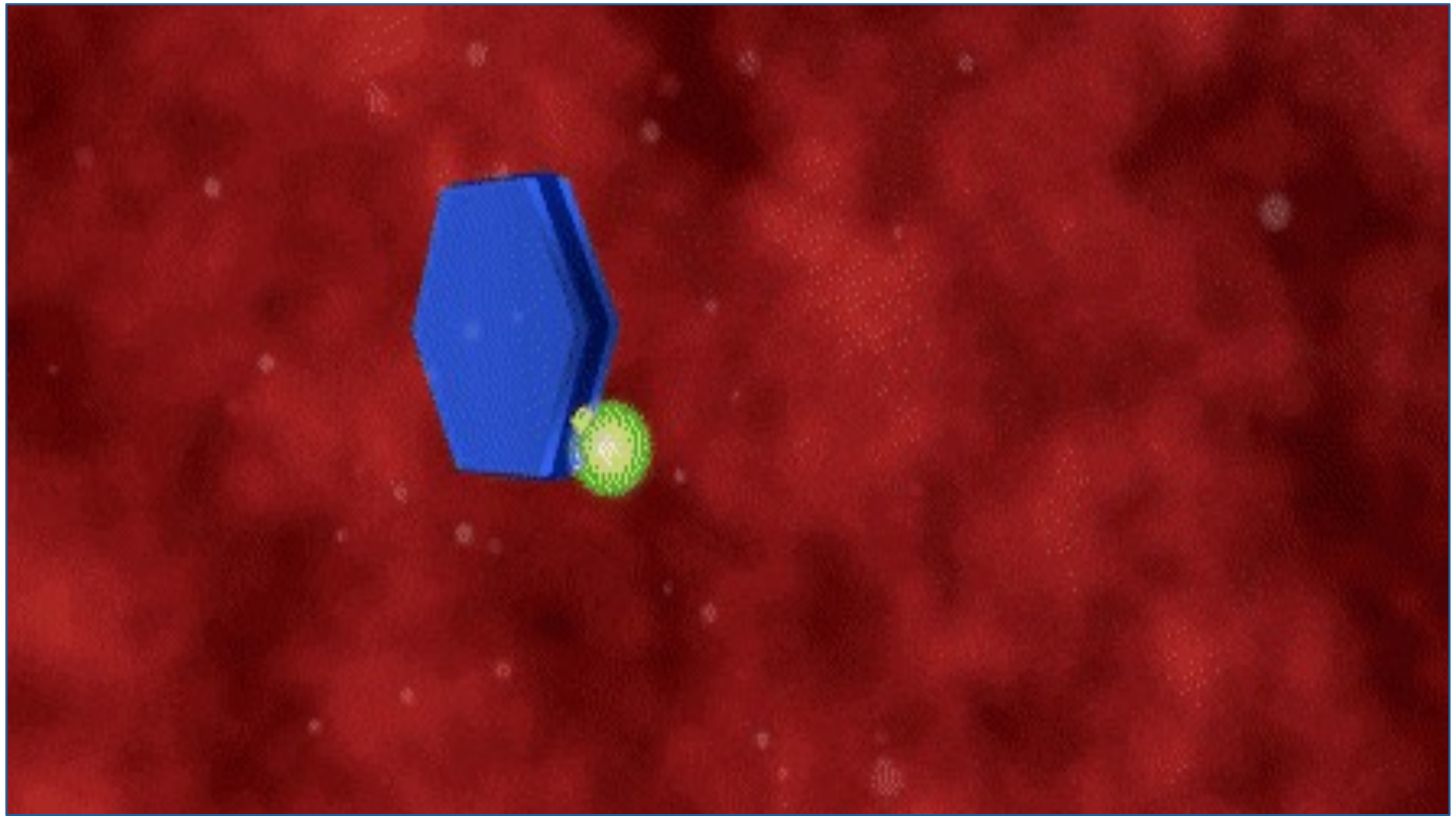

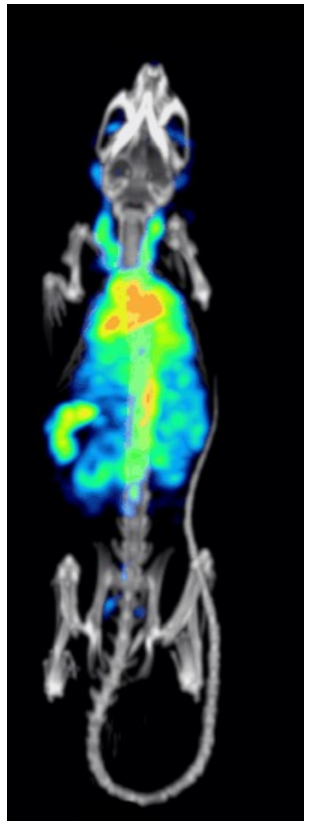

Videos available from: https://gfycat.com/selfassuredremorsefuldrever-positron-emission-tomography-diagnostic-test

PET Imaging

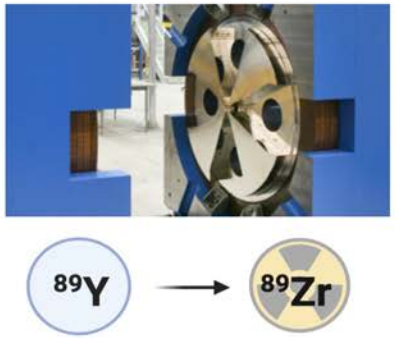

^{89}Y → ^{89}Zr

Production of radionuclide

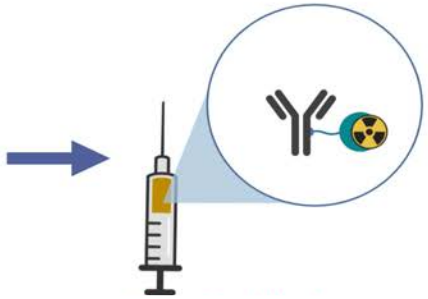

Preparation of radiotracer

Injection of radiotracer

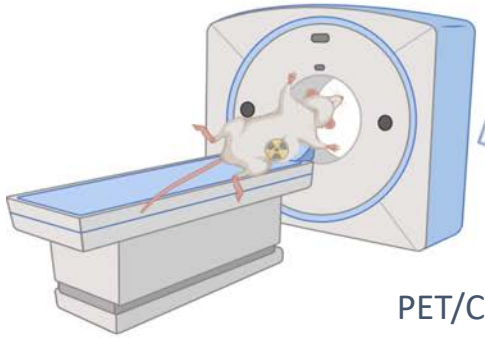

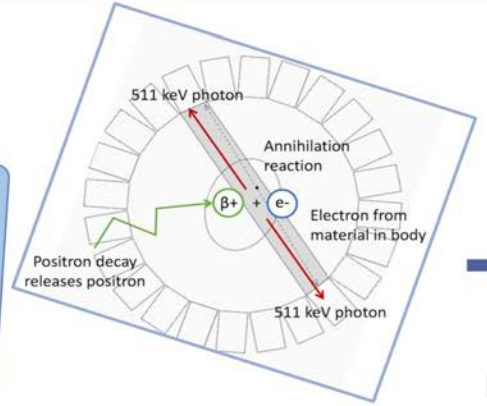

PET/CT imaging

Image processing and data analysis

PET/CT image of tumor-bearing mouse

Zirconium-89

- ^{89}Zr half-life matches biological half-life of antibodies
- Ideal for ImmunoPET
- Increased tumor to background ratio due to:
  - Extended imaging time
  - Residualizing property

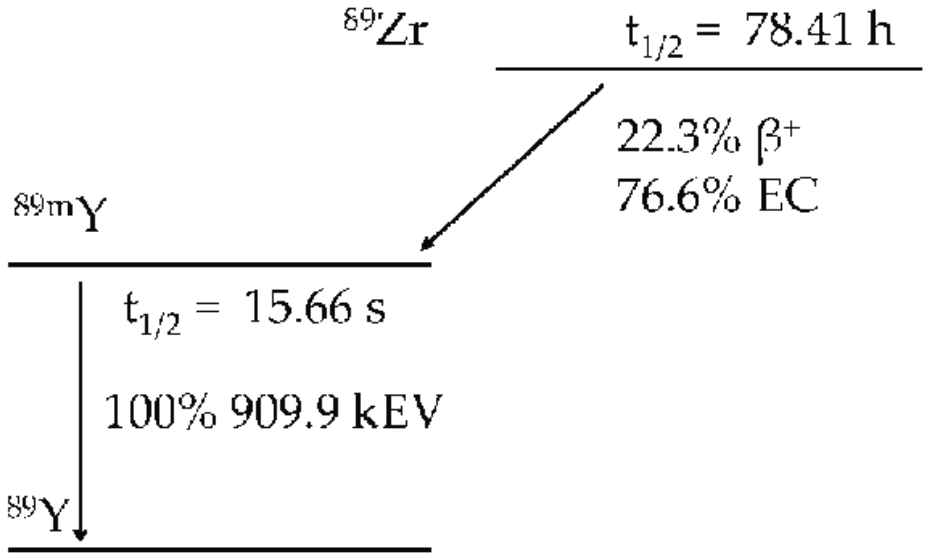

Designing ImmunoPET Agents: ^{89}Zr-AMI-DFO

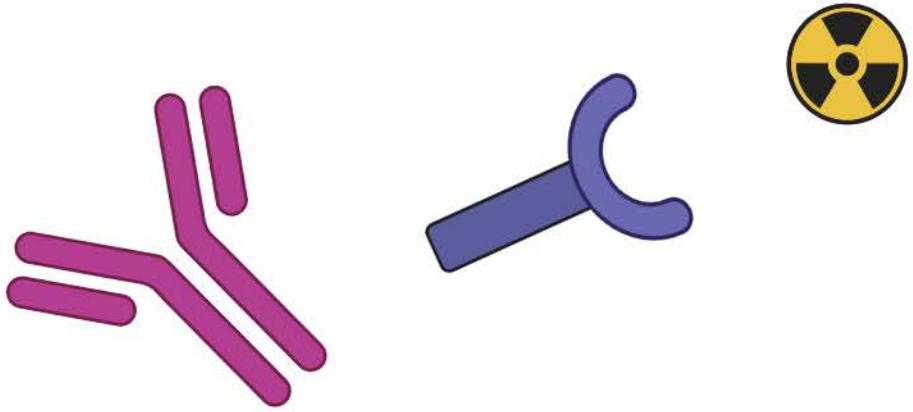

Targeting vector

Amivantamab (targeting EGFR and cMET)

Bifunctional metal chelate

Desferrioxamine (DFO)

Radiometal

^{89}Zr

Designing ImmunoPET Agents: ^{89}Zr-AMI-DFO

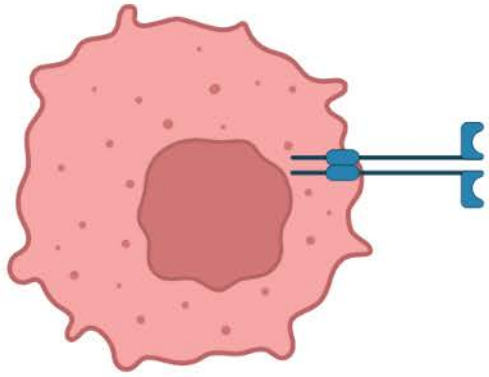

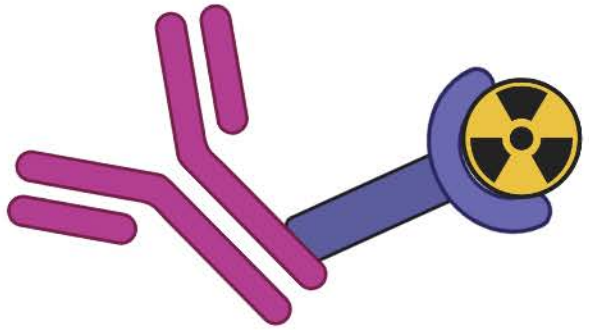

Tumor-associated protein target

Cell surface proteins (EGFR and cMET)

Targeting vector

Amivantamab (targeting EGFR and cMET)

Bifunctional metal chelate

Desferrioxamine (DFO)

Radiometal

^{89}Zr

Designing ImmunoPET Agents: ^{89}Zr-AMI-DFO

1. Radiolabeling of AMI-DFO with ^{89}Zr
   - pH 6.8-7.2
   - Room temperature

2. Characterization of ^{89}Zr-AMI
   - Radio-Thin Layer Chromatography
   - High Performance Liquid Chromatography

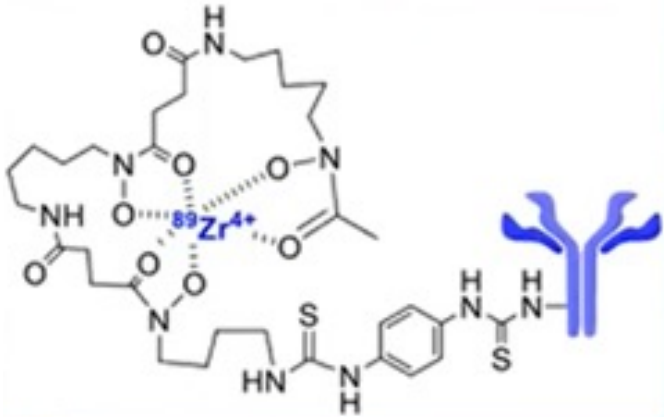

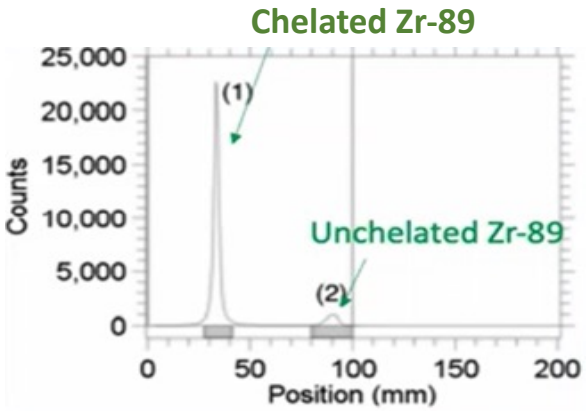

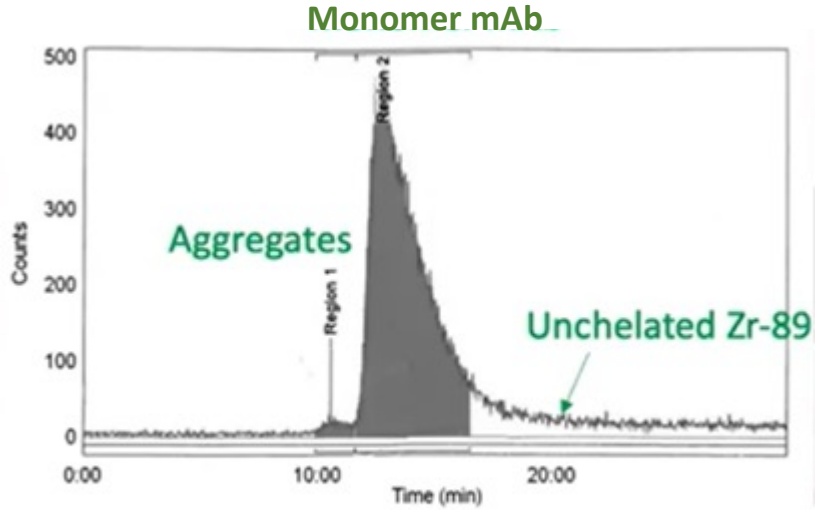

ImmunoPET for patient selection

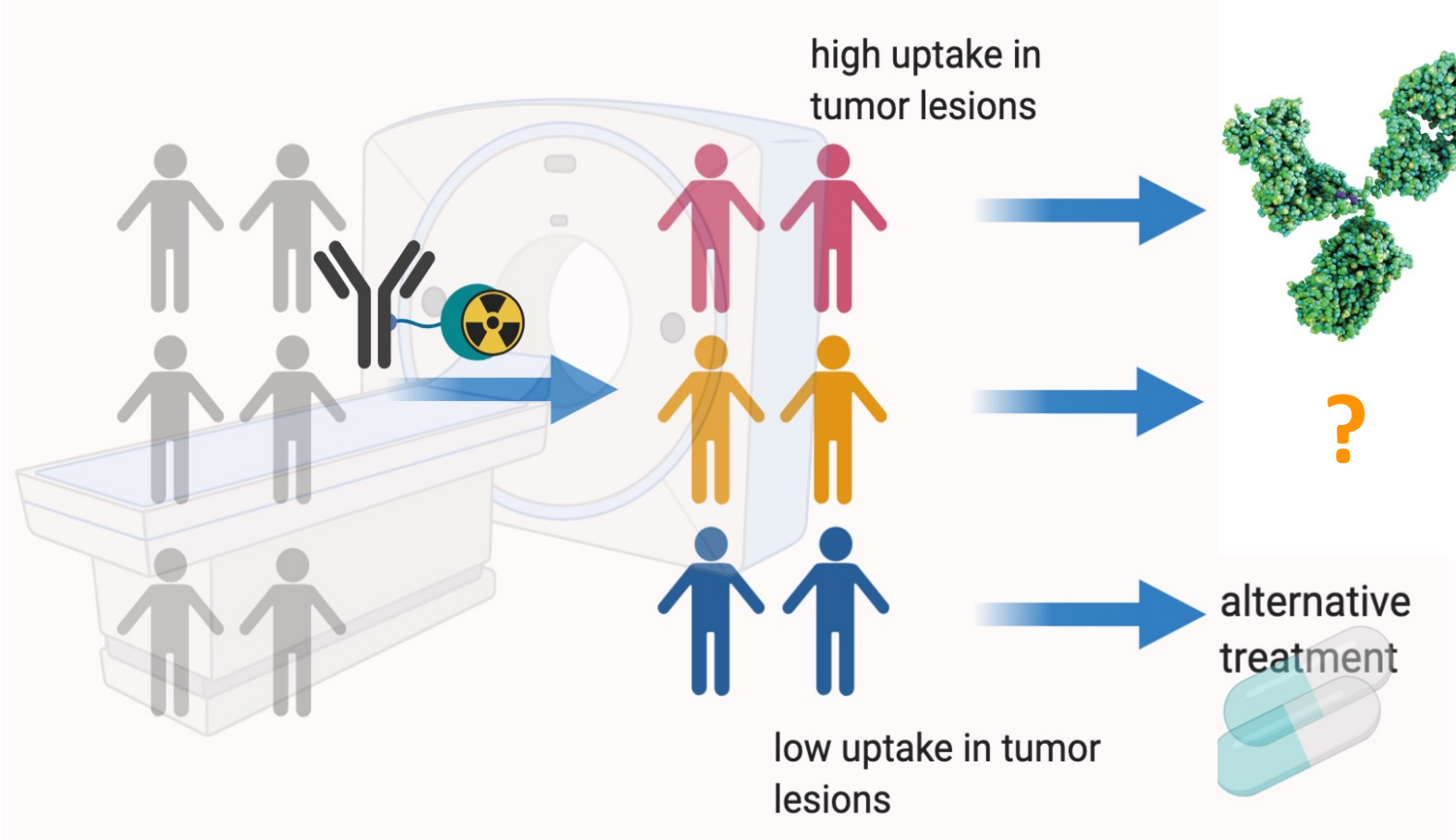

PET Imaging and Treatment Paradigm

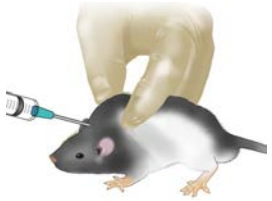

HCC-827 cell line injection

PET/CT Scan

PET/CT Scan

Days -30 -14 0 4 AMI Therapy 25 29

HCC-827 cell culture

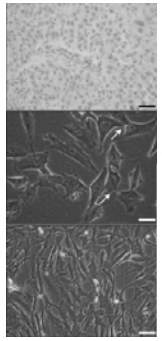

^{89}Zr-AMI injection

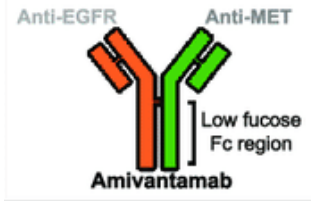

^{89}Zr-AMI injection

Tumor harvesting for ELISA

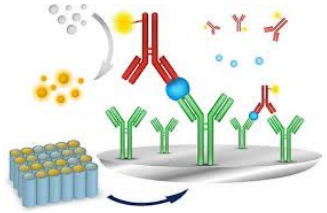

Yale University

Wright Laboratory

HOOL OF MEDICINE

Baseline CT/PET Imaging

Axial

Coronal

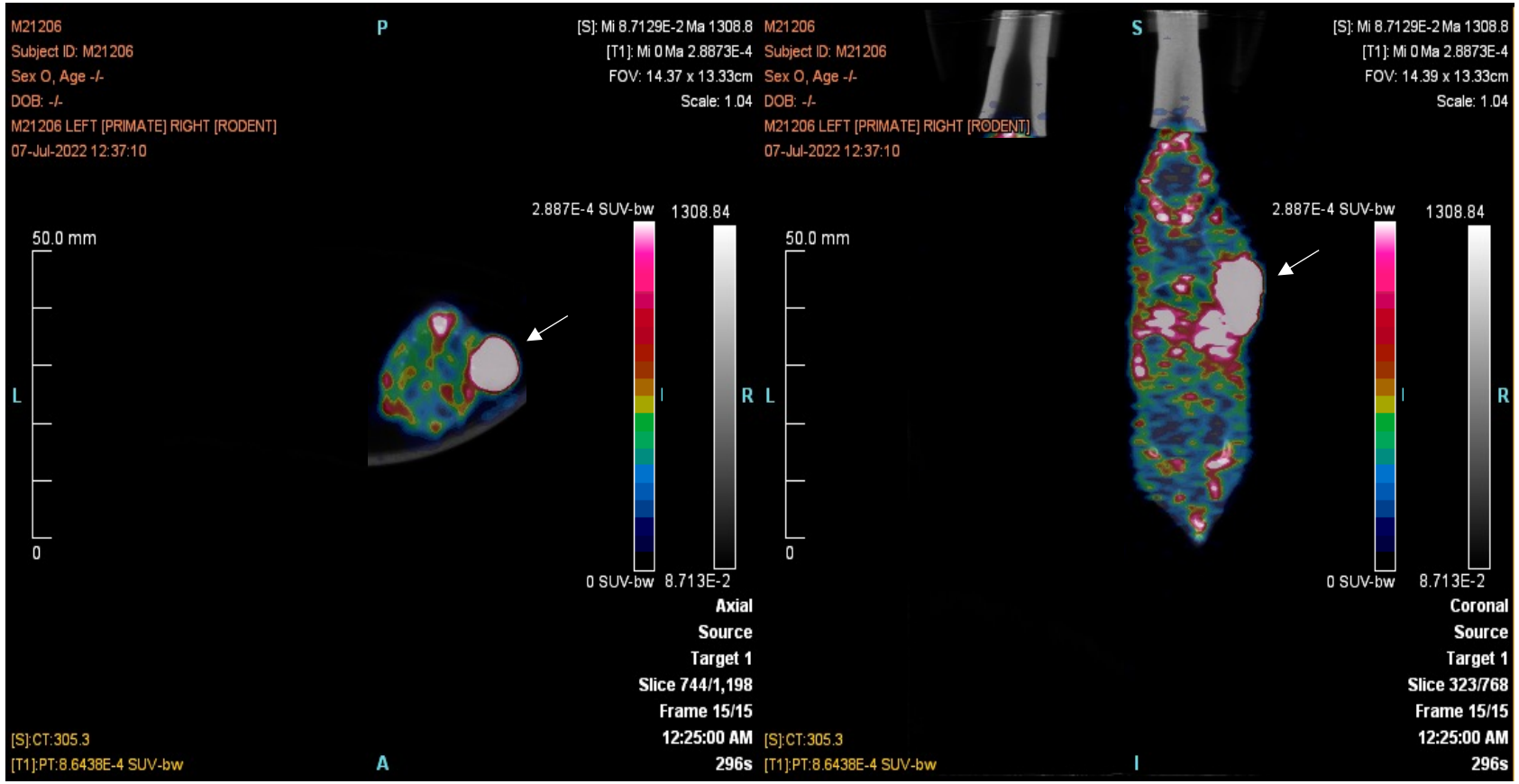

Tumor Growth Curve

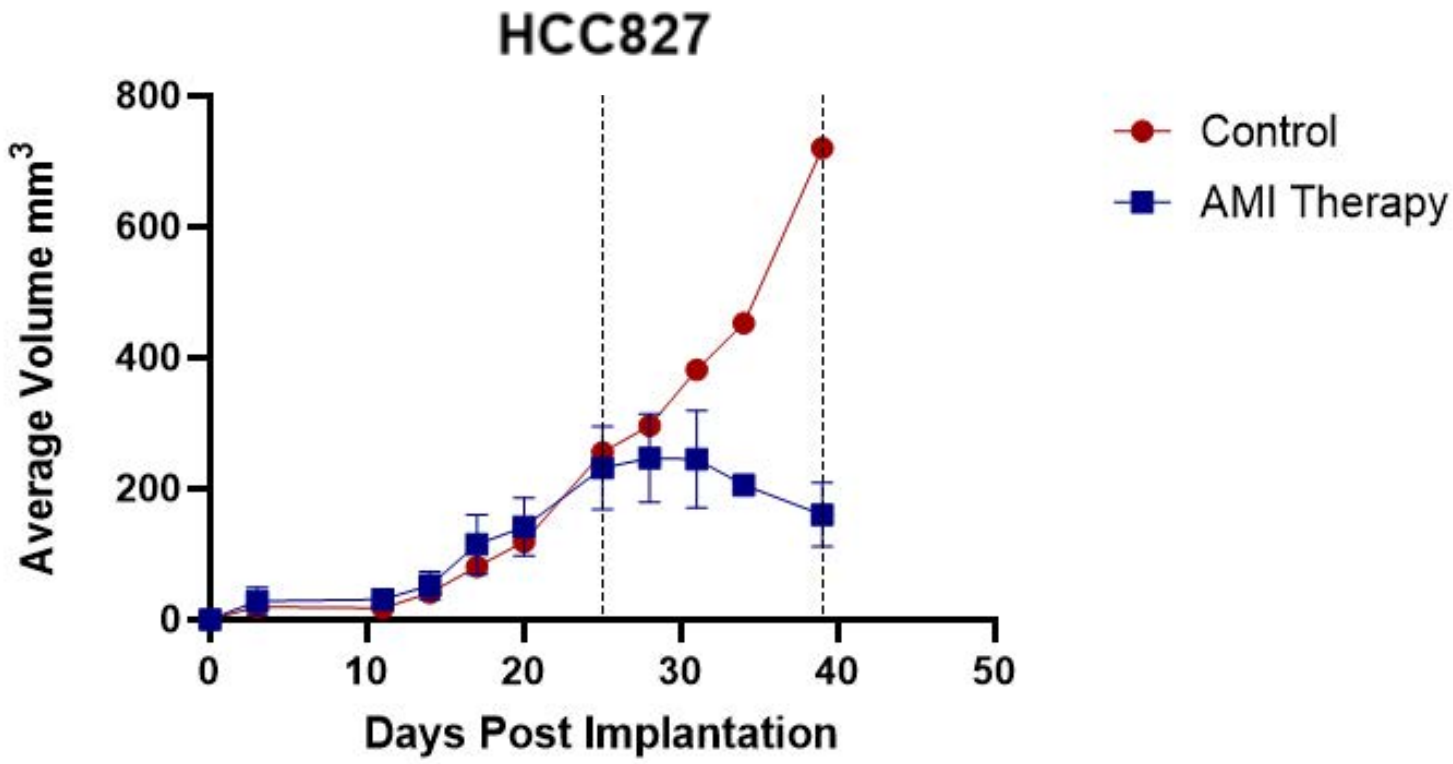

Tumor Growth Inhibition

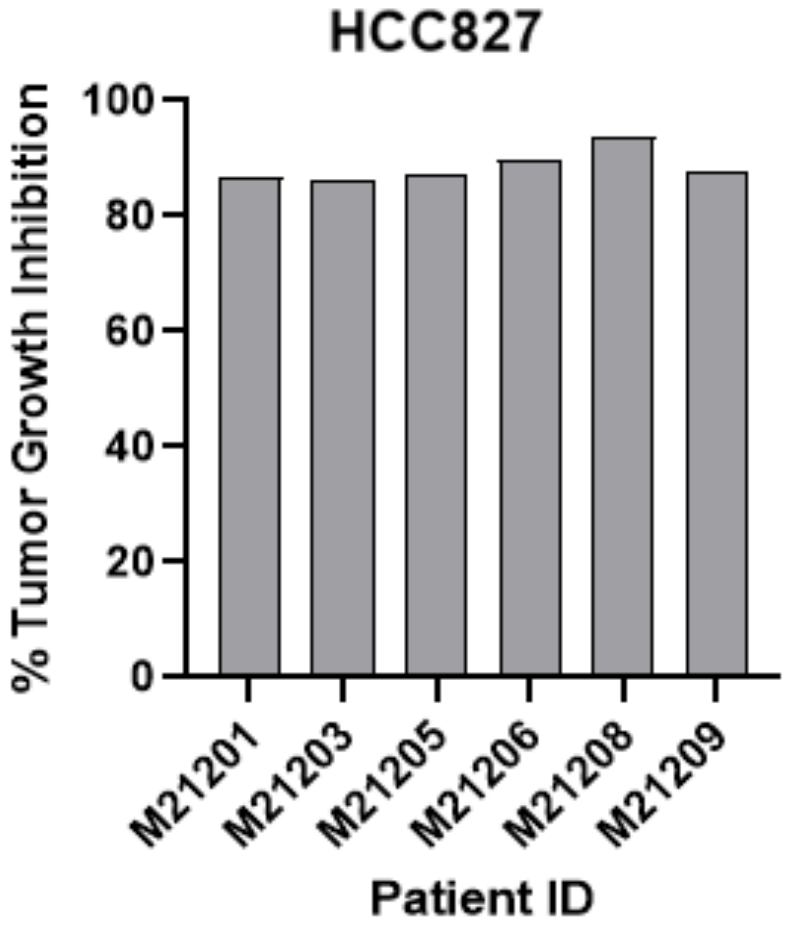

$$\%\,TGI = \left(1 - \frac{RTV_{\ treated\ group}}{RTV_{\ control\ group}}\right) \times 100(\%)$$

$$RTV = \frac{tumor\ volume_{\ day\ 25}}{tumor\ volume_{\ day\ 0}}$$

Baseline and post therapy comparison

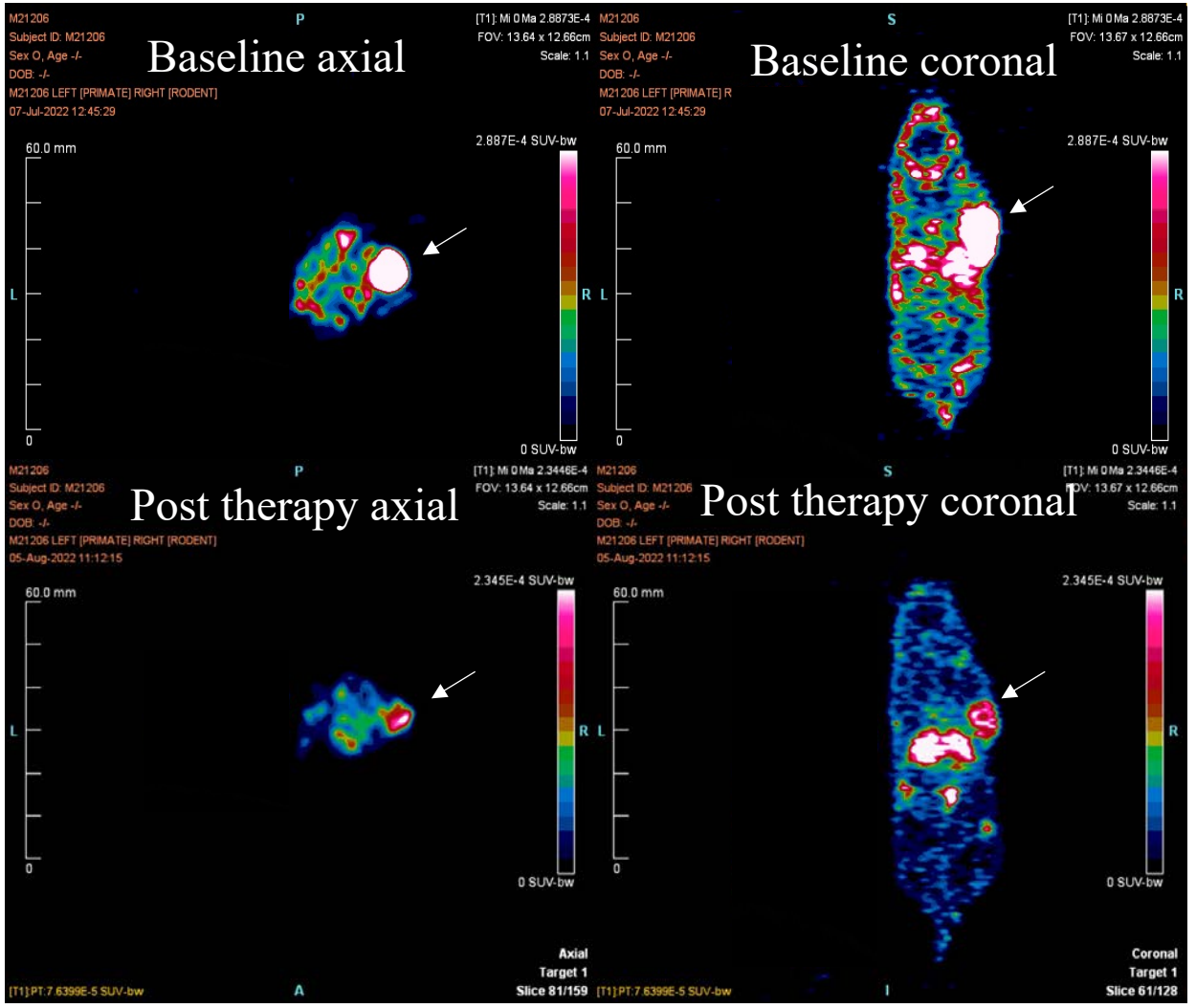

Maximum Intensity Projections

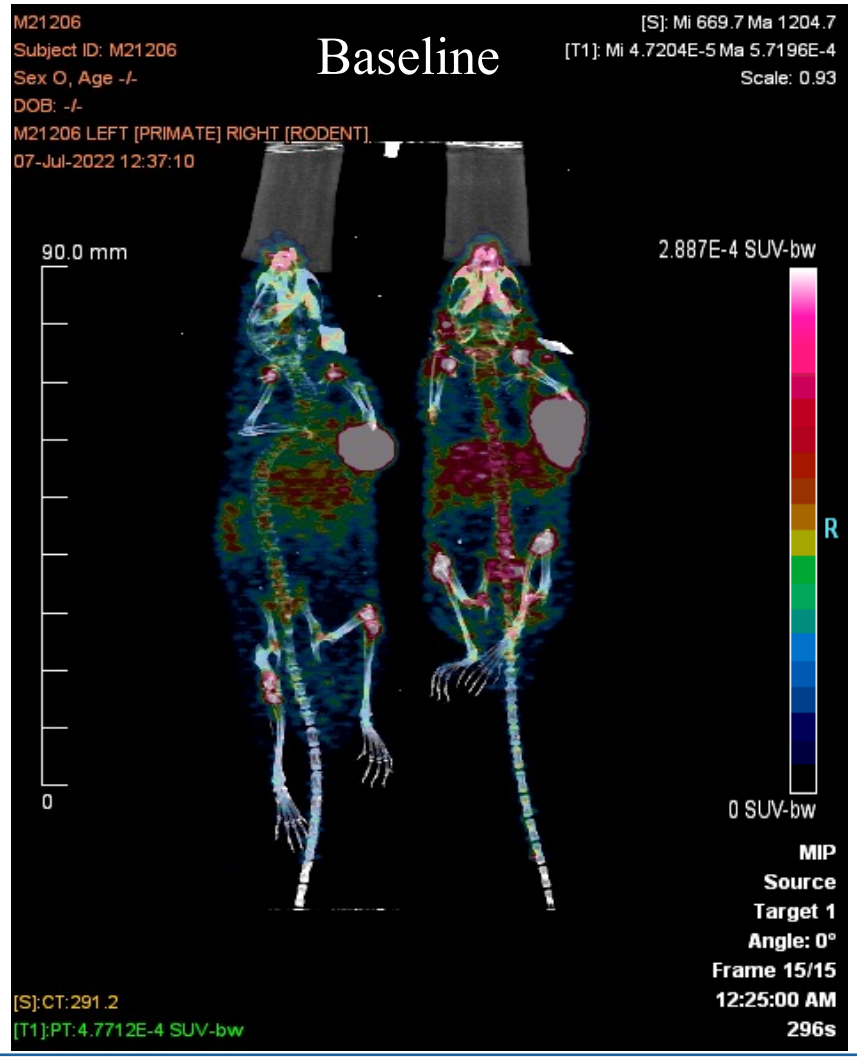

Yale University

Wright Laboratory

HOOL OF MEDICINE

Tumor-to-heart SUV ratios

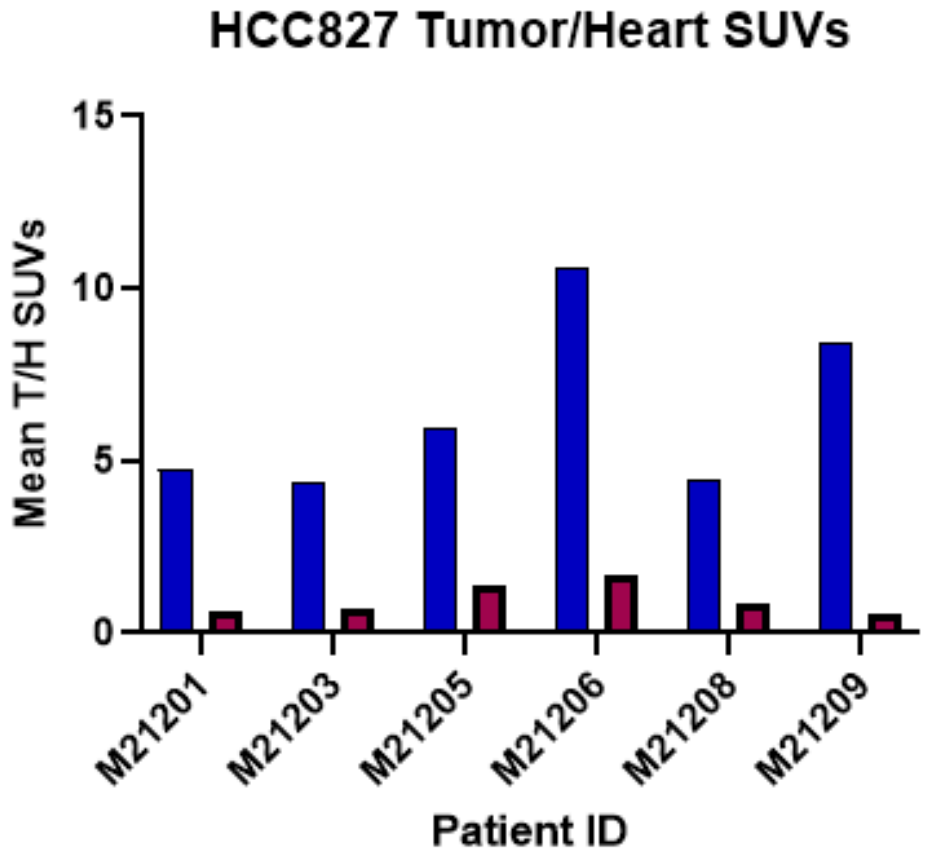

$$SUV = \frac{activity\ in\ tissue}{injected\ activity} \times mass$$

$$SUV\ ratio = \frac{mean\ SUV_{tumor\ ROI}}{mean\ SUV_{heart\ ROI}}$$

Learning Outcomes

- Interdisciplinary lab
- Team working in research
- Practical aspects of working in a lab
- A priceless opportunity to confirm my interest in research

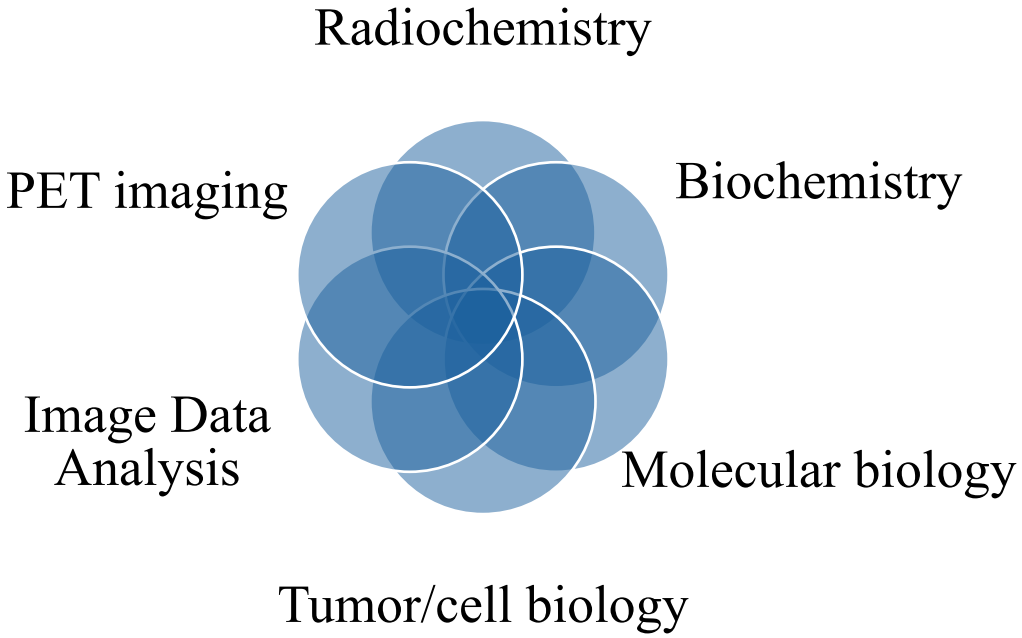

Instrumentation

Invion PET/CT scan for small animals

IVIS (In Vivo Imaging System)

EVOS (Digital Fluorescence Microscope)

Automatic Gamma Counter

HPLC

Radiation Well Counter

Softwares for image and data analysis

Prism

Yale University

Wright Laboratory

HOOL OF MEDICINE

Acknowledgements

Onaosi-Yale partnership

Antonio Ereditato, PhD
Bonnie Fleming, PhD
Victoria Misenti
Taylor Dunnigan
Emanuela Pallotta
Paolo Giovenali
Francesco Tavernese

CIT lab – Bernadette Marquez-Nostra, PhD

Current members

Samantha Katz, MS
Elisabeth Katz
Lindy Melegari

Alumni

Khashayar Rajabimoghadam, PhD
Erika Belitzky

Academic Collaborators

Evan Morris, PhD
Jocelyn Hoye, PhD
Alaaddin Ibrahimy

Yale PET Center

Tim Mulnix, PhD

Industry partners

Janssen Pharmaceuticals

Sheri Moores, PhD

Funding

Onaosi
NIH NCI R01CA255226

Onaosi-Yale program team

Lodovico, Tiziano, Giulia, Francesca, Andrea, Antonio

Yale University

Wright Laboratory

HOOL OF MEDICINE

Thank you!

Wright Laboratory

OPERA NAZIONALE ASSISTENZA ORFANI SANITARI ITALIANI
FONDAZIONE ONAOSI

CIT

Wright Laboratory

Yale University School of Medicine

FONDAZIONE ONAOSI

Prostate NLG diffusion phantom using PVP water solution

- Andrea De Simone

First, some questions

- What is diffusion?
- What is a non-linear gradient (NLG)?
- What is a phantom?

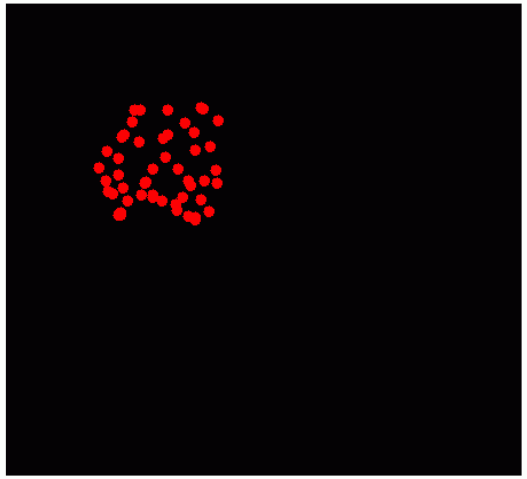

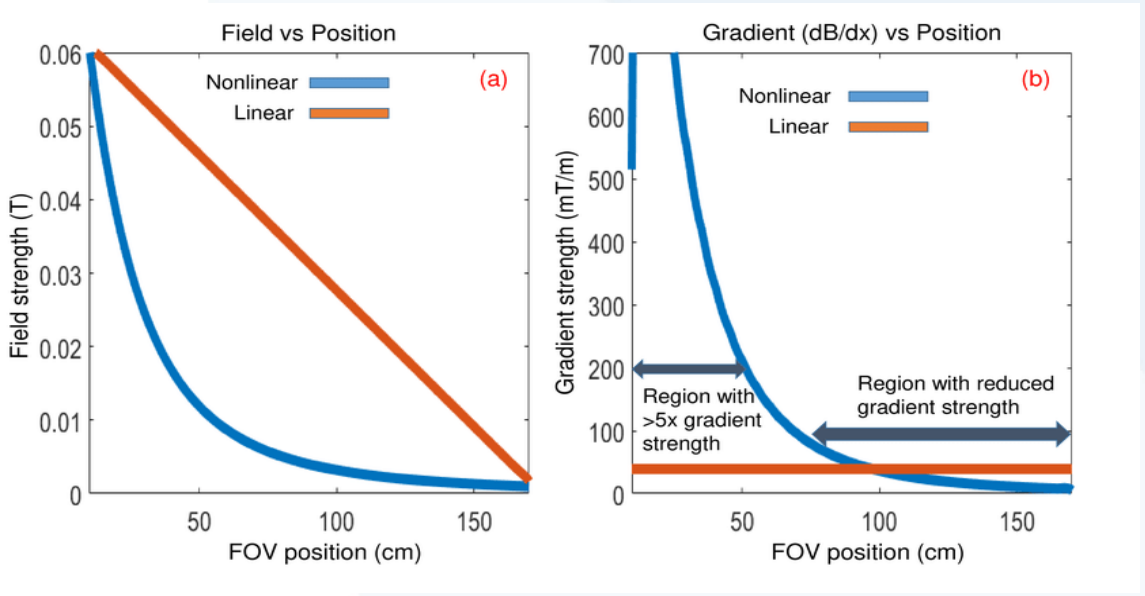

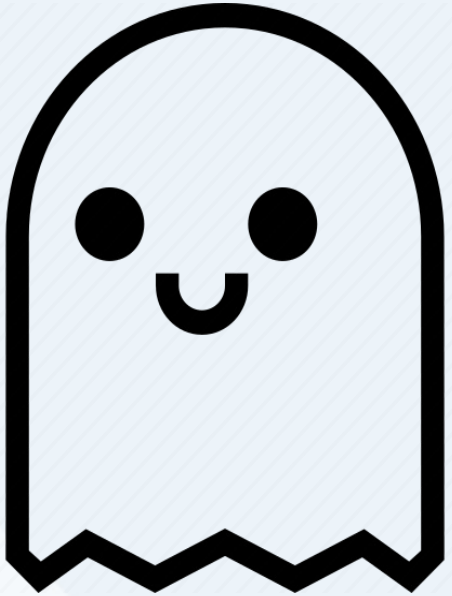

Diffusion-weighted imaging

- Diffusion-weighted imaging (DWI) is a form of MR imaging based upon measuring the random Brownian motion of water molecules within a voxel of tissue.

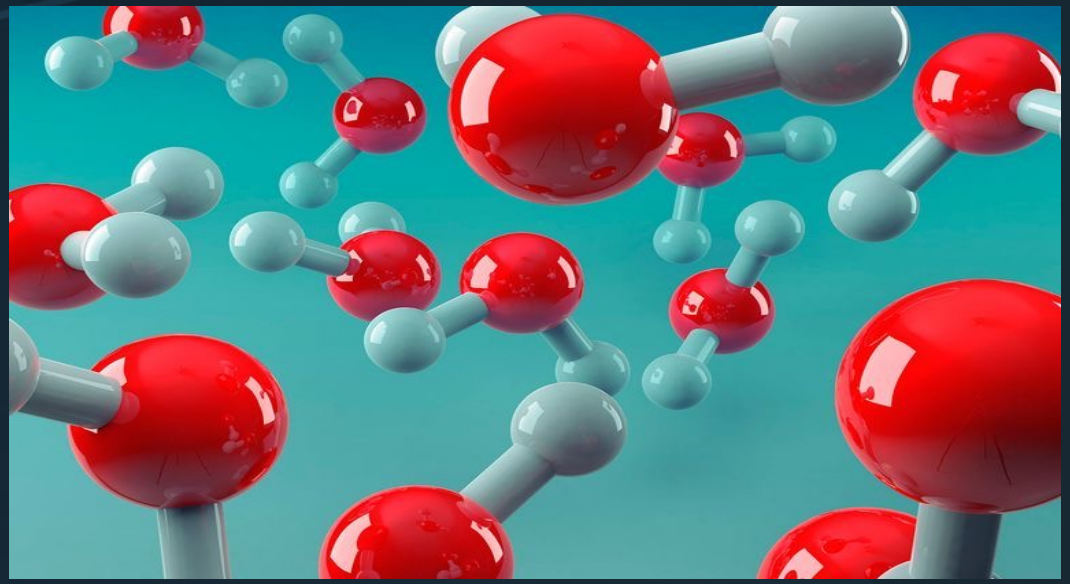

From DWI to ADC maps

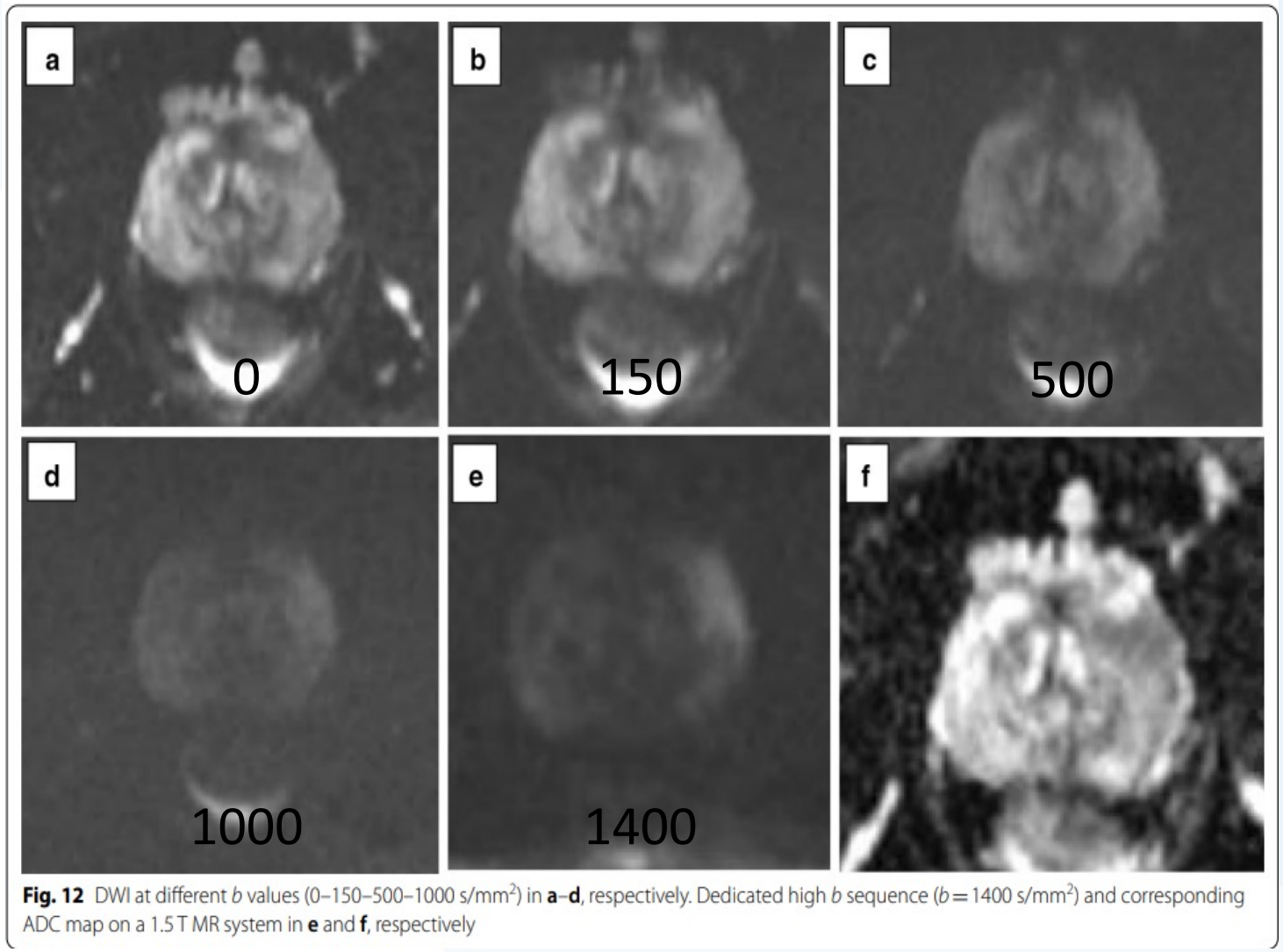

Fig. 12 DWI at different *b* values (0–150–500–1000 s/mm^2) in **a**–**d**, respectively. Dedicated high *b* sequence ($b = 1400$ s/mm^2) and corresponding ADC map on a 1.5 T MR system in **e** and **f**, respectively

How does MRI work?

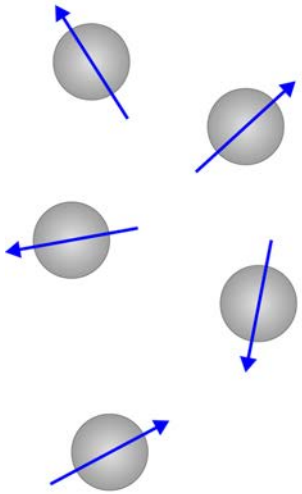

Larmor frequency: $\omega=-\gamma B$

Diffusion weighting (without diffusion)

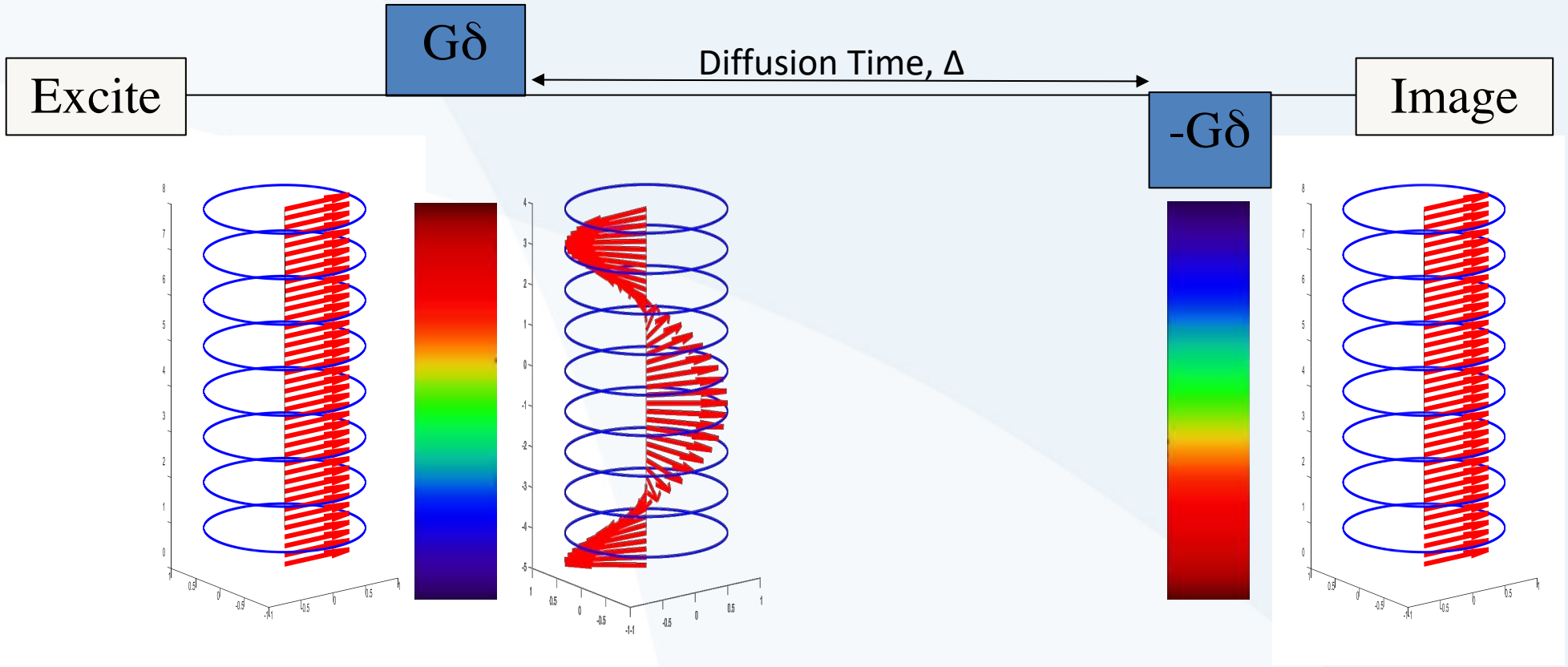

Maximum signal

Diffusion weighting (with diffusion)

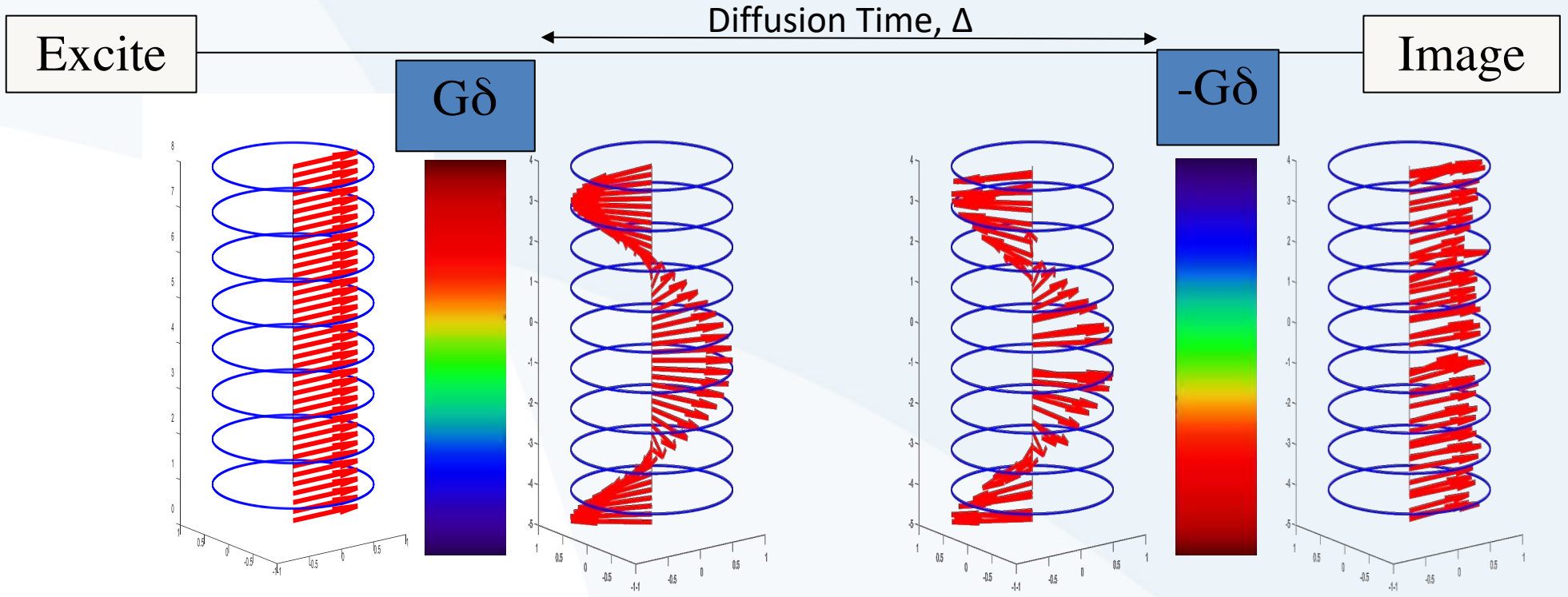

- Spins *approximately* return to x-axis
- But not perfectly aligned
- **Pixel gets darker!**

LOSS OF SIGNAL

Stronger diffusion weighting

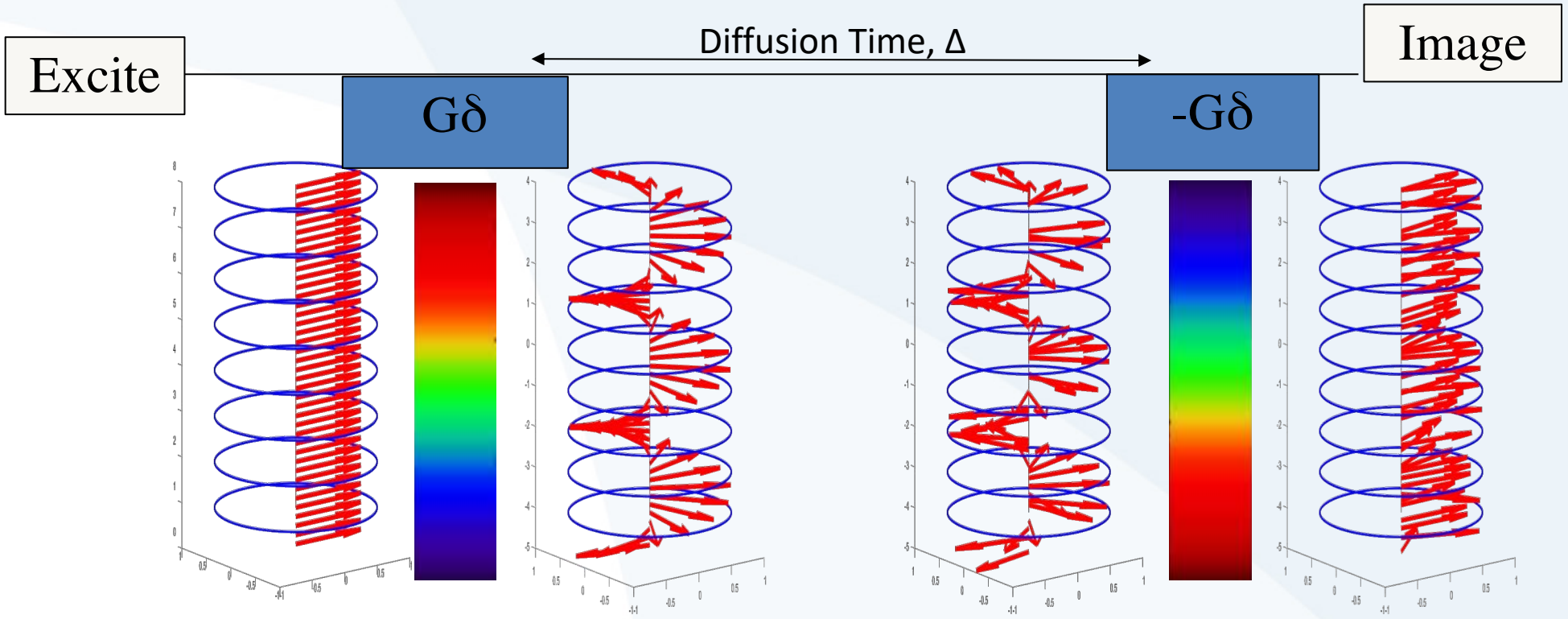

↑ randomization of direction = ↑ signal loss = ↑ sensitivity to diffusivity

What is a gradient in DWI?

- $S = S_o e^{-bD}$
- $b = \gamma^2 G^2 \delta^2 (\Delta - \delta/3)$

Stronger gradient

Better image

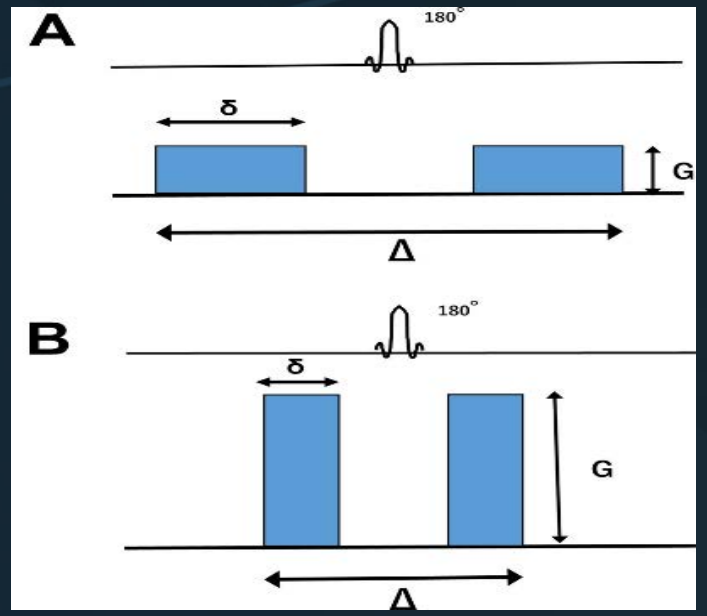

The benefits of NLGs

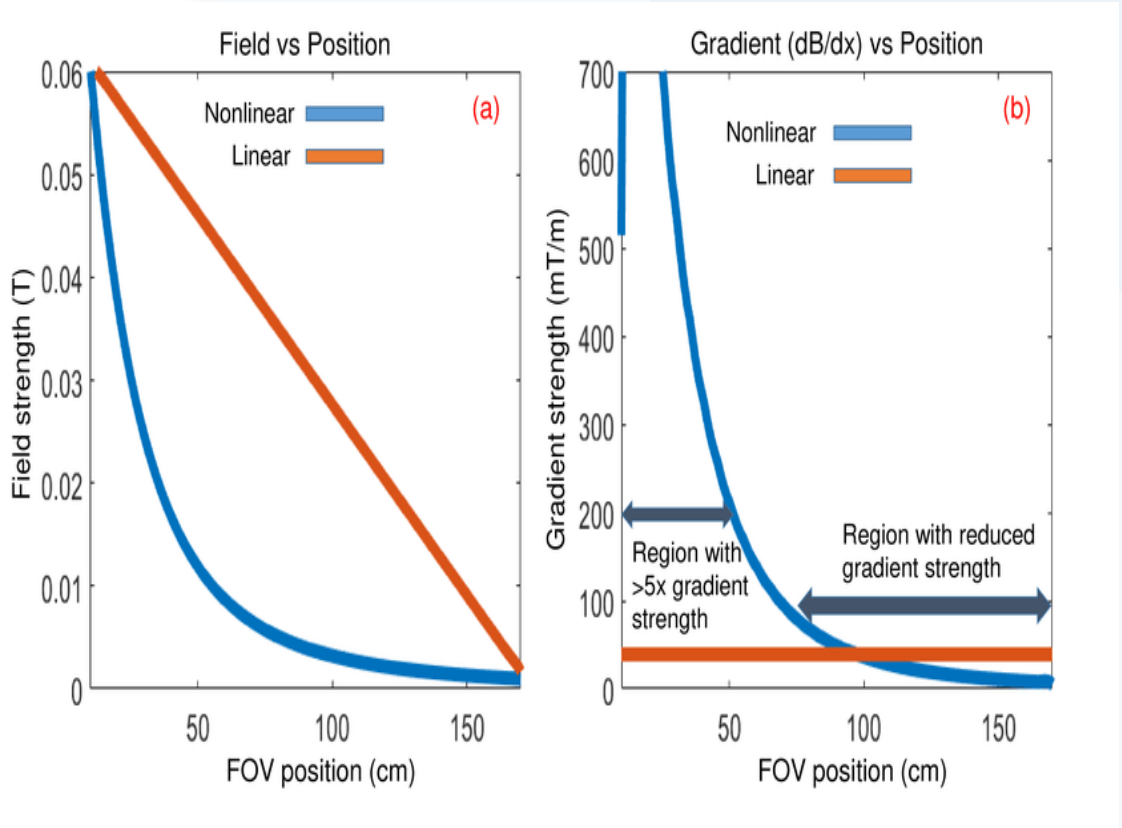

- Concentrates the field change
- Works well on the prostate (small, close to surface, relatively isotropic).
- High SNR
- *" […] Shorter encoding times and higher b-values increase the ability to distinguish benign and cancerous lesions ".*[1]

Let’s compare

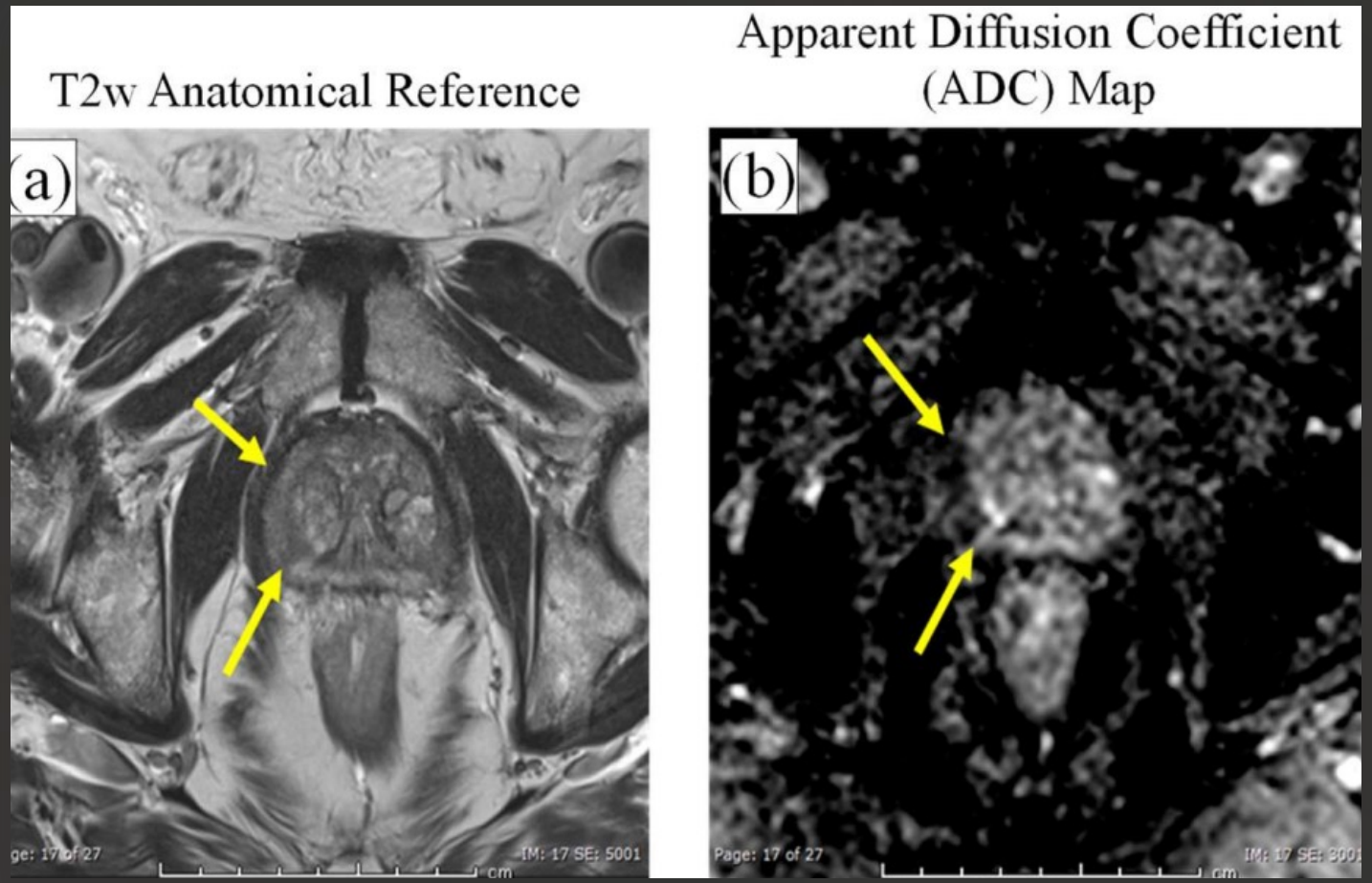

Our NLG

- The magnetic field is created right in front of the prostate, allowing for a much stronger gradient in our ROI.

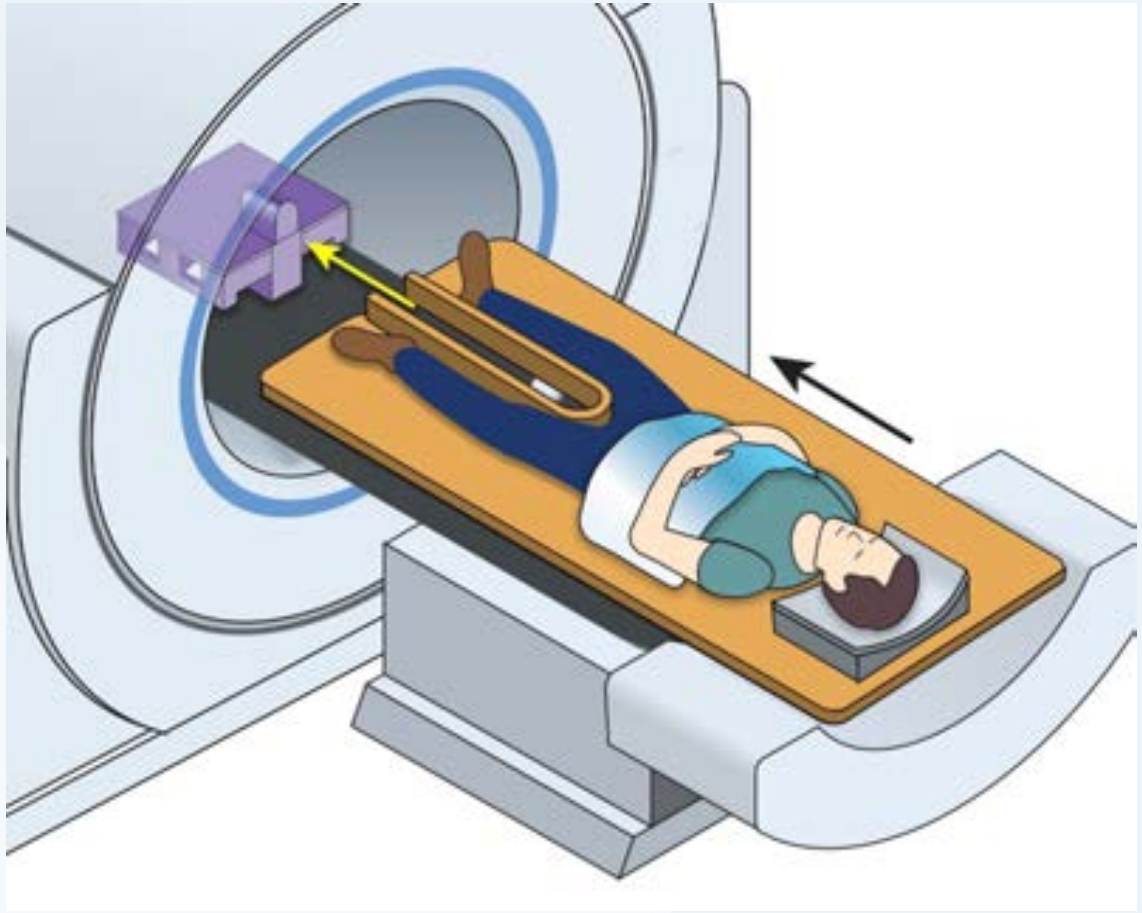

Our NLG hardware

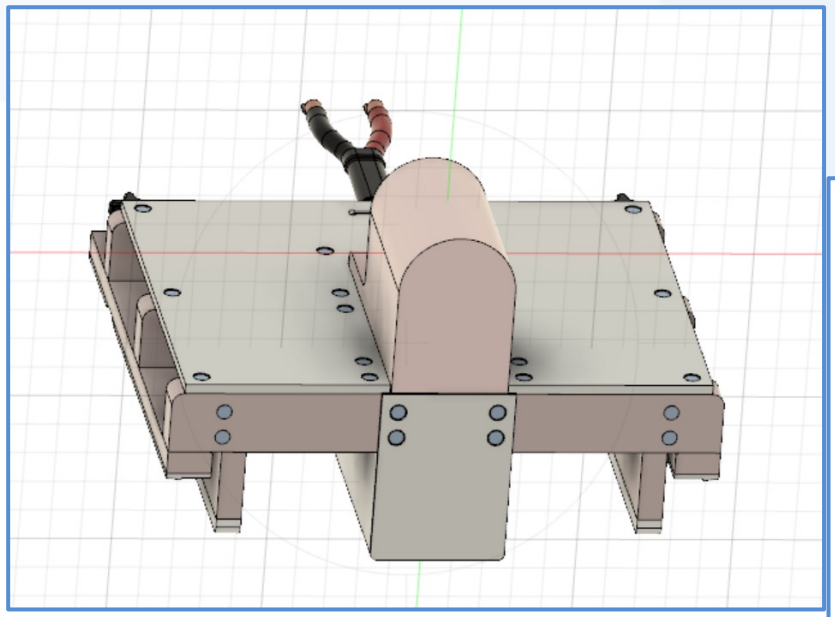

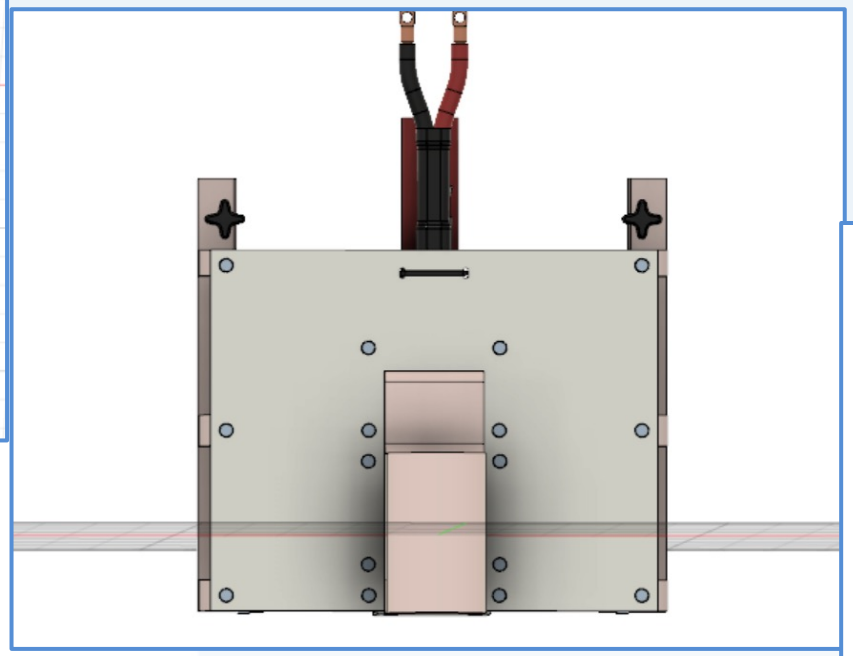

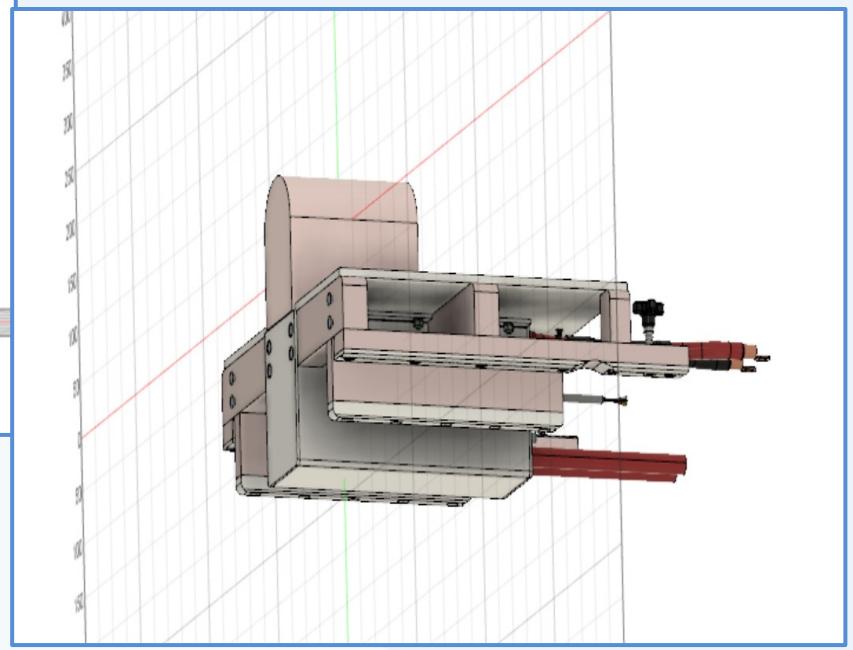

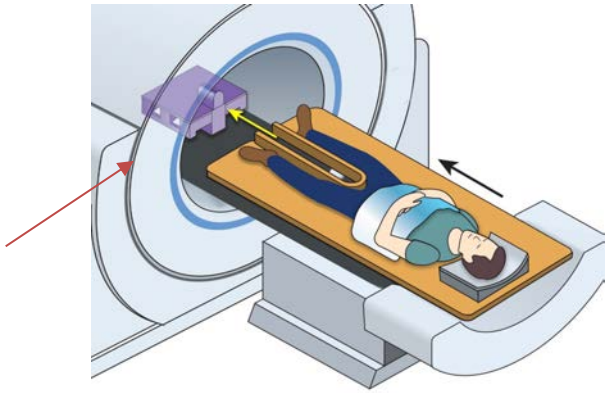

What is a phantom?

- A phantom is a specially designed object that is utilized as a “stand-in” for human tissue and can be scanned or imaged to evaluate, analyze, and fine-tune the performance of an imaging device.

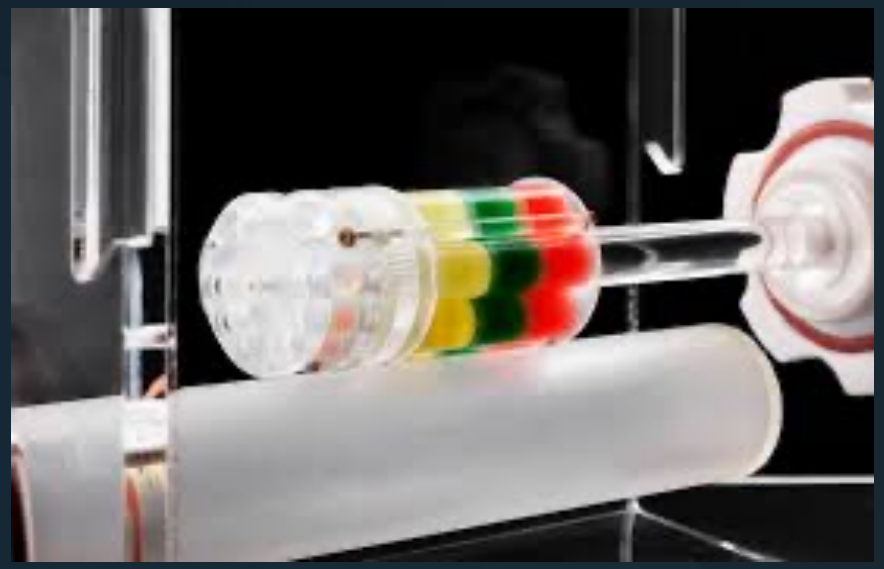

Okay…

…now what?

The purpose of our study

- *To validate the feasibility and accuracy of DWI and ADC mapping using NLGs [that are] designed to provide a high gradient at the prostate.*[1]

- *[This] could help distinguish between malignant and benign prostate lesions, thereby saving patients from unnecessary invasive procedures such as biopsies.*[2]

Step 1: designing the phantom

- The phantom was designed in two parts.
- 1) First, the **arch-like structure** was created to fit the gradient coil.
- 2) Additionally, we designed a **box** that could hold the six PVP vials plus a distilled water vial.
- Easier to switch between phantoms!

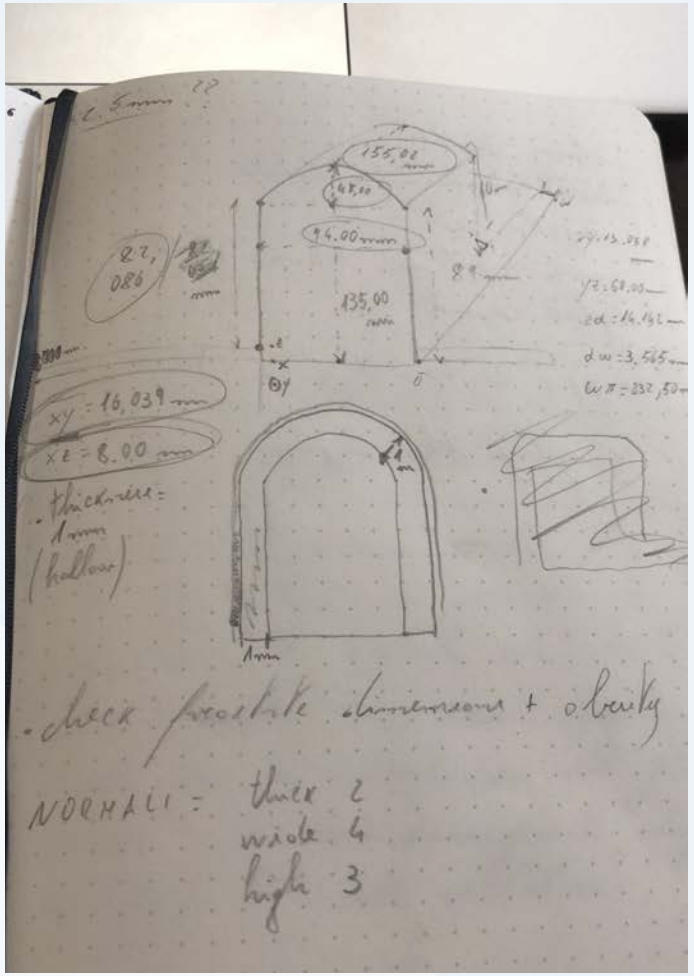

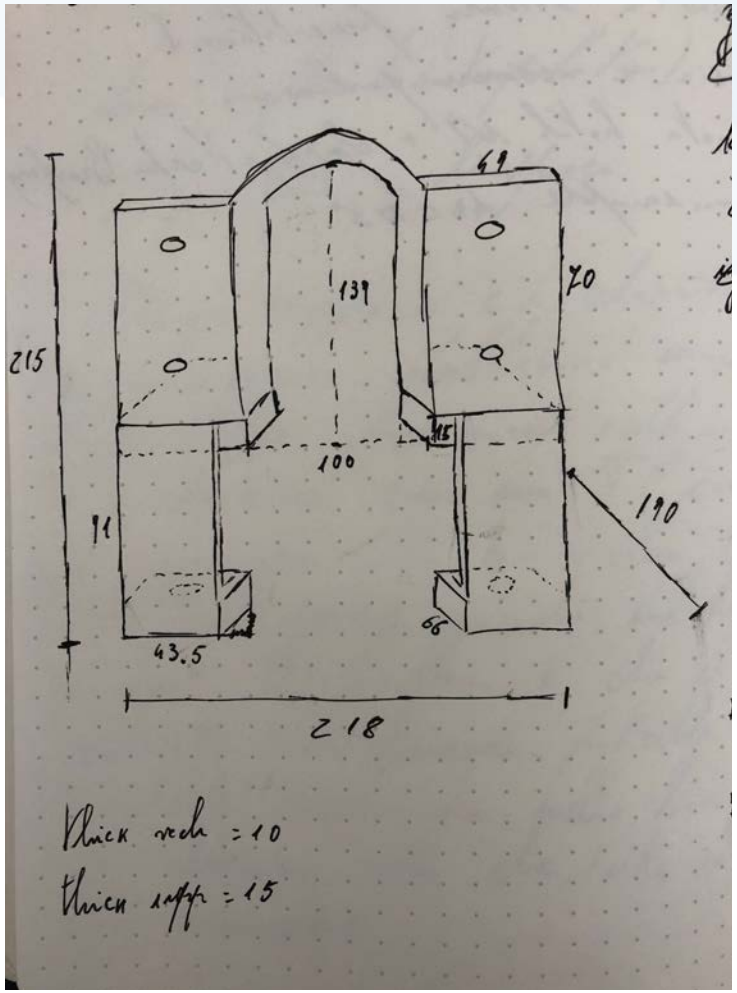
69
139
70
215
100
190
91
43.5
218
Dicke rechts = 10
Dicke Rippe = 15

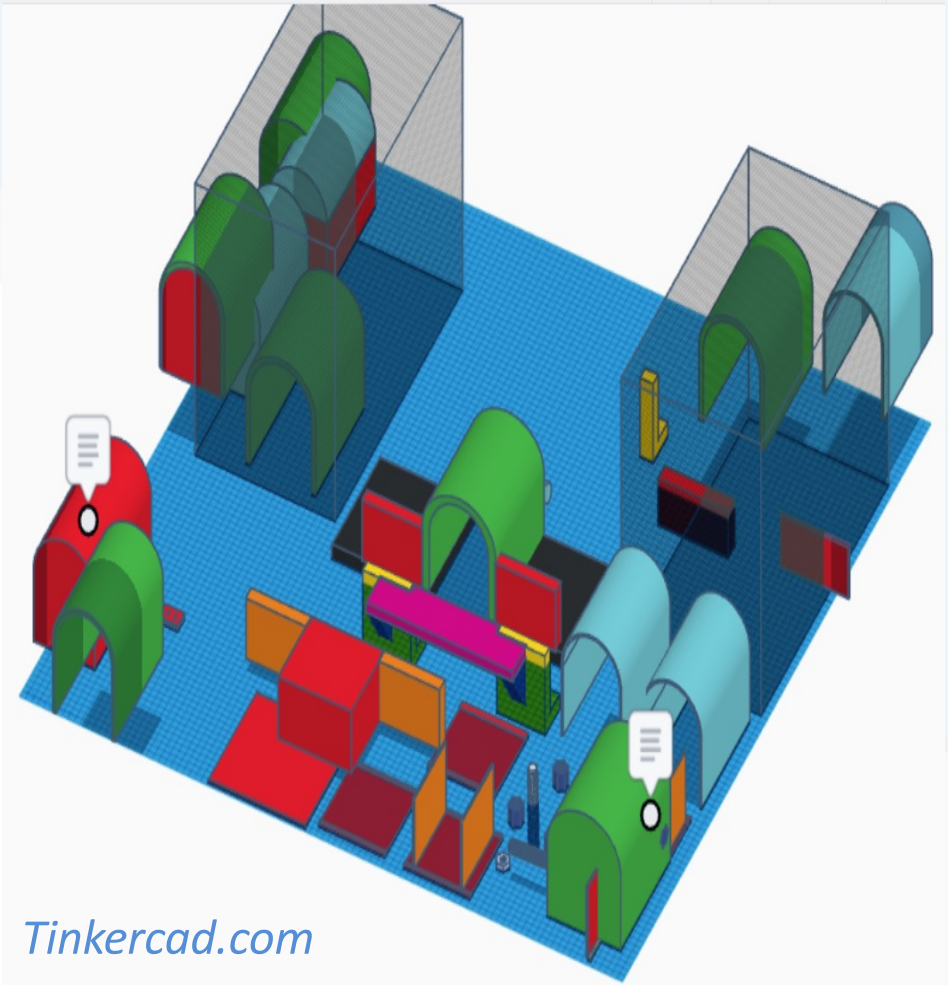
Tinkercad.com

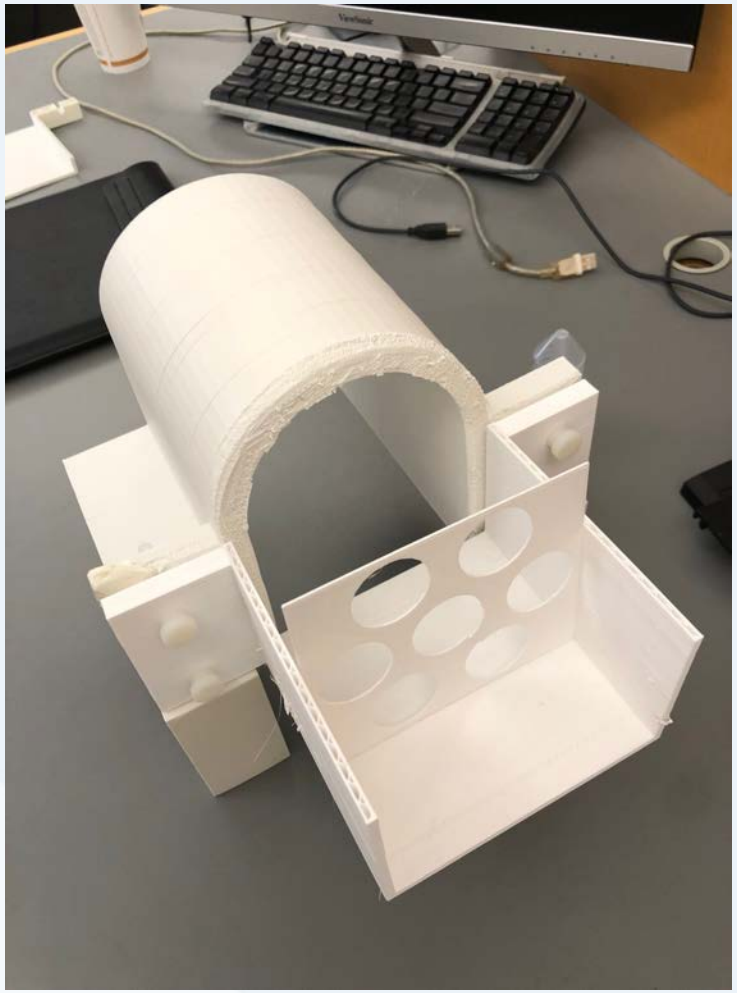

Step 2: PVP water solution

- In order to replicate and mimic the prostate tissue, we decided to use a PVP water solution with different PVP concentrations.[3]

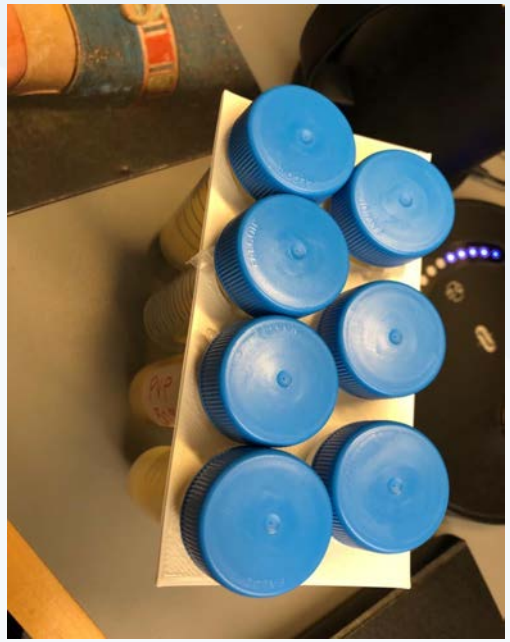

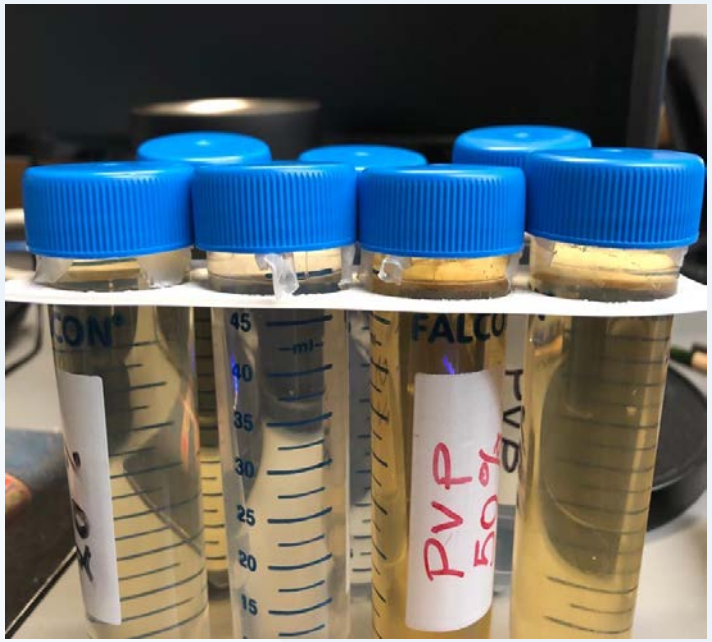

Final result!

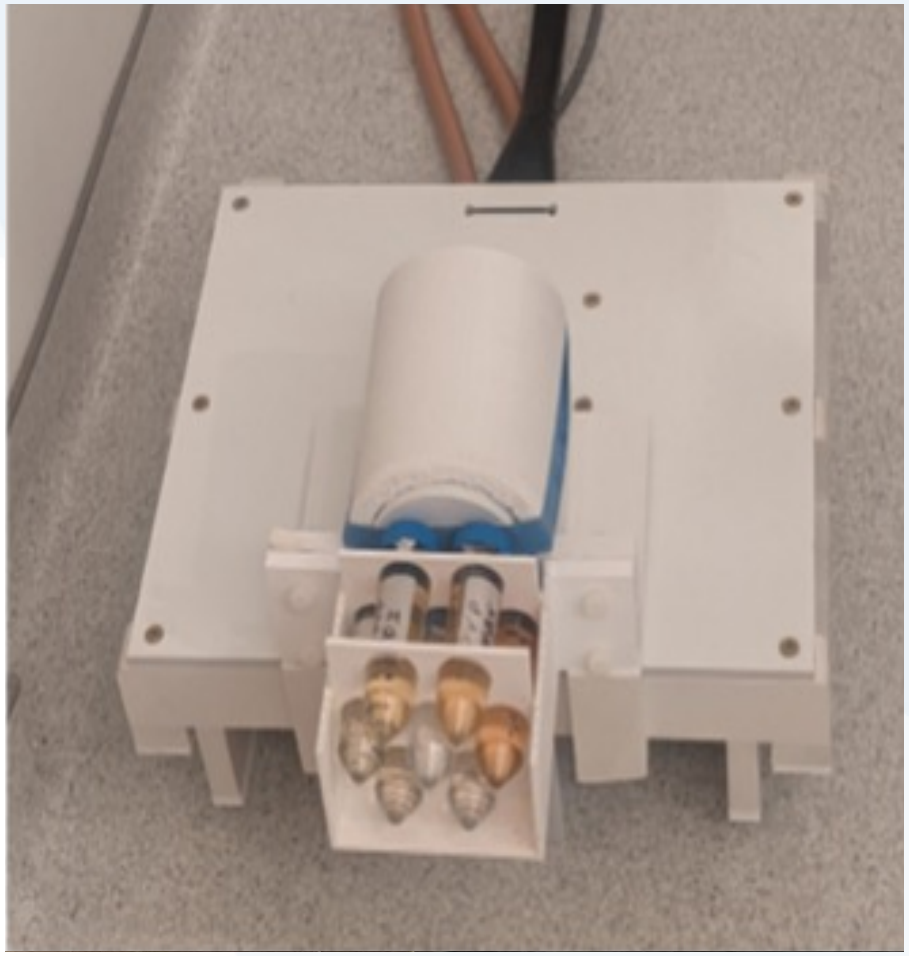

Step 3: scanning the phantom

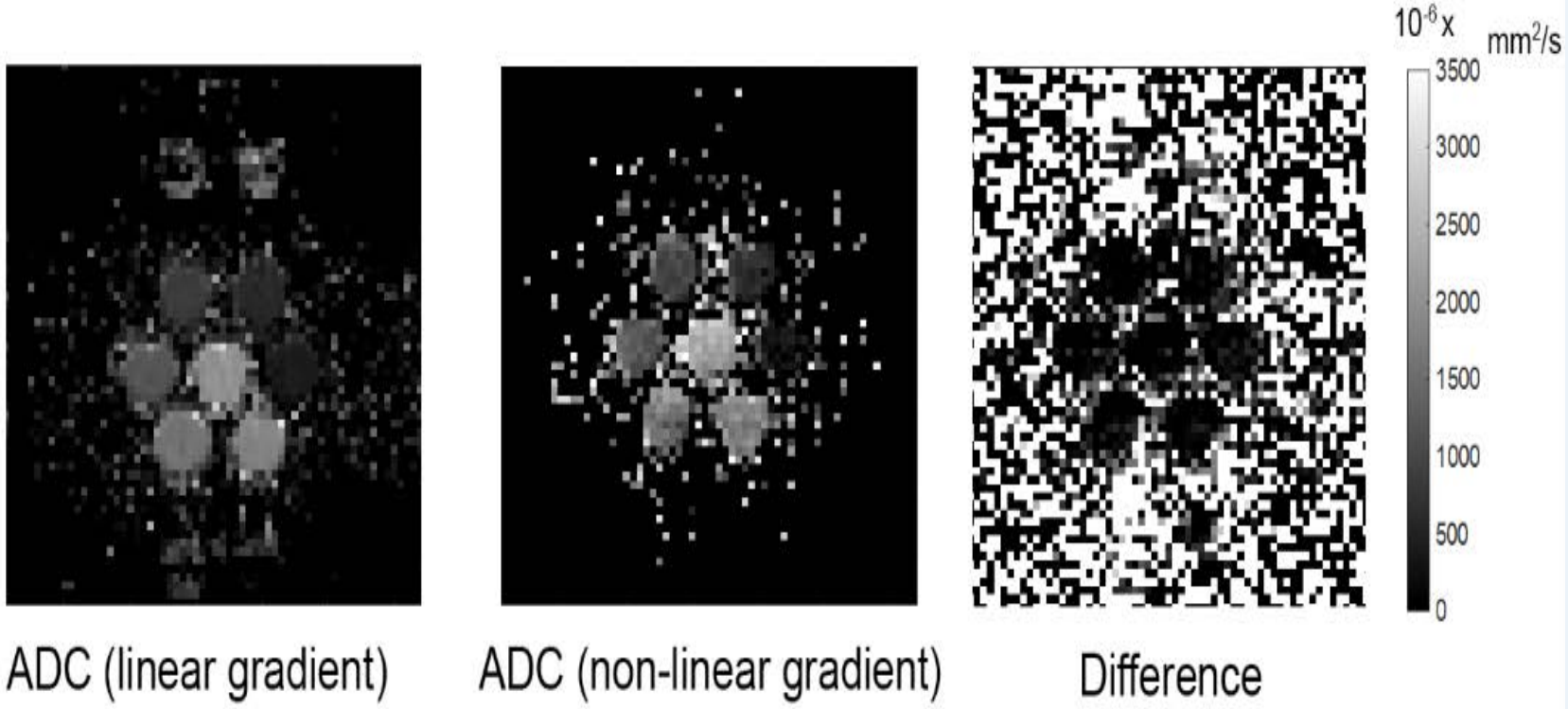

What we were expecting…

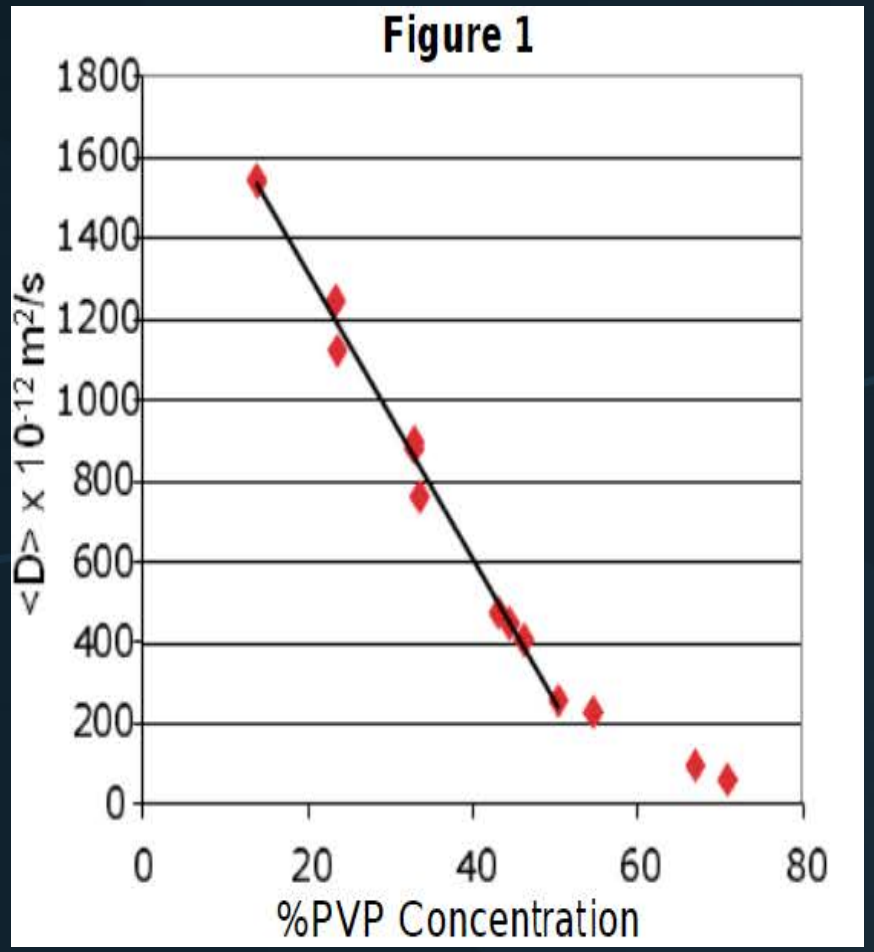

Pierpaoli et al. (2009), 1414

…what we got

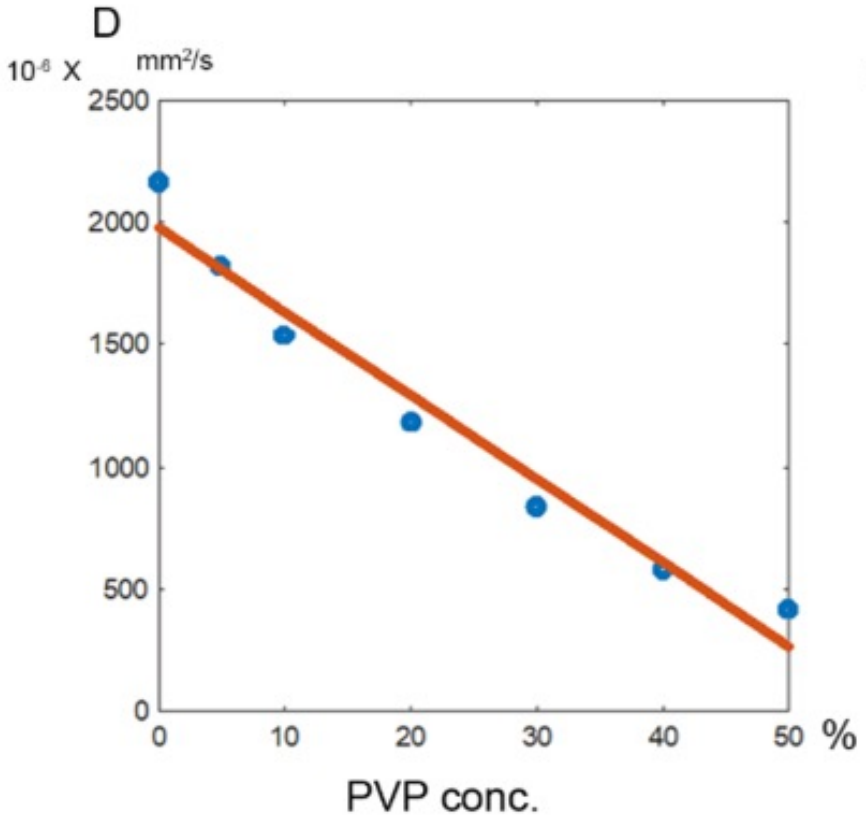

ADC vs. PVP conc. (linear gradient)

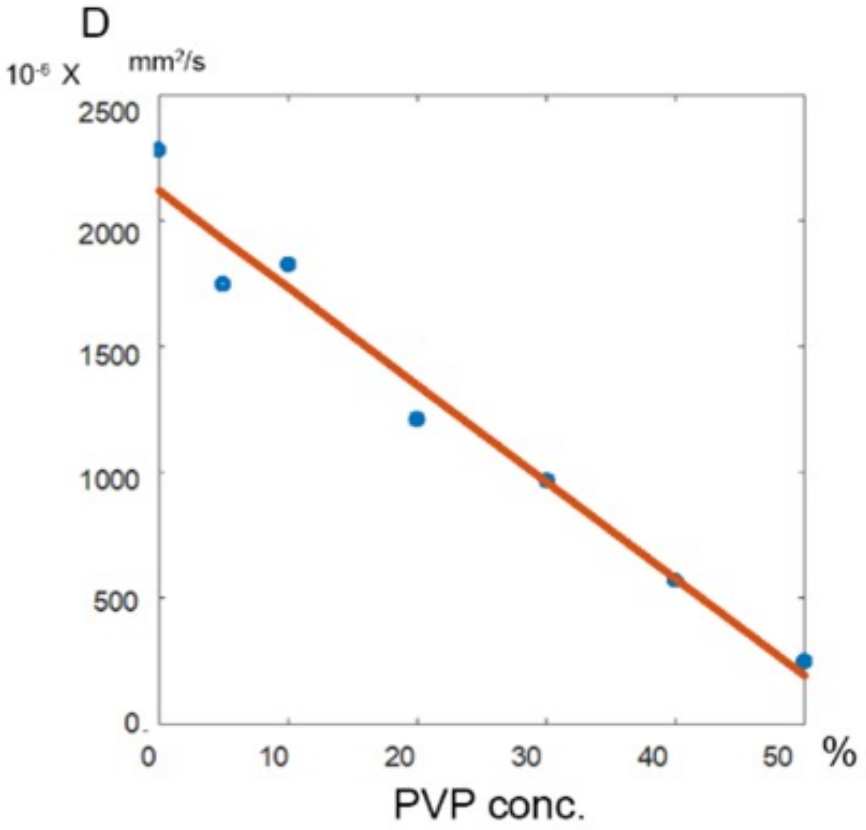

ADC vs. PCP conc. (non-linear gradient)

Eureka!

- The non-linear gradient coil produced similar diffusivity results with different PVP concentrations to those produced using the linear gradient coil.

- Future work will demonstrate accuracy gains obtainable from shorter diffusion encoding times.

References:

- [1] Hoque Bhuiyan et al., 2021 Oct;48(10):5804-5818. doi: 10.1002/mp.15100
- [2] Bauer et al., 87:1605-1612.https://doi.org/10.1002/mrm.29043
- [3] Pierpaoli et al. (2009), 1414

Acknowledgements:

The ONAOSI Foundation:
Dr.ssa Emanuela Pallotta
Dr. Paolo Giovenali
Dr. Francesco Tavernese

Anlyan Center:
Gigi Galiana Ph.D.
Nahla Elsaid Ph.D
Ates Fettahoglu

Wright Laboratory
Prof. Dr. Antonio Ereditato Ph.D.
Victoria Misenti
Taylor Dunnigan


The End

YALE RADIOLOGY

The role of physical exercise in Parkinson's disease: A clinical, radiological, and wearable tools analysis

Giulia Colonna,

Advanced Modeling Laboratory,

Yale PET Center,

Department of Radiology and Biomedical Imaging.

Wright Laboratory

OPERA NAZIONALE ASSISTENZA ORFANI SANITARI ITALIANI
FONDAZIONE ONAOSI

Background

Parkinson's Disease:

- Epidemiology:
  - Second most common neurodegenerative disorder in US
  - 60,000 new cases per year

- Pathology:
  - Degeneration of dopamine-producing neurons in the substantia nigra (SN) pars compacta.

- Symptoms:
  - Resting tremor
  - Rigidity
  - Bradykinesia
  - Postural instability.

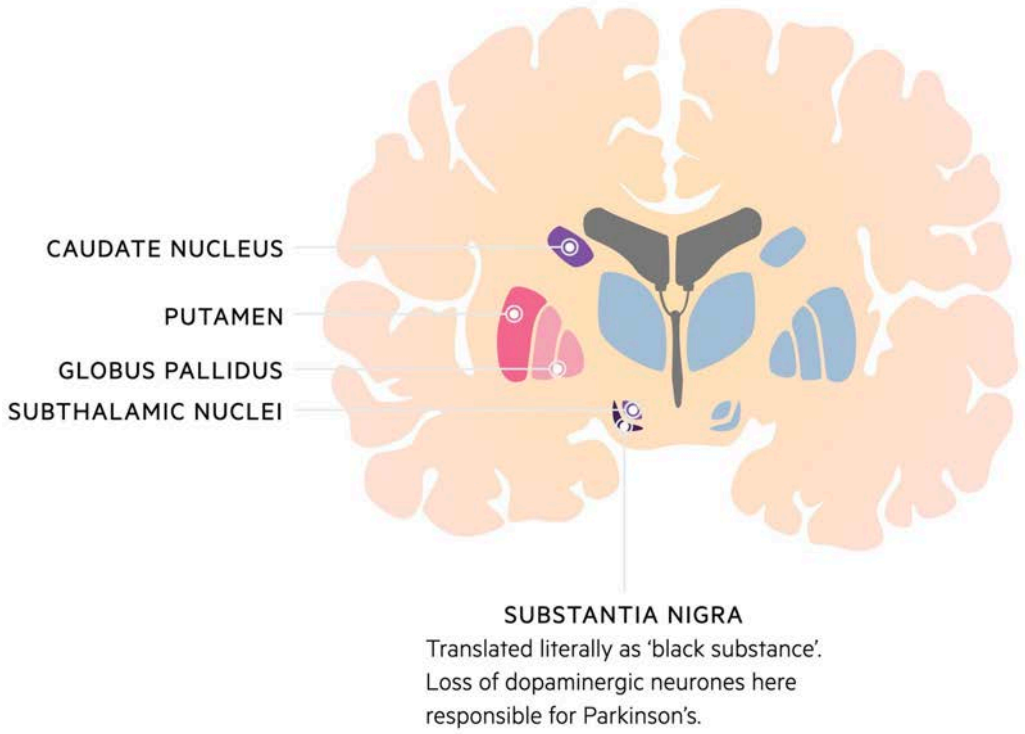

https://app.pulsenotes.com/medicine/neurology/notes/parkinson-s-disease

Treatment of Parkinson Disease:

- Levodopa
- Carbidopa
- MAO-B inhibitors
- Dopamine agonists
- Amantadine

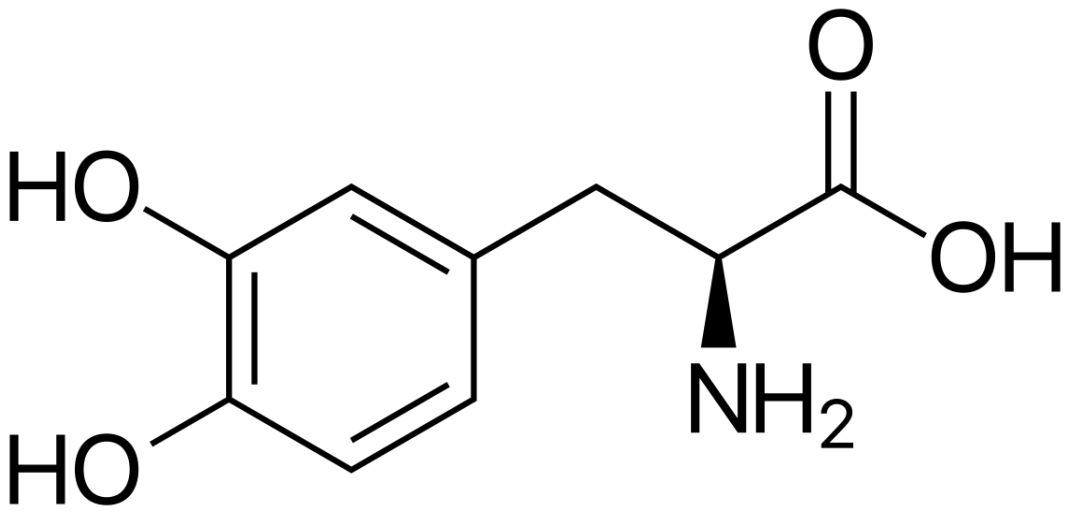

Parkinson's Disease and Exercise:

Effectiveness of home-ba supervised aerobic exercis double-blind, randomised

Nicolien M van der Kolk [1], Nienke M de Vries [1]

Nonpharmacological treatments for patients with Parkinson's disease

Bastiaan R Bloem [1], Nienke M de Vries [1], Georg Ebersbach [2]

Purpose of the study: potential neuroprotective effects of high-intensity exercise in humans with PD using multimodal neuroimaging techniques.

Boxing training for a case series

Stephanie A Combs [1], M Dyer Diehl
Katie Schaneman

Symptoms in Patients With De Novo Parkinson Disease: A Phase 2 Randomized Clinical Trial

Margaret Schenkman [1], Charity G Moore [2], Wendy M Kohrt [3 4], Deborah A Hall [5], Anthony Delitto [6], Cynthia L Comella [5], Deborah A Josbeno [2], Cory L Christiansen [1 4], Brian D Berman [7], Benzi M Kluger [7], Edward L Melanson [4 8], Samay Jain [9], Julie A Robichaud [10], Cynthia Poon [11], Daniel M Corcos [12]

Imaging study Methods:

MRI:

- The MRI will be used to assess **dopaminergic degeneration**, by targeting neuromelanin-containing neurons.
- NM can be measured accurately with MRI due to its **ferromagnetic properties**

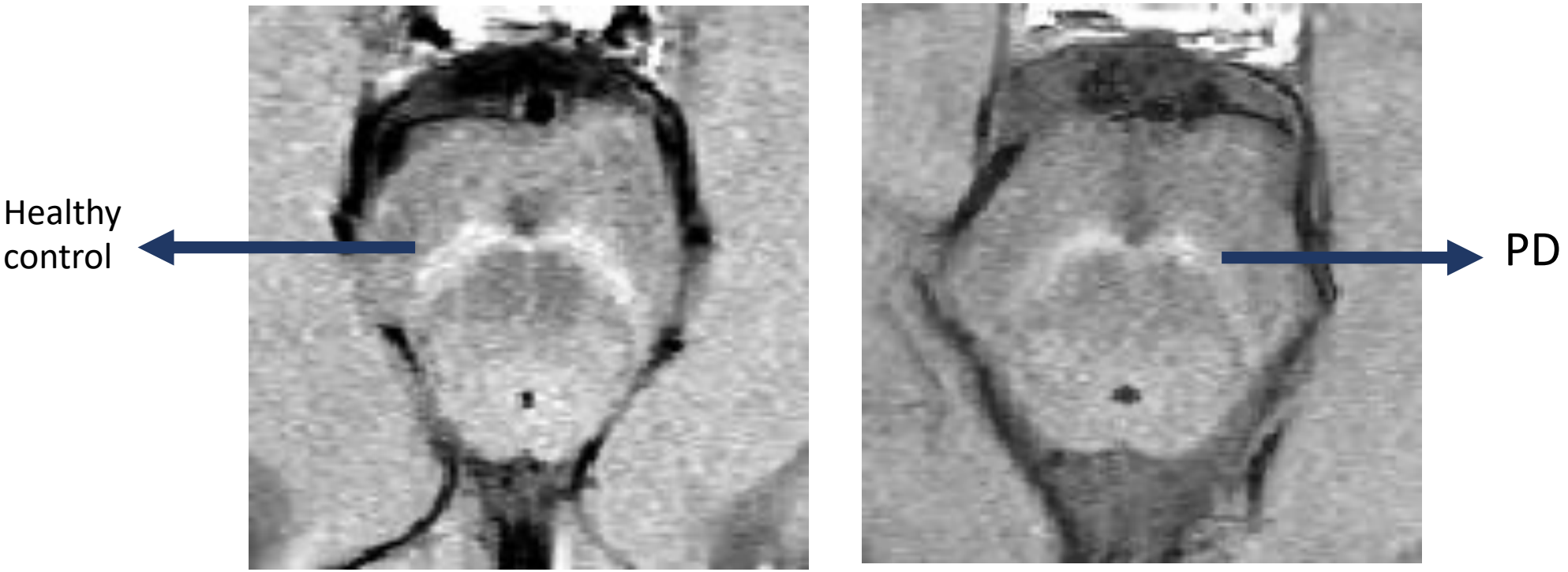

PET:

- The PET will be used to assess **the functionality of the dopaminergic system** by targeting the dopamine transporter **(DAT)** .
- novel radioligand **[18F]FE-PE2I**

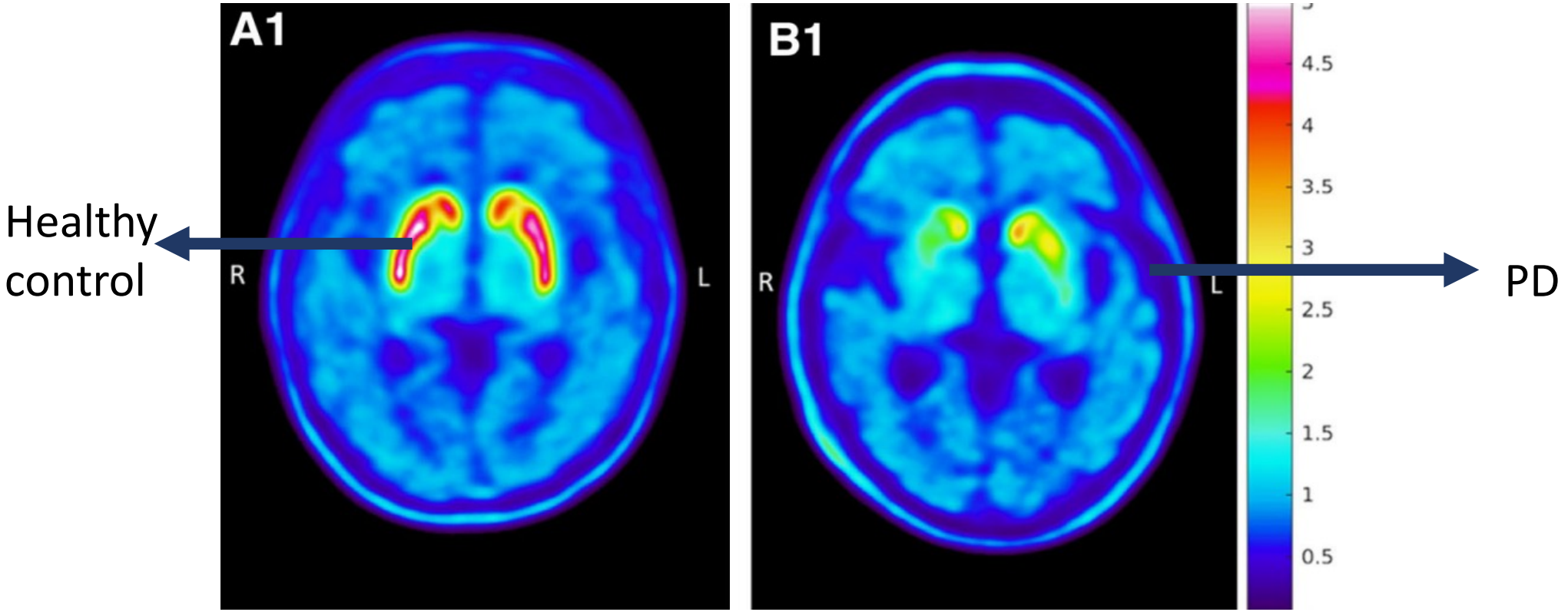

Dopamine transporter imaging with [18F]FE-PE2I PET and [123I]FP-CIT SPECT—a clinical comparison, Susanna J.

Patient Cohort and Study Design :

11 (6M, 5F) eligible subjects with PD defined according to the Movement Disorder Society (**MDS**)

- Clinical evaluation **(H&Y scale)**
- Motor function tests (**UPDRS**)
- Baseline NM-MRI
- [18F]FE-PE2I PET scan

- Clinical evaluation **(H&Y scale)**
- Motor function tests (**UPDRS**)
- NM-MRI
- [18F]FE-PE2I PET scan

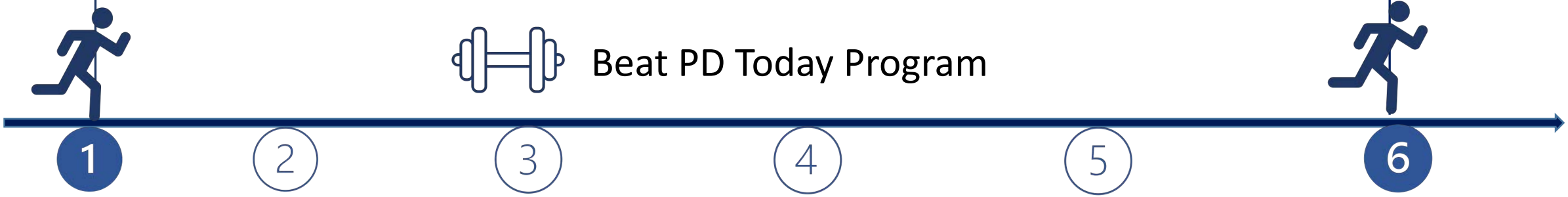

Beat PD Today

- **The Beat PD Today project**:
  - Individualized High-intensity training
  - Boxing
  - 1h session 3 times/week

- **HR Tracking devices**:
  - Fitbit
  - PolarH10 + HRVelite chest strap

- **Parameters**:
  - 70/80 % of maximum HR
  - High intensity Heart Zone (70%-85% of Heart Reserve)

Why two devices?

HRV polar:

- Measures the myocardial electric potentials (= electrocardiogram)
- Correlation with ECG: r=0.997[3]
- **Discomfort and complex interface**

Fitbit Charge 4 :

- Measures the volume changes in blood vessels throughout a PPG optical heart-rate sensor.
- Previous models **underestimate** HR measurments of an average of **6bpm** at baseline and **16 bpm** at higher HR.[4]
- **Confortable** and **convenient**

PolarH10 heart rate monitor vs Fitbit:

A validation study in PD patients

PolarH10 heart rate monitor vs Fitbit: A validation study in PD patients

To evaluate the **feasibility of Fitbit Charge 4 in measuring HR** compared to HRV polar Heart rate monitor.

Methods

Data Analysis :

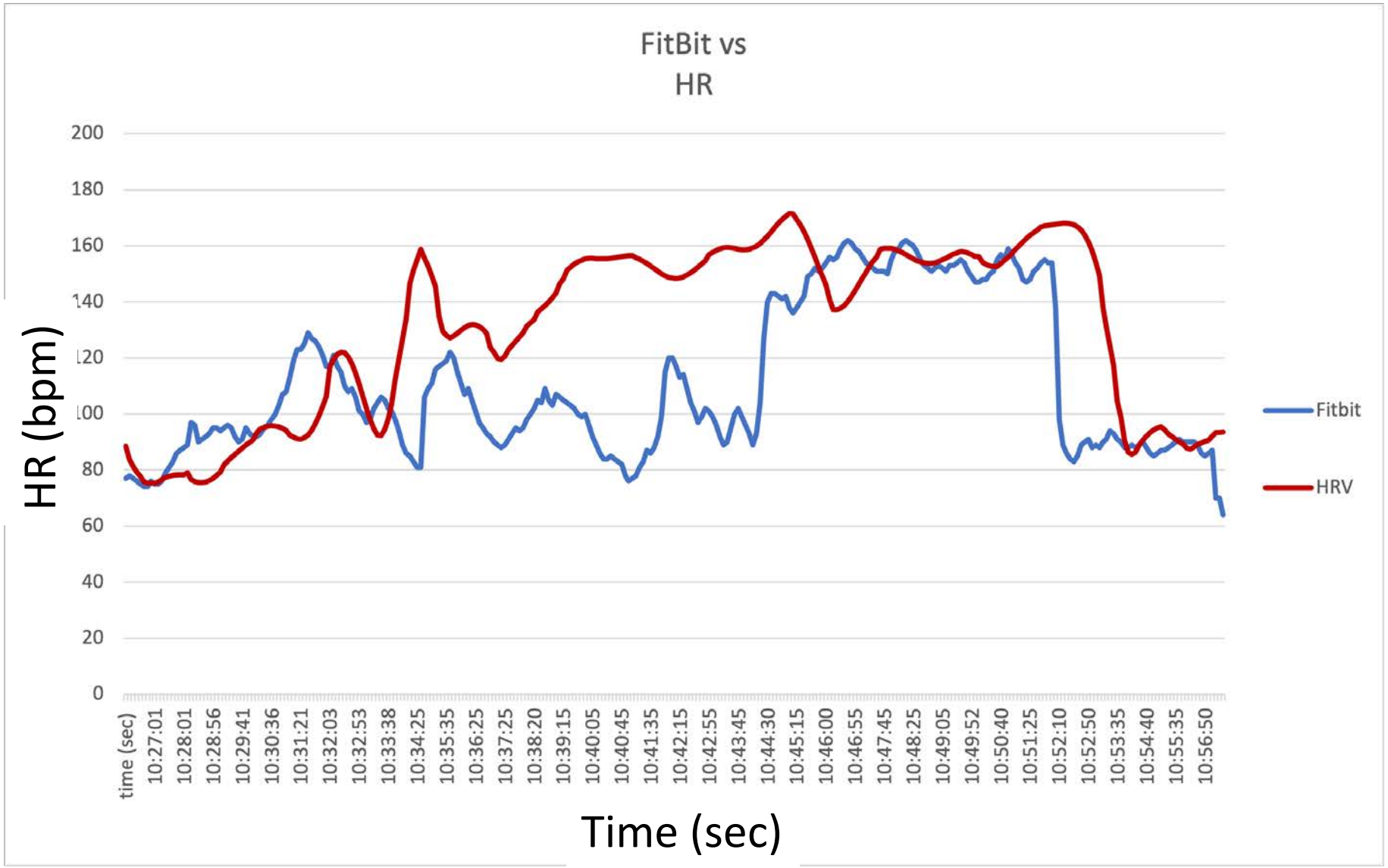

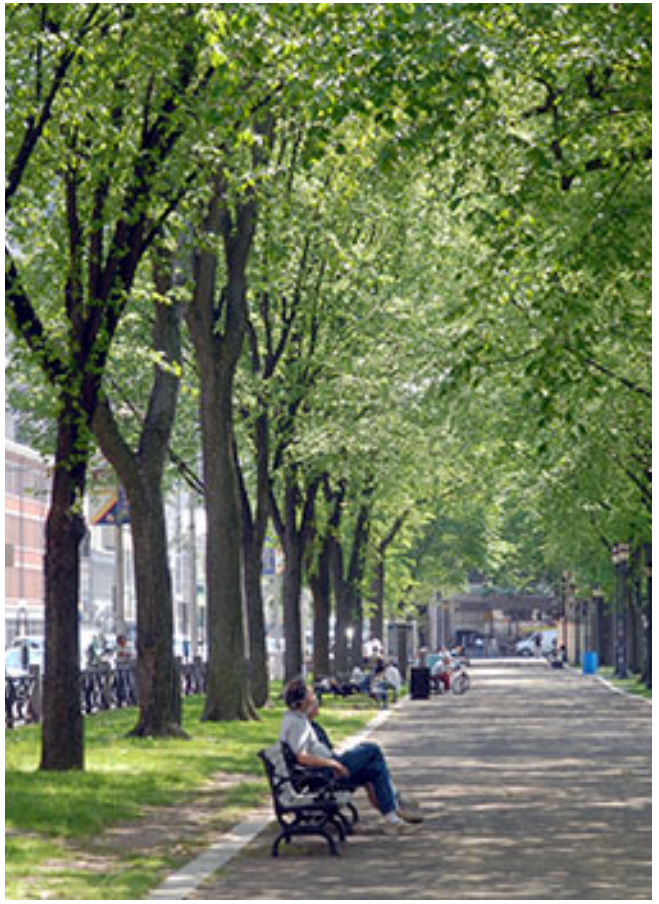

Data Analysis :

Fitbit Database:
14.717.423 values

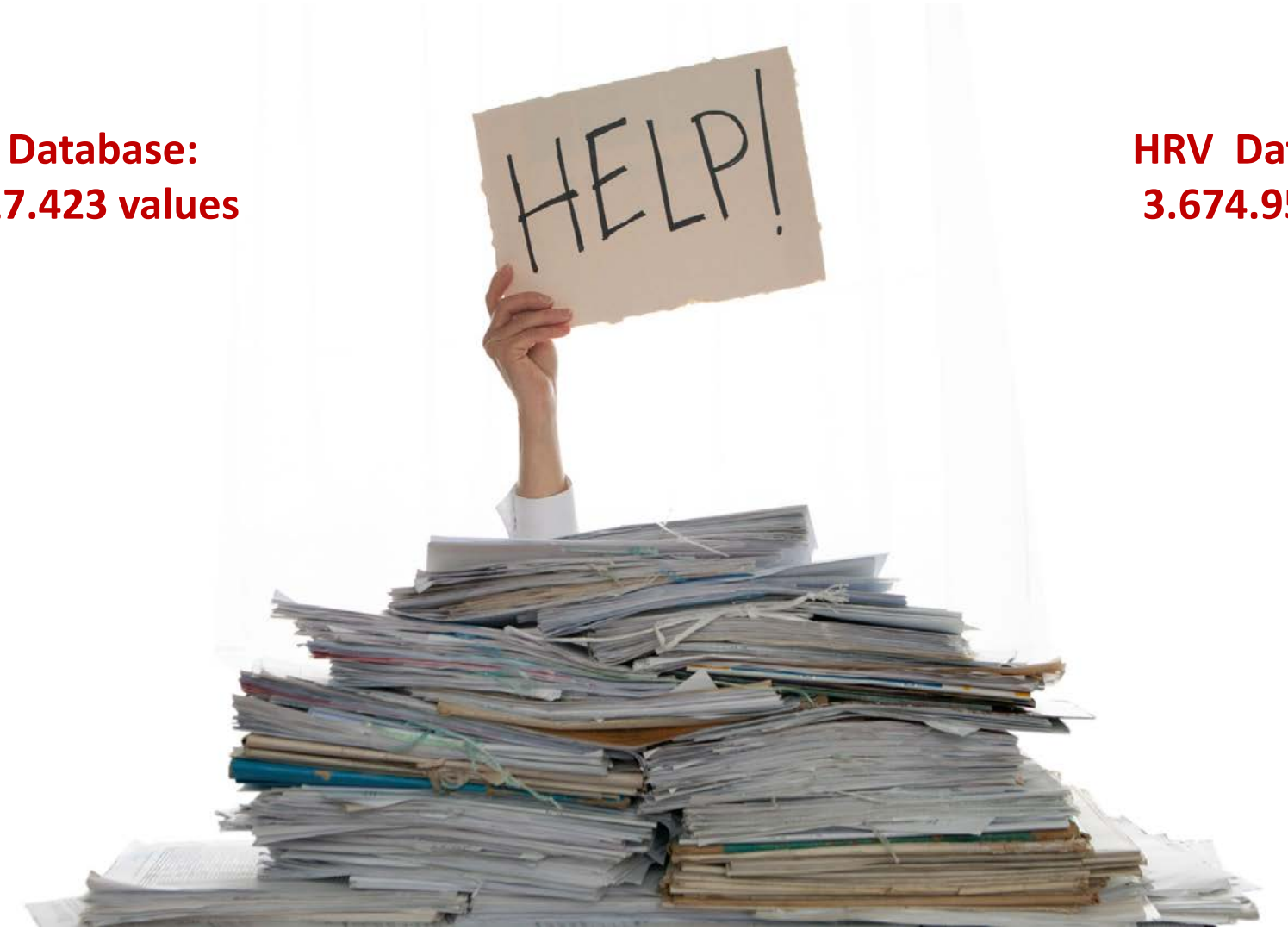

HRV Database:
3.674.957

Data Analysis :

- Time frame: 01/01/2021 – 08/06/2022
- Number of subjects: 10
- Session average duration: 1h
- Calculated values :
  - **Baseline AVG (<5min)**
  - **Highest AVG (20 min)**

<u>30 paired session (2,5 months) from each subjects,</u>
<u>for a total 300 calculated values to compare</u>

```
for one_df in groups:
 one_df.set_index('Time', inplace = True)
 a =one_df['HR_(BPM)'].resample('1T').mean()
 print(a)

#calculating statistics:
patient1=pd.DataFrame(columns = ['baseline_avg','total_avg','max_avg'])
for ii, one_df in enumerate(groups):
 baseline_avg=[(one_df['HR_(BPM)'].iloc[0:5]).mean()]
 total_avg=[(one_df['HR_(BPM)']).mean()]
 print(baseline_avg)
 print(total_avg)
 i = 0
 highest_avg = []

 while i < len(one_df)-20:
    highest_avg.append([(one_df['HR_(BPM)'].iloc[i:i+20]).mean()])
    i += 1
 max_avg = max(highest_avg)
 patient1 = patient1.append(pd.Series([baseline_avg,total_avg,max_avg], index=['baseline_avg
```

```
#filtering the Fibit file with the sessions Date and Time (from HRV):
y=range(len(df))
#y=range(60)
options3=df['new_date']
options2 = df['new_time'].dt.round('1min')
NewFitbit_df.reset_index(inplace=True)
results=[]
for x in y:
    options4 = [options2[x]]
    options5 = [options3[x]]
    NewFitbit_df['time1']= NewFitbit_df['Time'].dt.round('1min')
    NewFitbit2_df=NewFitbit_df[NewFitbit_df['time1'].isin(options4)& NewFitbit_df['Date'].is
    results.append(NewFitbit2_df)

#indexes of the starting time:
results= pd.concat(results)
#print(results['Date'].unique)
filtered_date=results['Date'].unique()
```

Results:

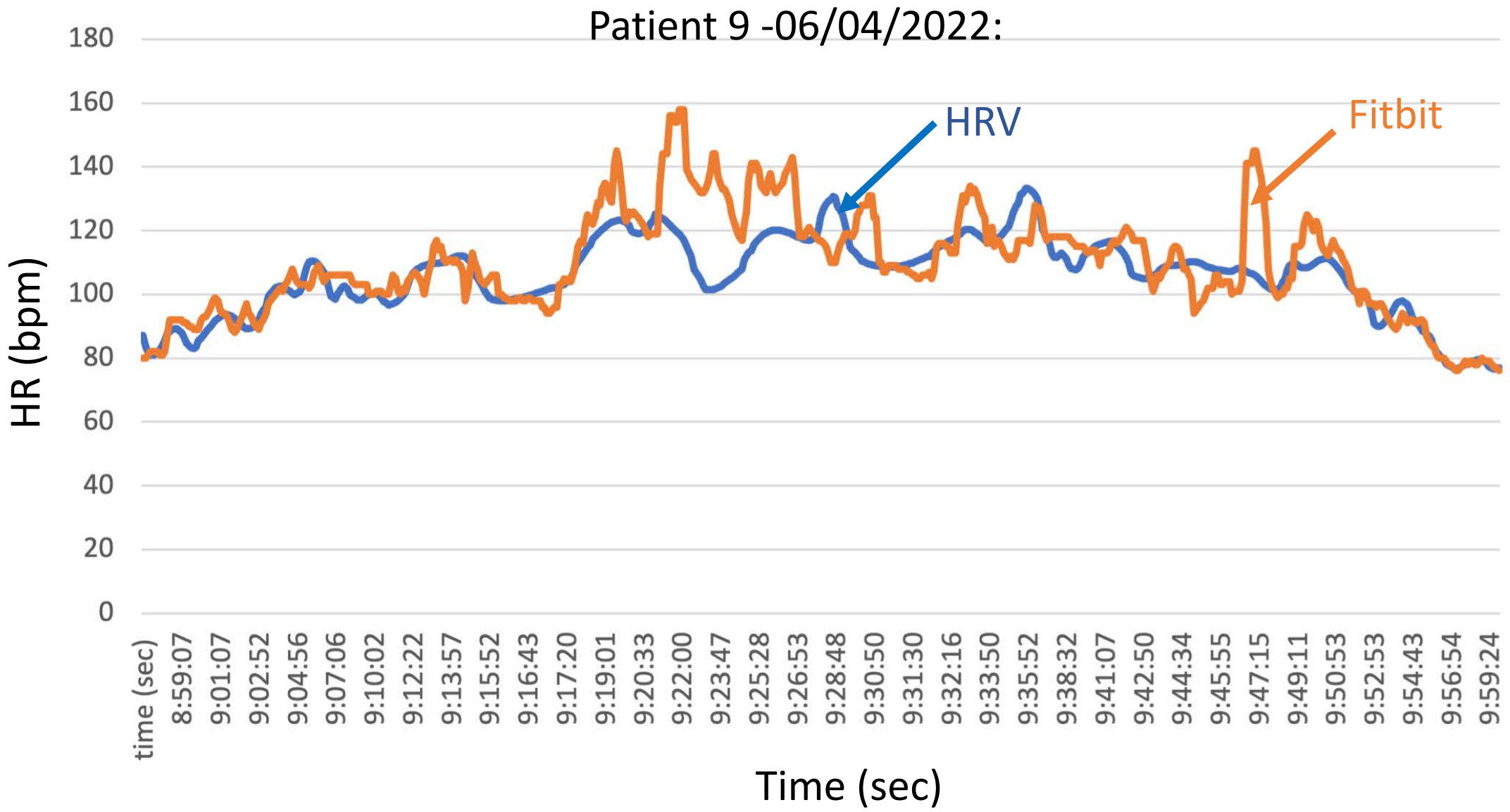
Patient 9 -06/04/2022:
HRV
Fitbit
HR (bpm)
180
160
140
120
100
80
60
40
20
0
time (sec)
8:59:07
9:01:07
9:02:52
9:04:56
9:07:06
9:10:02
9:12:22
9:13:57
9:15:52
9:16:43
9:17:20
9:19:01
9:20:33
9:22:00
9:23:47
9:25:28
9:26:53
9:28:48
9:30:50
9:31:30
9:32:16
9:33:50
9:35:52
9:38:32
9:41:07
9:42:50
9:44:34
9:45:55
9:47:15
9:49:11
9:50:53
9:52:53
9:54:43
9:56:54
9:59:24
Time (sec)

Results:

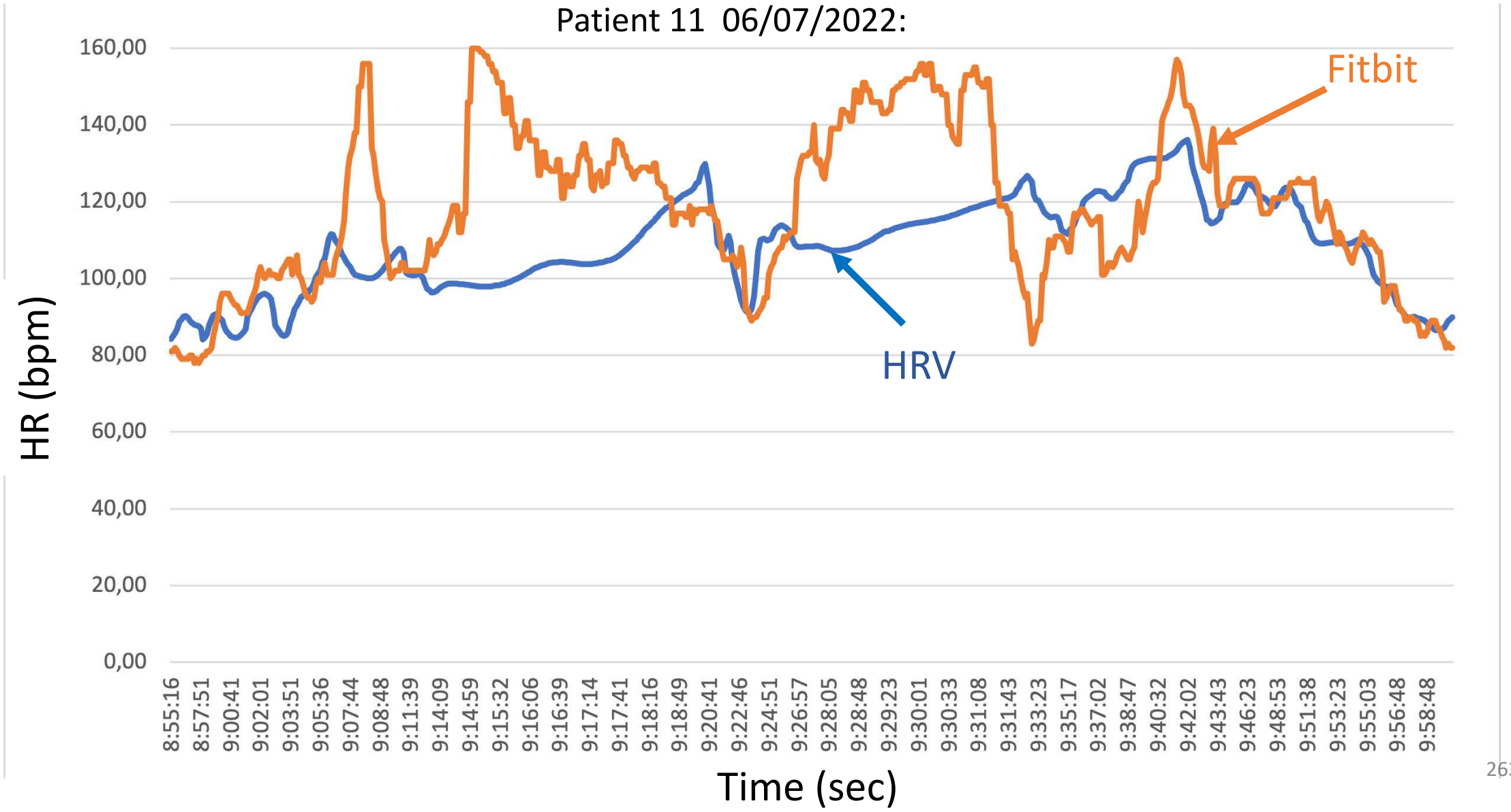
Patient 11 06/07/2022:
160,00
140,00
120,00
100,00
80,00
60,00
40,00
20,00
0,00
HR (bpm)
Fitbit
HRV
8:55:16
8:57:51
9:00:41
9:02:01
9:03:51
9:05:36
9:07:44
9:08:48
9:11:39
9:14:09
9:14:59
9:15:32
9:16:06
9:16:39
9:17:14
9:17:41
9:18:16
9:18:49
9:20:41
9:22:46
9:24:51
9:26:57
9:28:05
9:28:48
9:29:23
9:30:01
9:30:33
9:31:08
9:31:43
9:33:23
9:35:17
9:37:02
9:38:47
9:40:32
9:42:02
9:43:43
9:46:23
9:48:53
9:51:38
9:53:23
9:55:03
9:56:48
9:58:48
Time (sec)

Results:

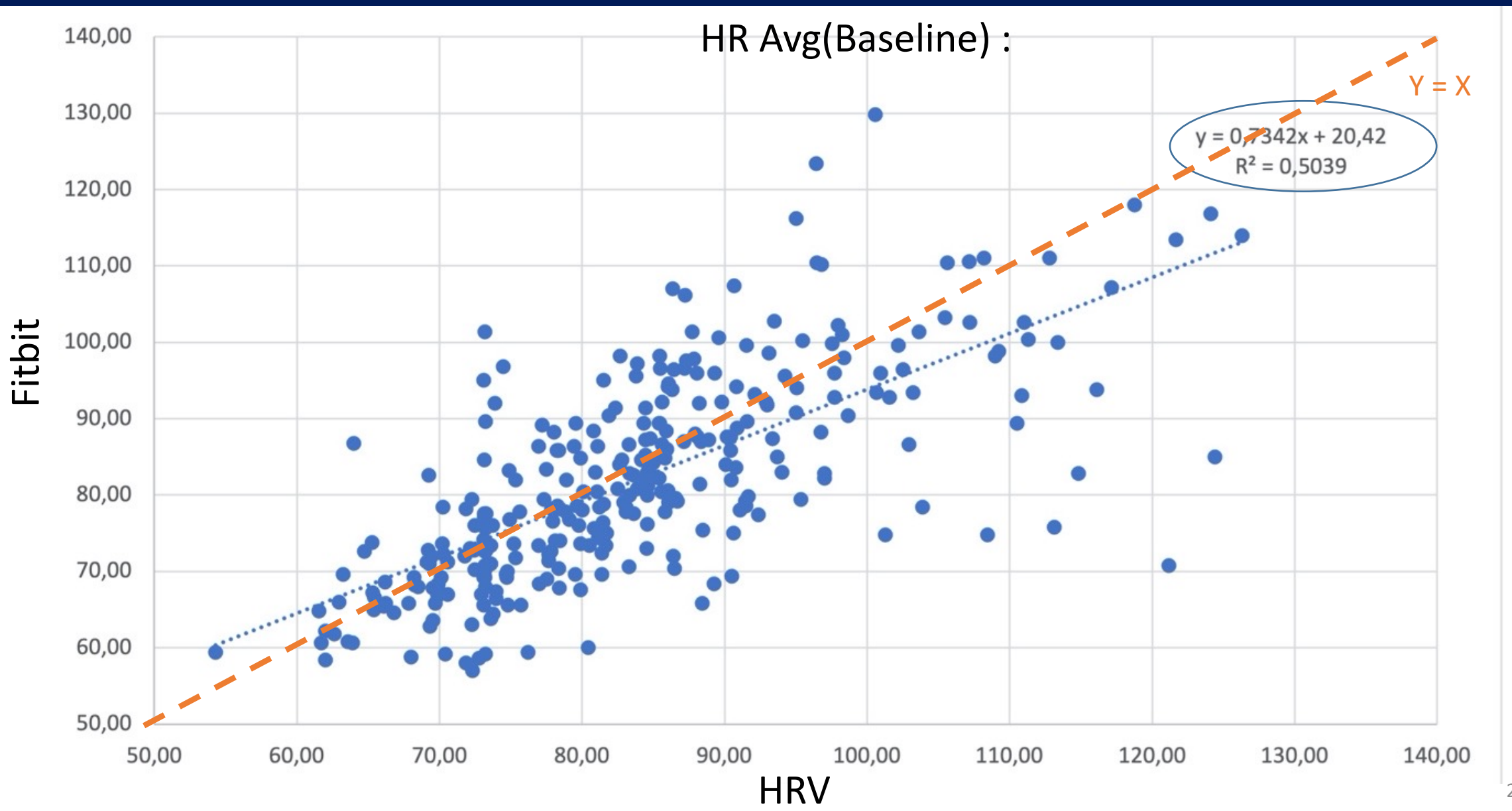
HR Avg(Baseline) :
Y = X
y = 0,7342x + 20,42
R² = 0,5039
Fitbit
HRV
140,00
130,00
120,00
110,00
100,00
90,00
80,00
70,00
60,00
50,00
50,00
60,00
70,00
80,00
90,00
100,00
110,00
120,00
130,00
140,00

Results:

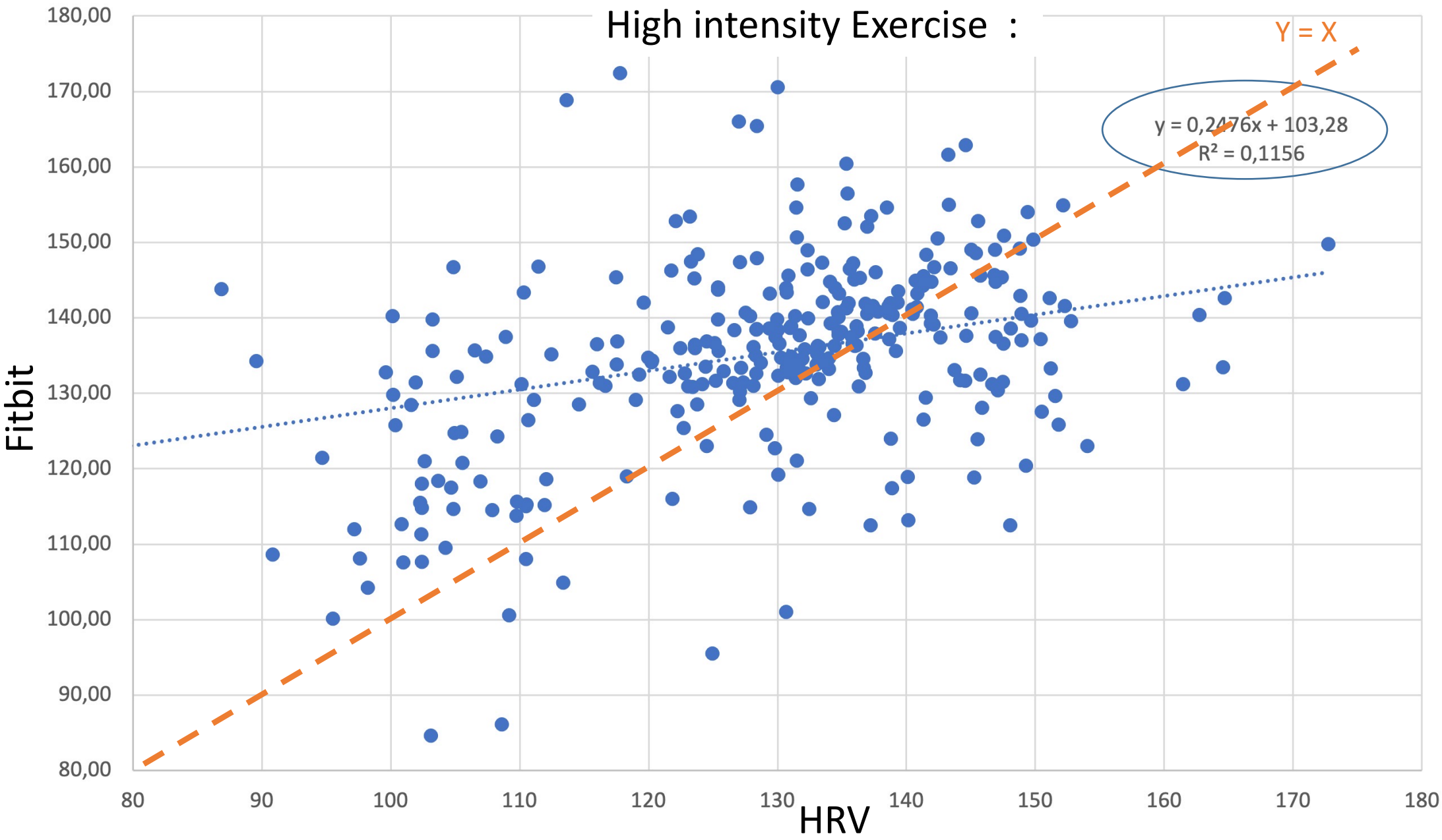
High intensity Exercise :
Y = X
y = 0,2476x + 103,28
R² = 0,1156
Fitbit
HRV
180,00
170,00
160,00
150,00
140,00
130,00
120,00
110,00
100,00
90,00
80,00
80
90
100
110
120
130
140
150
160
170
180

Results:

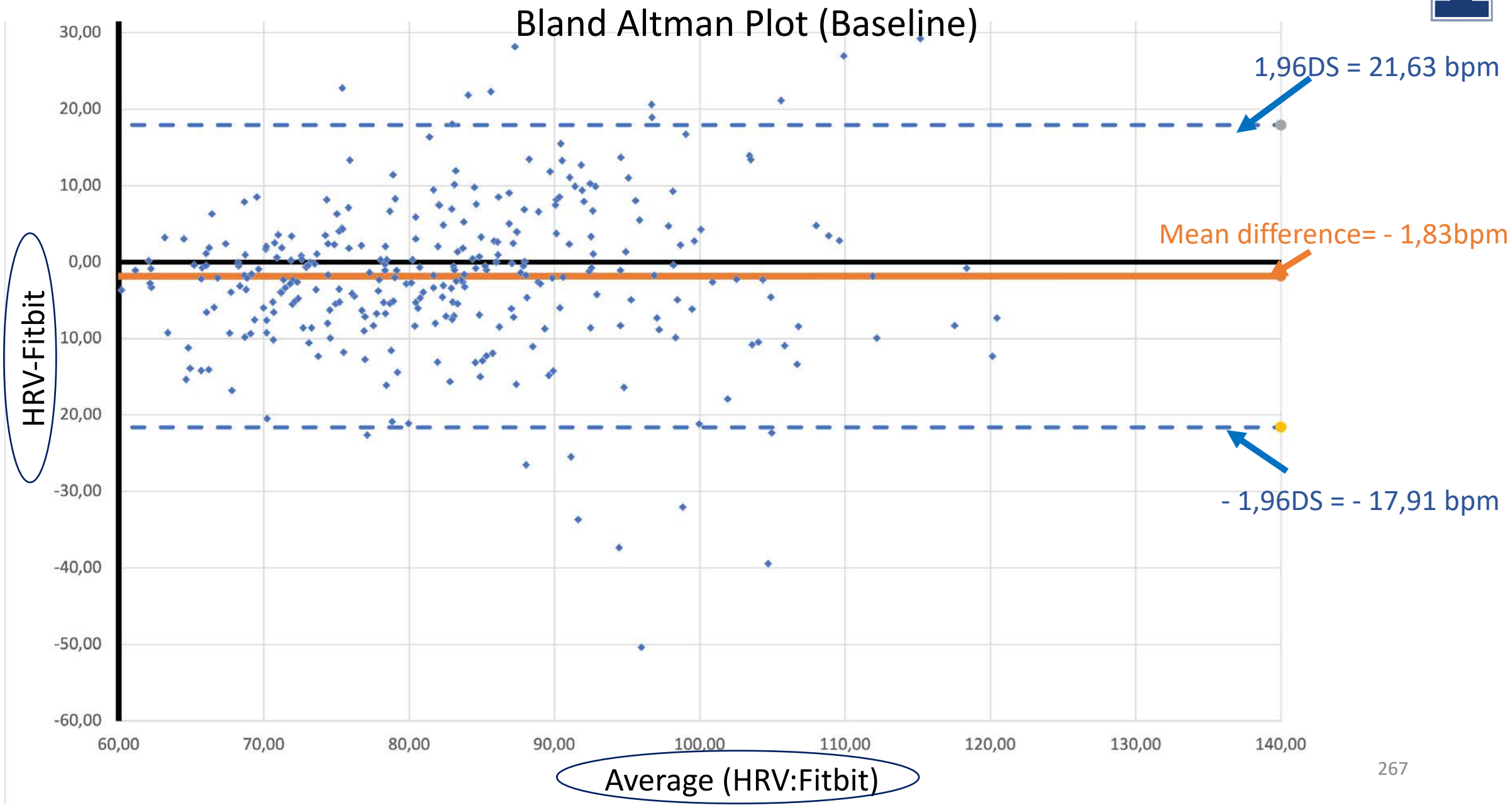
Bland Altman Plot (Baseline)
1,96DS = 21,63 bpm
Mean difference= - 1,83bpm
- 1,96DS = - 17,91 bpm
HRV-Fitbit
Average (HRV:Fitbit)
30,00
20,00
10,00
0,00
10,00
20,00
-30,00
-40,00
-50,00
-60,00
60,00
70,00
80,00
90,00
100,00
110,00
120,00
130,00
140,00

Results:

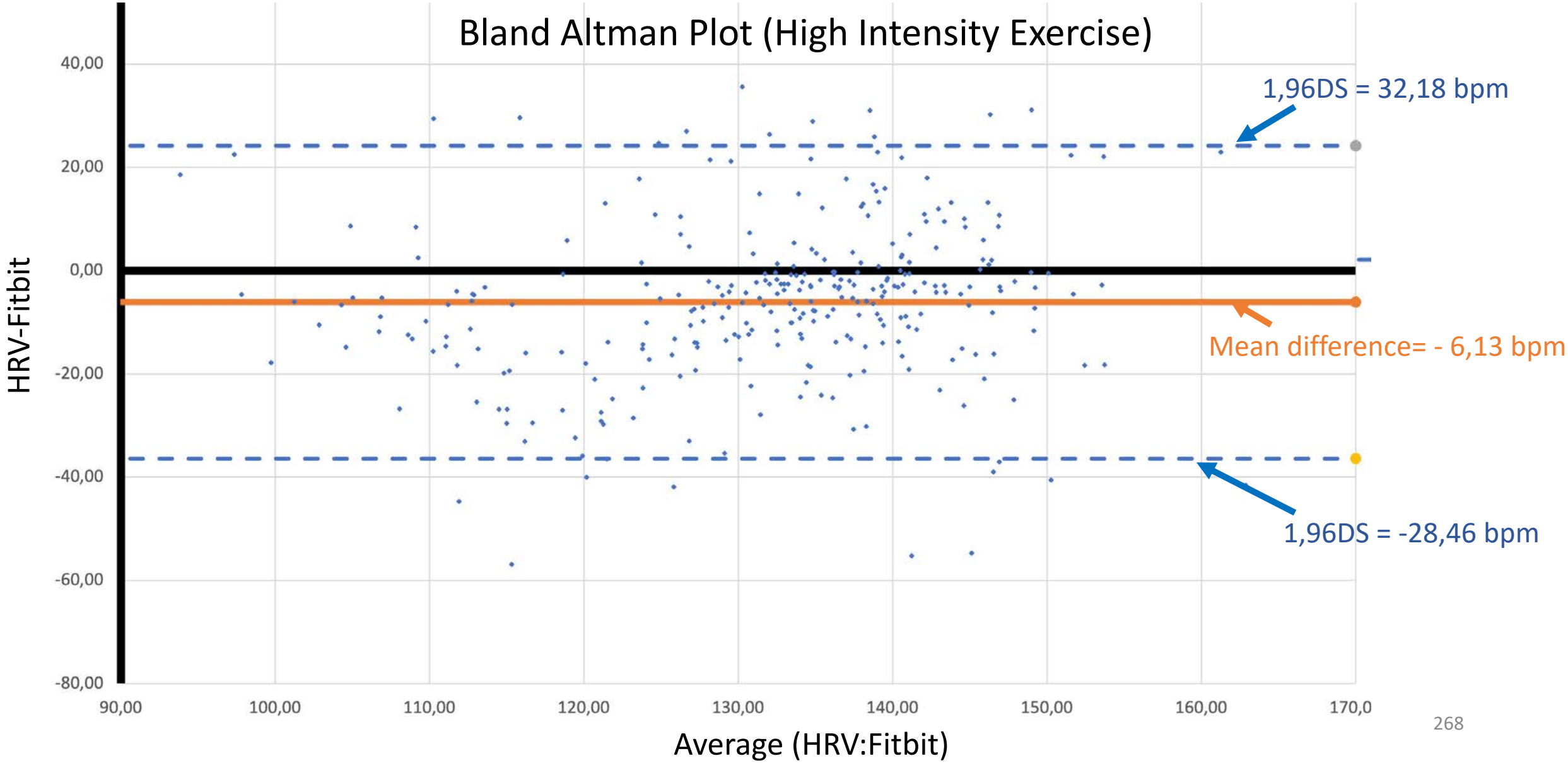
Bland Altman Plot (High Intensity Exercise)
1,96DS = 32,18 bpm
Mean difference= - 6,13 bpm
1,96DS = -28,46 bpm
HRV-Fitbit
Average (HRV:Fitbit)
40,00
20,00
0,00
-20,00
-40,00
-60,00
-80,00
90,00
100,00
110,00
120,00
130,00
140,00
150,00
160,00
170,0

Results:

Between-subjects variability :

Subject:	Baseline Difference (bpm) :	Highest AVG Difference (bpm)
Subject 1	1,55	-6,46
Subject 2	-2,86	-8,16
Subject 3	1,77	6,65
Subject 4	-0,69	-7,84
Subject 5	-1,09	-12,15
Subject 6	2,05	-7,97
Subject 7	-6,59	9,03
Subject 8	-10,95	-9,26
Subject 9	-0,58	-10,85
Subject 10	-2,47	-6,81

Results

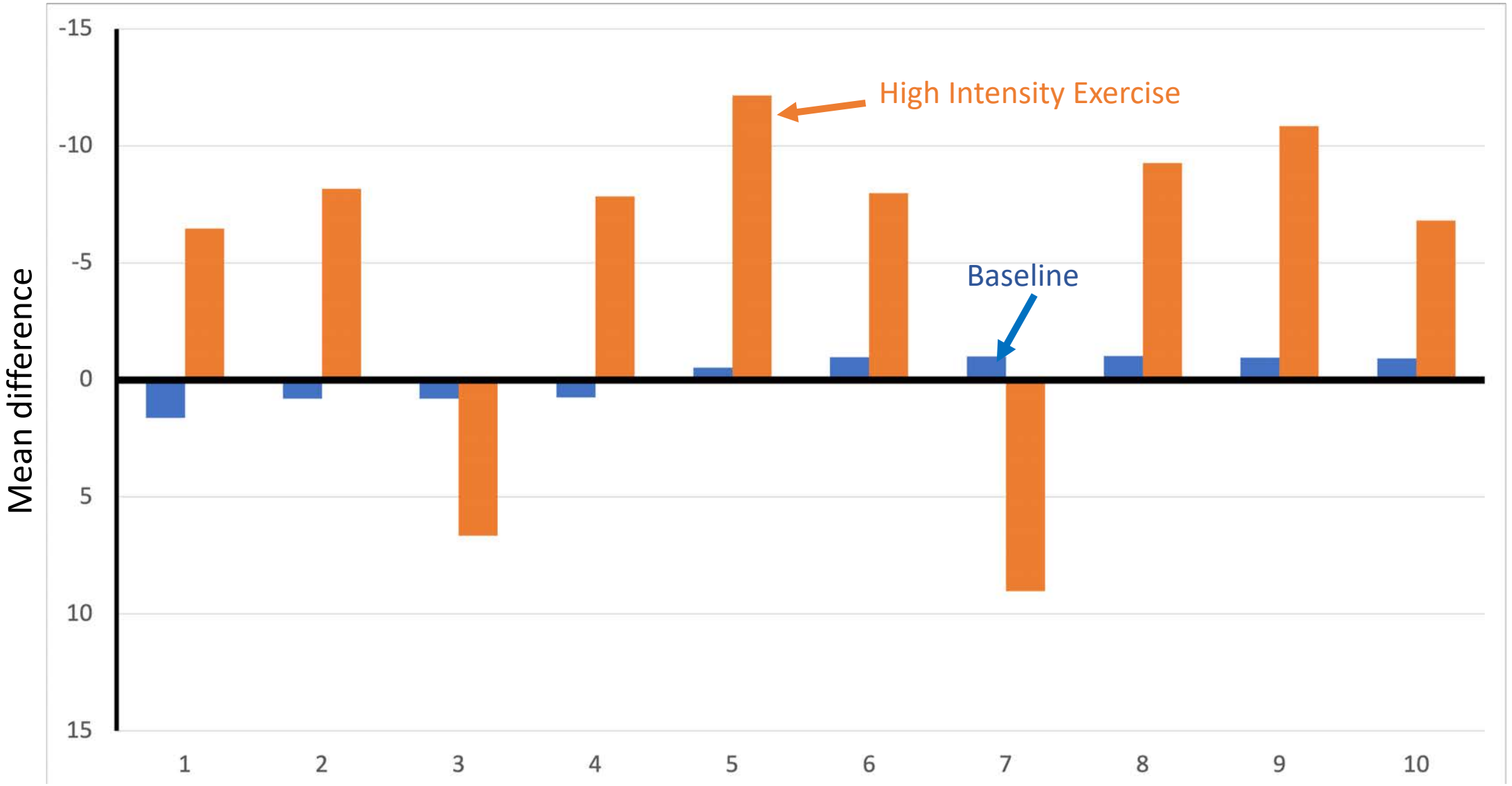
-15
-10
-5
0
5
10
15
Mean difference
High Intensity Exercise
Baseline
1
2
3
4
5
6
7
8
9
10
Subjects

Conclusions:

- Baseline condition = + **1,84 bpm**
- High intensity exercise **= + 6,13 bpm**
- Fitbit accuracy is HR-dependent, and there is a high between-subjects variability
- A larger study could be conducted just using the Fitbit

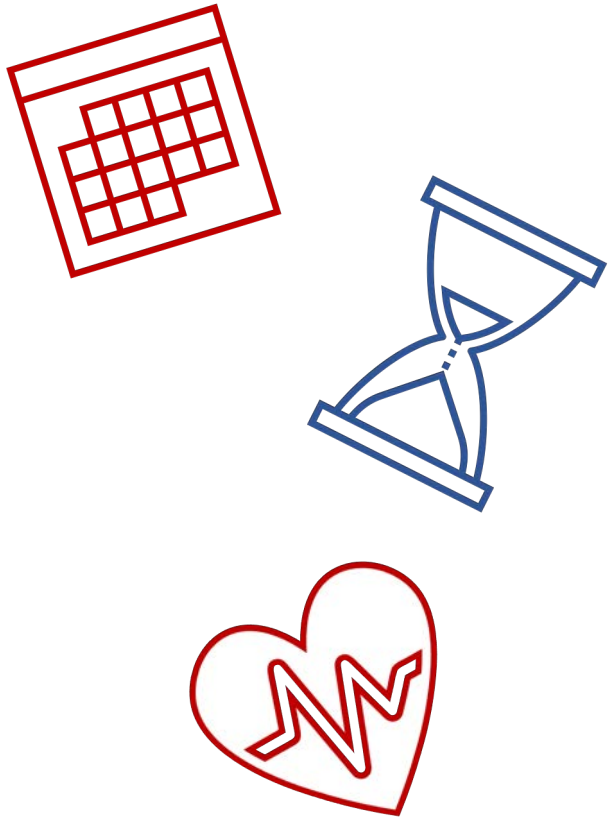

Thank you!

- **PET Center:**
  - Evan Morris
  - Jocelyn Hoye
  - Alaaddin Ibrahimy
  - Gelsina Stanley
  - Bart de Laat
- **Neurology, Movement Disorders**
  - Sule Tinaz
- **Wright Lab :**
  - Antonio Ereditato
  - Victoria Misenti
  - Taylor Dunnigan
  - Bonnie Fleming
- **Onaosi :**
  - Emanuele Pallotta
  - Paolo Giovenali
  - Francesco Tavernese

Wright Laboratory

OPERA NAZIONALE ASSISTENZA ORFANI SANITARI ITALIANI
FONDAZIONE ONAOSI